CONVECTIVE HEAT TRANSFER

IN A ROTARY KILN

by

SHONG HSIUNG TSCHENG

B.E.,   National Taiwan University, Taiwan, 1968

M.S.,   West Virginia University, U.S.A., 1972

A THESIS SUBMITTED IN PARTIAL FULFILMENT OF

THE REQUIREMENTS FOR THE DEGREE OF

DOCTOR OF PHILOSOPHY

in the Department

of

CHEMICAL ENGINEERING

We accept this thesis as conforming to the

required standard

THE UNIVERSITY OF BRITISH COLUMBIA

September, 1978

In presenting this thesis in partial fulfilment of the requirements for an advanced degree at the University of British Columbia, I agree that the Library shall make it freely available for reference and study. I further agree that permission for extensive copying of this thesis for scholarly purposes may be granted by the Head of my Department or by his representatives. It is understood that copying or publication of this thesis for financial gain shall not be allowed without my written permission.

Department of _Chemical Engineering_

The University of British Columbia
2075 Wesbrook Place
Vancouver, Canada
V6T 1W5

Date _September 29, 1978_

ABSTRACT

Convective heat transfer in a rotary kiln was studied as a function of operating parameters. The experiments were carried out in a steel kiln of 0.19 m in diameter and 2.44 m in length. The operating parameters covered included gas flow rate, solid throughput, rotational speed, degree of solid hold-up, inclination angle, particle size and temperature. To minimize radiation effects, air was used as the heating medium and maximum inlet air temperatures were limited to 650 K. Ottawa sand was used in all the runs except in the study of the effect of particle size where limestone was employed. The experiments were conducted under conditions where the bed height along the kiln was maintained constant and the bed was in the rolling mode.

Both the heat transfer coefficients from the gas to the solids bed and the gas to the rotating wall were found to be significantly influenced by gas flow rate. Increasing rotational speed increases the gas to bed heat transfer, but decreases the gas to wall heat transfer. The former effect is relatively small. The effect of degree of fill was slightly negative in the gas to solids bed heat transfer, and insignificant in the heat transfer from the gas to wall. The effects of inclination angle , solid throughput , particle size and temperature were

found negligible over the range tested. One of the major findings in this study is that contrary to suggestions in the literature, the coefficients for gas to bed heat transfer are about an order of magnitude higher than those for gas to wall. The higher coefficients for gas to solids bed are attributed to two factors, the underestimation of the true area by basing coefficients on the plane chord area and the effect on the gas film resistance of the rapid particle velocity on the bed surface.

The experimental data were correlated in a form suitable for design purposes, and the results compared with meager data available in the literature.

A mathematical model was developed for convective heat transfer from the gas to a rolling solids bed. The model requires the knowledge of the gas to particle heat transfer coefficient and the rolling velocity of the aerated particles. The model gives a reasonable prediction of the gas to bed coefficient in a rotary kiln using values of the gas to particle coefficient taken from the literature. The required data on the surface velocity of particles was obtained in a lucite kiln of the same size. Residence time distribution of particles was also studied briefly to verify that solids were nearly in axial plug flow.

A simple mathematical model of a rotary kiln heat exchanger is presented. This model predicts gas, solids and wall temperatures in a kiln as a function of the kiln design and

operating parameters using the heat transfer correlations

developed in this work.

TABLE OF CONTENTS

LIST OF TABLES

Appendix

TABLE OF FIGURES

Figure

ACKNOWLEDGEMENTS

CHAPTER 1

INTRODUCTION

The rotary kiln is one of the most widely used
industrial reactors for high temperature processes involving
solids. It consists of a metal cylinder, lined with brick,
rotated about its inclined axis as shown in Figure 1-1. The
solid feed is introduced into the upper end of the kiln by
various methods, including inclined chutes, overhung screw
conveyors and slurry pipes. The charge then travels down
along the kiln by axial and circumferential movements, due to
the kiln's inclination and rotation.

Kiln inclination depends on the process with a typical
range of values from 0.02-0.063 m/m. Different rotational
speeds are used depending on the process and kiln size from
very low, i.e., a peripherial speed of 0.015 m/s, for a TiO_2
pigment kiln, to 0.227 m/s for a cement kiln, to 0.633 m/s for
a unit calcining phosphate material. The sizes of industrial
kilns range from 1.7 m.I.D. x 11.8 m long for firing light
weight aggregate, to 5.9 m x 125 m for iron ore direct reduction.
Rotary kilns are versatile reactors in that particle size and
solid density are not restricted as in the case of fluidized
or spouted beds, direct firing or indirect heating may be used,
and the kiln can operate in either cocurrent or counter-current
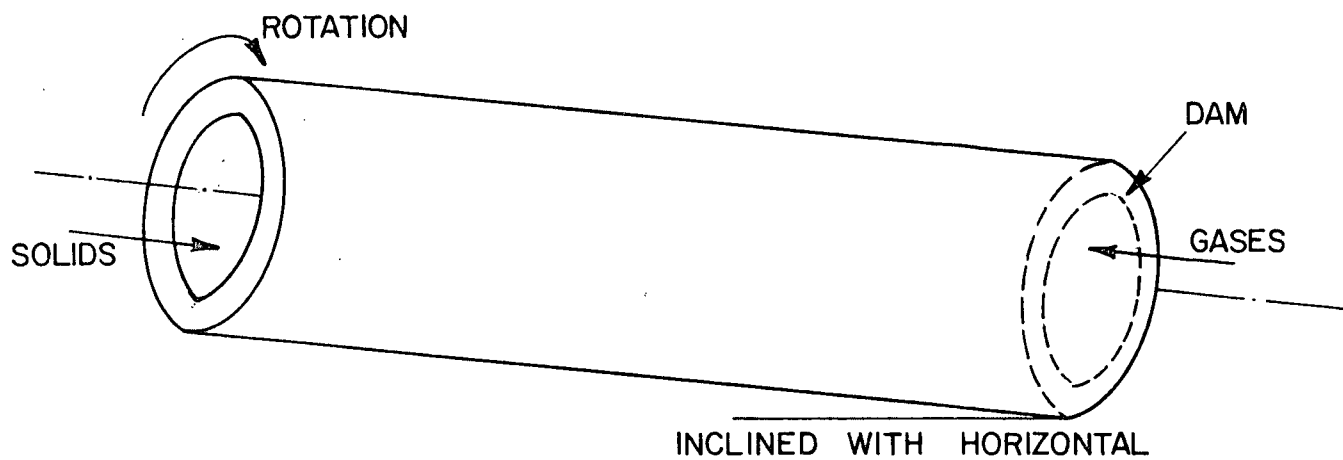
Figure 1-1 Basic Components of Rotary Kiln

flow. The latter feature is important where high extent of solid conversion is required. Solids may be fed either in the dry state, or as a wet paste.

The main uses of rotary kilns are in the processes of calcining, fusing, nodulizing, roasting, incinerating, and reducing of solid materials. Lime, magnesia and alumina are calcined to release carbon dioxide and water, at temperatures in the ranges of 1260-1500 K. The nodulizing process is applied to phosphate rock and certain iron ores with temperatures, 1500 to 1600 K. Roasting occurs at temperatures between 800 K and 1600 K, to oxidize and drive off sulfur and arsenic from various ores, including gold, silver, iron, etc. The rotary kiln is successfully used as a pre-combustion reactor for incineration of plastics wastes (1). The temperatures in this process are in the range of 570-970 K. Iron ore reduction is typical of reducing processes carried out in rotary kilns. The reaction temperatures are around 1300 K. Other major applications of rotary kilns include production of expanded aggregate, production of activated carbon (in two stages, carbonizing 670-770 K, and activation, 1170-1270 K), recovery of zinc from other metals (1200 K, Waelz process), and production of plaster of paris (382 to 404 K).

A considerable portion of the kiln length may be used to dry solids and bring them up to reaction temperature. In a typical wet process cement kiln, 60% of the 137 meter kiln length is required to dry the slurry and heat solids to 1100 K, whereas the calcining zone and burning zones occupy 22% and

18% of the length, respectively. Stelco reported (2) performance data for its first commercial iron ore direct reduction kiln in the SL/RN process. About 70% of the 125 meter kiln length is used to preheat the solids up to 1120 K, leaving only 30% for reduction. The thermal design of a rotary kiln is thus obviously important.

To design a kiln one should calculate the length of each individual zone for drying, heating, and chemical reaction based on heat transfer and kinetic data. Unfortunately there are few detailed data available in the literature for the calculation of heat flow.

The heat transfer process is complex, particularly in a fired kiln in which radiation, convection and conduction all provide contributions to the transfer of heat from and to the gas, the wall and the solids. The modes of heat transfer in a fired kiln are shown in Figure 1-2. The gas, a heat source, provides heat to the solids, a heat sink, and the wall, a regenerator. The wall, after receiving heat from the gas, transmits it by direct radiation to the solids bed surface, and by conduction when it rotates to the underside of the bed. A portion of the heat the wall receives passes to the surroundings through its outer shell as a heat loss. In a direct fired kiln of large diameter the major amount of heat that reaches the solid bed is transferred by radiation from the hot gas. Radiation from the exposed wall to the charge usually ranks next in importance. Convection from the gas and conduction from the underside wall provides less than one quarter of the total heat received by the solid charge. However, in
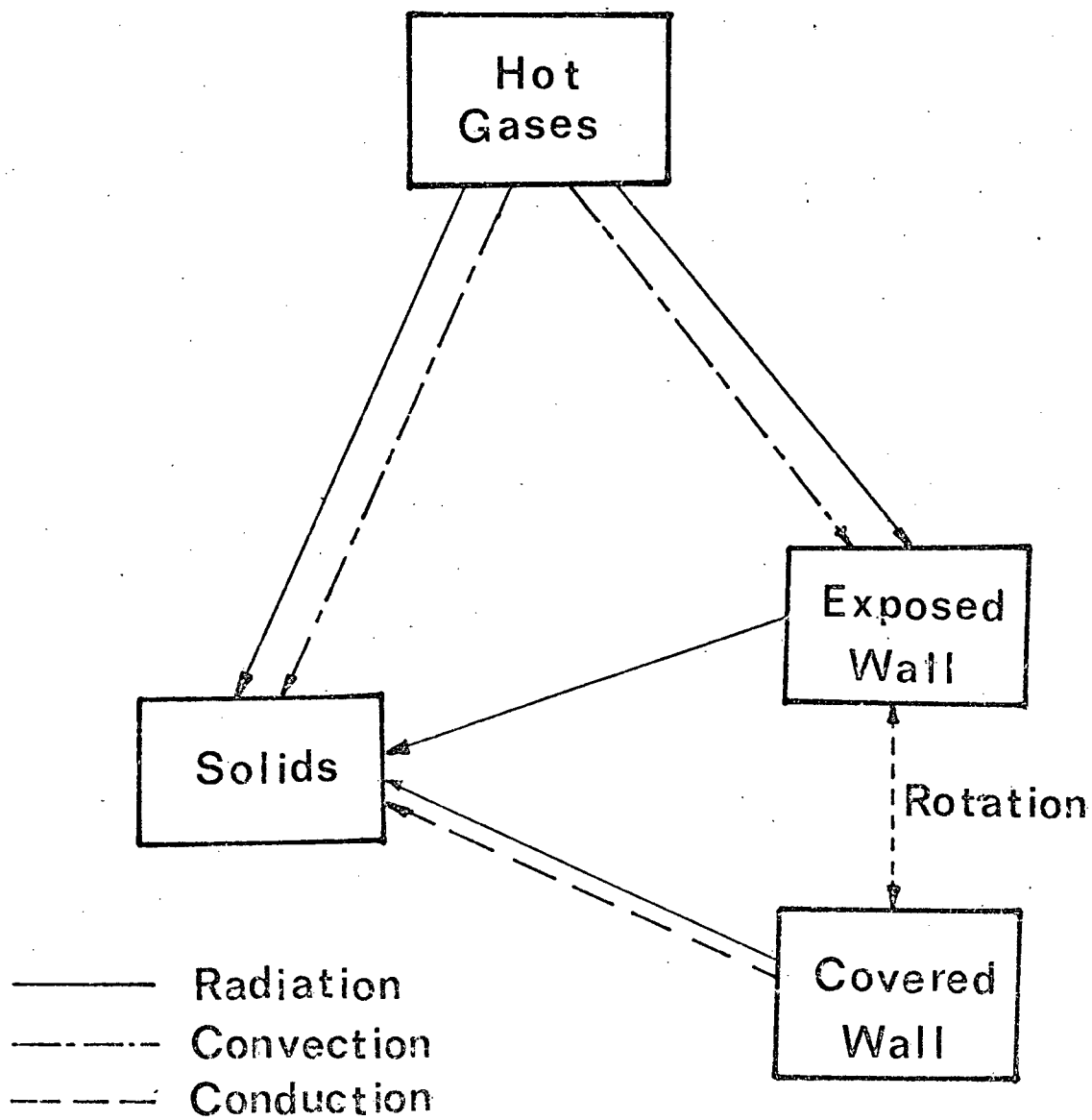
Figure 1-2 Heat Transfer Modes in Rotary Kiln.

kilns used for bicarbonate calcination (3) where the temperatures are around 450-470 K, and in the drying and parts of the heating sections of fired kilns, convection and conduction contributions are expected to outweigh that of radiation. Also, Brimacombe and Watkinson (4) have shown that in direct fired kilns of small diameter operating at solid temperatures up to 1100 K convection from the gas is the primary mode of heat transfer to the solids. However, there is no information available to determine under what conditions convection can be ignored in a fired kiln.

Recent investigators have attempted to simulate and model the performances of alumina kilns (5,6), cement kilns (7,8), iron ore reduction kilns (9,10), aggregate kilns (11) and simple heat exchanger kilns (12-17, 54). In these studies a number of differential equations were formulated to predict gas and solid temperature profiles along the kiln. The important parameters of the models included heat transfer coefficients for gas to solids, wall to solids, and gas to wall. Unfortunately there are no detailed data on heat transfer coefficients to incorporate into the models. The values of the coefficients were either calculated by using equations the reliability of which is to be verified, or values of the coefficients were assumed without further justification. The paucity of data for rotary kilns was also recognized by a working party report of the Institute of Chemical Engineers in 1971 (18). The report called for a comprehensive study of heat transfer processes over wide temperature ranges between solids bed, gas and wall in rotary kilns.

The purpose of the present work was to make an experimental investigation of convection heat transfer in the reaction-free system of a non-fired rotary kiln. The study was to cover the effects of a variety of operating parameters on heat transfer coefficients. These parameters included gas velocity and temperature, solid throughput, inclination angle, rotational speed, solid bed holdup, and particle size. The aim was to determine which of these factors were important in governing heat transfer from the gas to the solids in rotary kilns, and to report the results in a manner suitable for design purposes.

CHAPTER 2

LITERATURE REVIEW

To investigate the heat transfer mechanisms from the gas to the solids bed, it is essential to understand bed behavior and how it is affected by kiln operating parameters. During the movement of free flowing material in a rotating kiln, two velocity components appear: the radial motion of particles of the charge material due to the kiln's rotation and the axial motion of particles along the kiln mainly due to inclination. The latter type of particle motion determines the residence time of solid material in the kiln, whereas the former type of particle motion provides solid mixing.

2.1 Mechanism of Charge Movement

An excellent description of circumferential motion of the solid bed in a rotary drum was given by Rutgers (19). In a rotating cylinder a solid particle is taken up the wall to a particular height, depending on wall friction, specific gravity and shape. A mass of granules may be taken up higher on account of the interaction between the particles and the restricted relative movements of the individual grains within the mass. The center of gravity of the whole mass of the particles is displaced to a position eccentric to the axis of

the cylinder. The eccentricity decreases with increasing loading and it becomes somewhat greater with higher speeds of rotation.

For each drum radius there is a critical angular speed of rotation where centrifuging starts and a particle is taken along with the moving wall. This is given by

$$\omega_c = \sqrt{g/R} \quad \text{or} \quad N_c = 42.3/\sqrt{D} \qquad (2-1)$$

where R, D in meter. Below N_c, the critical rpm, several types of movement of decreasing intensity may be discerned. Figure 2-1 gives a cross-sectional picture of these types of radial motion. In cataracting, which takes place about 0.55 to 0.6 N_c depending somewhat on particle shape, some of the particles are showered through the upper section of the cylinder and fall downwards. At lower speeds of $0.1 < N/N_c < 0.6$ cascading occurs. Here the cross-sectional free surface has the typical lunar or kidney shape of Figure 2-1a. At speeds below 0.1 N_c, a relatively thin layer of particles rolls down the linear surface as shown in Figure 2-1b. If the speeds are considerably lower a slumping motion may occur where the particles no longer roll down the surface continuously.

The slumping phenomena, as depicted in Figure 2-2, was described by Zablotny (20) and Pearce (16). During rotary motion of the cylinder the surface of the charge gradually

(a)   (b)
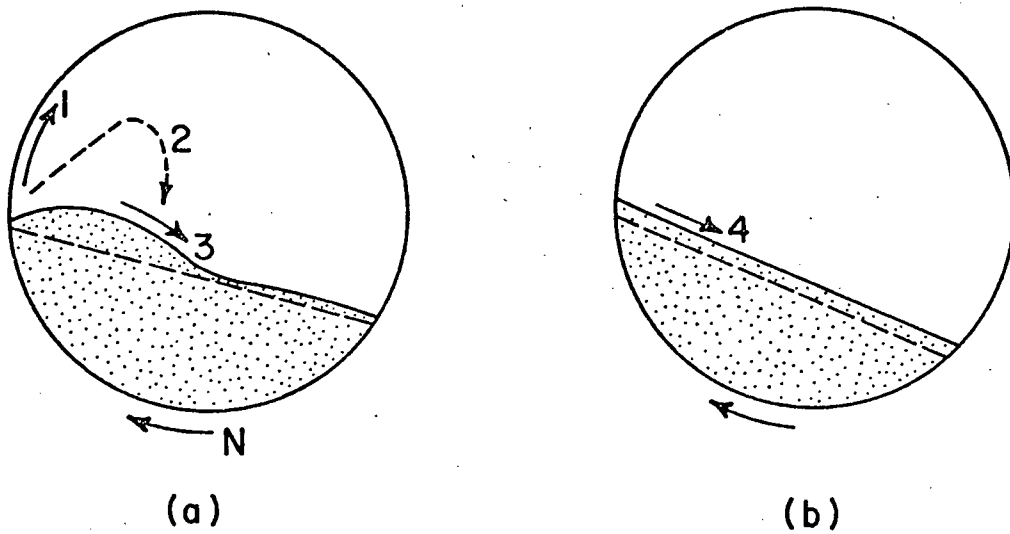
$$Nc \ (rpm) = \frac{42.3}{\sqrt{D}}$$ $D(m)$

I. CENTRIFUGING

    $N > Nc$

2. CATARACTING

    $Nc > N > 0.6 \ Nc$

3 CASCADING

    $0.6 \ Nc > N > 0.1 \ Nc$

4 ROLLING

    $0.1 \ Nc > N$

Figure 2-1 Types of Particle Movement in
Rotary Kiln (19).
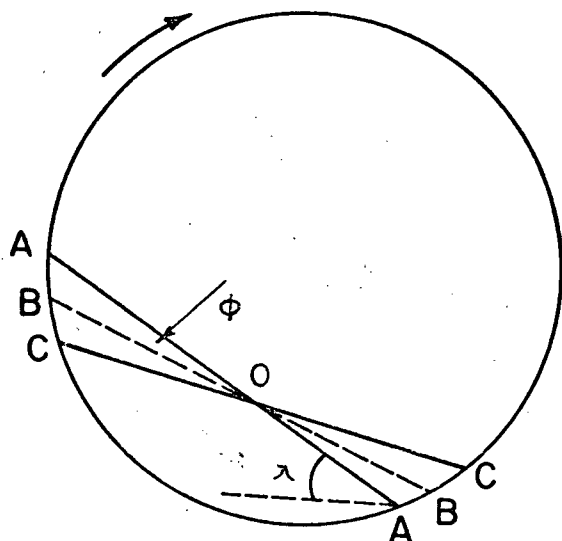
Figure 2-2   Mechanism of Slumping of Charge
in a Rotary Kiln (20).
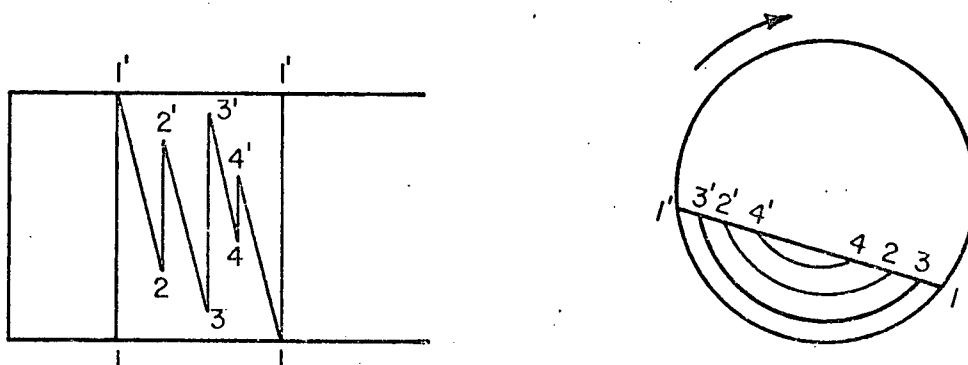
Figure 2-3   Path of a Particle in an Ideal
Rotary Kiln (20).

moves from position C-C into the position marked by the straight line A-A, forming the angle, λ, with the horizontal, which was defined as the angle of repose by Sullivan (21), or static angle of slide by Zablotny. In this thesis the term sliding will be restricted to motion related to slippage at the wall of the kiln and Zablotny's angle of slide will be called the angle of repose. At the moment when the surface of the charge attains position A-A the surface layer of the charge is detached in the upper part of the segment and then slumping of the material begins. The quantity of slumping material is shown schematically in Figure 2-2 by the A-O-B, which simultaneously forms the angle ϕ, called the shearing angle. After rapid slumping of that part of the material, the surface of the charge is in dynamic equilibrium, as it is situated under an angle defined as the dynamic angle of repose. A new surface B-O-B is then moved up to A-O-A, which results in a second slumping. The shearing angle must be determined experimentally. It depends on the physical properties of the charge material as well as the rotational speed. The shearing angle diminishes to zero as the rotational speed increases until a continuous rather than periodic slumping occurs. This action is referred to as rolling.

Henein, Brimacombe and Watkinson (22) reported experimental results on slumping and rolling beds in a 0.4 meter diameter rotary cylinder and kiln. They indicated that the transition between slumping to rolling not only depends on rotational speed, but also on the local holdup ratio of material

in the kiln, and on the size and shape of particles. They
have suggested that the mode of the bed behaviour may strongly
influence the transfer of heat in the kiln. The criteria for
transition from slumping to rolling have not yet been well
defined.

Industrial rotary kilns are rotated at speeds ranging
from 0.4 to 3 rpm depending on processes and sizes. The
diameters of typical industrial kilns are 1.8 to 5.9 m which,
in turn, have apparent critical speeds N_c of 32 to 17 rpm.
Most industrial kilns are thus operated at speeds of 0.1 >
N/N_c > 0.01, where the surface of the bed is expected to be
in rolling motion. For instance the 5.9 m diameter Stelco
kiln (2) operates at a rotational speed of 0.44 rpm or N/N_c =
0.0257.

Themelis, et al (23) stated that rotational speed was
the major factor of dynamic similarity for scale-up. In view
of the types of motion of particles in a kiln described above,
it would be appropriate to say the fraction of the critical
speed instead of the rotational speed may be a better factor
to use, so that similarity of bed motion be preserved in
scale-up. According to the latter criterion, to scale-up a
laboratory kiln of diameter 0.19 m with a rotational speed of
3 rpm to an industrial scale kiln of 3.0 m diameter, the
rotational speed has to be reduced to 0.75 rpm, according to

$$N = N' \sqrt{D'/D} \qquad (2-2)$$

This should maintain the same pattern of bed motion. Details of bed behaviour, solids motion, effect of particle size distribution and shape in kiln sections of various diameters are under study by Henein, Brimacombe and Watkinson (22).

Kilns used in industrial processes have inclination angles of about 1-4°, that is, considerably less than the dynamic angle of repose, which is about 30-40° for most solid materials. Thus the mass of material does not slide axially. During rotation of the kiln, individual particles of free-flowing material are reportedly (20) shifted along the axis of the kiln in flattened helical motion, the components of which are the path of a particle in the depth of the bed in the plane of rotation and a path on the surface of the charge as shown in Figure 2-3. A particle of material located in the bottom layer of the charge at point 1, during rotation, moves together with the charge along the path arc 1-1'. Then by the effect of the force of gravity, that particle rolls a short axial distance from point 1' along the slanting surface to point 2, from which it again travels together with the charge along the path 2-2', and emerges on the surface at point 2', etc. The progressive axial transport of the entire charge results, therefore, from the sum of the rolls of individual particles over the surface (i.e., 1-1' and 2-2') along the kiln. However, this picture is probably valid only for an ideally rolling bed.

2.2 Retention Time and Holdup

One of the most important factors in design of rotary kilns is the retention time or residence time of the charge for heating or chemical reaction. As early as 1927, Sullivan, Maier and Ralston (21) pioneered an extensive experimental study of the effects of operating parameters on retention time in rotary kilns. The experiments were conducted in 2.13 meter long kilns with varying diameters of 0.076, 0.152, 0.292 and 0.5 meters. The parameters covered inclination angle, rotational speed, angle of repose, solid feed rate, kiln diameter, temperature, and discharge constrictions. A wide range of materials was employed in their study, including Ottawa sand, coal, sawdust, and copper slag. They found that the retention time is proportional to the square root of the static repose angle of the solid, and inversely proportional to kiln diameter, rotational speed, and inclination angle of kiln. As expected the time of passage is independent of temperature at least up to 1170 K. At fixed rotational speed and inclination angle the retention time for a given material and kiln size is independent of the solid feed rate over a considerable range. Under these conditions increasing feed rate results in increasing hold-up of solids. The following empirical relationship was presented for a kiln with no discharge constrictions,

$$\bar{t} = \frac{1.77 \, L \, \sqrt{\Theta_0}}{\alpha_0 \, n \, D} \tag{2-3}$$

For a kiln with an end constriction, a lengthy coefficient was multiplied to the above equation.

Bayard (24) later proposed a formula based on his own data and that of Sullivan et al.,

$$\bar{t} = \frac{0.31 \ (24+\theta) \ L}{\alpha \ n \ D} \qquad (2-4)$$

This equation differs from equation 2-3 in the form of the dependence on the repose angle of the solid.

Analytical expressions for the relationship of retention time and other parameters were developed in 1951 by Saeman (25) for light loading kilns,

$$\bar{t} = \frac{L\sin\theta}{\pi \ D \ n \ (\alpha+\psi \ \cos\theta)} \qquad (2-5)$$

and by Pickering et al. (26)

$$\bar{t} = \frac{L\sin\theta'}{\pi \ D \ n \ \sin\alpha} \qquad (2-6)$$

where θ and θ' are static and dynamic angle of repose, respectively. ψ is angle between bed surface and kiln axis.

Varentsov and Yufa (27) applied dimensional analysis

to investigate role of various factors affecting the moving rate of solids in a rotary kiln. A series of experiments was conducted in kilns 6 m long with inside diameters of 0.3 and 0.55 m. Solid material used in these tests included marble chips, sand, coke and pyrite. Four particle size ranges were investigated: 0.35-0.56, 1.51-1.70, 3.81-4.40 and 7.07-7.28 mm. The following equation was proposed:

$$\bar{t} = m^* \; \frac{L}{\pi D n} \; Re^{0.01} \; Ga^{-0.33} \; (\frac{\theta}{\alpha})^{0.66} \; (\frac{4d_p^2}{\pi D^2 n})^{0.08} \; (\frac{d_p}{D})^{0.93} \qquad (2-7)$$

where m^* is a coefficient depending on the kiln diameter. The value of m^* was correlated by utilizing the data of Sullivan et al. for various diameters. For $D = 0.5$ m, the value of m^* is 1.7×10^{-3}; 0.75×10^{-3} for $D = 1.0$ m; 0.25×10^{-3} for $D = 2.0$ m. Gas velocity, in equation 2-7, has little effect on retention time ($\bar{t} \propto Re^{0.01}$), and particle size doesn't exercise a significant influence as seen in the equation since the sum of the powers of particle size, d_p, appearing in Ga ($-d_p^3$), $4d_p^2/\pi D^2 \eta$ and d_p/D, is 0.1. It was also concluded that gas temperature doesn't affect the solid throughput in the kiln. The holdup, η, although appearing in $4d_p^2/\pi D^2 \eta$, does not have a significant effect on retention time either.

Zablotny (20) also employed dimensional analysis and carried out experiments in a kiln of 3.55 m long and 0.352 m diameter. The following equation was presented,

$$\bar{t} = \frac{1.36 \; L}{\pi \; D \; n} \; (\frac{\theta}{\alpha})^{0.85} \qquad (2-8)$$

The retention time, obtained from the ratio of bed weight/discharge rate, gives the average time of solids residing in the kiln by assuming uniform bed depth and constant axial volumetric rate of solids along the kiln. These assumptions are not always valid in industrial kilns where the bed depths along the kiln are not uniform or the particles change in physical properties due to reaction or drying.

Vahl and Kingma (28) showed that differentials in bed height exist along a horizontal rotating cylinder and thus solids can be transported continuously through it. This contradicts the empirical equation of Sullivan et al., according to which the transport would be nil in horizontal rotary kilns. Vahl and Kingma derived a differential equation which related the solid throughput to the bed height τ with distance x from the feed for a horizontal cylinder. Based on this equation Kramers and Croockewit (29) introduced the inclination angle and gave the following equation for rotary kilns:

$$F = \frac{4}{3} \pi n R^3 \left(\frac{\tan\alpha}{\sin\theta} - \frac{d\tau}{dx} \cot\theta\right) \left(2 \frac{\tau}{R} - \frac{\tau^2}{R^2}\right)^{3/2} \qquad (2\text{-}9)$$

By approximation of

$$2 \left(\frac{\tau}{R} - \frac{\tau^2}{R^2}\right)^{3/2} \approx 1.24 \frac{\tau}{R} \qquad (2\text{-}10)$$

and introducing the dimensionless group, $N_\phi = \dfrac{F \sin\Theta}{nR^3 \tan\alpha}$ and
$N_k = \dfrac{R \cos\Theta}{L \tan\alpha}$, and the boundary condition, $\tau = \tau_L$ for $x = L$,
equation 2-9 becomes

$$\frac{\tau_L}{RN_\phi} - \frac{\tau}{RN_\phi} + 0.193 \quad \frac{\dfrac{\tau_L}{RN_\phi} - 0.193}{\dfrac{\tau}{RN_\phi} - 0.193} = \frac{L-x}{LN_k \, N_\phi} \tag{2-11}$$

This equation shows, in dimensionless form, the relationship
of bed height $\dfrac{\tau}{R}$ (or holdup η) and distance $\dfrac{x}{L}$, and other
operating parameters. When $\dfrac{\tau_L}{RN_\phi} = 0.193$, a constant height
is obtained over the whole length of the kiln. After re-
arrangement this equation can be rewritten as

$$F = 1.295 \, \tau_L \, n \, D^2 \, \tan\alpha / \sin\Theta \tag{2-12}$$

τ_L is the bed depth, which is related to holdup by the
expressions

$$\eta = \frac{1}{2\pi} (\beta - \sin\beta)$$

$$\text{and } \frac{\tau_L}{R} = 1 - \cos\frac{\beta}{2} \tag{2-13}$$

where β is the central angle of the sector occupied by the
solids in the cross-section of the kiln.

The retention time can be derived from the ratio of bed weight/solid throughput,

$$\bar{t} = \frac{\frac{\pi}{4} D^2 L\eta}{F} \qquad (2-14)$$

Substitution of equations 2-12 and 2-13 into equation 2-14 and approximation of $\tan \alpha \simeq \alpha$ yields

$$\bar{t}_\tau = 1.21 \frac{L\sin\Theta}{nD\alpha} \frac{\eta}{1-\cos\frac{\beta}{2}} \qquad (2-15)$$

The retention time for a uniform bed depth is thus not only a function of the group, $L\sin\Theta/nD\alpha$, but also depends on holdup η.

Saeman (25) obtained a similar analytical expression for an inclined kiln with various degrees of loading,

$$F = \frac{\pi}{6} nD^3 \sin^3 \frac{\beta}{2} (\psi\cos\Theta + \alpha) / \sin\Theta \qquad (2-16)$$

For uniform bed depth, $\psi \cos\Theta = 0$, and substitution of equation 2-13 into equation 2-11 gives

$$\bar{t}_\tau = 1.5 \frac{L\sin\Theta}{nD\alpha} \frac{\eta}{\sin^3 \frac{\beta}{2}} \qquad (2-17)$$

The retention time in this equation has a different
dependence of holdup term from equation 2-12.   (Note that β
is function of η).

From equation 2-9 one will note that there are four
operating parameters, which are interrelated in a rotary
kiln operated at uniform bed depth: solid throughput,
holdup, rotational speed and inclination angle. For example,
at constant holdup and inclination angle, rotational speed
can not be increased without solid throughput being increased.
Thus, three of the four operating variables in a uniform bed
depth kiln are independent.

2.3   Residence Time Distribution

The conversion of solids in a rotary kiln reactor
depends not only on chemical parameters and the mean residence
time of particles in the reactor but also, in general, on
the spread in residence times and the way the spread is
brought about. It is therefore important to know what
spread in residence time distribution is caused by the flow
pattern of the solids in the kiln. As indicated above, the
particles in a rotary kiln have velocity components in both
the longitudinal (axial) direction and the transverse (radial)
direction. Due to their more or less random behaviour, the
movements are often described mathematically by a type of
diffusion or mixing coefficient, in the axial and radial
directions. The axial velocity profile as well as the axial
mixing coefficient will contribute to a spread in residence

time. Conversely, the radial mixing coefficient will
diminish the effect of the axial velocity profile and
thereby reduce the spread in residence time. In a rotary
kiln the radial mixing coefficient causes a more or less
uniform distribution of element particles over the cross-
section of the kiln, which tends to make the radial gradient
of solid concentration in a reacting system zero.

A survey of the mixing of granular materials in
rotary cylinders has been given by Rutgers (19) together
with some experimental data on axial dispersion. A 0.16 x
0.50 meter rotary cylinder was equipped with varying dimen-
sions and shapes of the inlet and outlet sections, which
resulted in various holdups of the solids. His results
showed that axial dispersion coefficient is directly pro-
portional to the square root of rotational speed at constant
residence time in a horizontal cylinder, and approximately
inversely proportional to the square root of holdup at
constant rotational speed. The Peclet number in his work
is in the order of magnitude of two to three.

Tracer methods are usually used to study residence time
distribution. In rotary kiln tests tracer particles identical
to the feed except for color are readily prepared by use of
food dyes. If c_o, the initial concentration of tracer par-
ticles, represents the number of tracer particles injected
divided by the total weight of particles in the holdup volume,
and c (ζ, z) is the concentration at $z = \frac{x}{L}$ and $\zeta = \frac{t}{\bar{t}}$ $(\bar{t}$,
average residence time), then the axial dispersion model for

the tracer in dimensionless form is (30, 31, 32):

$$\frac{\partial C(\zeta,z)}{\partial \zeta} + \frac{\partial C(\zeta,z)}{\partial \zeta} = \frac{1}{Pe}\frac{\partial^2 C(\zeta,z)}{\partial z^2} \qquad (2\text{-}15)$$

where $\qquad C(\zeta,z) = c(\zeta,z)/c_o$

and $\qquad Pe = \bar{u}L/D \quad$ Peclet number

For an impulse input of tracers injected into the inlet of the rotary cylinder, which initially contained no tracer, Abouzeid et al. (30) presented the following set of initial and boundary conditions

$$C(o,z) = o \qquad\qquad\qquad (2\text{-}16a)$$

$$C(\zeta,o) - \frac{1}{Pe}\frac{\partial C(\zeta,o)}{\partial z} = \delta(\zeta) \qquad (2\text{-}16b)$$

$$\frac{\partial C(\zeta,1)}{\partial z} = o \qquad\qquad\qquad (2\text{-}16c)$$

where $\qquad \delta(\zeta) = 1 \quad \zeta = o$

$$= o \quad \zeta > o$$

Moriyama and Suga (32) replaced the second boundary condition,

equation 16c, with

$$C(\zeta,\infty) = \text{finite} \qquad\qquad (2\text{-}16\text{d})$$

and solved equation 2-15. This condition, they argued,
corresponds to the fact that the mixing region of the par-
ticles is limited to the surface region of the bed in the
kiln and that this region is almost unaffected by the dam
near the discharge end.

The solutions of equation 2-15 with initial and
boundary conditions (equations 2-16a, b or c) were lengthy
and given in the publication by Abouzeid et al. (30). The
Peclet numbers are usually derived from the variance σ_t^2 or
the relative variance σ_Θ^2 of the experimental residence time
distribution,

$$\sigma_\Theta^2 = \left(\frac{\sigma_t}{\bar{t}}\right)^2 \qquad\qquad (2\text{-}17)$$

instead of from the solution of equation 2-15. The relation-
ship of relative variance and Peclet number is obtained (19,
33) for a closed-closed system in the axial dispersion model:

$$\sigma_\Theta^2 = \frac{2}{Pe} - \frac{2}{Pe^2}\left[1-\exp(-Pe)\right] \qquad\qquad (2\text{-}18)$$

The values of Pe, in rotary kilns, are large enough that
the following approximation is valid.

$$Pe \simeq \frac{2}{\sigma_\theta^2}$$
(2-19)

Moriyama and Suga (32) applied dimensional analysis
to obtain the relationship of Pe and other operating variables.
Based on their data on a plastic horizontal cylinder (0.20 x
2.0 meter) and that of Matsui (34), the following equation
was presented,

$$Pe = 1.06 \times 10^4 \, (F/D^3n)^{0.516} \, (L/D)^{0.524} \, (d_p/D)^{5.55-0.604f}$$
(2-20)

where f is friction coefficient (= tanθ'). The Peclet numbers
in their studies are in the range of 250-5000. Axial dis-
persion coefficients were found to be directly proportional
to rotational speed.

The effects of operating parameters in addition to
rotational speed on residence time distribution were reported
by Abouzeid, et al. (30). The experiments were conducted in
a small scale cylinder of 0.08 x 0.24 m. It was found that
the axial dispersion coefficient increases with increasing
inclination angle, rotational speed and solid feed rate, but

is independent of particle size. Lu, et al. (35) applied a
multi-stage combined model to describe the mixing condition
of particles in a rotating cylinder with cross air flow.
The model consisted of a series of stages, each stage com-
prising a plug-flow reactor, a complete-mixing reactor with
back flow and a dead volume. Although the model was claimed
to fit their experimental data well, the resultant equation
is probably too complicated to be practical and requires too
many parameters to be specified.

A study of the effect of particle segregation on
particle motions was presented by Sugimota and co-workers
(36-38). The effect of cross air flow was shown by Lu, et
al. (35).

The transport of solids in rotary cylinder devices is
well represented by the axial dispersion model according to
several investigators, (30-32). Unfortunately there are no
detailed data to predict the values of D except the correla-
tion equation of Moriyama and Suga (equation 2-20). This
equation was established from the data obtained from
laboratory scale horizontal cylinders of L/D $\simeq$ 10.

The results of several investigations on the relation-
ship of axial dispersion coefficient and rotational speed are
compared in Figure 2-4. As shown in the figure there is
still no agreement on how the axial dispersion coefficient is
related to rotational speed, i.e. whether $D \propto N$ or $D \propto \sqrt{N}$ or other
types. As well, the dispersion coefficients differ by an
order of magnitude depending on the physical properties of the
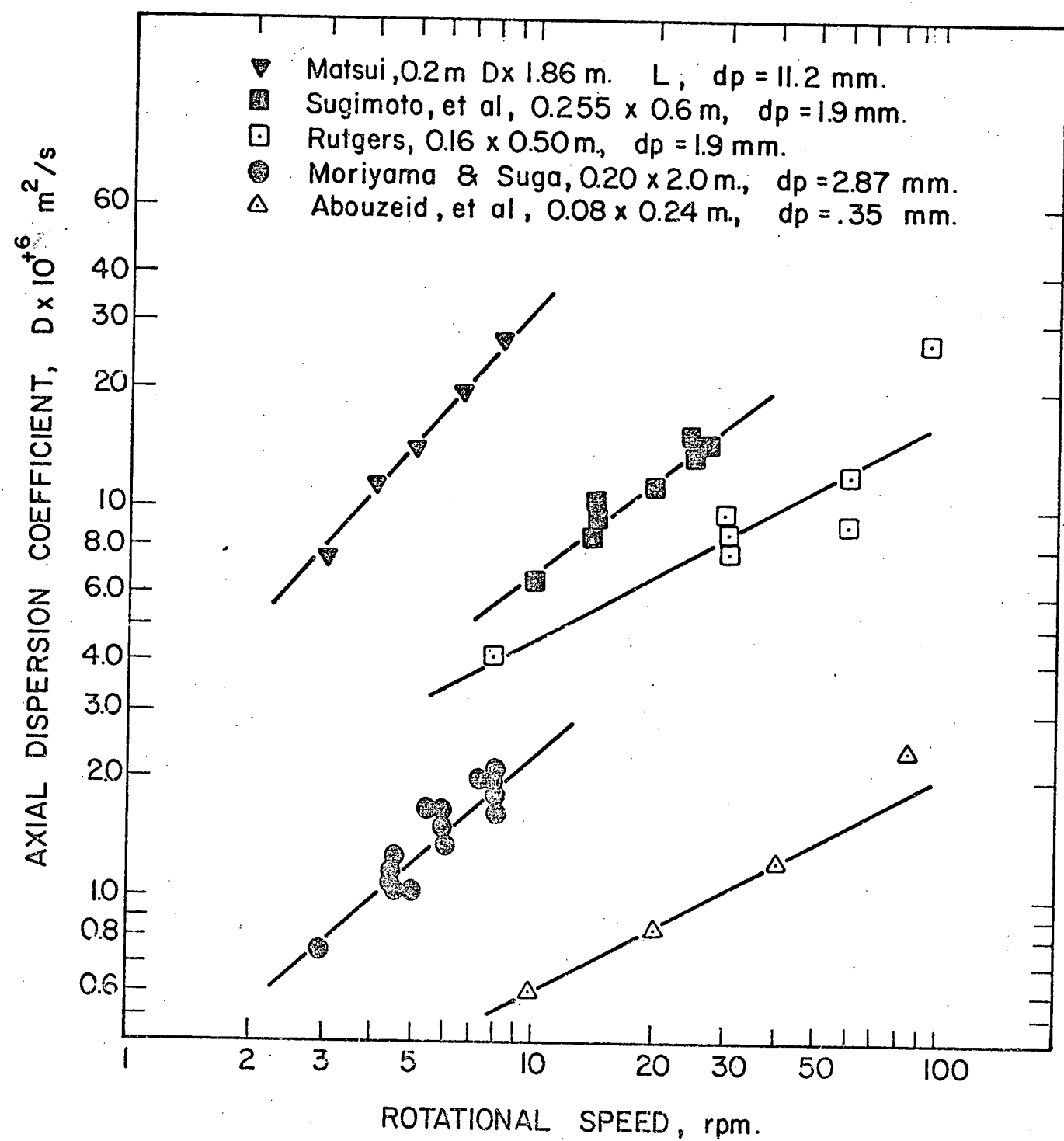
Figure 2-4   Relationship of Axial Dispersion
Coefficient and Rotational Speed.

particulate material (particle size, internal friction, shape), kiln dimensions, degree of fill, and solid through-put. There are very few data points in the rotational speed region typical of the rotary kiln. As indicated in equation 2-20 the ratio of L/D has a significant effect on Peclet number. In typical industrial kilns (39) the ratio of L/D ranges from 14 for petroleum coke kilns to 30 for long lime kilns. However the experimental kilns used for the RTD experiments have a smaller L/D ratio, about 3 for cylinders of Rutgers, Abouzeid et al. and Sigumoto et al., and about 10 for Matsui and Moriyama and Suga. These investigators did not study the influence of L/D.

Wes et al. (31) used an industrial scale drum, 0.6 m I.D. x 9.0 m long to study the RTD. In their experiments the samples were taken at 3.65 m from the entrance and at the end of the rotating drum, which may represent two different L/D ratios. The results of their experiments are given in Table 2-1. Pe increases from 55 to 204 at N=6 rpm, and from 46.9 to 145 at N=2 rpm, when L/D increases from 6.09 to 15. This suggests that the Peclet number in industrial kilns may be even higher. This high Peclet number then characterizes the solid flow in a rotary kiln as essentially plug flow (33).

2.4 Surface Time

The surface time is the time the individual particle spends on the aerated surface layer before it returns to the bed. After residing in the bed and moving along with the wall,

TABLE 2-1

Effect of Kiln Length on D and Pe (Wes, et al.)

L (m)	L/D (−)	N (rpm)	η (%)	$\bar{t}$ (s)	D (m^2/s)	Pe (−)
3.65*	6.08	6	20.1	2.33×10^3	10.4×10^{-5}	55.1
		6	20.0	2.26	12.3	47.9
		2	35.4	3.97	7.15	46.9
9	15	6	19.8	5.63	7.05	204
		6	19.8	5.65	7.59	189
		2	31.4	8.94	6.24	145

*The midway distance where samples were taken.

it returns to the surface layer. The time this particle resides in the bed is referred as bed time. The sum of surface time and bed time is called the cycle time. Cycle time, surface time and bed time are functions of rotational speed, holdup, kiln diameter, particle physical properties and radial position in the kiln. Since the particle travels along the kiln in a helical motion, cycle time, surface time and bed time are defined as averages taken over a certain length of the kiln.

Surface time is expected to be important in heat transfer processes where particles in the surface layers are exposed to hot gases. Heat transferred from the gas phase to the surface layer of the solids is distributed to the bulk material by solid mixing taking place in the circulatory bed. In a direct fired kiln it has been estimated (18) that surface temperature will rise by 80 K in 0.1 seconds, and by 270 K in one second, in which latter period the surface is renewed. At a depth of 1 mm below the surface layer the heat supply may account to only one percent of that radiated to the surface. Surface time is also believed to play an important role in the convective heat transfer process. The experimental results of Wes et al. (31) showed that some sort of penetration mechanism might exist for convection from the gas to the downflowing particles. Thus, according to penetration theory, a short surface time gives a higher average heat transfer coefficient. In addition a short time yields more particles flowing down the surface that certainly

increases the heat flux.

Although heat transmission by radiation and convection to the aerated surface layer is important, there is very little information in the literature about surface time except from the work of Hogg, Shoji and Austin (40). They reported that in their rotary cylinder, 0.095 m in diameter and 0.248 m long the fraction of surface time to cycle time is 0.49 at a rotating speed of 90 rpm or N/N_c = 0.64. In a rotary kiln where rotating speeds are operated below 6 rpm, the fraction of surface time to cycle time is far below 0.49.

There is also lack of information in the literature about the thickness of the surface layer. It is believed that the thickness depends on rotational speed, internal particle friction, inclination angle, holdup, etc. In rotary soda calciners (3) the thickness of the layer was stated theoretically equal to the diameter of the particles at 4 rpm where the rolling pattern starts. No sizes of the calciners and the particles were given.

In the present work some experiments are carried out to study the influence of operating variables on surface time, and a film study on the thickness of the surface layer is reported.

2.5 Heat Transfer

Bowers and Reed (41) correlated heat transfer data from four industrial kilns: limestone calcination, dry cement burning, dolomite calcination and shale expansion. From the

former two kilns they concluded that the overall gas-bed
heat transfer coefficient has the following relationship
with kiln diameter,

$$U_O = 18.6 \ D \qquad\qquad (2-21)$$

where U_O : overall gas-solid heat transfer
coefficient $(W/m^3 K)$

D : kiln diameter (m)

Equation 2-21 is obviously unsatisfactory for design purposes
and can only show the order of magnitude of heat transfer
coefficients, because the correlation was based on a limited
number (6) of scattered data. It also excludes the effects
of rotational speed, solid and gas throughput, inclination
angle, particle size and does not reflect the complexity of
the actual process that occurs in the kiln.

2.5a Conduction

    Heat transmission by conduction occurs at the under-
side of the bed which is in contact with the rotating wall.
At the moment when the particles return from the surface
layer to the bed, in which they become at rest relative to
the wall and to their neighbours, the particles adjacent to
the wall receive heat from the wall (Point A in Figure 2-5),
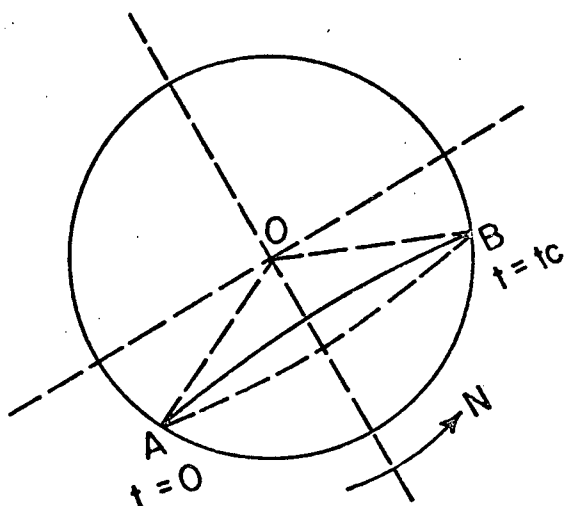
Figure 2-5   Bed-Wall Heat Transfer by
              Conduction.
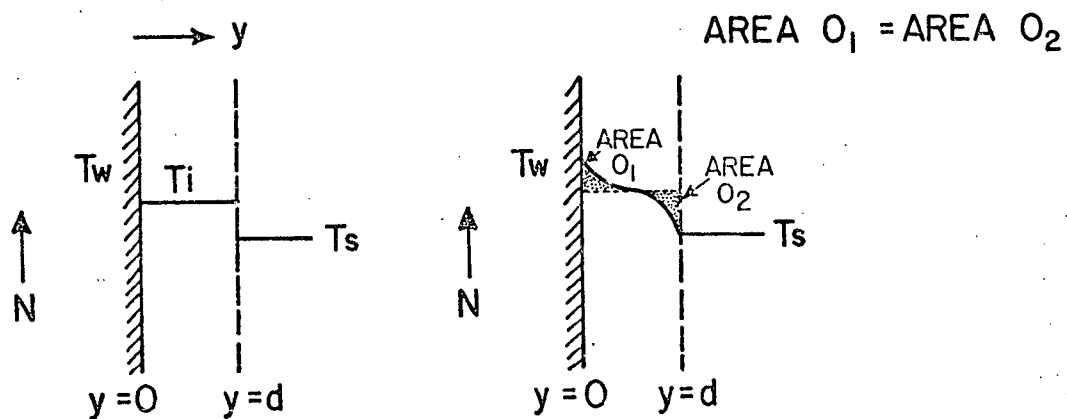
Figure 2-6   Penetration Model for Bed-to-Wall
              Heat Transfer Proposed by Wachters
              and Kramers (3).

until they move up to the point (B in Figure 2-5) and roll
on the surface again. Therefore, Wachters and Kramers (3),
Wes et al. (42), Lehmberg et al. (43) and Nikitenko (44)
proposed an unsteady state penetration model for heat con-
duction. The following assumptions were made:

a) The temperature of the bulk material far from the
   wall is constant during the contact time tc.

b) The region at the wall in which heat conduction
   takes place is thin compared with the radius of
   the cylinder, so that the curvature may be neglected.

c) Tangential heat conduction can be neglected.

d) At t $\simeq$ o the contents of the wall layer are mixed
   with the bulk material.

A heat balance for a circumferential element consisting
of particles adjacent to the wall yields

$$\frac{\partial T}{\partial t} = a \frac{\partial^2 T}{\partial y^2} \qquad (2-22)$$

where a is the heat diffusivity of particles, m^2/s. The
initial and boundary conditions used by Wes et al. were

$$T(o,y) = T_s$$
$$T(t,o) = T_w \qquad (2-23)$$
$$T(t,\infty) = T_s$$

Experimental measurements were made by Wes et al. in an industrial scale drum of 0.6 x 9.0 m. Potato starch and yellow dextrine solids with particle sizes of 15~100 µm, were used in the heating process to determine heat transfer coefficients, h_{ws} from the wall to the solids. The experimental results were claimed to be in agreement with the following equation, which is derived from the simple penetration model with equation 2-23.

$$h_{ws} = \frac{2 \ k_s}{\sqrt{\pi a t_c}} \quad \text{or} \quad 2 \ k_s \ \sqrt{\frac{n}{a\beta}} \qquad (2-24)$$

Nikitenko (44) used the following set of initial and boundary conditions.

$$T \ (0,y) = T_s$$
$$T \ (t,0) = T_w \qquad (2-25)$$
$$\frac{dT \ (t,\infty)}{dy} = T \ (0,y)$$

and obtained the following relationship.

$$h_{sw} = 0.15 \ \rho_s \ \sqrt{\frac{n}{\beta}} - 8 \qquad (2-26)$$

No explanation was made of the use of the last boundary condition, and no experimental results were displayed in his paper.

In a study by Wachters and Kramers (3), experiments were conducted in a 0.152 x 0.475 m copper cylinder and values of h_{ws} were reported to be 1/3 to 1/2 of those predicted from equation 2-24. They assumed that whereas the bulk of the granular bed has a uniform temperature there is a thin layer at the wall always consisting of the same particles and that when these roll back, they only mix among themselves. Based on these assumptions, the wall layer d' in thickness, was proposed that was initially at a temperature T_i for o<y<d' as given in Figure 2-6. The average temperature of the layer was assumed to not change during the time of contact, etc. Thus the following boundary conditions were used,

$$T (o, o<y<d) = T_i$$

$$T (o, y>d) = T_s \qquad\qquad (2-27)$$

$$T (t,o) = T_w$$

$$T (t,\infty) = T_s$$

Their experimental results indicated that at higher speed (or lower t_c) where $d' > 4\sqrt{at_c}$, the wall layer reduces the

heat transfer coefficients by a factor of 3 with respect to that obtained from a simple penetration model,

$$h_{ws} = \frac{2 \; k_s}{3 \; \sqrt{\pi a t_c}} \qquad 10 \; \text{rpm} \leq N \leq 40 \qquad (2\text{-}28)$$

At relatively low speed (high contact time, t_c), h_{ws} gradually changed according to

$$h_{ws} = \left[\frac{\sqrt{\pi a t_c}}{2 \; k_s} + \frac{\sqrt{\pi}}{2 \; k_s} \; d' \right]^{-1} \qquad N \leq 10 \qquad (2\text{-}29)$$

The wall layer thickness, d', was obtained by extrapolating the experimental data from the above equation,

$$d' = 1.12 \times 10^{-3} \; \sqrt{\beta} \qquad (2\text{-}30)$$

The values of d' were 1.8 mm and 1.5 mm with $\beta=2.53$ and 1.83 radians, respectively in their experiments. However the dependence of d' in equation 2-30 on β, the central angle

of the solids bed, can not be physically explained.

Recently Lehmberg et al. (43) introduced the concept of the presence of a gas film between the wall and the solids into the penetration model. The presence of a gas film was also recognized by Epstein and Mathur (45) for wall to bed heat transfer in the annulus of a spouted bed. In order to fit their own experimental data Lehmberg et al. proposed two heat transfer regions near the wall. The simple penetration model as given in equation 2-24 was applied in the region between the wall and δ_u, the thickness at the contact point between wall and particle. The basis of the model is illustrated in Figure 2-7. In the second region, bounded by δ_u and the particle radius, the gas film was added to the model. In addition to the first parameter δ_u, they introduced a second parameter h', (termed the relative heat transfer coefficient), which is the ratio of the gas film heat transfer coefficient h_g' to the effective thermal conductivity of solids, k_s. The overall wall-bed heat transfer coefficients across these two regions was given in lengthy form as follows:

$$h_{ws} = \frac{\sqrt{\rho_p C_{pp} k_s}}{\sqrt{t_c}} \left[\frac{2}{\sqrt{\pi}} - \frac{1}{h'\sqrt{at_c}} + \frac{1}{h'\sqrt{at'}} \exp(h'^2 at_c) \, \text{erfc}(h'^2 at_c) \right]$$

$$\text{where } h' = \frac{h_g'}{k_s} \tag{2-31}$$

$$= 4 \frac{k_g}{k_s} \cdot \frac{1}{d_p} \left(\ln \frac{d_p}{2\delta_u} - 1 + \frac{2\delta_u}{d_p} \right)$$
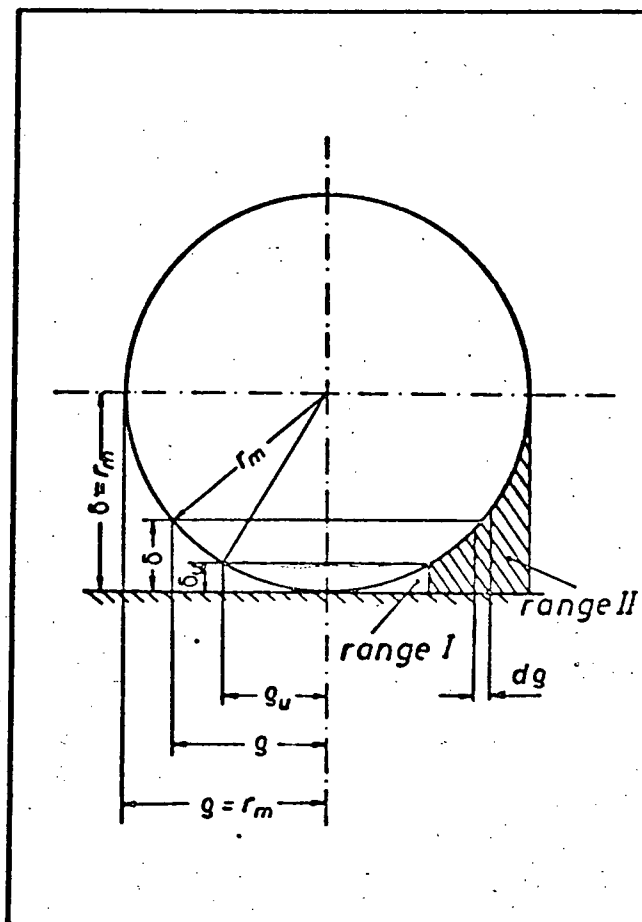
Figure 2-7 Two-region Penetration Model for
Wall-Bed Heat Transfer Proposed by
Lehmberg et al. (43)

By adjusting the values of h' and δ_u equation 2-31
was reported in good agreement with their own experimental
data. δ_u was found equal to 9μm, compared to the particle
sizes of 157, 323, 794 and 1038 μm. The mean thickness of
the gas film (^{1}/h') increases with increasing particle
sizes. The parameters, h' and δ_u were determined
experimentally, therefore equation 2-31 for wall to bed
heat transfer coefficient is not readily used for design
purpose. For long contact time, δ_u was also reported to
be a function of time. In addition equation 2-31 can not
fit the data of Wes et al. unless h' → ∞ (or ^{1}/h'→ 0).

Since no model yet proposed could satisfactorily
represent all the published experimental data, an attempt
was made in this work to correlate all the available data
within the frame of the penetration model. This correlation
is discussed in Chapter 6.

2.5b Convection

The following empirical relationship

$$h_{gw} = 0.0981 \ G_g^{0.67} \qquad\qquad (2-32)$$

where G_g = gas mass flux kg/hr m^2 (cross section kiln)
is recommended by Porter et al. (46) for the convective heat
transfer coefficient from gas to wall in a rotary kiln, and
is also used to predict the gas to bed coefficient. In an

earlier publication (47) the same authors used an equation with a smaller exponent on gas mass flux, and which included the effect of kiln diameter:

$$h_{gw} = 0.0608 \ G_g^{0.46}/D \qquad (2-33)$$

A third expression used for convective heat transfer coefficient in kilns is a modified Nusselt type equation for heat transfer in tubes,

$$h_{gw} = 5.2 \times 10^{-2} \ (\frac{k_g}{D}) \ (\frac{Du_g P_g}{\mu_g} \ . \ \frac{\mu_g C_{pg}}{k_g})^{0.786} \qquad (2-34)$$

Gygi (48) used this expression to calculate convective heat transfer coefficient for cement kiln in the preheating zone.

However, no expression has been reported to evaluate heat transfer coefficient from the gas to the solid bed. Several investigators (5, 12) have used equation 2-32 for gas to wall convection to calculate heat flow from gas to charge. The area is taken to be the chord length times the kiln length. This convective coefficient is apparently independent of the speed of rotation, particle size, and inclination of the kiln. The equations $h_{gs} = h_{gw} = 0.023 \ \frac{k_g}{D} \ R_e^{0.8} \ P_r^{0.4}$ were also used for modelling iron ore reduction (9) and $h_{gs} = h_{gw} = c(k_g D)^{0.2}$

$(U_g/C_{pg})^{0.8}$ for an alumina kiln (6). In other modelling studies specific values were used with no reported justification including h_{gs} = 22.8 W/m^{2}K, h_{gw} = 28.4 W/m^{2}K for wet process cement kilns (7,8); h_{gs} = h_{gw} = 14.0 W/m^{2}K for a light weight aggregate kiln (11); and h_{gs} = 1.5 W/m^{2}K for a rotary kiln heat exchanger (15).

Wes et al. (42) published experimental values of 5.1 and 4.9 W/m^{2}K for wall to air heat transfer coefficient in an empty drum equipped with flights, with 550 and 336 kg/hr m^2 air mass flux, respectively. They also reported local convective heat transfer coefficients from potato starch and yellow dextrine to cool air in a horizontal rotating drum. The results are given in Figure 2-8. Wes et al. claimed there might exist a kind of penetration mechanism for the heat transfer to the down flowing solids on the surface because of a linear relationship of h_{sg} $\propto$ $\sqrt{N}$ between 3 rpm to 6.5 rpm. One can conclude from the work of Wes et al. that the gas to solids convection coefficient is roughly 12 to 25 times the magnitude of the gas to wall convection coefficient in a rotary kiln with low flights. Friedman and Marshall (49) gave h_{gs} of 26.5 W/m^{2}K at G_g = 782 kg/hr m^2 air mass rate, and of 20.4 and 38.2 W/m^{2}K at G_g = 15.60 kg/hr m^2.

Brimacombe and Watkinson (4) recently reported experimental data of 120 to 240 W/m^{2}K for gas to solids convection coefficients. The experiments were conducted in a pilot scale fired rotary kiln, which has 0.406 m I.D. and

Figure 2-8   Convective Heat Transfer Coefficient from
Bed to Air, Data of Wes, et al (42)

5.5 m long.   The gas flow rates ranged 545 to 820 kg/hr m^2

with average temperature, 675 to 830 K, and the solid

throughput were 70 to 135 kg/hr.   Their data show that heat

transfer coefficient increases with increasing gas tempera-

ture and gas flow rate, and the effect of solid throughput

is insignificant.

Chen et al. (50) studied the effect of air cross

flow on the gas to particle heat transfer in a rotary dryer.

The dryer was constructed with two concentric cylinders.

The inside cylinder was o.15 m in diameter and made of per-

forated plate with 1.5 mm holes, 10 mm square pitch, covered

by a screen of 150 mesh.   Hot air was allowed to flow through

the annualar space into the inside cylinder.   The heat

transfer coefficients between gas and particles were found

to be in the same range of the data in the fixed bed.

2.5c   Radiation

The Stefan-Boltzmann equation has been widely used

for the thermal analysis of a rotary kiln, due to the lack

of reported data.   The radiative heat transfer coefficient

is strongly dependent on the form, $(T_i{}^4 - T_j{}^4)/(T_i - T_j)$.

Table 2-2 lists equations used for radiant heat transfer by

several investigators who were modelling rotary kilns.   A

similar table was drawn up by Venkateswaren (54).   The

temperature dependence of Lyon et al. was simplified to

$2(T_i{}^3 + T_j{}^3)$.   These sets of equations have different values

of factors which are dependent on emissivities of gas, solid

and wall. Kaiser and Lane (51) have recommended in Saas' equations that the term $f\varepsilon_s$ in $h_{ws,r}$ should be replaced by the expression of Eckert and Drake (52) given in Table 2-2 which takes into account re-radiation from solids. T_s, the solid bed temperature, was used in the equations shown in Table 2-2, instead of the bed surface temperature. The latter may be larger than T_s by a few hundred degrees as indicated by Luethge (53). Since radiation takes place to the aerated charge surface, the calculated value of h_r based on the equations in Table 2-1 would appear to overestimate the radiation contribution.

TABLE 2-2   Radiant Heat Transfer Coefficient

Investigators	$h_{gw,r}$	$h_{gs,r}$	$h_{ws,r}$
Saas (12)	$\rho\varepsilon_g(T_g^4-T_w^4)/(T_g-T_w)$	$\rho\varepsilon_g(T_g^4-T_s^4)/(T_g-T_s)$	$\rho\varepsilon_{sf*}(T_w^4-T_s^4)/(T_w-T_s)$
Lyons et al. (7)	$2\rho\varepsilon_g\varepsilon_w(T_s^3+T_w^3)$	$2\rho\varepsilon_g\varepsilon_s(T_g^3+T_s^3)$	$2\rho\dfrac{A_w}{A_s}\varepsilon_s\varepsilon_w(T_w^3+T_s^3)$
Toyama et al. (11)	$\dfrac{\rho}{M**}\varepsilon_w\varepsilon_s\left[1+(1-\varepsilon_g)(1-\varepsilon_g)\dfrac{A_s}{A_w}\right]\dfrac{T_g^4-T_w^4}{T_g-T_w}$	$\dfrac{\rho}{M}\varepsilon_s\varepsilon_g\left[1+(1-\varepsilon_w)(1-\varepsilon_g)\dfrac{A_s}{A_w}\right]\dfrac{T_g^4-T_s^4}{T_g-T_s}$	$\dfrac{\rho}{M}\varepsilon_s\varepsilon_w(1-\varepsilon_g)\dfrac{A_s}{A_w}\dfrac{T_w^4-T_s^4}{T_w-T_s}$
Manitius et al. (6)	$4.96\times10^{-8}\varepsilon_w\left[\hat{\varepsilon}_g T_g^4-\varepsilon_g(T_w)T_w^4\right]$	$4.96\times10^{-8}\varepsilon_s\left[\hat{\varepsilon}_g T_g^4-\varepsilon_g(T_s)T_s^4\right]$	$4.96\times10^{-8}\varepsilon_s\varepsilon_w\left[(1-\varepsilon_g)T_w^4-(1-\varepsilon_g)T_s^4\right]$
Riffaud et al. (5)	$\rho\varepsilon_g(T_g^4-T_w^4)/(T_g-T_w)$	$\rho\varepsilon_g(T_g^4-T_s^4)/(T_s-T_s)$	$\rho\varepsilon_1^*(T_w^4-T_s^4)/(T_w-T_s)$
Wingfield et al. (9)	$\rho\varepsilon_g(T_s^4-T_w^4)/(T_g-T_w)$	$\rho\varepsilon_g(T_g^4-T_s^4)/(T_g-T_s)$	$\rho\varepsilon_s(T_w^4-T_s^4)/(T_w-T_s)$

* ε_{sf} is recommended (47) by substitution of $\left[\dfrac{1}{\varepsilon_s}+\dfrac{A_s}{D}\left(\dfrac{1}{\varepsilon_w}-1\right)\right]^{-1}$

** $M=1-(1-\varepsilon_w)(1-\varepsilon_g)'\left[1-(\varepsilon_s+\varepsilon_g-\varepsilon_s\varepsilon_g)\dfrac{A_s}{A_w}\right]$

* ε_1 function of ε_s and ε_w

CHAPTER 3

SCOPE OF PRESENT WORK

As has been shown above few experimental data on heat
transfer coefficients have been published for convection in
rotary kilns. No systematic study of the effects of
operating parameters on convective heat transfer could be
found in the literature. Some equations (46,47,48) have
been proposed for the convection process, but none have had
experimental verification, and included effects of
operating parameters other than gas velocity.

It was the objective of the present work, therefore,
to make an experimental study of the influence of kiln
operating parameters on convective heat transfer coefficients
in a non-fired rotary kiln. Conditions were chosen to mini-
mize radiative effects. The parameters to be studied
included kiln rotational speed, inclination angle, gas velocity,
solid charge feed rate, degree of fill, particle size and tem-
perature.

In order to understand the heat transfer process,
knowledge of the particle motion in the kiln is required.
The secondary objective, therefore, was to study the relation-
ship of solid charge feed rate, charge load, kiln rotational
speed and inclination angle, especially under conditions of

uniform bed depth along the kiln. It was also intended to
investigate the factors influencing the time particles
spend on the surface of the bed. A brief study of residence
time distribution in the kiln was also included in this work.

With this experimental information, a model of the
convection process in a rotary kiln was to be formulated
and design equations presented.

CHAPTER 4

APPARATUS AND MATERIALS

4.1 Apparatus

A schematic diagram of the experimental system used
for heat transfer and particle motion experiments is shown
in Figure 4-1. It consists of five primary components:
the rotary kiln, the solid feeding system, the receiving
system, the air heating system and the instrumentation and
recording system. Two kilns of the same size were used.
A lucite cylinder was primarily used in the investigation
of particle motion in the kiln, and a steel cylinder was used
for the heat transfer experiments.

4.1a Kilns

The transparent lucite rotary cylinder was 2.44 m in
length, 0.1905 m I.D. and 6.35 mm in wall thickness, and
provided with end flanges of 0.254 m diameter. The solids
inlet flange had an opening of 0.076 m diameter, whereas
three different flanges with openings of 0.133, 0.114 and
0.089 meters were used at the solids outlet end to maintain
the desired bed depths. During the initial experiments slip
was found between the smooth kiln wall and the solids bed.
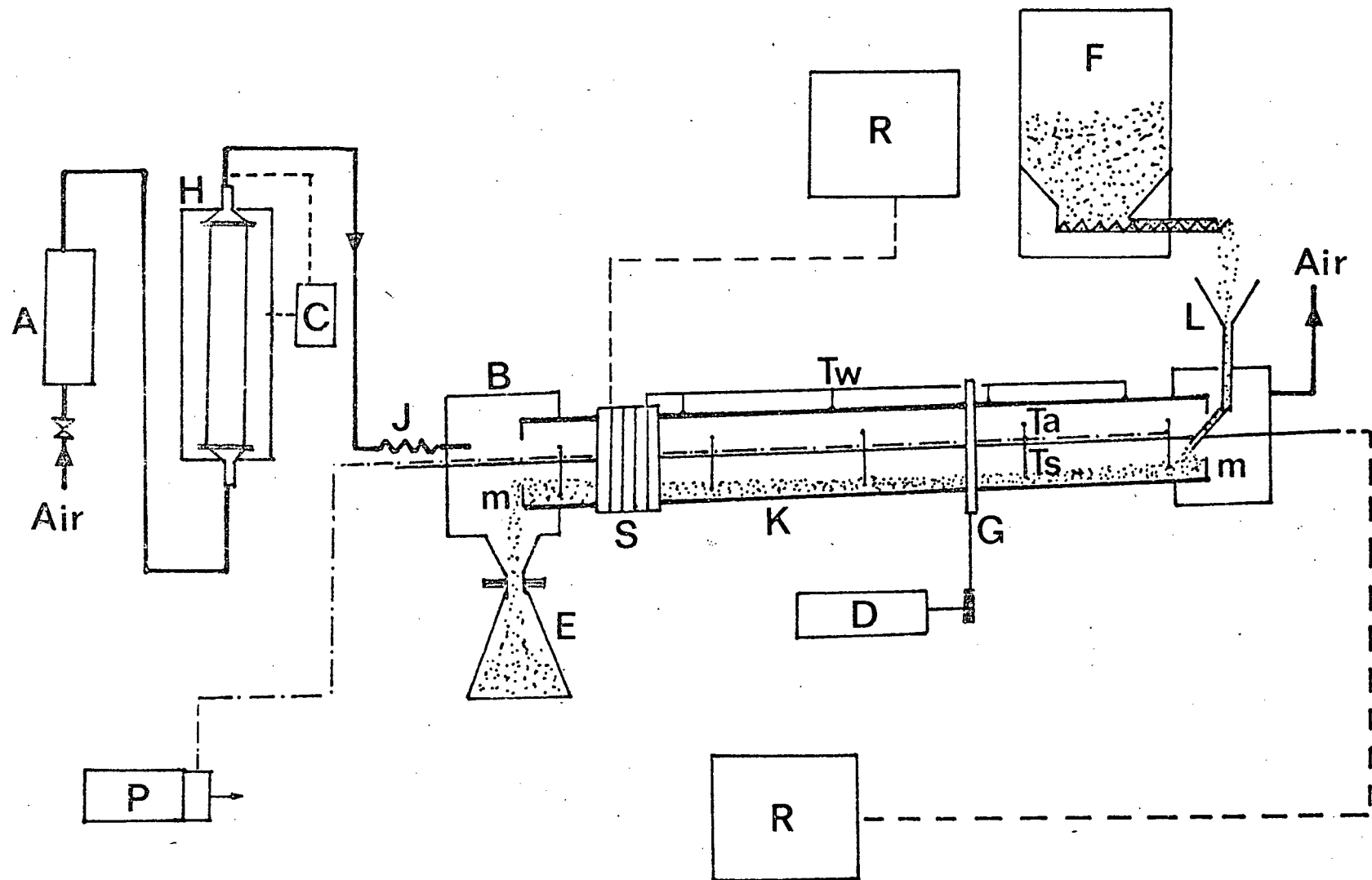
Figure 4-1   Schematic Diagram of Apparatus.

TABLE 4-1

Key to Figure 4-1

A	Rotameter
B	End box
C	Temperature controller
D	Variable speed drive
E	Solid receiving cone
F	Screw feeder
G	Chain and sprocket
H	Electric furnace
K	Rotary kiln
L	Funnel and chute
M	Dam
P	Suction pump
R	Temperature recorder
S	Slip ring
Ta	Air temperature probe
Ts	Solids bed temperature probe
Tw	Wall temperature probe
————	2.54 cm steel pipe
— · — · —	Suction line
— — —	Potential transmitting line

Eight equally spaced strips were then glued along the interior surface of the cylinder, parallel to its longitudinal axis. The strips were 4.80 mm wide and 3.2 mm high. The cylinder sat on six metal 0.067 m x 0.10 m long rollers, equipped with rubber O-rings. The cylinder was rotated on the rollers by a friction belt driven by a ¼ horsepower variable speed motor. The kiln with the accessories was supported by a steel frame which could be adjusted to a desired inclination angle to the horizontal.

The kiln used for the heat transfer experiments was constructed of seamless, cold drawn mild steel pipe. It was the same size as the lucite cylinder, 0.1905 m I.D. x 2.44 m long x 6.35 mm wall thickness. The L/D ratio was thus 12.8. The interior surface of the tube was coated with 1 mm thick layer of refractory cement, and was roughened to prevent the solids bed from slipping during rotation. The outside wall was insulated with two layers of 3.2 mm thick ceramic paper, then covered with 0.208 m diameter, 0.076 m thick fiberglass pipe insulation. The opening of the steel inlet end plate was 0.076 m diameter. Three outlet plates with openings of 0.133, 0.114 and 0.089 m diameter allowed holdups of 6.5%, 11% and 17%, respectively. Both ends of the rotating kiln were sealed with carbon rings in 0.254 m diameter x 0.254 m long end boxes. The construction of the end boxes and carbon rings is shown in Figure 4-2. The kiln was rotated on four metal rollers by a sprocket and chain driven by a ½ horsepower variable speed motor. The support for the

CARBON RING

$\phi = 0.19$ m

ROTATING KILN
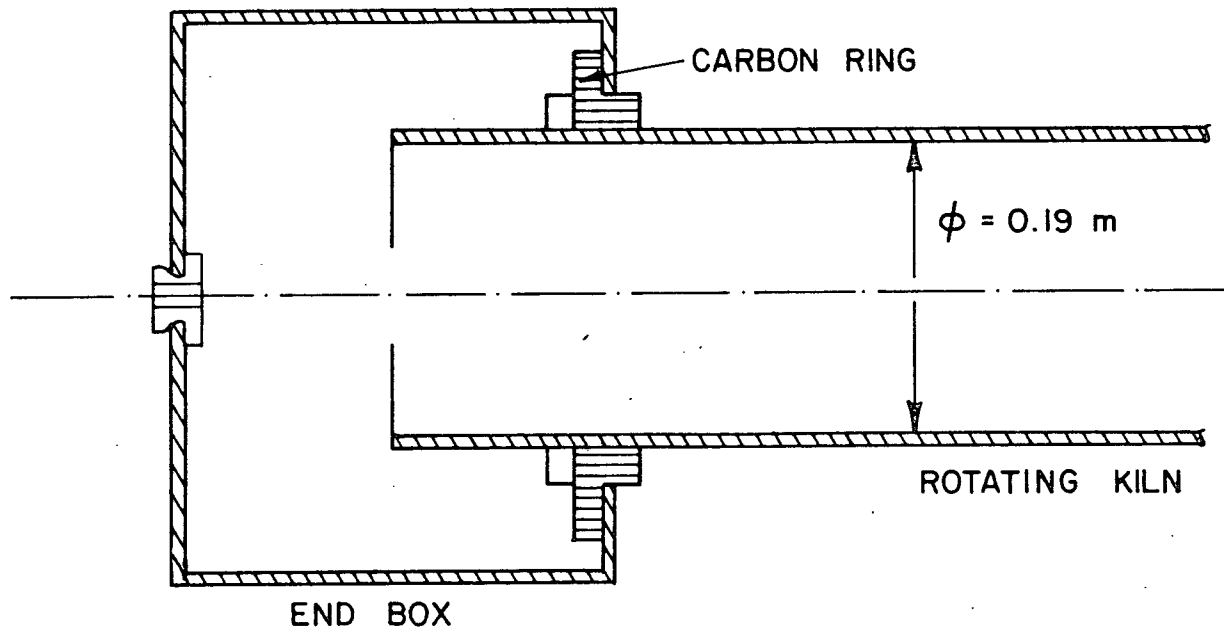
END BOX

Figure 4-2   End Box and Seal System

steel kiln was the same construction as that for the lucite cylinder.

4.1b Feeding System

The feeding system consisted of a bulk material storage hopper, a screw feeder with a constant rate controller, and a feed chute. The feeding equipment was manufactured by Mechanical Development Corporation, Wisconsin, Model #400 SCR. The hopper capacity was 0.035 m^3, and the maximum feed rate was 0.142 m^3/hr. The feed rate was controlled manually by an adjustable controller capable of achieving an accuracy of 1 - 2% for most dry materials. The calibration of this equipment for Ottawa sand and polystyrene is given in the appendix. The material delivered by the feeder was dropped essentially instantaneously into the rotary kiln through a feed chute, which was made of a funnel and a 45 degree 0.013 m diameter copper tube, bent into the end of the kiln.

4.1c Receiving System

For the heat transfer experiments a cone of about 0.04 m^3 volume was attached to the discharge end box. The construction is shown in Figure 4-3. The bottom side of the discharge box was welded with a 0.102 m diameter short pipe with a flange at the other end of the pipe. The cone was sealed and clamped to the discharge flange. Under the average solid throughput the cone became full every thirty minutes.
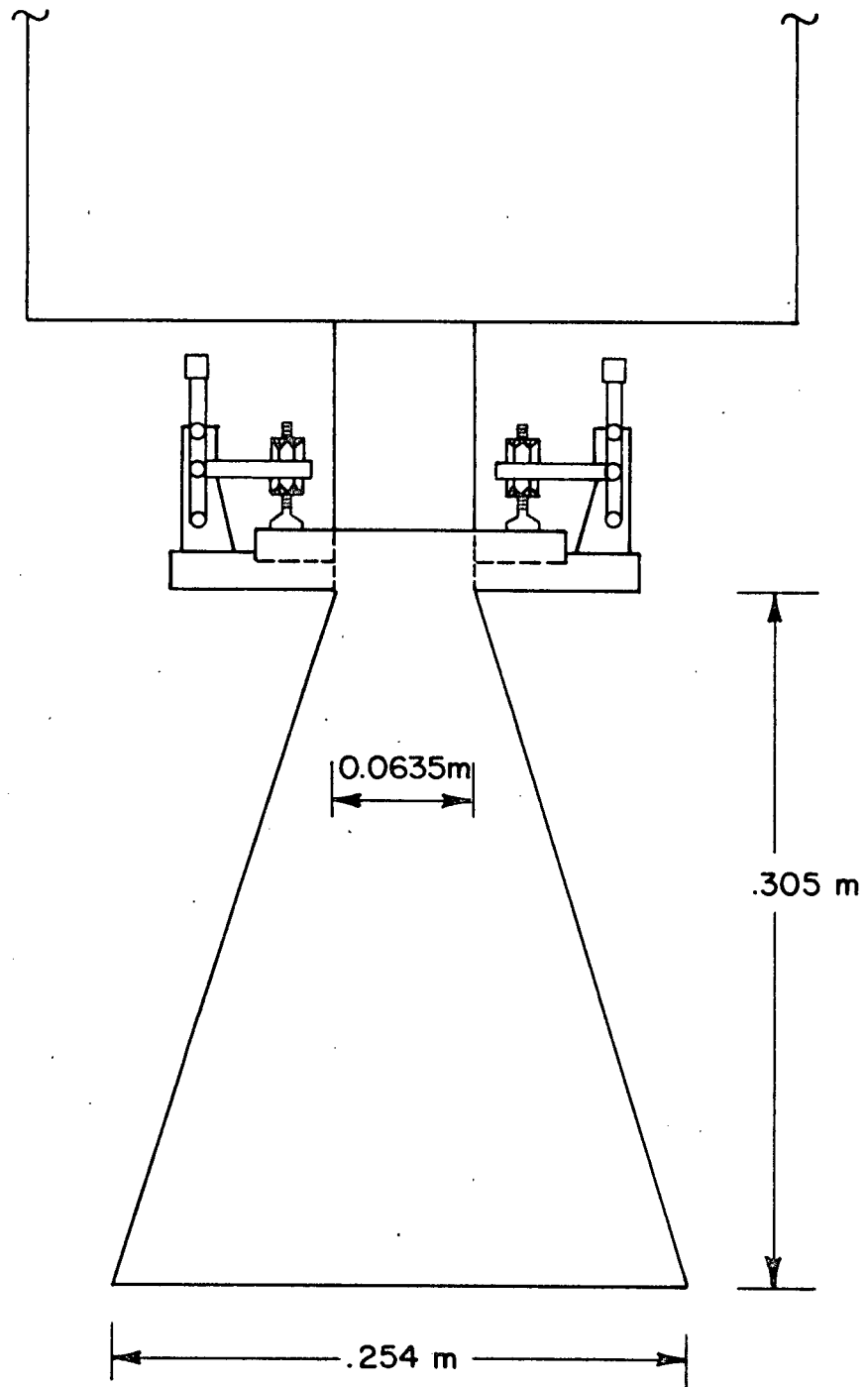
Figure 4-3 Conical Receiver

Then the cone was replaced with another empty one. The
interchange took only a few seconds so that it would not
disturb the system. For residence time distribution studies,
the conical receivers were not used.

4.1d Air Heating System

An electric furnace was used to heat air before it
entered the kiln. The furnace was constructed of a 0.0635 m
diameter and 0.62 m long stainless steel tube, packed with
0.0177 m ceramic Berl saddles. The tube was heated by two
semi-cylinder heating elements, each having 3.6 kW capacity.
The system, then, was insulated in a 0.30 m x 0.30 m x 0.76 m
long fire brick box. The furnace was controlled by an on-off
temperature controller which had a temperature deviation = 2K.

4.1e Thermocouples

Twenty thermocouples were used to measure the tempera-
tures of solids bed and air at five axial locations along
the kiln - three for solids bed and one for air at each
location. The arrangement of the thermocouples is shown
schematically in Figure 4-4. The original purpose of the
installation of the three thermocouples for solids bed at
one location was to measure radial temperature distribution
in the bed.

The thermocouples were constructed of 30 gauge iron-
constantan, and supported by a 0.0127 m diameter, 2.54 m
long steel tube. The probes were situated at the distances,
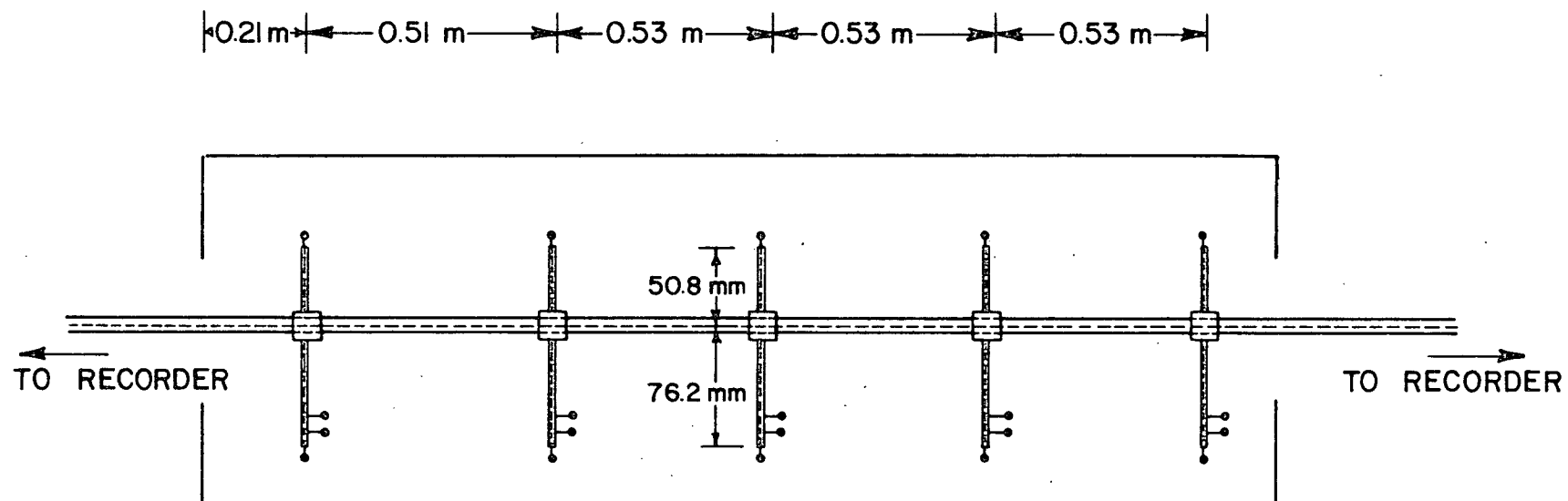
Figure 4-4   Schematic Diagram of Thermocouples Arrangement

0.21, 0.72, 1.25, 1.78 and 2.32 meters from the solid feed
end of the kiln. All the probe wires were extended through
the supporting tube out of its two ends to the recorder.
The supporting tube was passed through the center of the
rotary kiln.

The thermocouples were calibrated in a white oil
constant temperature bath up to 400 K. They were also cali-
brated in freezing tin (504.8 K) and zinc (692.4 K) baths.
The calibration data given in the appendix showed a maximum
deviation of 1.8 K against the ASTM standard table (55).
The air temperature probe was shielded, and air was sucked
through it by a pump located outside the kiln. The construction
of the shield and suction system is shown in Figure 4-5.
The design of the shield suction thermocouples was modified
from the design of Hills et al. (56). In their study the
minimum suction rate for the efficient operation of a 1.5 mm
pt - pt/Rh thermocouple was 15×10^{-6} m^3/s at an air flow
rate of about 1.5×10^{-3} m^3/s. A similar curve was obtained
for the iron-constantan thermocouples used in this study.
The minimum necessary suction rate was about 25×10^{-6} m^3/s,
as shown in Figure 4-6. At a typical kiln operation in this
study the suction rate was about 0.6% of the air flow rate
through the kiln. The wall temperatures were measured by
four iron-constantan thermocouples which were installed on
the kiln wall at positions, 0.31 m, 0.91 m, 1.52 m and 2.13 m
from the solid charge end. Since the kiln rotated it was
necessary to construct commutator rings to transmit the
thermocouple potentials to a suitable measuring device. The

6.4 mm

GAS SUCTION
THERMOCOUPLE

SUCTION

12.7 mm
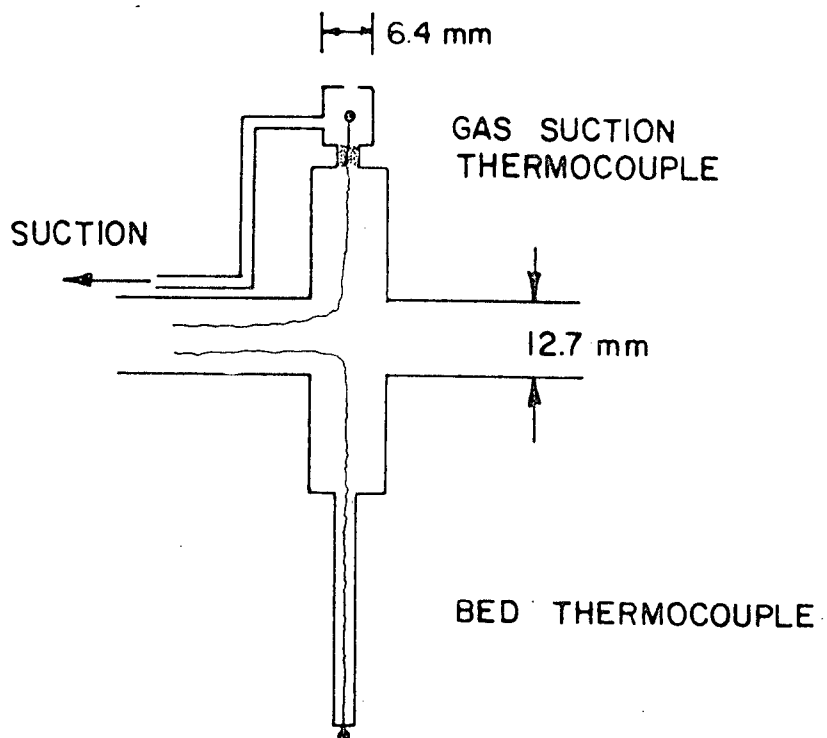
BED THERMOCOUPLE

Figure 4-5   Diagram of Suction Thermocouple
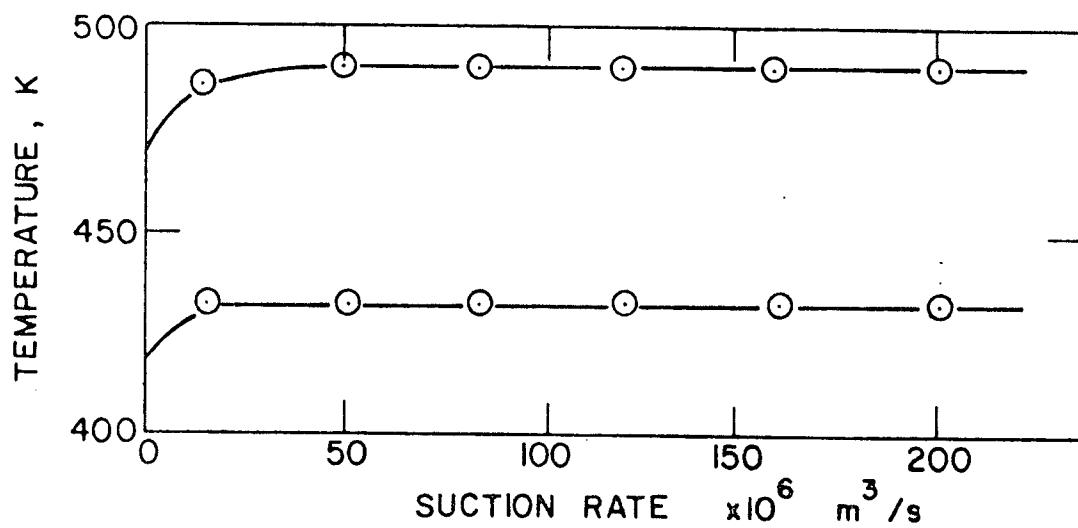
Figure 4-6   Typical Response of Suction Thermocouple

construction of commutator rings is shown in Figure 4-7.
Eight suitable rings, 0.254 m O.D., made of 6.35 mm diameter
copper wire, were constructed and mounted in electrical and
thermally insulating plastic rings attached to the kiln wall.
Copper strips were then used to connect the commutator ring
and iron-constantan wires to a multipoint recorder. Cali-
bration of this device indicated its error within ± 2 K.
The variation which was noted was believed to be caused by
thermal and electrical effects in the commutator assembly.
Four additional thermocouples were installed in the insulation
layer at the same axial locations as the wall thermocouples.
The thermocouples were located at 6.35 mm from the outside
wall. The temperature measurements by these thermocouples
permit a calculation of the wall heat loss.

4.2 Materials

In the residence time distribution (RTD) experiments
transparent STYRON polystyrene particles supplied by Dow
Chemical of Canada Ltd were used. These particles are of
elliptic cylinder shape with dimensions of 1.9 x 3.1 x 3.6 mm
and apparent density of 653 kg/m^3. Tracer particles were
colored by a red food dye and thus were not different in
physical properties from the bulk material.

Alumina was used in a film study of particle lateral
and radial velocity. To obtain the particle velocity an
individual particle was identified at a location in the kiln's
cross section and was traced for a certain time. Thus large
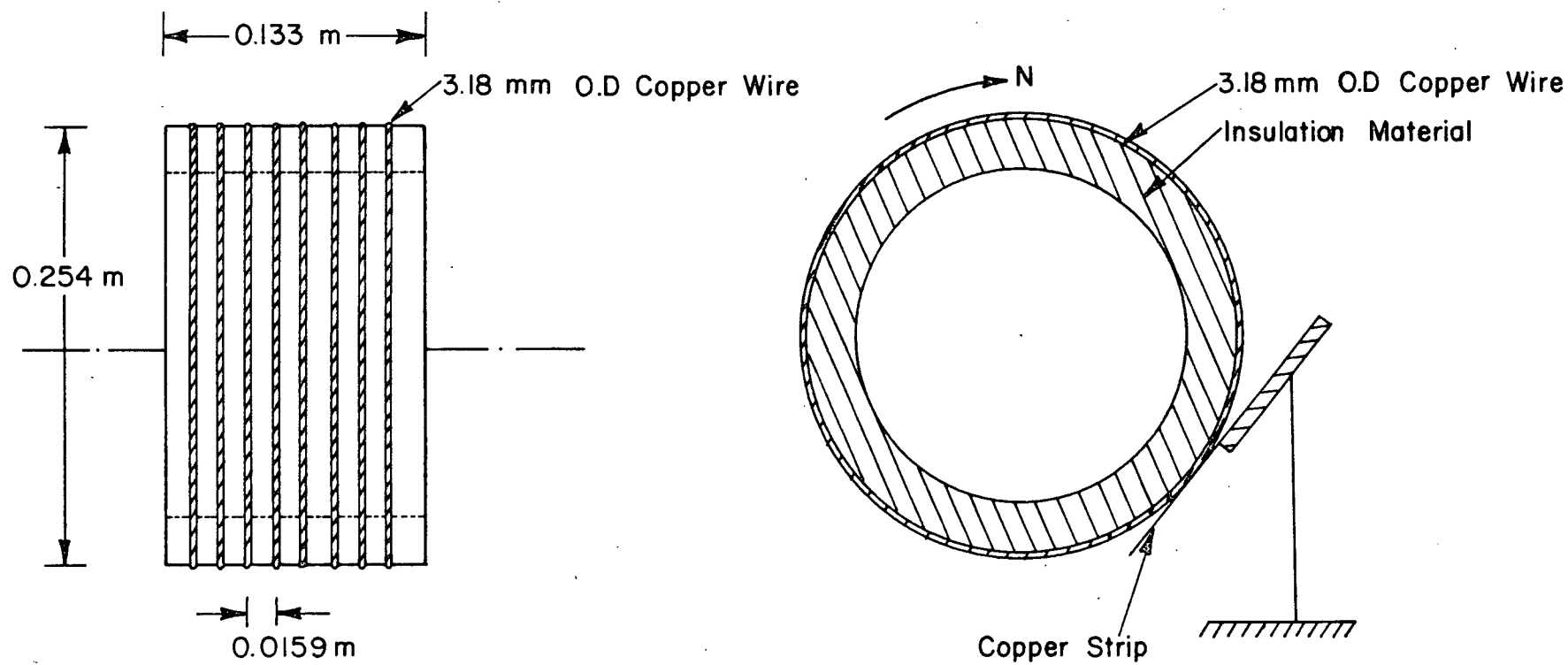
Figure 4-7   Commutator Copper Rings

Labels in figure:
- 0.133 m
- 3.18 mm O.D Copper Wire
- 0.254 m
- 0.0159 m
- N
- 3.18 mm O.D Copper Wire
- Insulation Material
- Copper Strip

particles of opaque alumina of 6.35 m in diameter were used.

In the major part of the heat transfer study inert Ottawa sand was used. The particle size was 20-30 mesh (average diameter 0.73 mm). The physical properties of Ottawa sand have been reported by others (46, 57) and are listed in Table 4-2.

Limestone was used to study the effect of particle size on heat transfer. Limestone was sieved into three sizes, 10-20 mesh, 20-28 mesh and 28-35 mesh. The average particle sizes were 1.26, 0.73 and 0.51 mm, respectively. Physical properties are also given in Table 4-1.

No gas flow was used during the particle motion study, since the effect of gas flow on the particle throughput in a rotary kiln was reported (21, 27) to be negligible.

In the heat transfer experiments where convection is of primary interest preheated air was used rather than combustion gases because of its transparent property to radiation. Since air contains only minimal amount of water vapor and carbon dioxide, gas to wall and gas to solids radiation can be neglected. Measurement of moisture in the incoming air showed a partial pressure of water of 0.004 atm. At the temperatures of the present study, gas/wall radiation coefficients were about 0.07 W/m^2K, a factor of 35 to 70 times less than the convective coefficients measured. Air transport and thermodynamic properties are given in the literature (46, 58, 59).

TABLE 4-2

Physical Properties of Ottawa Sand and Limestone

Ottawa sand (49, 59)

Thermal conductivity	0.268	W/m K
Bulk density	1650	kg/m^3
Particle density	2627	kg/m^3
Specific heat	0.775	kJ/kg K at 373 K
	0.821	kJ/kg K at 448 K

Limestone

Thermal conductivity (58)	0.692	W/m K
Bulk density*	1680	kg/m^3
Specific heat*	0.914	kJ/kg K at 373 K
	0.966	at 423 K
	1.018	at 473 K

*Measured

CHAPTER 5

EXPERIMENTAL PROCEDURE

5.1 Retention Time and Solid Throughput

Polystyrene particles were used for solid throughput runs in the lucite cylinder, while Ottawa sand was used in the steel cylinder. In the latter runs the end boxes and the long tube for thermocouples were removed.

Before starting, the cylinder was set at a predetermined inclination angle. Then the end plates were attached at the both ends of the cylinder. The cylinder was rotated at a fixed rotational speed. The solid material was then fed into the cylinder through the screw feeder until the desired holdup was reached. Mass throughput was measured by collecting and weighing the material leaving the discharge end in a definite time interval (1˜5 minutes depending on flow rate). Rotation was continued until a steady state condition was attained. This was achieved when the constant discharge rate became equal to the feed rate from the screw feeder. About 30˜60 minutes were required to reach steady state in most cases.

To ensure that a uniform bed depth was obtained the bed depth had to be constantly monitored at both ends of the cylinder. If the bed depth was not uniform, adjustments were made

to the feed rate. When the uniform bed depth at steady state condition was obtained, the feeder was switched off and the material in the cylinder was removed, and weighed to determine the holdup. The retention time was then calculated by dividing the bed weight by the solid throughput.

5.2 Residence Time Distribution

Prior to introduction of tracer material steady state flow conditions for the uniform bed depth were assured as described in the previous section. A known number of colored tracer particles was injected into the feed chute at an arbitrary zero time and samples were taken as soon as the first tracer arrived at the end of the cylinder. It was assumed that the tracer was injected over a sufficiently small time interval that the idealized impulse stimulus was realized. Separate samples were taken over thirty seconds intervals until all the tracer material had discharged from the kiln. The rotation was then stopped and the material holdup was determined.

Tracer concentration in each of the discharge samples was evaluated by direct counting of the colored particles and weighing of the total sample. This gave information on the concentration $c(t_i)$, at a number of discrete times, t_i, i = 1,2, ...M, where M denotes the last sampling interval in which tracer appeared in the discharge.

The relationships are given below of the mean, $\bar{t}$, and variance, σ_t^2, of the residence time distribution for the tracer as functions of the exit age distribution function E. Thus,

$$\bar{t} = \int_0^\infty tE(t)dt \qquad (5-1)$$

and

$$\sigma_t^2 = \int_0^\infty (t - \bar{t})^2 E(t)dt \qquad (5-2)$$

The above equations can be approximated (30) for the discrete system

$$\bar{t} \approx \sum_{i=1}^{M} t_i E(t_i) \Delta t \qquad (5-3)$$

and

$$\sigma_t^2 \approx \sum_{i=1}^{M} (t_i - \bar{t})^2 E(t_i) \Delta t \qquad (5-4)$$

where

$$E(t_i) = \frac{c(t_i)}{\sum_{i=1}^{M} c(t_i) \Delta t_i} \qquad (5-5)$$

About 1.0 g tracer was used in a 0.08 m x 0.24 m drum of Abouzeid et al (30) at a solid throughput of 8.64 kg/hr and rotational speed of 42 rpm. In this study the tracer weight was 13.7 g. Only one of the runs used 115 g of tracer material.

The relative variance and Peclet number were then calculated as outlined in Chapter 2:

$$\sigma_\theta^2 = \frac{\sigma_t^2}{\bar{t}^2} \qquad (2\text{-}17)$$

and

$$Pe \approx \frac{2}{\sigma_\theta^2} \qquad (2\text{-}19)$$

The second equation allowed the calculation of axial dispersion coefficient, D, according to

$$D = \frac{\bar{u}L}{Pe}$$

where $\bar{u}$ is the average axial velocity, $\bar{u} = \dfrac{L}{\bar{t}}$.

5.3   Surface Time

Steady state flow was first achieved as described in Section 5.1. A limited number of colored particles were dropped into the cylinder through the feed chute. A length of 0.2 m in the middle of the lucite cylinder was chosen as the test section. When the colored particle reached the test section, the time count was started and the number of the cycles which this colored particle

reappeared on the surface was noted until it passed the other
end of the test section. The above procedure was repeated at
least five times and the average value was taken.

The average axial distance the particle advanced on the
surface for each cycle was

$$d_a = \frac{l_t}{n_t} \qquad (5-6)$$

where l_t :   the length of test section

n_t :   the total number of cycles in the section

and the cycle time, t_t, i.e. the time the particle spent for
each cycle was calculated by dividing the total time in the
test section by n_t. To obtain the surface time t_s, the time the
particle residing in the bed, t_b, must be known and this was ob-
tained with the following equation

$$t_b = \beta/2\pi n \qquad (5-7)$$

where β is the central angle the solids bed occupied. The
surface time, therefore, was obtained by

$$t_s = t_t - t_b \qquad (5-8)$$

The particle axial speed on the surface was calculated
as:

$$V_a = d_a/t_s \qquad\qquad (5-9)$$

This value represents the actual axial speed of the individual particle on the surface. The lateral speed was equal to that of the bed width divided by t_s.

$$V_1 = l_s/t_s$$

5.4 Heat Transfer

5.4a Experimental Procedure

The kiln was first adjusted to the desired inclination angle and the conical solid receiver was attached at the discharge end. The air system was then turned on and the air flow was measured by a calibrated rotameter. The electric furnace was switched on and the temperature controller was set at a desired temperature. The kiln was allowed to heat up for about 3 to 4 hours before rotation of the kiln was started and the feeding began. The feed rate was determined according to Figure 6-9. The temperatures of the air, the bed and the wall were continuously recorded.

The conical receiver was filled up every 15~45 minutes at 50~18 kg/hr solid throughput. Just before the receiver was full, it was removed and replaced by another empty one. The exchange of the cones was done within a few seconds and there was no fluctuation of air temperature observed in the measurements. About one hour was required for the solid flow to reach

the steady state condition. Then the material in the conical receiver was emptied and weighed, and the solid discharge rate calculated. The solid flow was assumed to be at steady state if both the feed rate and the discharge rate were equal.

The recordings of the temperature readings were continued until the steady conditions prevailed. Then the suction pump was switched on and the readings of air temperature taken once the temperatures levelled off.

A complete run usually took 5 to 8 hours.

5.4b. Preliminary Tests

In early heat transfer tests, the kiln was insulated with 6.35 mm ceramic insulation paper, and covered with 3.2 mm asbestos cloth and 25.4 mm thick fiberglass insulation material. Heat balances on these tests indicated that as much as 50% of the heat given up by the air was lost through the kiln wall. To reduce these large heat losses from the kiln, fiberglass was replaced with 0.203 m fibred asbestos pipe insulation, 51 mm thick. The kiln end boxes and discharge system were also insulated. By this procedure the heat loss under most operating conditions was reduced to less than 20% of the total heat given up by the air in passing through the kiln. A similar problem was indicated by Friedman and Marshall (49) for heat transfer experiments in a rotary cylinder. In addition the heat loss was found to be non-uniform along the kiln making interpretation of the data subject to some error. This was due to the presence of the sprocket, rollers and slip rings which could not be in-

sulated. The commutator was located between 1.02 and 1.22 meter from the charge end. The central section of the kiln between 1.25 m and 1.78 m was chosen as the test section of the kiln since this section was far enough away from the two ends of the kiln to minimize the end effects on heat transfer and particle motion, and did not suffer from non-uniform heat loss because of the presence of sprocket, roller or slip ring.

5.4c Operating Range

Table 5-1 shows the range of operating variables covered in this study. Air throughput ranged from 18.6 to 95 kg/hr. On an empty kiln basis the air flux was from 650 to 3300 kg/hr-m^2 which is about in the range of industrial kilns. The inlet air temperature was varied from 373 K to 650 K. The solid feed rate was in the range of 11~66 kg/hr or 400~1750 kg/hr-m^2. The ratio of air/solid feed rate ranges from 0.5 to 5 which compares with 1~2 typical for industrial kilns. Rotational speeds covered a range of 0.9 to 6.0 rpm. The kiln bed was always in the rolling mode at these rotational speeds. One run was carried out at 0.4 rpm during which the bed was in the slumping state. The slope of the kiln was varied from 1.36° to 4.1° and the degree of fill was set in the range of 6.5 to 17%.

Table 5-1   Kiln Operating Conditions

Air throughput   18.6 - 95 kg/hr

Air mass velocity*   650 - 3300 kg/m^2 hr

Air inlet temperature   373 - 650 K

Solids used   Ottawa - sand and limestone

particle sizes   0.51 - 1.26 mm

solids throughput   11 - 50 kg/hr

solids mass velocity*   400 - 1750 kg/hr m^2

Rotational speed   0.9 - 6 rpm

Kiln slope   1.36°- 4.1°

percent fill   6.5 - 17%

*   Superficial - based on cross-sectional area of
    empty kiln

CHAPTER 6

RESULTS AND DISCUSSIONS

Particle Motion

6.1 Type of Bed Movement

Figure 6.1 gives a series of photographs showing different types of bed movement in the cross section of rotating cylinder. The photographs were made using a bed of polystyrene particles at various rotational speeds. As shown in the figure the rolling type of movement is seen at a rotational speed of N/N_c less than 0.1..   Showering of particles is observed at rotational speeds above $N/N_c = 0.6$. The results are in agreement with the observation and description by Rutgers (19). The first three photographs for the rolling type of particle movement give a measured value of the dynamic angle of repose of 27° for polystyrene.

6.2 Lateral and Radial Velocity

A film study of particle movement in the cross section was made. Alumina spheres of 6.35 mm diameter were used. The rotational speed was set at 4.78 rpm, which gave a rolling bed at the holdup ratio of 26%. Figure 6-2 shows traces of the positions of two individual particles with time. The first particle was taken on the aerated surface about 0.06 m from Point A as

N/N$_c$=0.031   0.056   0.091

Rolling
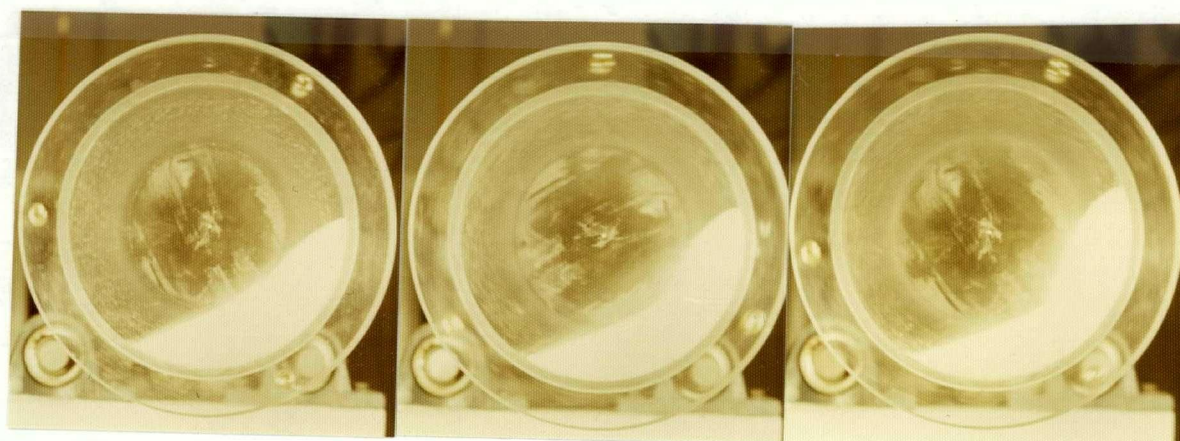
N/N$_c$=0.135   0.387   0.526

Cascading
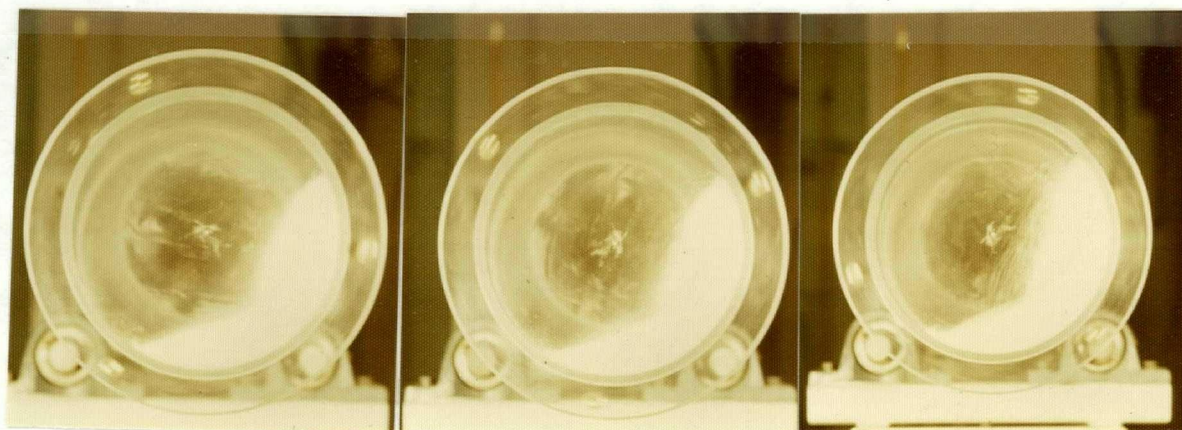
N/N$_c$=0.684   0.747   0.808

Cataracting

Figure 6-1   Photographs of Bed Motions

N = 4.78 (rpm)
Di = 0.195 (m)
dp = 6.35 (mm)(Alumina sphere)

▨▨▨▨▨ Particle trace
▬◄▬◄▬ Boundary between surface layers and bed
⊜ Starting point

Parameter, the time in seconds after the particle moves at starting point.
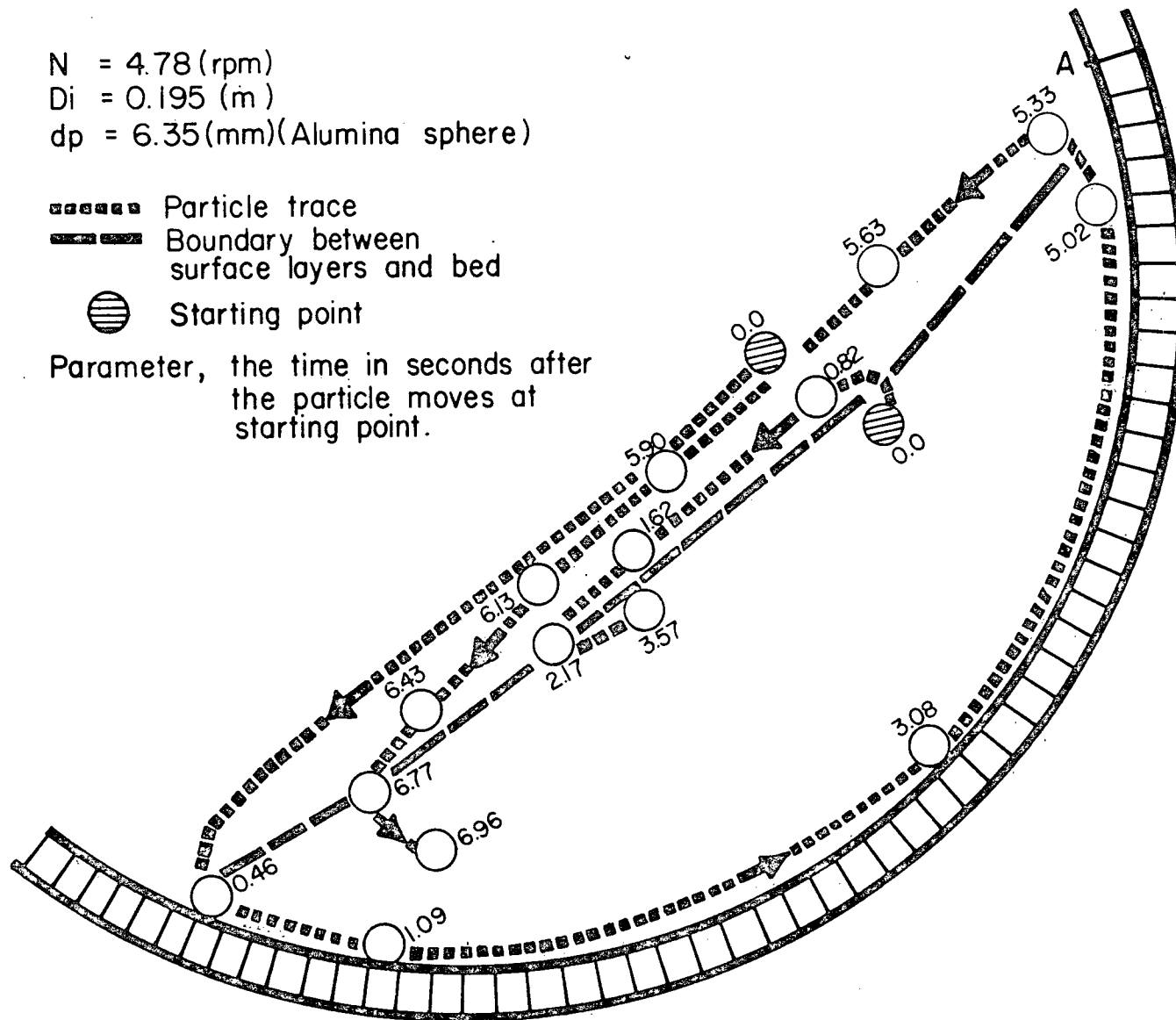
Figure 6-2 Trace of Individual Particles in Kiln

shown in the figure. It took 0.46 seconds to roll a distance
of 0.11 m down the surface (at a speed of 0.24 m/s) before it
returned to the bed. Once in the bed, adjoining the wall it
rotated at the same angular speed as did the kiln. It spent
almost 5 seconds to travel a distance of 0.23 m (at a speed of
0.046 m/s) before it returned to the bed surface. It stayed
on the top of the surface layers for a while, then entered a
second layer, in which it travelled at a lower velocity than it
did in the first layer. However it did not return to the bed
at the same location as the first time. The lateral velocity
of particles decreased from 0.24 m/s in the first layer to
0.107 m/s in the second layer. Thus it is interesting to see
the particle velocity profile across the surface layers. A
second particle was traced which travelled in the surface layer
near the boundary between the surface layers and the bed as
seen in Figure 6-2. It took more time to travel even a shorter
distance than the first one. The velocity was 0.042 m/s.

Figure 6-3 plots both radial and lateral velocity pro-
files against kiln radius position. The ordinate is the kiln
radius along the centerline, OB, of the bed as shown in Fig-
ure 6-3. There are two regions, evident in Figure 6-2 and in
Figure 6-3, the surface region in which particles roll down
the inclined bed, and the bed region where particles move as
a rigid body with the kiln rotation. The boundary between
them is defined as the dividing line, beyond which the parti-
cles on both sides move in opposite directions. The boundary
is shown in Figure 6-2 and Figure 6-3, and is approximated by
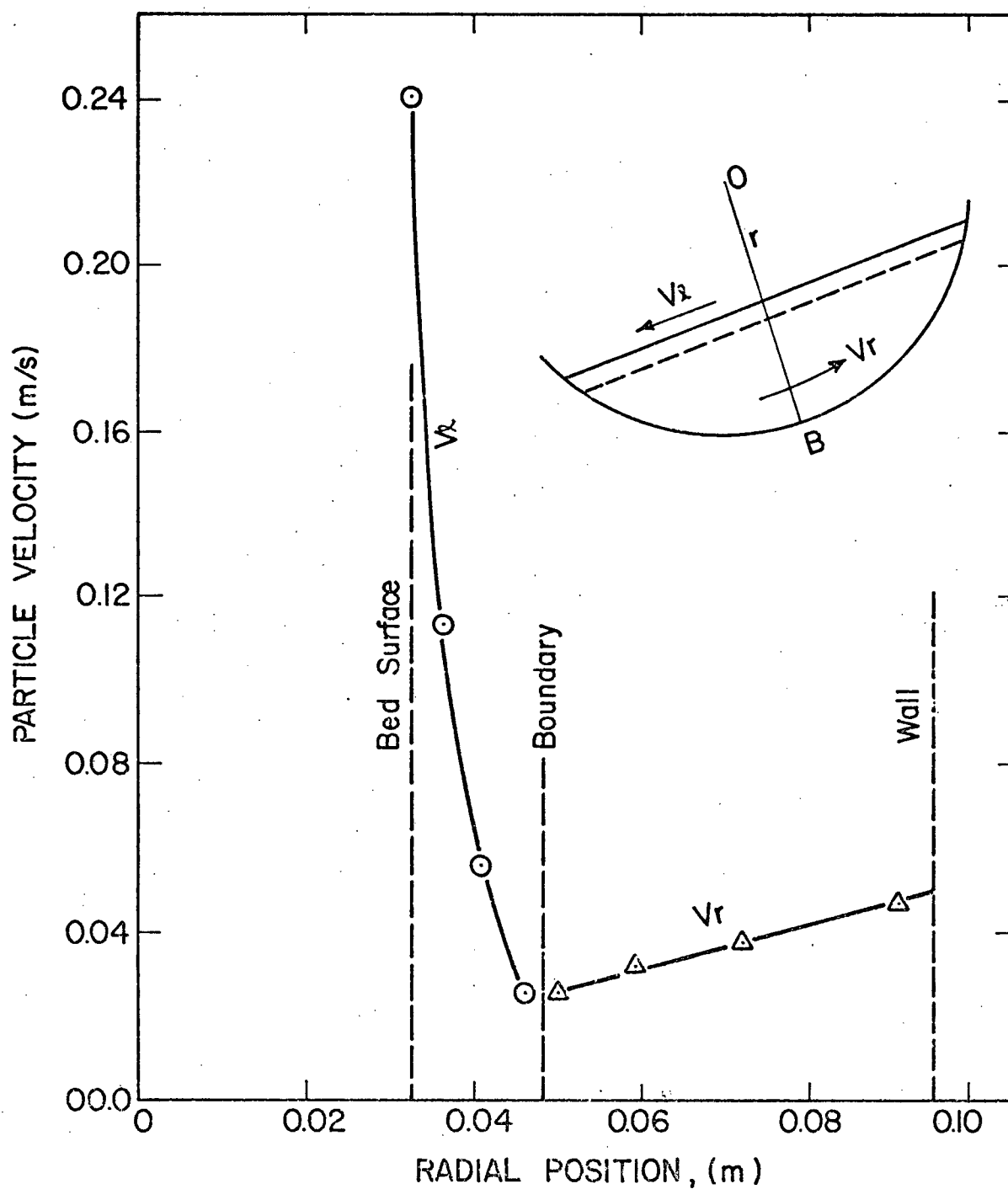
Figure 6-3   Particle Velocity in a Rotary Kiln.

2.5 particle diameters below the surface. The particle velocities
in the surface region and the bed region are referred as lateral
velocity and radial velocity, respectively. In the region of
surface layers the velocity drops significantly from the aerated
surface to the boundary. This is attributed to the internal friction of
surface layer particles. The frictional force exerted on the particle
increases substantially with the distance down from the aerated
surface. Inside the bed the particles move together with neigh-
bouring particles at the angular speed. Their linear radial
speeds are represented by

$$V_r = 2\pi n r \qquad\qquad (6-1)$$

which agrees with the measured speed as given in Figure 6-3.

6.3 Surface Time

It has been postulated above, that the surface time or
particle velocity on the surface plays an important role on
heat transfer and chemical reaction. Inasmuch as the relation-
ship of retention time with the operating parameters is well
established, it is worthwhile to obtain a relationship of re-
tention time and surface time.

A set of experiments using colored polystyrene as tracers
in a bed of the same material was carried out by visual obser-
vation using a stopwatch. The rotational speed was varied and
the solid flow rate also varied in such a way that the holdup
ratio was maintained constant. Retention time and surface time

were calculated by the procedures described in Chapter 5. The results plotted in Figure 6-4 show the relationship of retention time and surface time to rotational speed. Retention time, as expected varies as N^{-1}, whereas surface time is proportional to rotational speed to the power -0.5.

It is also of interest to know the effect of rotational speed on the ratio of surface time to retention time. Figure 6-5 shows the replot of Figure 6-4 and includes the data of Hogg et al (40) for comparison. Hogg et al calculated a value of 0.49 for the ratio of surface time to retention time at a much higher rotational speed, 90 rpm, which resulted in a cataracting type of bed in their 0.095 x 0.248 m rotary cylinder. The data of the present study were obtained in both rolling and cascading types of beds. As seen in Figure 6-5 an increase of rotational speed results in a higher fraction of time the individual particles are exposed to the fluid for heat transfer and chemical reaction. However, it also reduces retention time and surface time in a given length of the kiln as attested by Figure 6-4. The implication of this result is important for analysis of chemical reaction and heat transfer.

Figure 6-6 gives a plot of lateral velocity and axial velocity of the particles on the aerated surface versus rotational speed. The lateral velocity in Figure 6-6 represents an average value. The slopes for both of lateral velocity and axial velocity vs. rotation speed in the log-log plot are about 0.5. Lateral velocity, V_l shows much higher values than axial velocity, V_a. However, the ratio of V_l/V_a is little affected by rotational
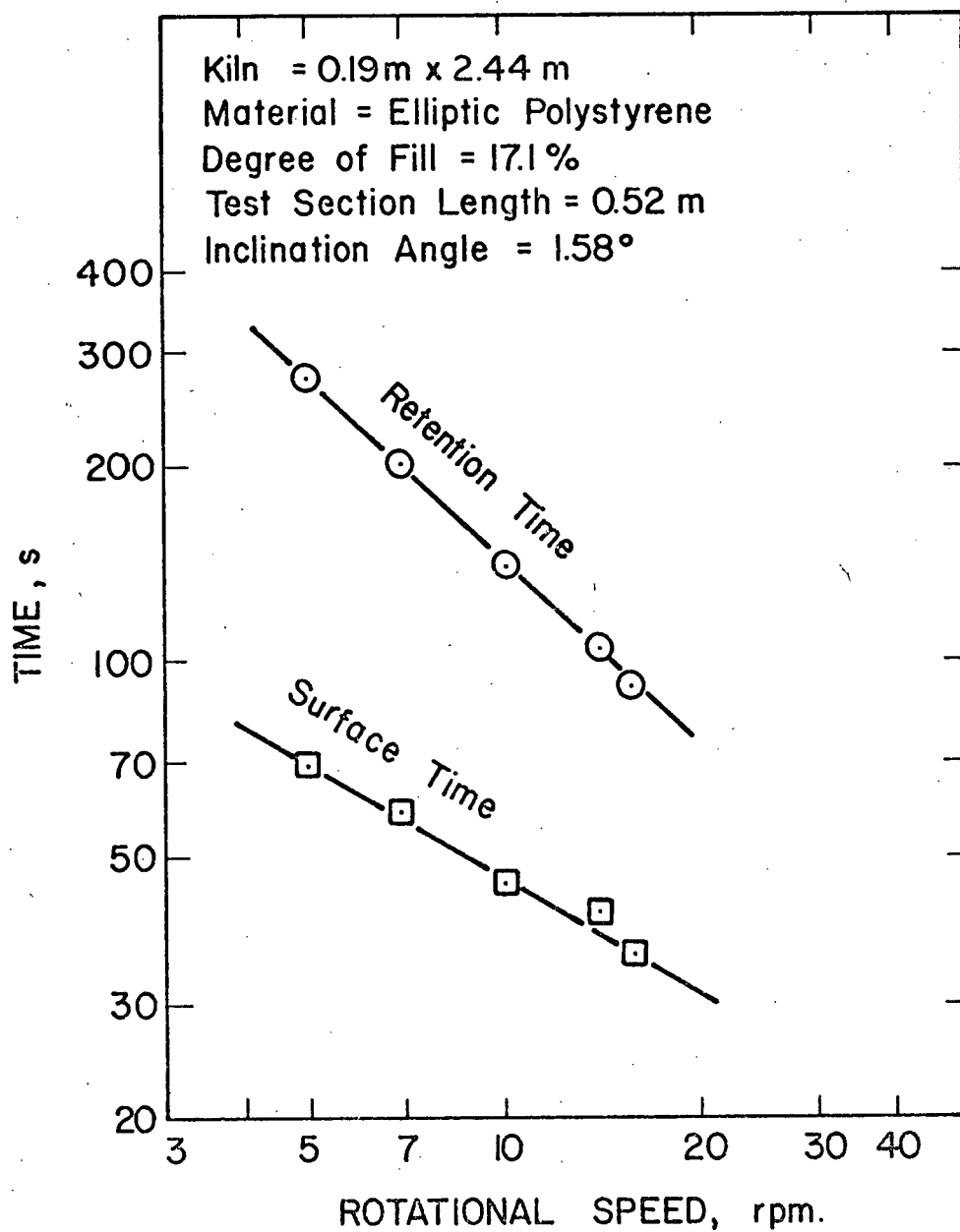
Figure 6-4   Retention Time and Surface Time
versus Rotational Speed.
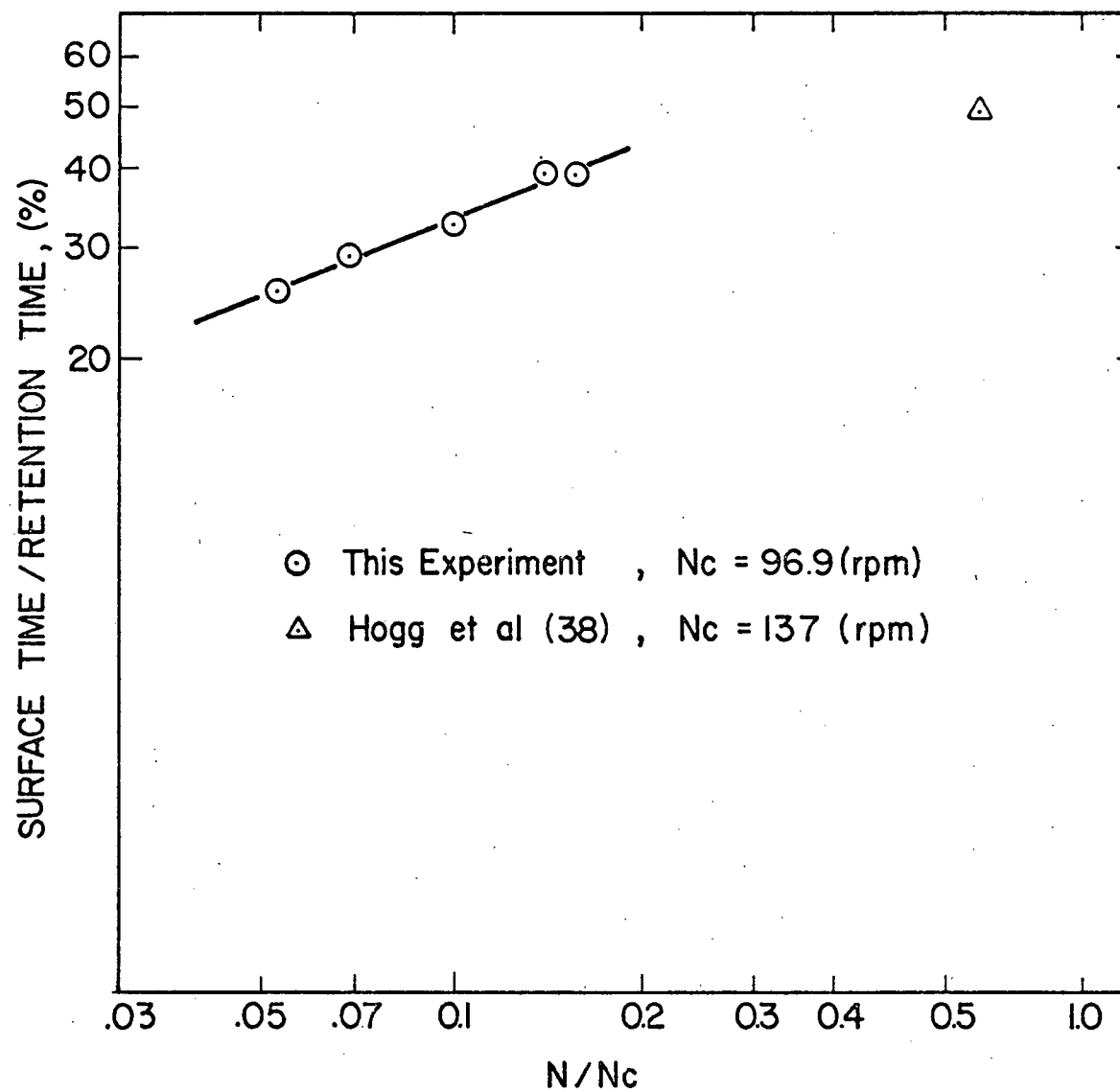
Figure 6-5   The Ratio of Surface Time to Rotation Time versus N/N_c.
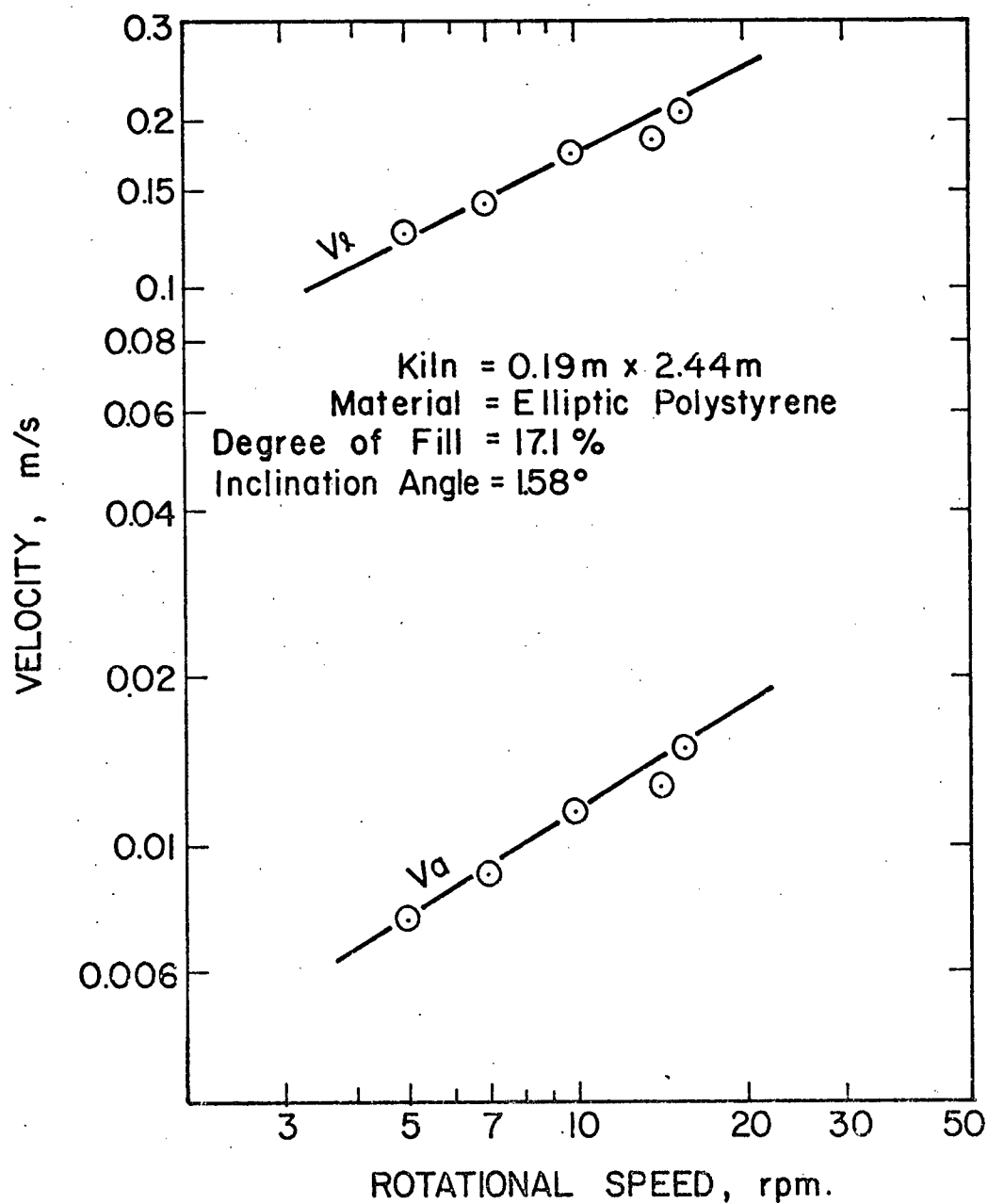
Figure 6-6   Surface Velocity versus Rotational
            Speed.

speed as given in Table 6-1. This is in agreement with the analytical result (25),

$$\frac{V_1}{V_a} = \frac{\sin\theta}{\alpha + \psi\cos\theta} \qquad (6-2)$$

where θ is the dynamic angle of repose, α the angle of inclination and ψ the angle between the surface of the particle and the cylinder axis.

For the present experiments the dynamic angle of repose is 27° and α is 1.58^O. By assuming $\psi = 0$, a value of V_1/V_a, 16.5 is obtained. This value is a little higher than the values given in Table 6-1.

Equation 6-2 gives the effect of inclination angle, α, on the ratio of V_1/V_a. The inclination angle, the angle of the kiln axis to the horizontal is obviously a major factor for axial transport of particles, V_a. The effect of α on V_1 is expected to be insignificant.

Table 6-1   Relationship of V_1/V_a vs. N

N (rpm)	V_1/V_a (-)
5	16.3
6.9	16.0
10	15.1
14	14.5
15.4	13.8

6.4 Solid Throughput and Retention Time

Although the effects of rotational speed and inclination
angle on solid throughput were studied theoretically and experi-
mentally in the literature, none of these studies reported the effects on solid
throughput in a system in which the bed height or degree of fill
is uniform along the kiln. The degree of fill is thought to
be one of major factors influencing the heat transfer processes
since it relates to the surface area for heat transfer. One
industrial kiln was reported (2) to have 5% fill at the charge
end up to 31% at the discharge end. The local heat transfer
processes are therefore expected to be affected by the degree
of fill along the kiln.

In order to eliminate this effect the bed height should
be maintained as uniform as possible along the kiln. An attempt
was made in a series of experiments to determine the throughput
with varying inclination angle and rotational speed. The ex-
periments were carried out under conditions of uniform bed
height along the kiln by carefully monitoring bed depth at the
two ends of the kiln. In all experiments the angle, ψ, between
the bed surface and the kiln axis was no larger than 0.0014
radians or about 0.1 degree. Ottawa sand was used.

The experimental results under these conditions are de-
picted in Figures 6-7, 8, and 9. Figure 6-7 illustrates the
effect of rotational speed with varying inclination angle. The
extrapolation of the line to a rotational speed of zero gives
no throughput of solids. The linear relationship of the through-
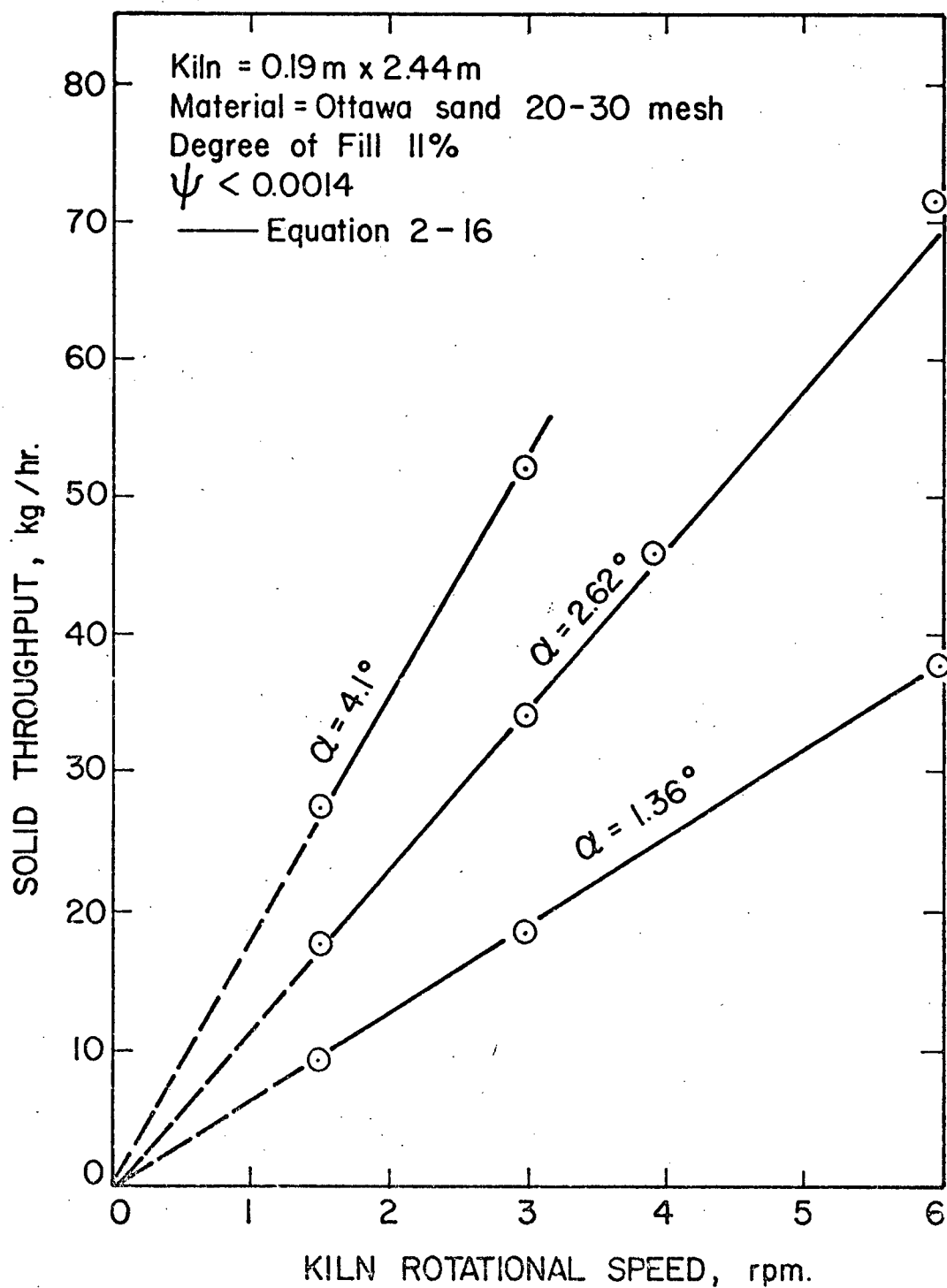
Figure 6-7   Effect of Rotational Speed on Solid
              Throughput in a Uniform Bed Depth
              Rotary Kiln.
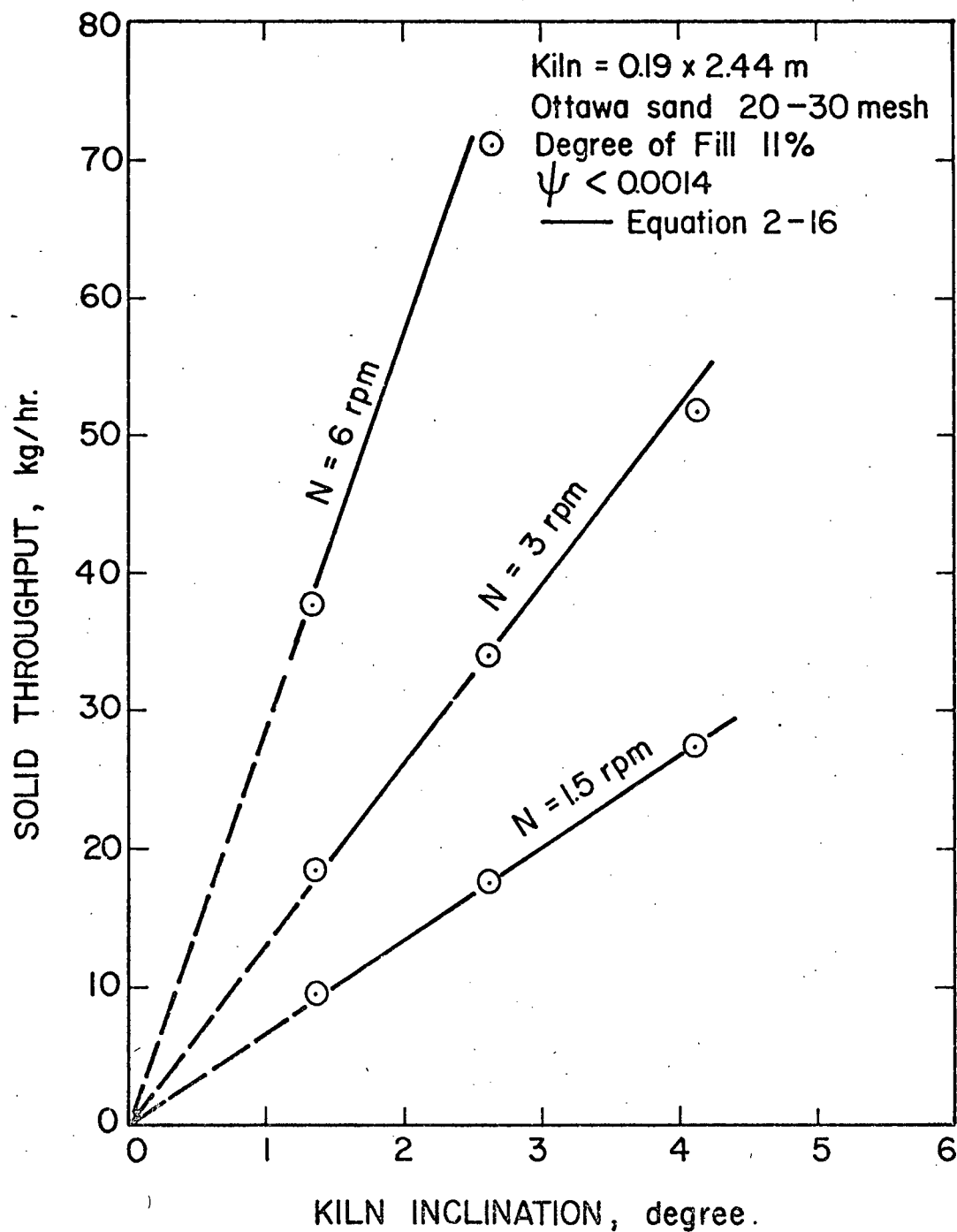
Figure 6-8 Effect of Inclination Angle on Solid
Throughput in a Uniform Bed Depth
Rotary Kiln.
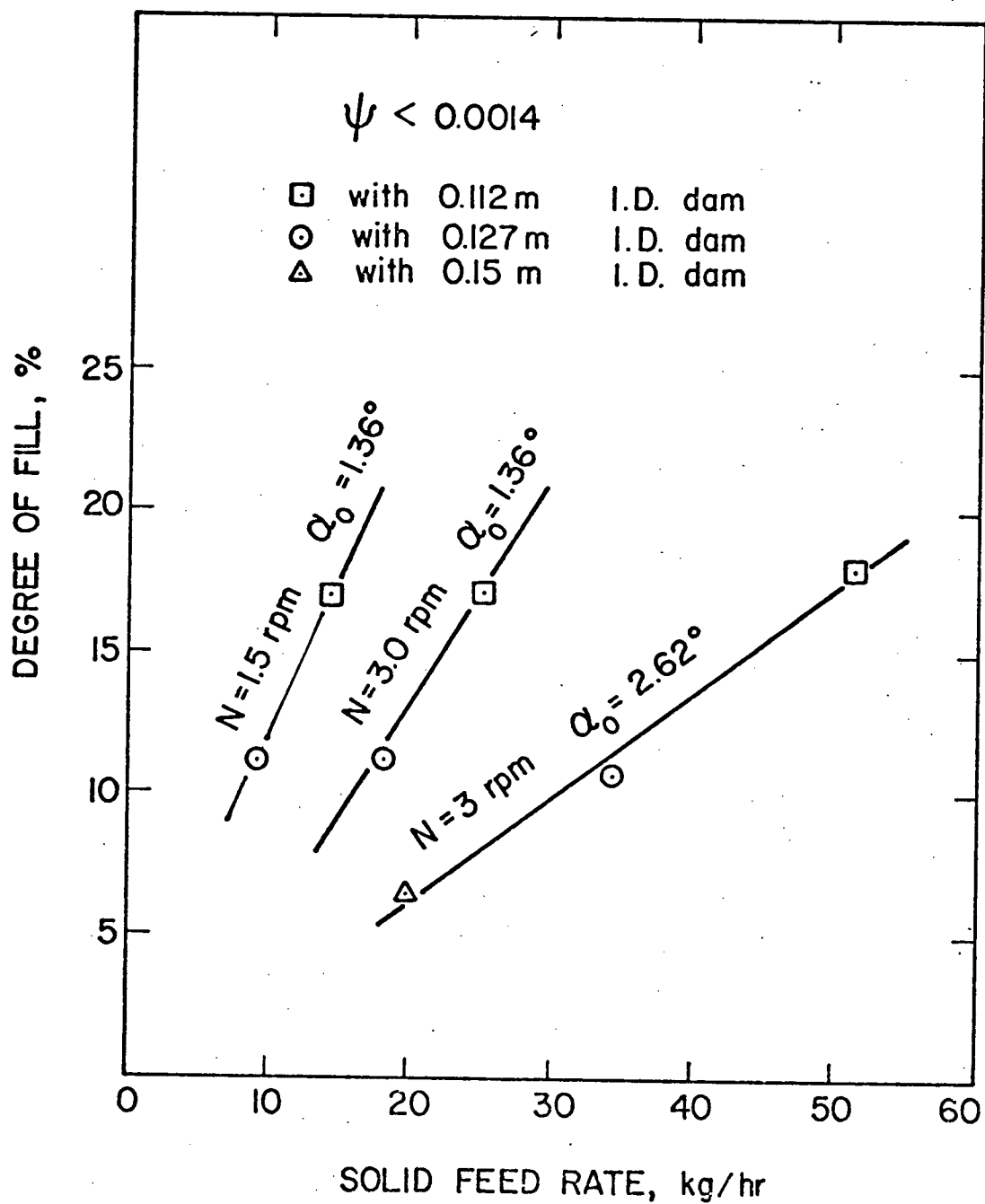
Figure 6-9 Relationship of Solid Throughput and Degree of Fill in a Uniform Bed Depth Rotary Kiln.

put and rotational speed is in agreement with previous work
(19-21, 24-29, 40, 60-62). It has been shown above that in-
creasing rotational speed increases the frequency of the solid
particle appearing on the bed surface. Since axial movement of
particulate material takes place only on the bed surface, the
increasing frequency of appearance of particle on the bed sur-
face increases axial movement in a given time, which increases
axial velocity. Since the solid throughput is equal to axial
velocity multiplied by the cross section area which is uniform
along the kiln, the solid throughput correspondingly increases
in a way that it is linearly proportional to rotational speed.

The solid lines in Figures 6-7 and 6-8 represent the
following equation (25)

$$W_s = \frac{\pi}{6} nD^3 \rho \alpha \sin^3 \frac{\beta}{2} \Big/ \sin\theta \qquad (2-16)$$

The experimental data are found in good agreement with the
theory.

The effect of inclination angle on the solid throughput
is given in Figure 6-8. The linearity of the relationship can
be explained as follows. Increasing inclination angle increases
the axial displacement of the particle while it is on the surface.
It also means that axial velocity increases in proportion.

Degree of fill is plotted against solid throughput in
Figure 6-9 for a uniform bed-depth kiln at various rotational
speeds and inclination angles. In order to operate at a higher

degree of fill, the solid feed rate must be increased to maintain the uniform bed depth.

In previous work (19-21, 24-29, 40, 60-62) the solid throughput was determined by setting two operating variables, rotational speed and inclination angle. In doing so the degree of fill might vary significantly from one end of the kiln to the other. The average degree of fill was usually experimentally determined by removing the holdup out of the kiln and dividing the volume of holdup by the kiln volume. Although a theoretical analysis was done (29), the equation for the degree of fill was lengthy and complex.

By operation under conditions for uniform bed depth in the heat transfer study, four independent operating variables, solid throughput, rotational speed, degree of fill, and inclination angle, are reduced to three through equation 2-16. Therefore if one sets rotational speed and feed rate, there is only one inclination angle that will give a certain uniform bed depth. The retention time was simply obtained by dividing the bed weight by solid throughput. The results for the same series of experiments are given in Figure 6-10. As expected the retention time is inversely proportional to the rotation speed. However degree of fill has little impact on retention time for a uniform bed kiln as shown in Figure 6-11. Increasing degree of fill requires an increase of feed rate to maintain the bed at the same height. As a result, retention time, as a ratio of bed weight to solid throughput remains constant.
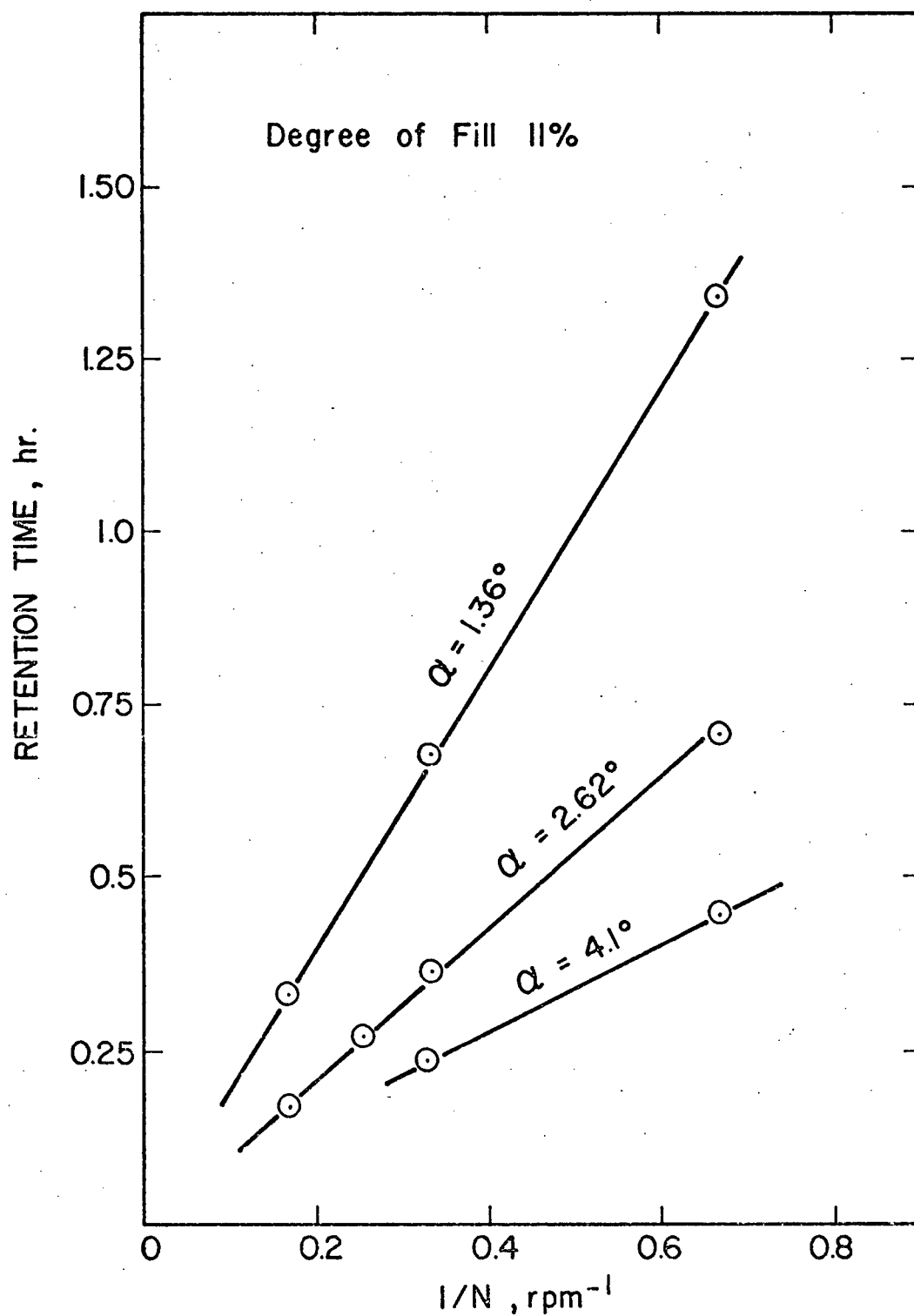
Figure 6-10   Effect of Rotational Speed and
Inclination Angle on Retention
Time in a Uniform Bed Depth
Rotary Kiln.
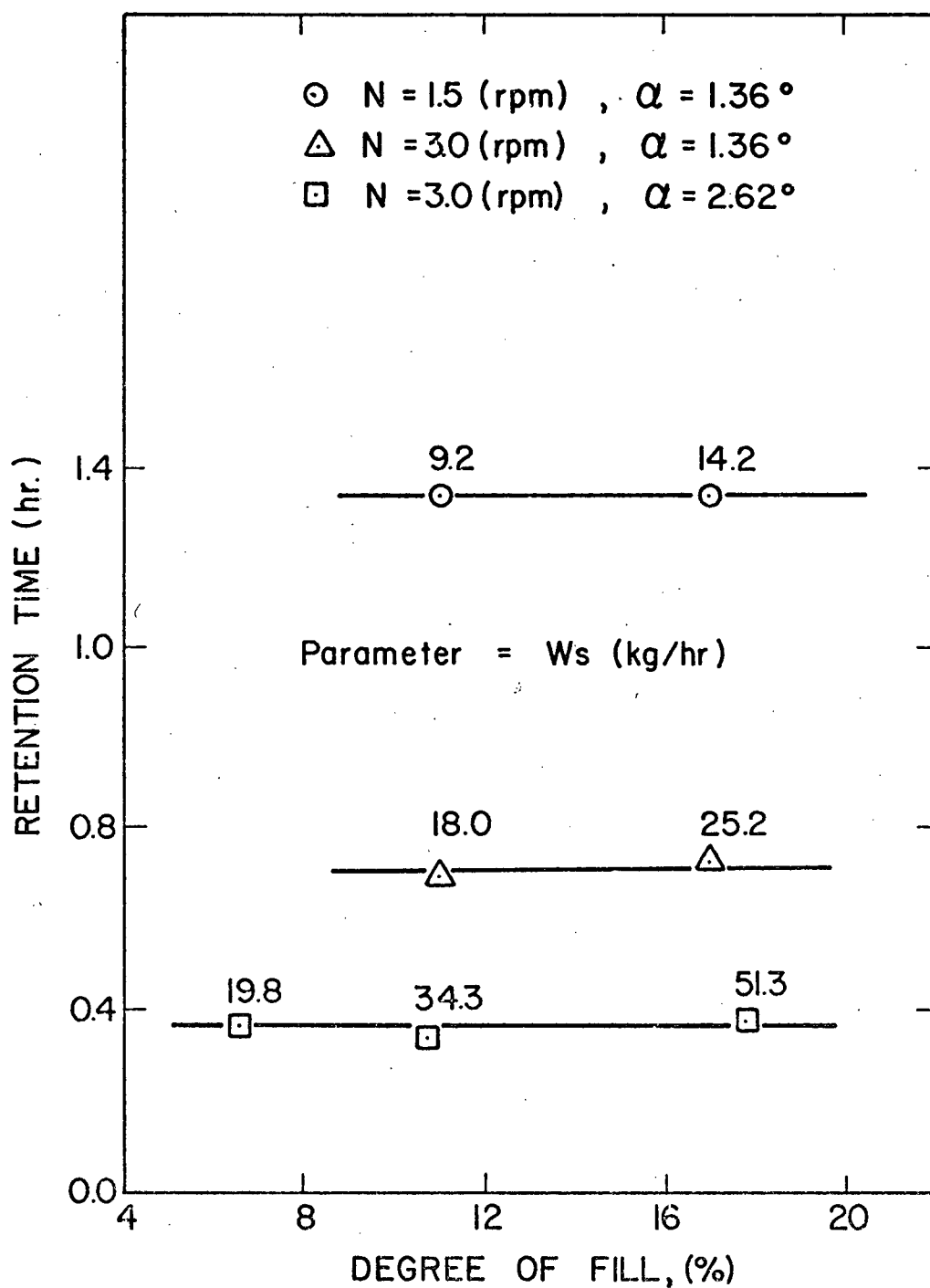
Figure 6-11   Effect of Degree of Fill on
               Retention Time in a Uniform
               Bed Depth Rotary Kiln.

6.5 Residence Time Distribution

For modelling of heat transfer and/or chemical reaction in a rotary kiln it is generally assumed that solid moves in plug flow in the axial direction and is completely mixed in the radial direction. The validity of the former assumption can be examined by the use of the axial dispersion model. The Peclet number was reportedly (30, 31, 38) high enough (above 50) that the solid flow in axial direction can be considered as plug flow.

In this study four RTD runs were conducted in the lucite cylinder. The impulse stimulus method was used. The experimental conditions are listed in Table 6-2 and the results are given in Figure 6-12, plotted as the F-curve versus time. The tracer of 115 g was used in Run R1 whereas about 13.7 g was used in other runs. Based on the experimental results the standard deviation, Peclet number and axial dispersion coefficient were calculated and also are given in Table 6-2. The results indicate the Peclet numbers are in the range 371 to 567 and increase with decreasing rotational speed. However decreasing rotational speed decreases axial dispersion coefficient.

Now it is of interest to compare the experimental data with that calculated from the axial dispersion model with the obtained Peclet numbers.

The axial dispersion model was represented by equation 2-15. Moriyama and Suga (32) solved this equation with initial and boundary conditions as given in equations 2-16a, b and d. The last boundary condition describes a rotary kiln having

Table 6-2

Operating Conditions and Calculation Results

of RTD Experiments

Run No.	R1	R2	R3	R4
Tracer weight (kg)	0.115	0.0137	0.0138	0.0136
Bed Weight (kg)	8.7	9.4	8.4	9.3
Rotation speed (rpm)	6.87	15.6	5.5	4.8
Solid Throughput kg/hr	28.7	61.2	19.8	19.8
Inclination angle (degree)	1.5	1.5	1.5	1.5
$\sigma_\theta \times 10^{+2}$ (-)	7.04	7.34	5.94	7.24
Pe (-)	404	371	567	382
$D \times 10^5$ (m^2/s)	1.28	2.91	0.69	0.90
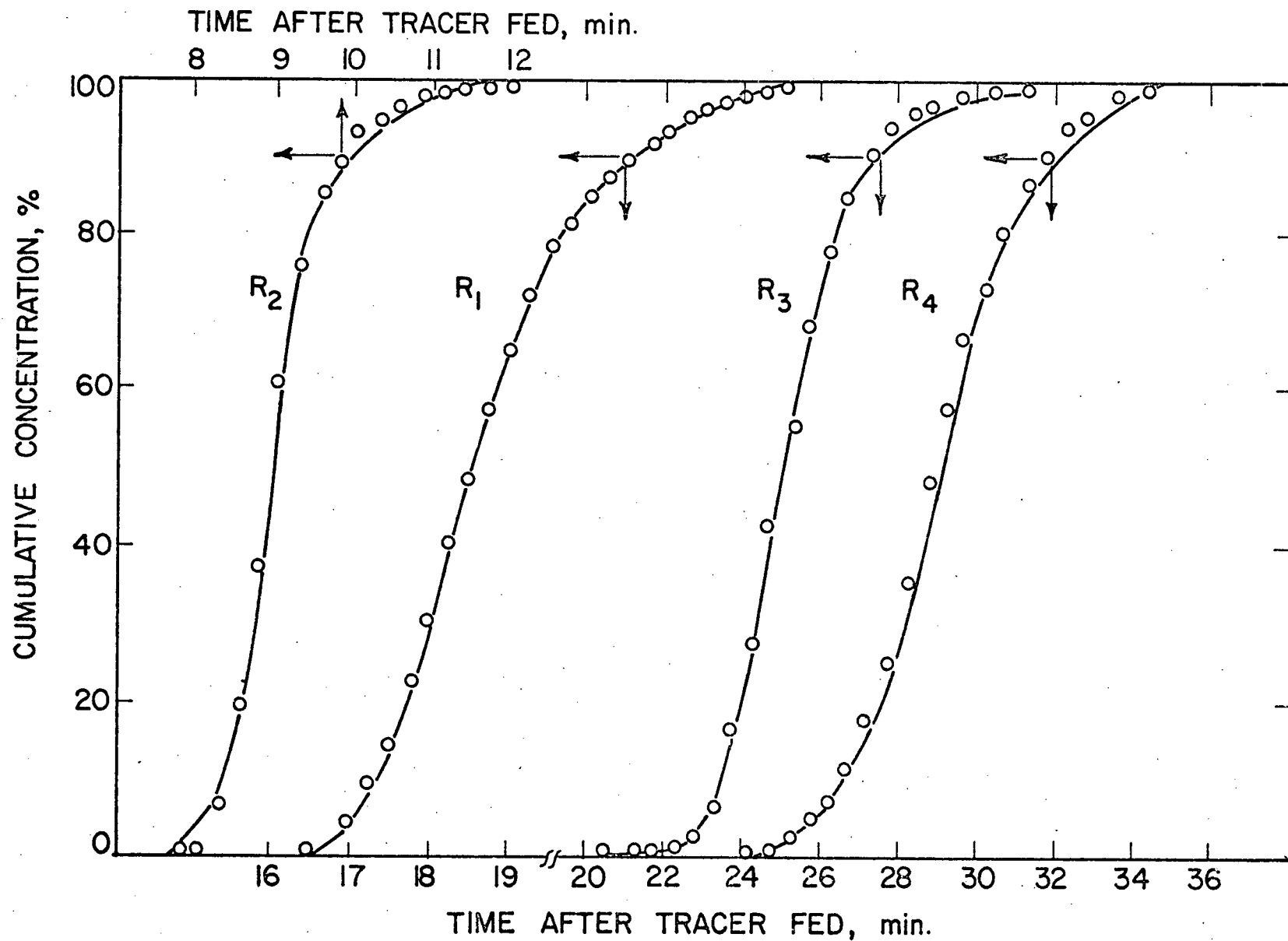
Figure 6-12   Cumulative Response Curve in a Rotary Kiln.

constriction at the discharge end more reasonably than equation 2-16c proposed by Abouzeid et al (30). The solution of Moriyama and Suga for large Pe (>50) is given in equation 6-3.

$$C(\xi) = \frac{\xi}{1+\xi} \sqrt{\frac{Pe\xi}{\pi}} \; Exp \left[- \frac{(1-\xi)^2 Pe}{4\xi} \right] \qquad (6-3)$$

In this equation Pe, the only parameter in the model, is determined from the experimental data and is given in Table 6-2. Figures 6-13, 14, 15 and 16 compare the experimental data and equation 6-3. The figures show a reasonable agreement, however the peak concentration is underestimated in each case.

Since solid transport through a rotary kiln can be represented by the axial dispersion model, it is useful to investigate the effects of kiln operating parameters on Peclet number or the axial dispersion coefficient D. The effect of operating parameters, especially rotational speed, on D has been studied by many investigators (19,30-32, 34, 36, 62). The relationship between D and N/N_c based on the present experiments is shown in Figure 6-17, along with the experimental results of other investigators. D is plotted against N/N_c, instead of N, because N/N_c is able to indicate the flow pattern of particles in a rotary cylinder, as described in Section 2-1. As discussed in Section 2-3 and seen in Figure 2-4 there has been little agreement on the relationship between D and N. The experimental results of Abouzeid, et al (30), Rutgers (19) and Sugimoto et
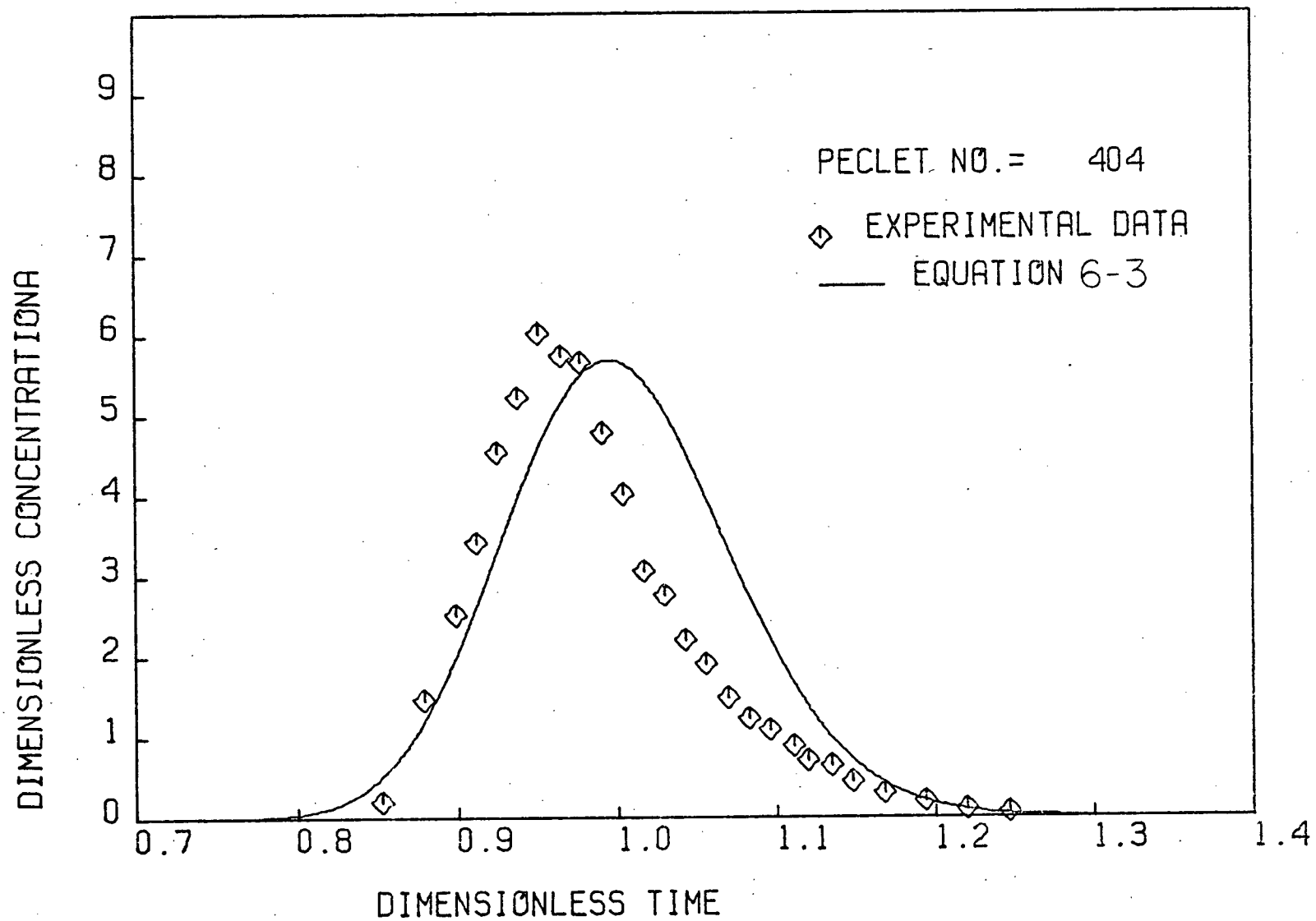
Figure 6-13   Residence Time Distribution (Pe = 404)
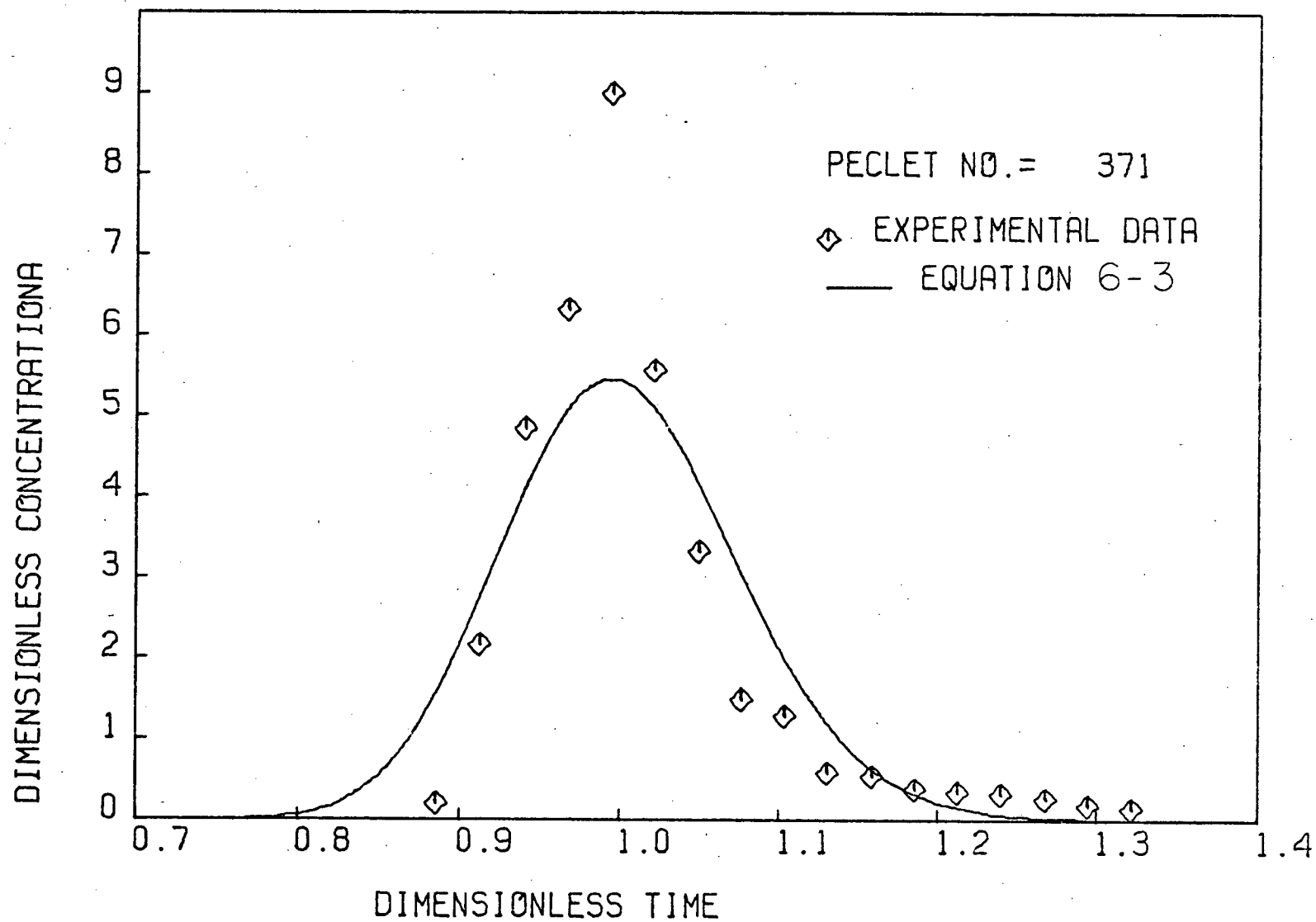
Figure 6-14   Residence Time Distribution (Pe = 371)
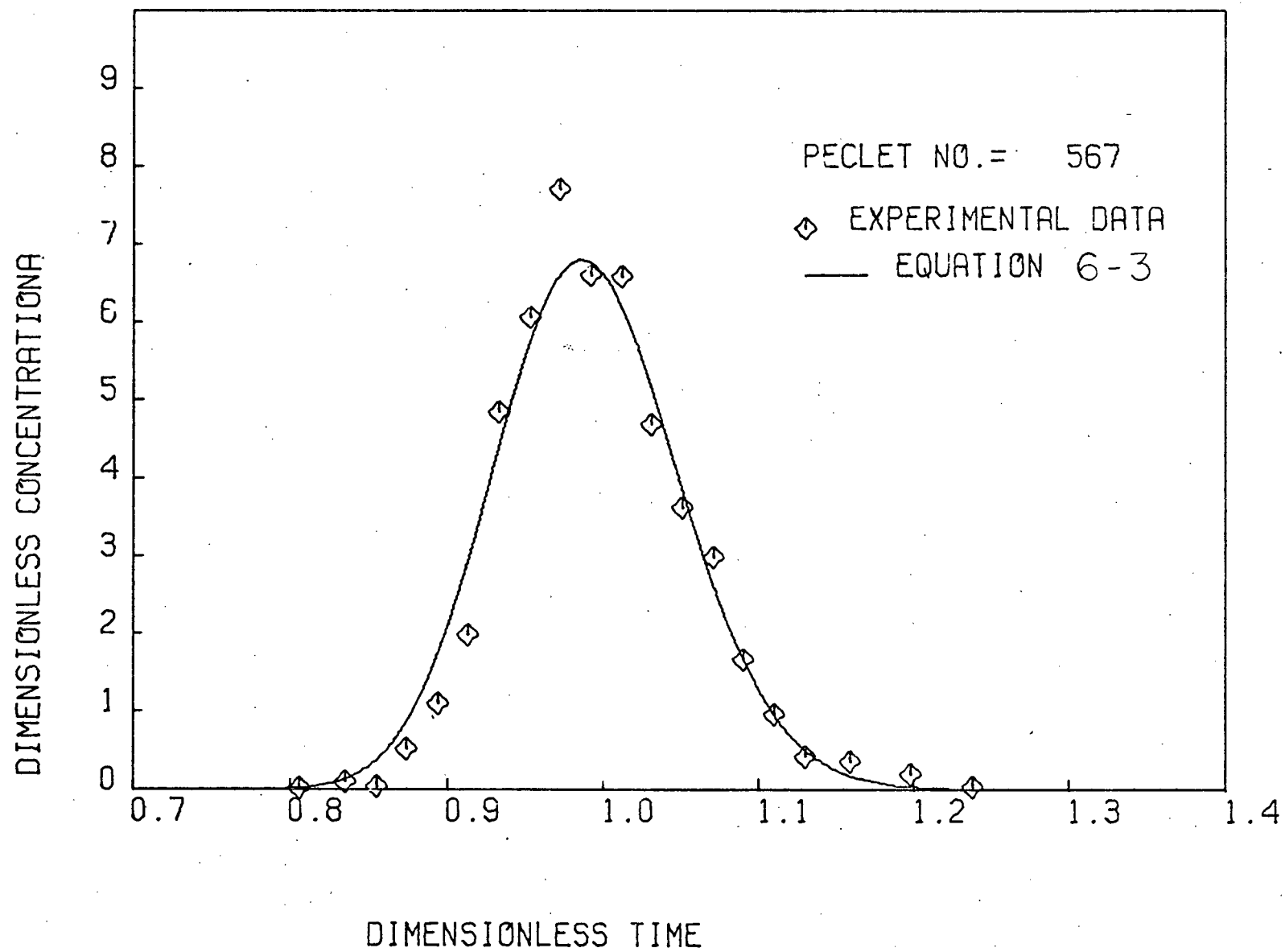
Figure 6-15   Residence Time Distribution (Pe = 567)
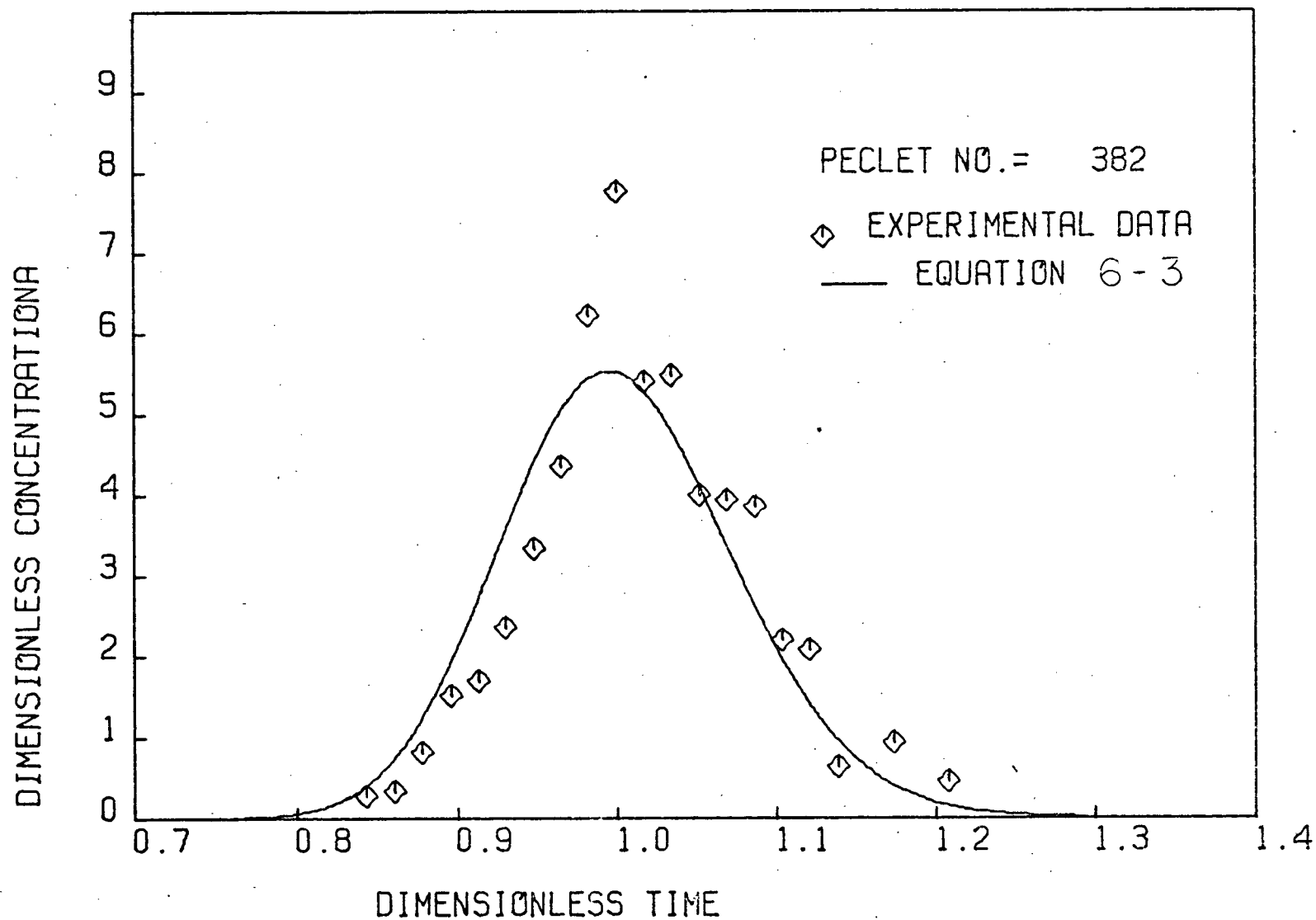
Figure 6-16 -Residence Time Distribution (Pe = 382)
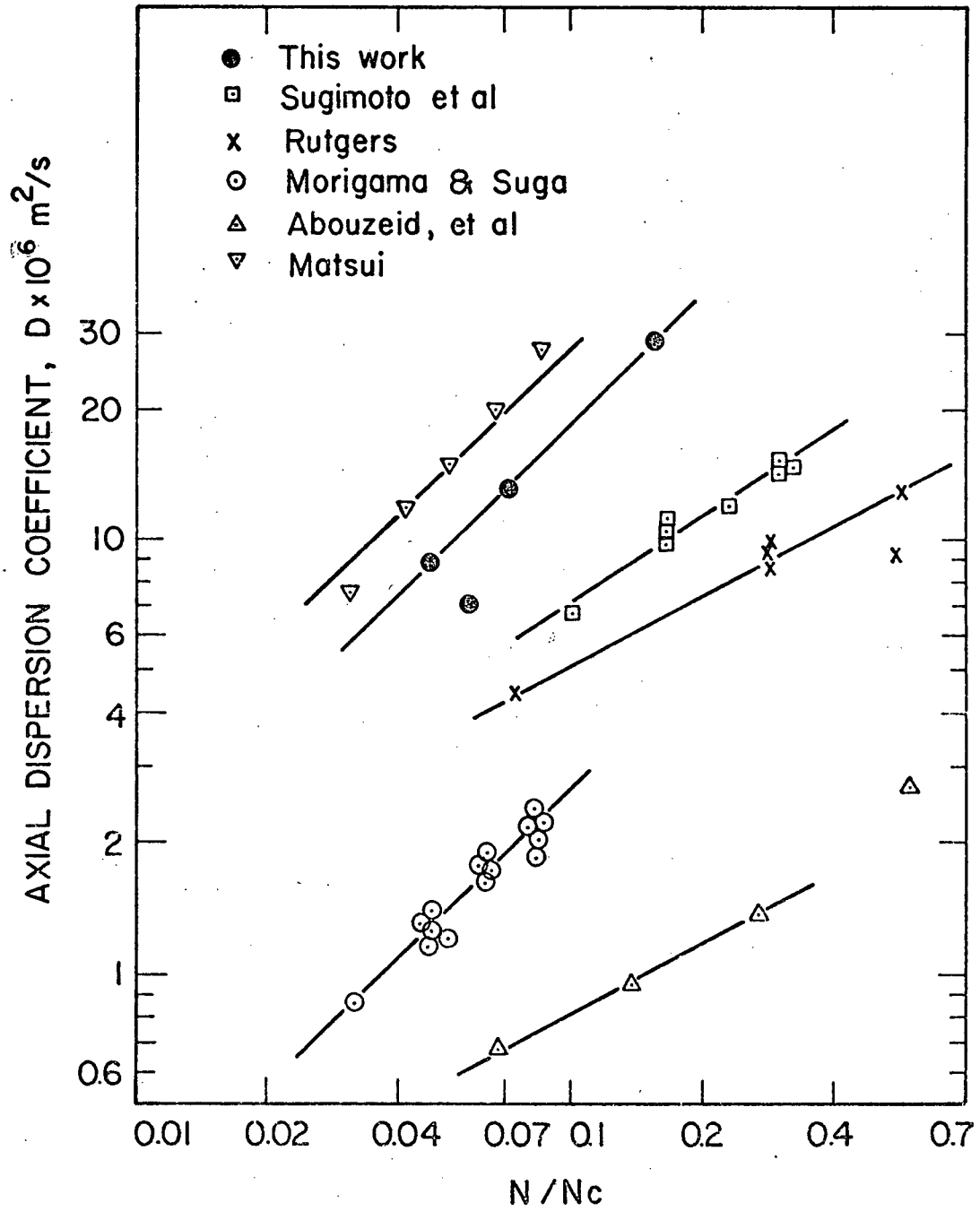
Figure 6-17   Relationship of D and N/N_c.

al (36-38) indicated that D was proportional to the square root of rotation speed, however those of Matsui (34) and Moriyama and Suga (32) reported D was directly proportional to rotation speed. The result of the present experiments agree with Matsui, and Moriyama and Suga. The discrepancy in slopes seems to be related to differences in flow regimes of bed particles. Figure 6-17 clearly indicates that D is directly proportional to N at $N/N_c < 0.1$ where the rolling type of bed movement was obtained, whereas for the cascading bed, $N/N_c > 0.1$, D is proportional to the square root of N.

The high Peclet numbers obtained indicate that the solid flow can be considered as plug flow in kilns of the size used in this study.

Heat Transfer

6.6   Solid and Gas Temperature

6.6a   Solid Temperature

The bed temperature in radial direction is usually assumed uniform in the modelling of a rotary kiln although the surface temperature is likely to be higher. The former assumption was confirmed in this study by measurements with three radially spaced thermocouples inserted into the bed. The radial bed temperatures along the kiln in two sets of data are given in Figure 6-18. Temperatures at different bed depths are within $\pm$ 2 K, and the bed can be taken as radially isothermal in the bulk.

Effective radial mixing is a major contribution to uni-
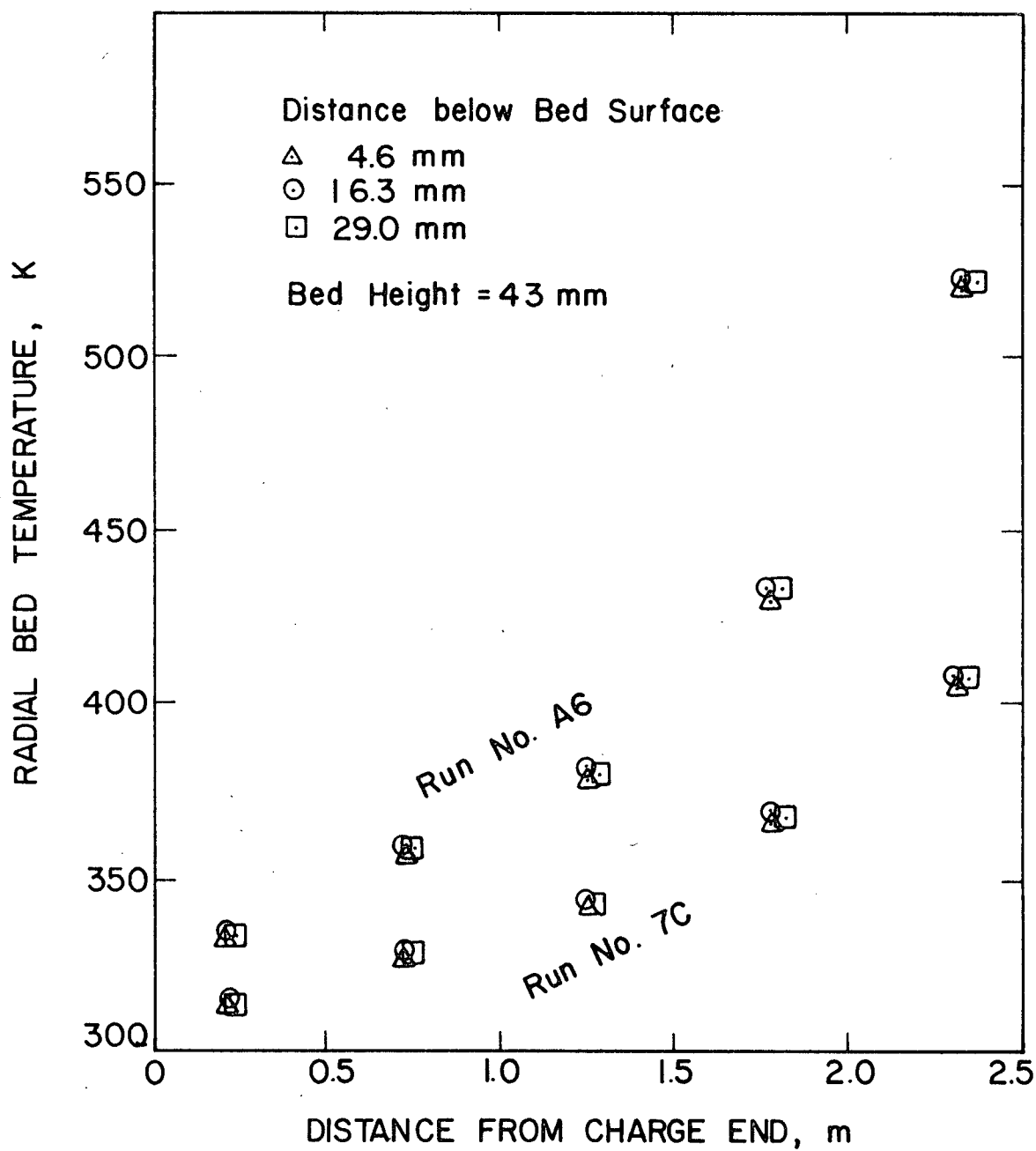
Figure 6-18 Radial Solid Temperature in the Bed

formity of radial bed temperatures. The radial solid flows
are in the rolling pattern under conditions tested. Heat is
transferred from air to the exposed surface layer which is well
mixed when rolling down to the foot of the bed surface. Immed-
iately a new fresh layer repeats the same phenomena as the
previous layer. With such fast turnover of solid material and
short exposure time on the surface, the material appears to be
thermally mixed when it emerges into the bed. Thus, a single
bed temperature can adequately represent the solid temperature
at a given axial position.

6.6b Gas Temperature

The calculations of heat balance and heat transfer require
the average gas temperature at a given axial position. To de-
termine a true bulk temperature both radial gas temperature and
velocity profiles would be required along the kiln.

Figure 6-19 shows a radial gas temperature profile taken
at 1.7 m from the gas entrance using a portable shielded probe.
In the absence of gas velocity data, the average gas temperature
was calculated assuming plug flow of gas using the following
equation:

$$\bar{T}_g(x) = \sum_i T_{g_i}(x,r) \, A_i / \Sigma A_i \qquad\qquad (6-3a)$$

For the present test, the average gas temperature was 409.2 K,
compared to the centerline gas temperature of 412.5 K. If a
velocity distribution that accounted for the velocity decrease
near the wall were used to calculate a bulk temperature, the value
would be even closer to the centerline temperature. The wall and
solids temperatures are shown as 347K and 376K respectively. The
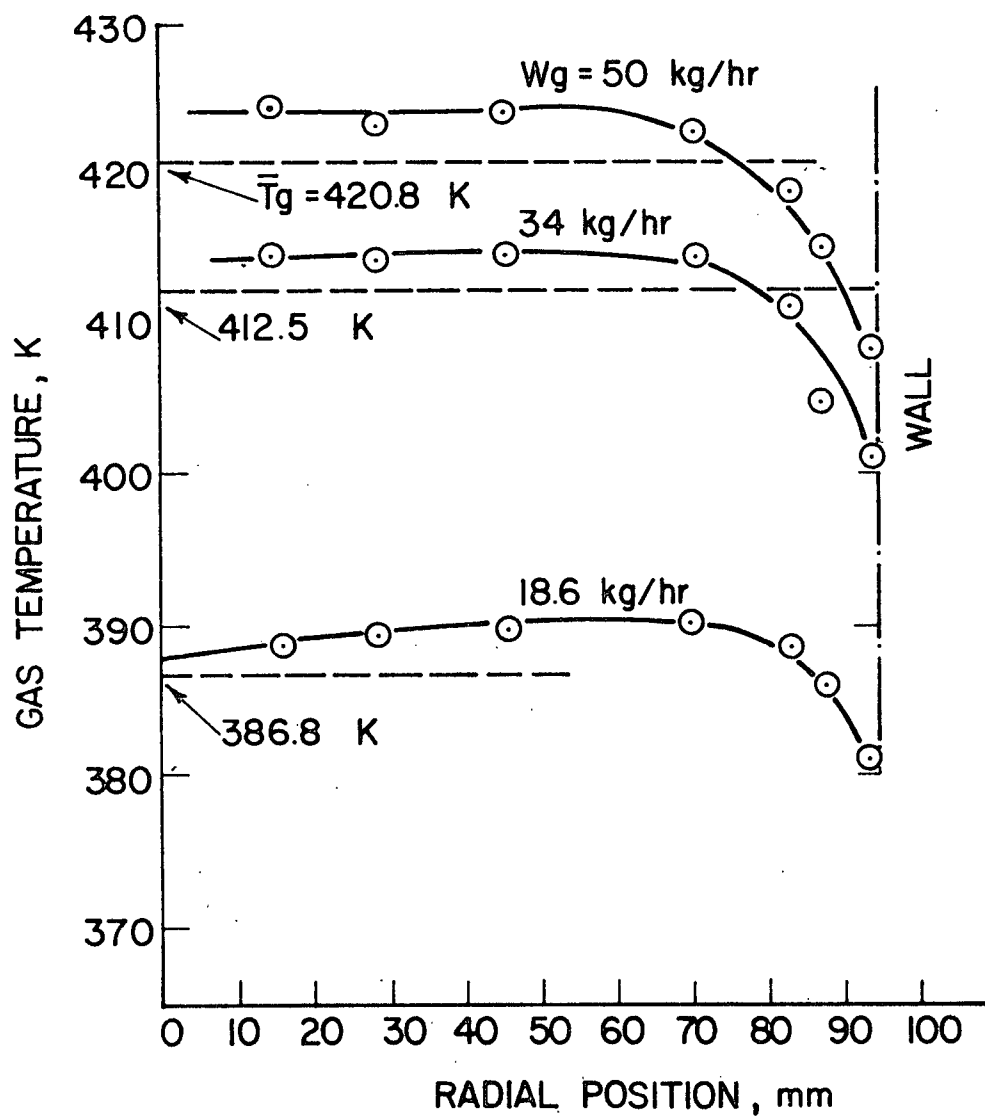
Figure 6-19 Average Radial Temperature Profile

appropriate driving forces for heat transfer are thus ΔT_{gw} = 409.2-347=66.2 K and ΔT_{gs} = 409.2-376=33.2 K. Experimental difficulties precluded the routine measurement of both radial and axial temperatures. Instead the temperature 25.4 mm from the centerline was used to approximate the average temperature at a given axial position. This will give a slightly larger calculated ΔT for both gas/solids and gas/wall coefficients. In the present case the $\Delta T_{gs} \simeq 412.5-376=36.5$ K, and ΔT_{gw} = 412.5-367= 65.5 K. Thus reported heat transfer coefficients will be conservative. The effect of using the near-centerline temperature rather than the bulk temperature will be small since on average $\Delta T_{gs} \simeq 67K$ and ΔT_{gw}=70 K. However a 3K deviation in T_g will make coefficients about 10% low at low percentage fill, and low solids throughputs where ΔT_{gs} are about 30-40 K. On average the reported coefficients will be about 4% low.

6.7 Axial Temperature Distribution

Figure 6-20 is a typical curve of the axial temperature distributions found along the kiln. Air temperatures and sand temperatures were taken at five locations, whereas wall temperatures were taken at four locations. The smooth curves along experimental curves were obtained by the use of spline functions. For most runs the sand temperature is higher than the wall temperature until they approach each other near the discharge end. This reflects the greater rate of heat transfer to the bed than to the wall, and the relatively high heat loss through the wall. In this typical run as shown in Figure 6-20 the temperature profiles are not linear and the temperature difference between gas and solids temperature is fairly constant along the kiln at about 55 K. The temperature driving force will be reduced to
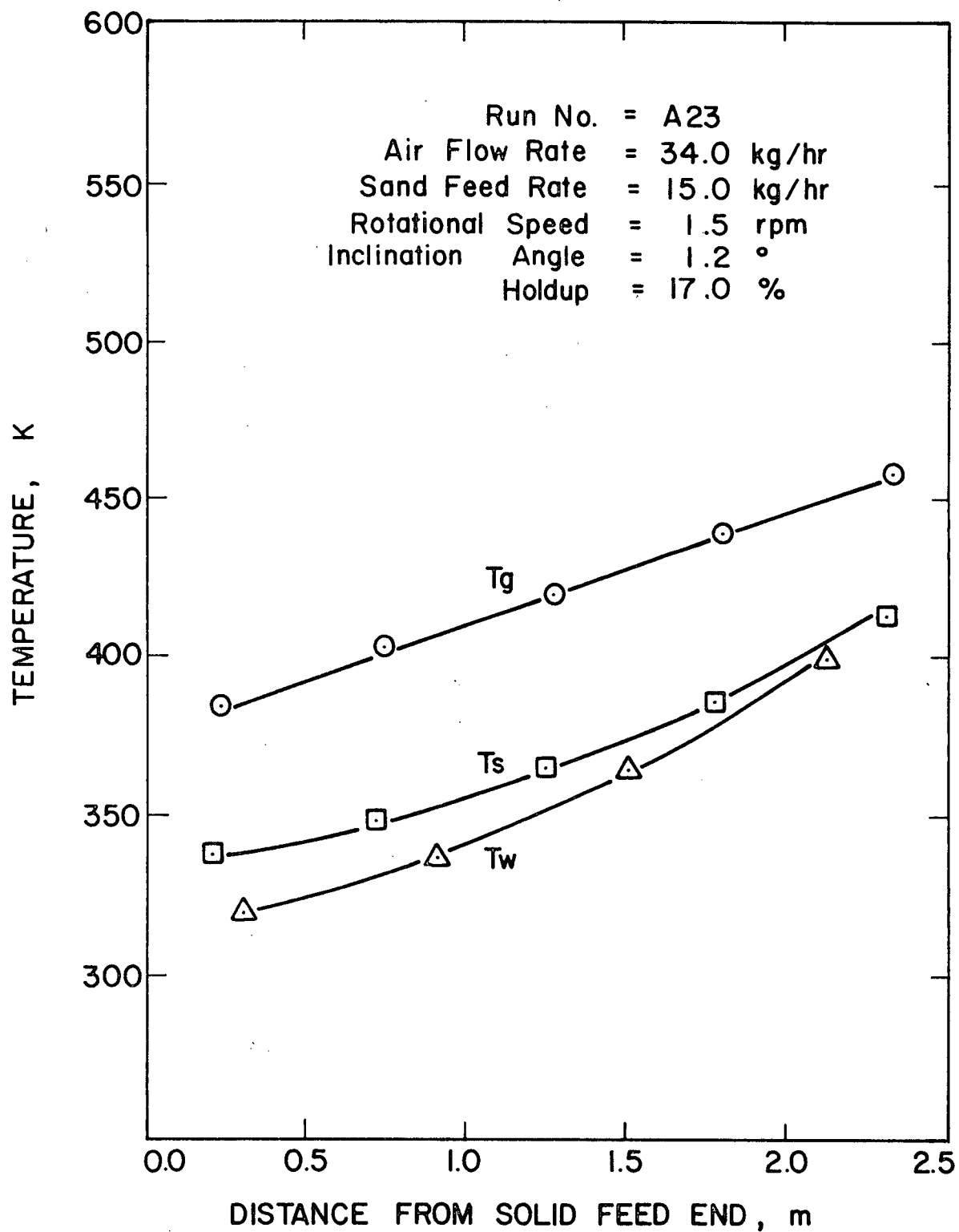
Figure 6-20 Typical Axial Profiles along a Rotary Kiln

53 K if the average gas temperature as discussed in the previous section is used. This results only in 4% increase of heat transfer coefficient if the average gas temperature is used instead of the centerline temperature.

Figure 6-21 shows the reproducibility of temperature readings for two runs at the same operating conditions carried out two days apart. The data were reproducible within 2.5 K for solids temperature, 1.5 K for wall temperature and 1.0 K for gas temperature. The effect of air flowrate on temperature distribution is depicted in Figure 6-22. The air entering the kiln for these two runs was kept at the same temperature. The temperatures of air, sand and wall for high air flowrate were found to be higher than those for lower flowrate. The reason can be explained as follows. The heat transfer coefficient from gas to solids is a function of gas flowrate as $h \propto W_g^n$, where n is less than unity. Then an increase of gas flowrate increases the heat flow rate from gas to solids accordingly if $T_g - T_s$ remains about the same. Since $Q \propto W_g C_{pg} \Delta T_g$, thus ΔT_g, the gas temperature drop, becomes depending on gas flowrate in a form of $W_g^{-(1-n)}$. Therefore increasing gas flowrate decrease the gas temperature drop.

The effect of rotational speed and sand throughput on the temperature profiles is given in Figure 6-23. The temperatures of air, sand and wall for a higher rotational speed were found to be lower than those for a low speed. These effects are explained below. As noted in Section 6.4, in order to main-
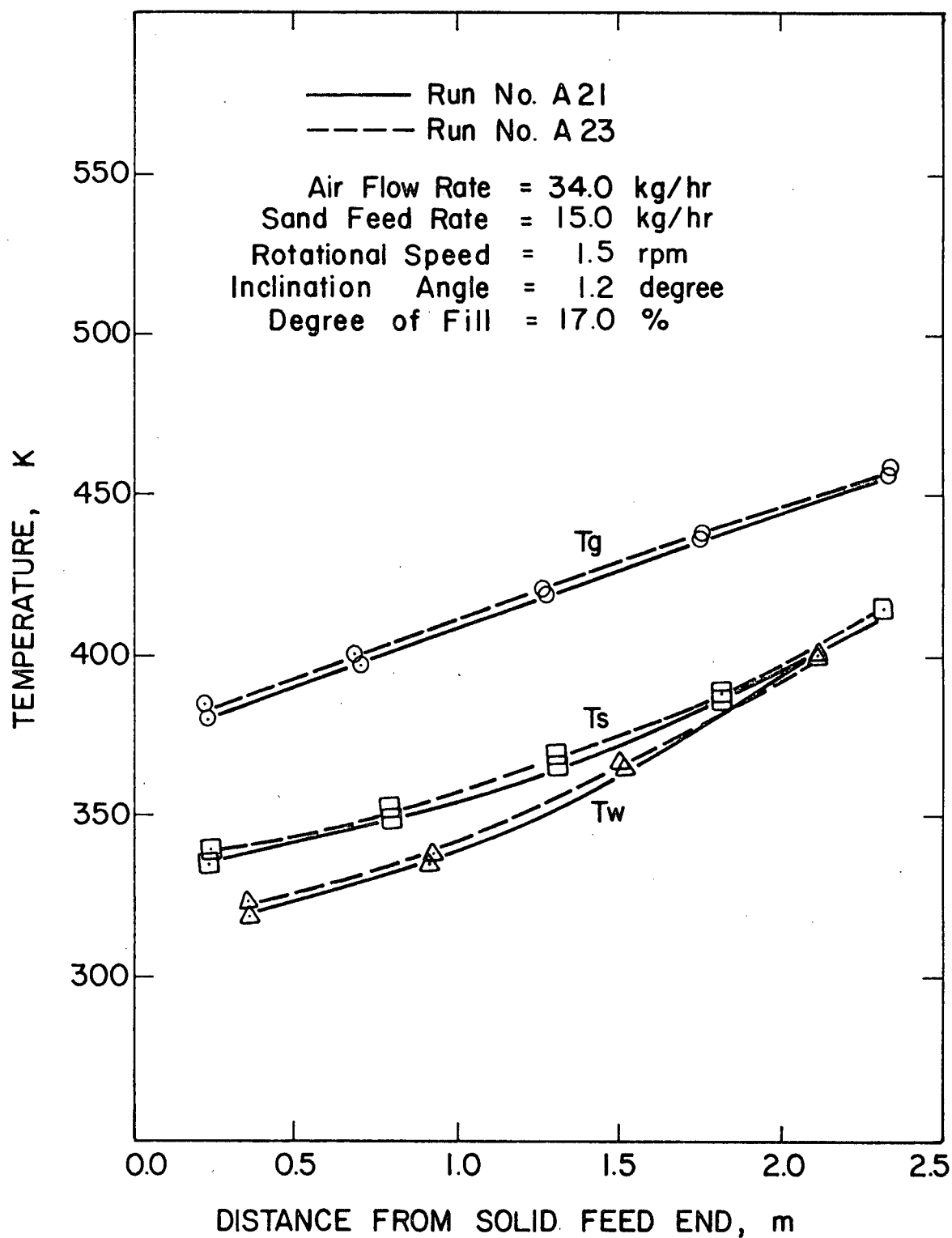
Figure 6-21 Reproducibility of Axial Temperature Profiles along Rotary Kiln
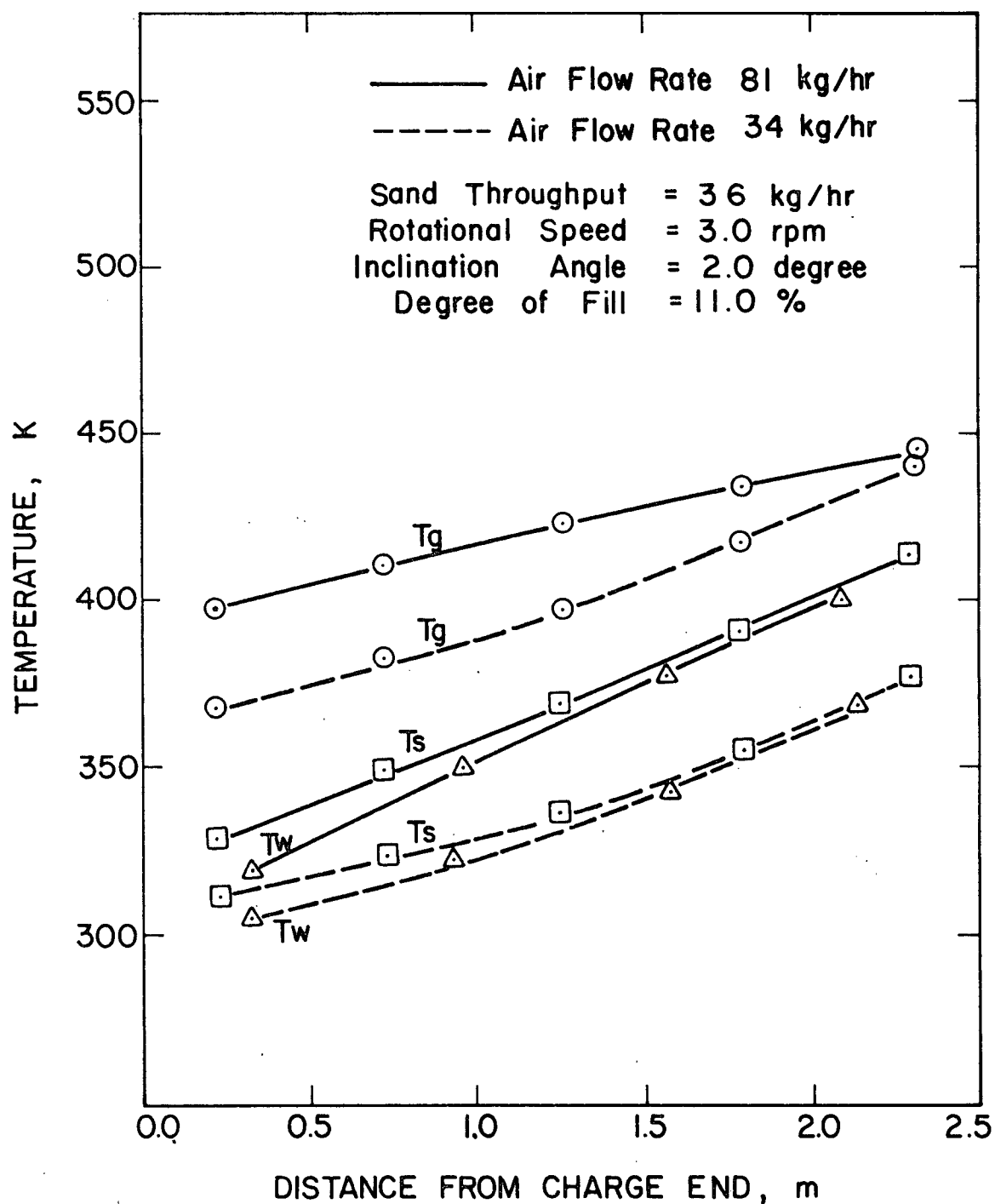
Figure 6-22   Effect of Air Flow Rate on Axial Temperature
             Profiles along Rotary Kiln
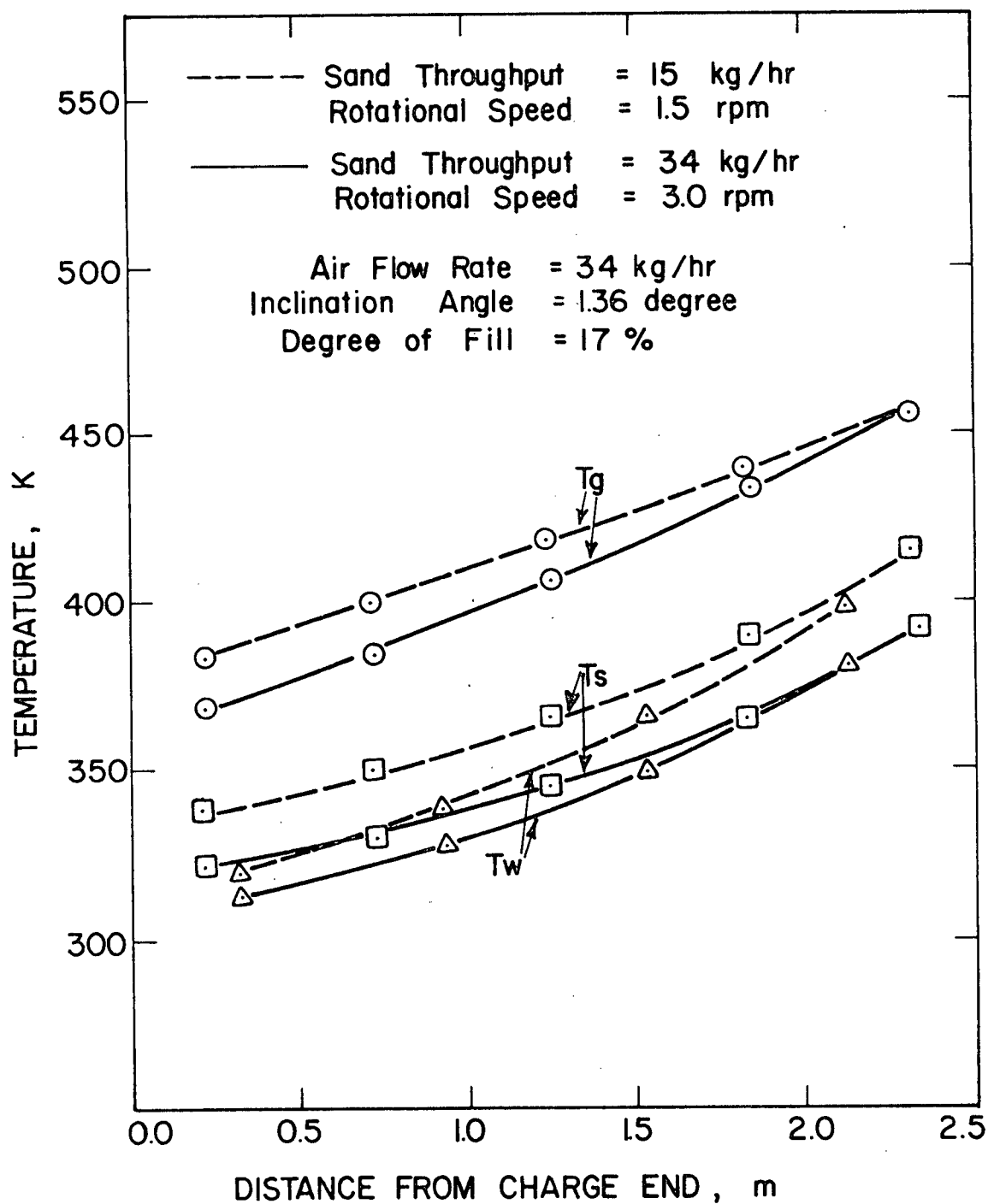
Figure 6-23   Effect of Sand Throughput and Rotational
Speed on Temperature Distribution

tain a uniform bed depth along the kiln, doubling rotational
speed requires a double sand feedrate. Meanwhile an increase
of rotational speed increases the gas to solids heat transfer
coefficient as will be demonstrated in Section 6.10, which re-
sults in an increase in heat flow from gas to sands accordingly.
Since $Q \propto W_g \Delta T_g$, the gas temperature drop is expected to be
higher for a higher rotational speed at a constant gas flowrate,
W_g. Thus the solid temperature is also expected to be lower for
a high rotational speed. Figure 6-24 shows the effect of air
inlet temperature. Air temperature near the discharge end drops
much more quickly for the high inlet temperature run than for
the low temperature run.

6.8 Calculation Method for Heat Transfer Coefficient

The calculation of heat transfer coefficients was based
on a simple but realistic equation with the following assumptions:

1. The gas phase is in plug flow and at uniform temperature
   at each axial position.
2. Since the solid bed temperature is radially uniform,
   therefore, the solid temperature is a function of axial
   distance only. Solids move in plug flow.
3. The wall temperature is taken to be independent of angle
   and time. The experimental results show insignificant
   fluctuations of wall temperature under conditions used.
4. The bed surface is assumed flat, and in the calculation
   of gas/bed coefficients its area is taken equal to the
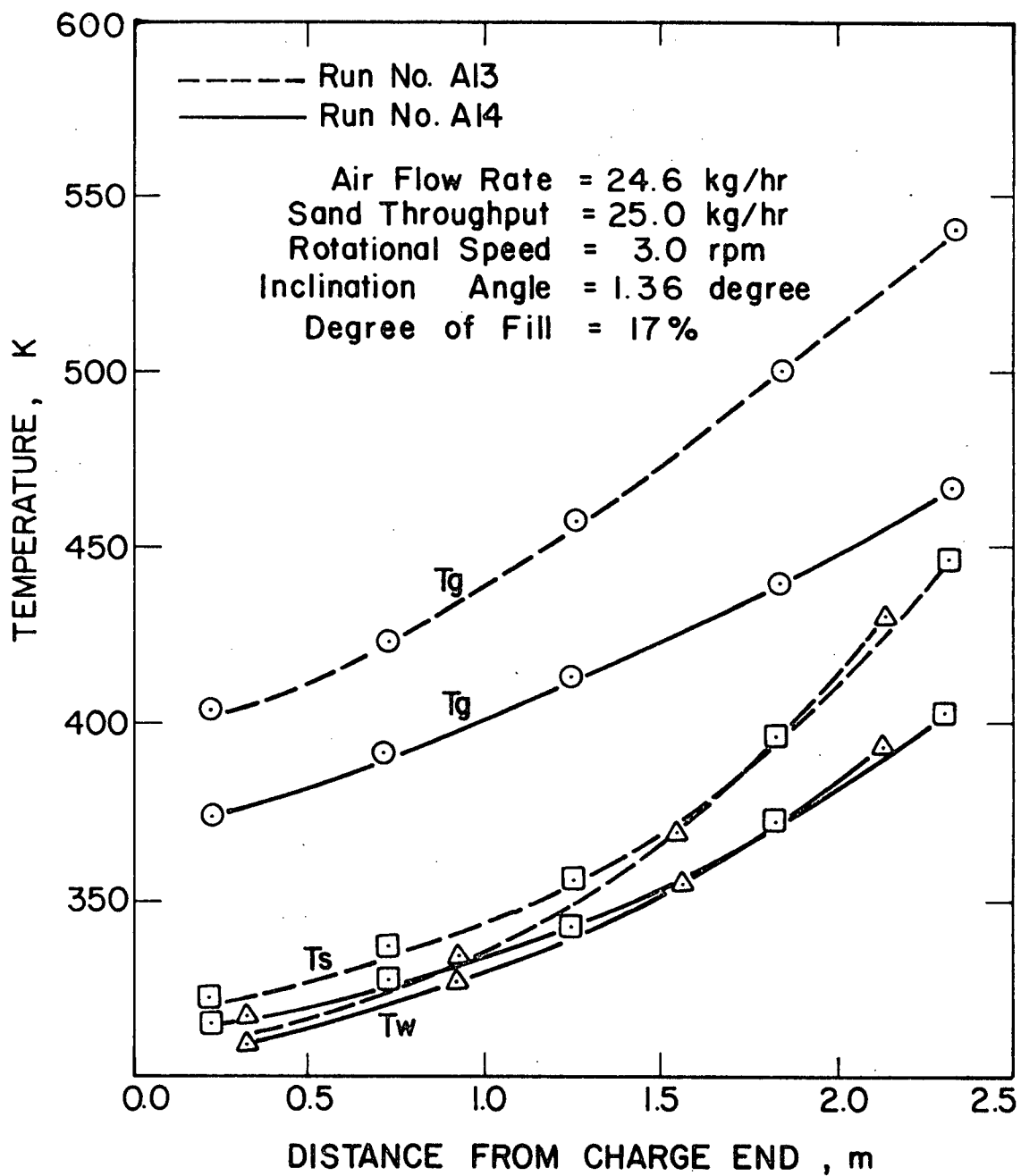
Figure 6-24   Effect of Air Inlet Temperature on
              Temperature Distribution

chord length times the bed length.

The above assumptions are valid for the whole length of the kiln except the zone of the solid inlet, where the particles fall from the feeding chute and shower through the air stream. In this region the temperature of the particles rises rapidly.

From an enthalpy balance taken over an incremental axial length of kiln as illustrated in Figure 6-25, the following equations can be easily derived:

Gas phase

$$\frac{dH_g}{dx} = q_{gs}(x) + q_{gw}(x) \tag{6-4}$$

Solid phase

$$\frac{dH_s}{dx} = q_{gs}(x) - q_{sw}(x) \tag{6-5}$$

The second term in equation 6-5 is written with the sign appropriate to the case where $T_s > T_w$. H is the enthalpy and is defined as

$$H_g = W_g \overline{C}_{pg}(T_g - T_{g_r}) \tag{6-6}$$

and

$$H_s = W_s \overline{C}_{ps}(T_s - T_{s_r}) \tag{6-7}$$
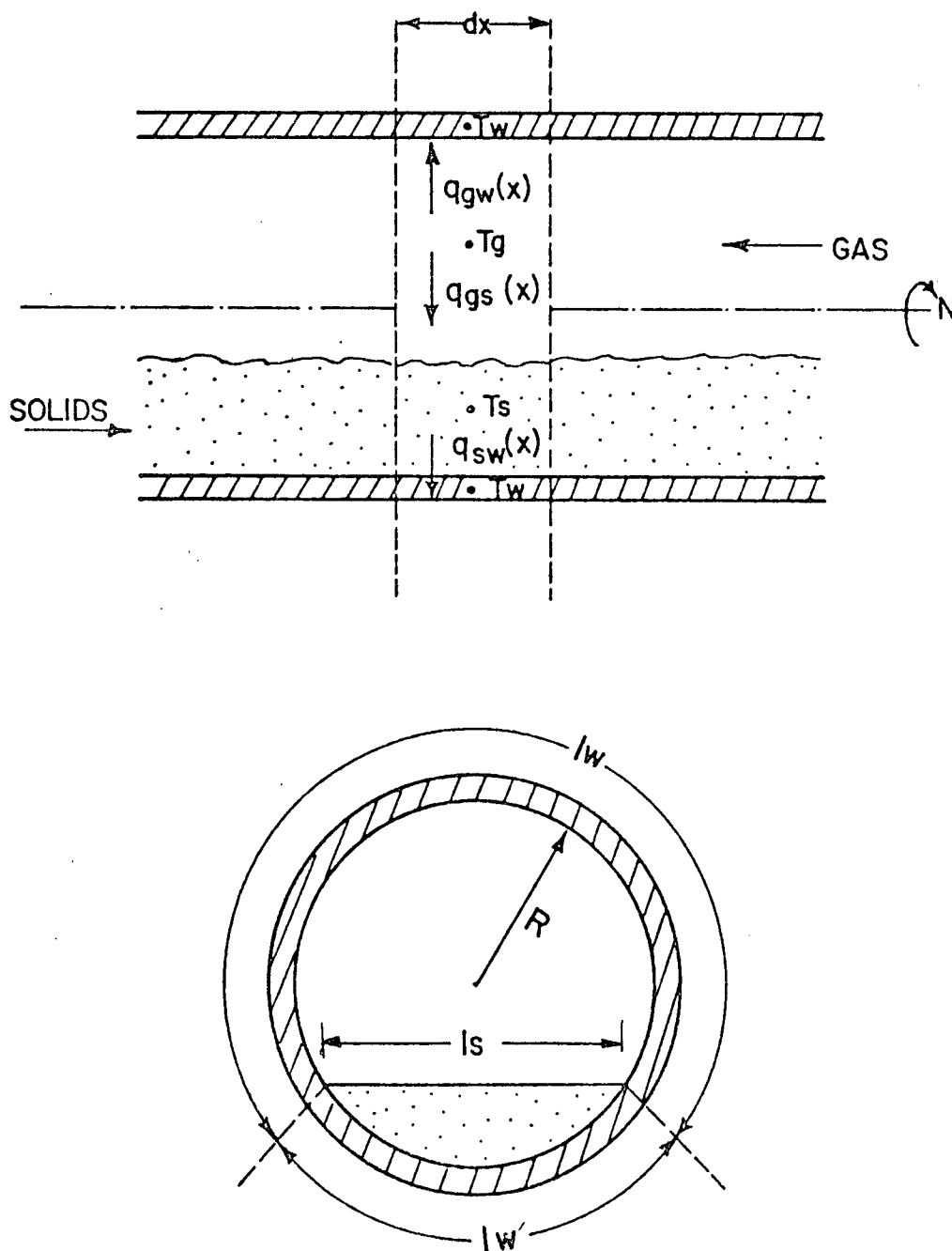
Figure 6-25 Differential Section of Rotary Kiln.

where T_{g_r}, T_{s_r} are reference temperatures for gas and solid respectively and q represents a heat flow per unit length. The substitution of equations 6-6 and 6-7 into equations 6-4 and 6-5 respectively, gives

$$\frac{dH_g}{dx} = C_{pg} W_g \frac{dT_g}{dx} \tag{6-8}$$

$$\frac{dH_s}{dx} = C_{ps} W_s \frac{dT_s}{dx} \tag{6-9}$$

The heat transfer terms, $q_{gs}(x)$, $q_{gw}(x)$ and $q_{sw}(x)$ are defined in terms of heat transfer coefficients,

$$q_{gs}(x) = h_{gs}(x) l_s (T_g - T_s) \tag{6-10}$$

$$q_{gw}(x) = h_{gw}(x) l_w (T_g - T_w) \tag{6-11}$$

$$q_{sw}(x) = h_{sw}(x) l_w (T_s - T_w) \tag{6-12}$$

With equations 6-8 to 6-12, equations 6-4 and 6-5 become

$$C_{pg} W_g \frac{dT_g}{dx} = h_{gs}(x) l_s (T_g - T_s) + h_{gw}(x) l_w (T_s - T_w) \tag{6-13}$$

$$C_{ps} W_s \frac{dT_s}{dx} = h_{gs}(x) l_s (T_g - T_s) - h_{sw}(x) l_w \cdot (T_s - T_w)$$

$$(6-14)$$

In these two equations, T_g, T_s are obtained from experimental measurements and the axial gradients, $\frac{dT_g}{dx}$ and $\frac{dT_s}{dx}$ are calculated from the temperature distribution along the kiln by use of spline functions. However, there are three unknown variables, $h_{gs}(x)$, $h_{gw}(x)$ and $h_{sw}(x)$ in equations 6-13 and 6-14. In order to evaluate the heat transfer coefficients from gas to solid, and gas to wall, one must know $h_{sw}(x)$, the heat transfer coefficient from solid to wall. Fortunately the solid bed-wall heat transfer coefficients are available in the literature and these experimental data have been correlated under the frame of penetration model. The result is given in the next section. Once $h_{sw}(x)$ is known, then heat transfer rate from gas to solid bed is calculated by

$$q_{gs}(x) = \frac{dH_s}{dx} + q_{sw}(x) \qquad (6-15)$$

that, in turn, is used to calculate heat transfer rate from gas to wall, $q_{sw}(x)$ by

$$q_{gw}(x) = \frac{dH_g}{dx} - q_{gs}(x) \qquad (6-16)$$

$q_{gs}(x)$, $q_{gw}(x)$ are local heat transfer rates. The average heat transfer rate per unit length of kiln can be calculated as

$$\bar{q}_{gs} = \int_{x_1}^{x_2} q_{gs}(x) \, dx \; / \; (x_2 - x_1) \qquad (6\text{-}17)$$

and

$$\bar{q}_{gw} = \int_{x_1}^{x_2} q_{gw}(x) \, dx \; / \; (x_2 - x_1) \qquad (6\text{-}18)$$

The logarithmic mean heat transfer coefficients for gas to solids and gas to wall are represented by

$$h_{gs} = \bar{q}_{gs} \; / \; l_s (T_g - T_s)_{lm} \qquad (6\text{-}19)$$

$$h_{gw} = \bar{q}_{gw} \; / \; l_w (T_g - T_w)_{lm} \qquad (6\text{-}20)$$

respectively, where

$$(T_g - T_s)_{lm} = \frac{(T_g - T_s)_{x_2} - (T_g - T_s)_{x_1}}{\ln \dfrac{(T_g - T_s)_{x_2}}{(T_g - T_s)_{x_1}}}$$

and

$$(T_g - T_w)_{lm} = \frac{(T_g - T_w)_{x_1} - (T_g - T_w)_{x_1}}{\ln \dfrac{(T_g - T_w)_{x_2}}{(T_g - T_w)_{x_1}}}$$

The heat lost through the kiln wall to the surroundings can be estimated by the heat conduction equation for the insulation material

$$q_1(x) = \frac{2\ k_i\ (T_w - T_{in})}{\ln\ (D_{in}/D_w)} \tag{6-21}$$

where k_i: thermal conductivity of insulation material. D_w, D_{in}, diameters where temperature probes for wall and insulation material.

From experimental measurements of wall temperature and the temperature of insulation material the heat loss through the wall may be calculated.

A heat balance over a section of the wall yields

$$q_1(x) = q_{gw}(x) + q_{sw}(x) \tag{6-22}$$

The subtraction of equation 6-4 from equation 6-5 also gives the sum of $q_{gw}(x) + q_{sw}(x)$

$$\frac{dH_g}{dx} - \frac{dH_s}{dx} = q_{gw}(x) + q_{sw}(x) \tag{6-23}$$

These two equations are used to check the heat loss through the wall. A local heat balance deviation was defined:

Local Deviation = $100 \left[q_s(x) + q_l(x) - q_g(x) \right] / q_g(x)$

Thus negative deviations indicated that more heat was lost from the gas than was gained by the solids and lost through the wall.

6.9   Bed to Wall Heat Transfer

In order to evaluate heat transfer from gas to solids bed and wall, heat transfer from solids bed to wall or vice versa must be known. Although some experimental data for wall to solids bed heat transfer (3, 42, 43), together with proposed models are available in the literature, as described in Chapter 2 no proposed model yet satisfactorily represents all the published experimental data. An attempt was made to correlate the data within the frame of the penetration model. The simple penetration model with I.C. and B.C. as given in equations 2-23 leads to the following dimensionless equation

$$\frac{h_{sw} l_w'}{k_s} = 2 \sqrt{\frac{nR^2 \beta 2}{a}} \qquad (6-24)$$

Figure 6-26 plots the published data (3, 42, 43) in terms of $\dfrac{h_{sw} l_w'}{k_s}$ versus $\dfrac{nR^2 \beta}{a}$. The correlation in the figure shows

a very interesting result. The Nusselt number, $\dfrac{h_{sw} l_w'}{k_s}$ increases
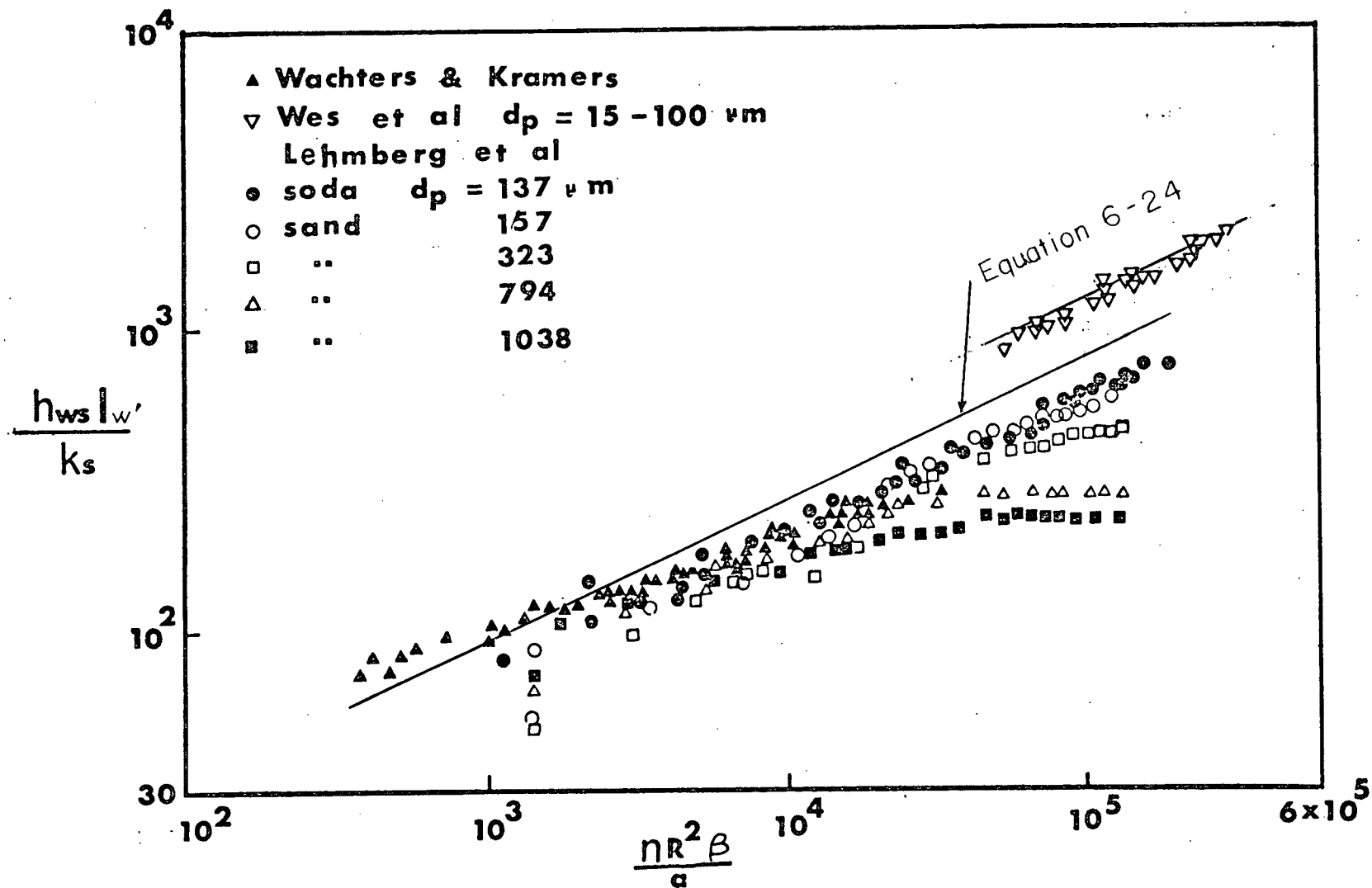
Figure 6-26 Correlation of Solids Bed-to-Wall Heat Transfer Coefficient.

with increasing $nR^2\beta/a$ according to the following equation,

$$\frac{h_{sw}l_{w'}}{k_s} = 11.6\left[\frac{nR^2\beta}{a}\right]^{0.3} \qquad \left[\frac{nR^2\beta}{a}\right] \le 10^4 \qquad (6\text{-}25)$$

At values of $nR^2\beta/a > 10^4$ the dependence of $h_{sw}l_{w'}/k_s$ on $nR^2\beta/a$ becomes stronger, then $h_{sw}l_{w'}/k_s$ approaches a limiting value which depends on particle sizes. The data with coarse particles tend to level off quickly beyond $nR^2\beta/a = 10^4$, whereas with fine particles, $h_{sw}l_{w'}/k_s$ continues to increase. The values of $h_{sw}l_{w'}/k_s$ estimated from equation 6-25 are lower than those from the simple penetration model from which equation 6-24 is derived. The negative deviation can be readily explained by the presence of a gas film near the wall, as postulated by Botterill et al (63) for the fluidized bed, Epstein and Mathur (45) for the spouted bed and Lehmberg et al (43) for the rotary kiln.

Ernest (64) carried out experiments on moving beds with definite contact time, t_c, using particle sizes 100 μm - 700 μm. A limiting value of heat transfer coefficient between wall and bed was found at very short contact time, $t_c < 0.1$ second. The limiting value depended on particle size. The contact time between the wall and the particles near the wall is approximately of the order of ten seconds under conditions of this study. The range of $nR^2\beta/a$ is from 10^3 to 10^4. Therefore equation 6-25 is used to calculate the heat transfer coefficients for the solids

bed and the wall.

6.10   Heat Transfer Coefficients

6.10a   Local Heat Transfer Coefficient

The length of the kiln taken to be the test section in
this study is the central 0.53 meters which gives a x/D ratio
of 2.78. The test section is situated between 1.25 m (L/D
= 6.56) from the solid charge end and 0.66 m (L/D = 3.46) from
the discharge end of the kiln.

The local heat flow per unit length from the gas and to
the solids was calculated as described in Section 6.8. Table
6-3 shows the results of heat flow determination within the
test section from a typical experiment. In the test section
the gas gives up the overall heat of 211.2 W of which about
73% goes to heat up the solids. The heat flow from the solids
to the wall accounts for the one third of the heat lost through
the wall. The local heat balance deviation varies from -5.9%
towards the charge end to +5.1% in the middle of the test sec-
tion, then to -12.4% near the hot end. However the overall
heat balance in the test section deviates only -1.4%. In their
high temperature experiment in the pilot kiln, Brimacombe and
Watkinson (4) reported the local heat balance deviation of +20%
near the charge end to -20% near the hot end. The change in
deviation, in their result, from negative to positive was
thought to be due to the neglect of downstream radiation.

The local heat transfer coefficients from the gas to

Table 6-3

Local Heat Flows and Heat Transfer Coefficients

x (m)	1.25	1.30	1.40	1.50	1.60	1.78
T_g (K)	462.0	464.3	469.3	474.6	480.4	492.0
T_s (K)	374.0	377.0	384.1	392.2	400.9	417.0
T_w (K)	369.2	372.9	380.3	388.0	395.7	410.5
T_c (K)	343.6	346.1	351.5	357.7	364.7	380.5
q_{sw} (W/m)	57.2	50.0	45.1	50.1	61.4	77.9
q_s (W/m)	169.2	190.8	226.5	252.1	267.3	268.1
q_{gs} (W/m)	226.4	240.8	271.7	302.2	328.7	345.9
q_g (W/m)	322.6	335.0	361.5	390.6	422.2	485.3
q_{gw} (W/m)	96.3	94.1	89.9	88.4	93.4	139.4
$q_{gw}+q_{sw}$ (W/m)	153.6	144.1	135.0	138.5	154.8	217.3
q_l (W/m)	134.0	140.2	150.7	158.6	162.2	157
local deviation, (%)	-5.9	-1.2%	4.3	5.1	1.3	-12.4
$h_{gs_{local}}$ (W/m^{2}K)	16.13	17.3	20.0	23.0	25.9	28.9
$h_{gw_{local}}$ (W/m^{2}K)	2.53	2.51	2.47	2.49	2.69	4.17

the solids and to the wall were calculated based on equations 6-10 and 6-11. The calculation results are included in Table 6-3 and shown in Figure 6-27 in which the local heat transfer coefficients are plotted against x, the distance from the charge end and against the ratio of x/D. As shown in Figure 6-27 both $h_{gs}(x)$ and $h_{gw}(x)$ increase as x increases towards the hot end. The $h_{gs}(x)$ gradually increases from 16.1 w/m^2K to 28.9 W/m^2K. The same trend was also obtained by Brimacombe and Watkinson (4) in their pilot kiln. In a typical run of their experiments the local heat flow received by the solids doubled from one end of the test section to the another end. Since the temperature difference, (T_g-T_s) remained the same over the test section in their study, the local heat transfer coefficients, thus, doubled from one end of the test section to another end. The shape of the increasing $h_{gw}(x)$ as shown in Figure 6-26 is found consistent with that for hot gas flowing through a tube near the entry region. As reported by Rohsenow and Hartnett(65) the local Nus- selt number increases sharply towards the gas entry region. Comparisons of the present results with those in the literature are given in section 6-10h.

The logarithmic mean heat transfer coefficients h_{gs} and h_{gw} over the test section are calculated by equations 6-19 and 6-20. The values of h_{gs} and h_{gw} are 22.4 W/m^2K and 3.0 W/m^2K respectively for the typical run as given in Table 6-3.
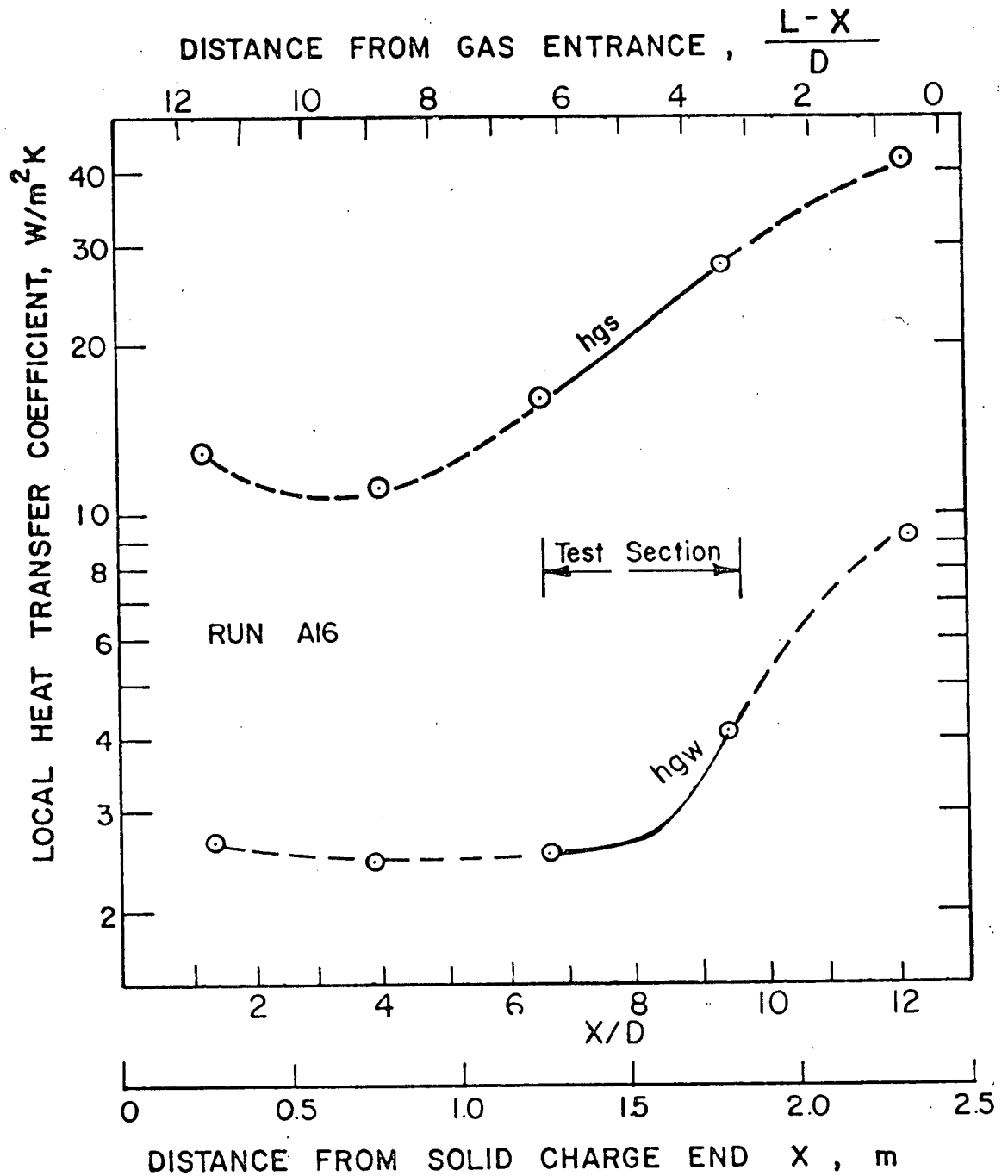
Figure 6-27   Local Heat Transfer Coefficient

6.10b   Effect of Air Temperature

Figure 6-28 shows the effect of average air temperature on heat transfer coefficient. Air temperatures, in this investigation, range from 350 K to 570 K. The air temperature has no effect on the gas to solids bed heat transfer coefficient. Watkinson and Brimacombe (63) reported a significant effect of gas temperature, ranging 650 K to 830 K, in a direct-fired rotary kiln. The average convective gas-solid coefficients, in their results, are in the range of 120 to 240 $W/m^2 K$. These values are much higher than the values, 18-53 $W/m^2 K$ obtained in the present study for a non-fired kiln. Figure 6-28 also shows that air temperature has little effect on h_{gw}. The values of h_{gs} are about an order of magnitude higher than h_{gw}. This difference is discussed below.

6-10c   Effect of Gas Flowrate

The effect of gas flowrate on heat transfer coefficients for both gas-solids and gas-wall was studied at constant solids throughput, rotational speed and inclination angle, which, in turn, results in constant degree of fill. The gas flow rate was varied over the range of 18.6 to 95 kg/hr, or 653 to 3334 $kg/hr-m^2$ (kiln cross section). The Reynolds number in the gas phase varied from 1600 to 7800. The heat transfer coefficients, h_{gs} and h_{gw}, are plotted against gas flow rate in Figure 6-29. As expected, raising the gas flow rate increases both gas to solids and gas to wall heat transfer coefficients.
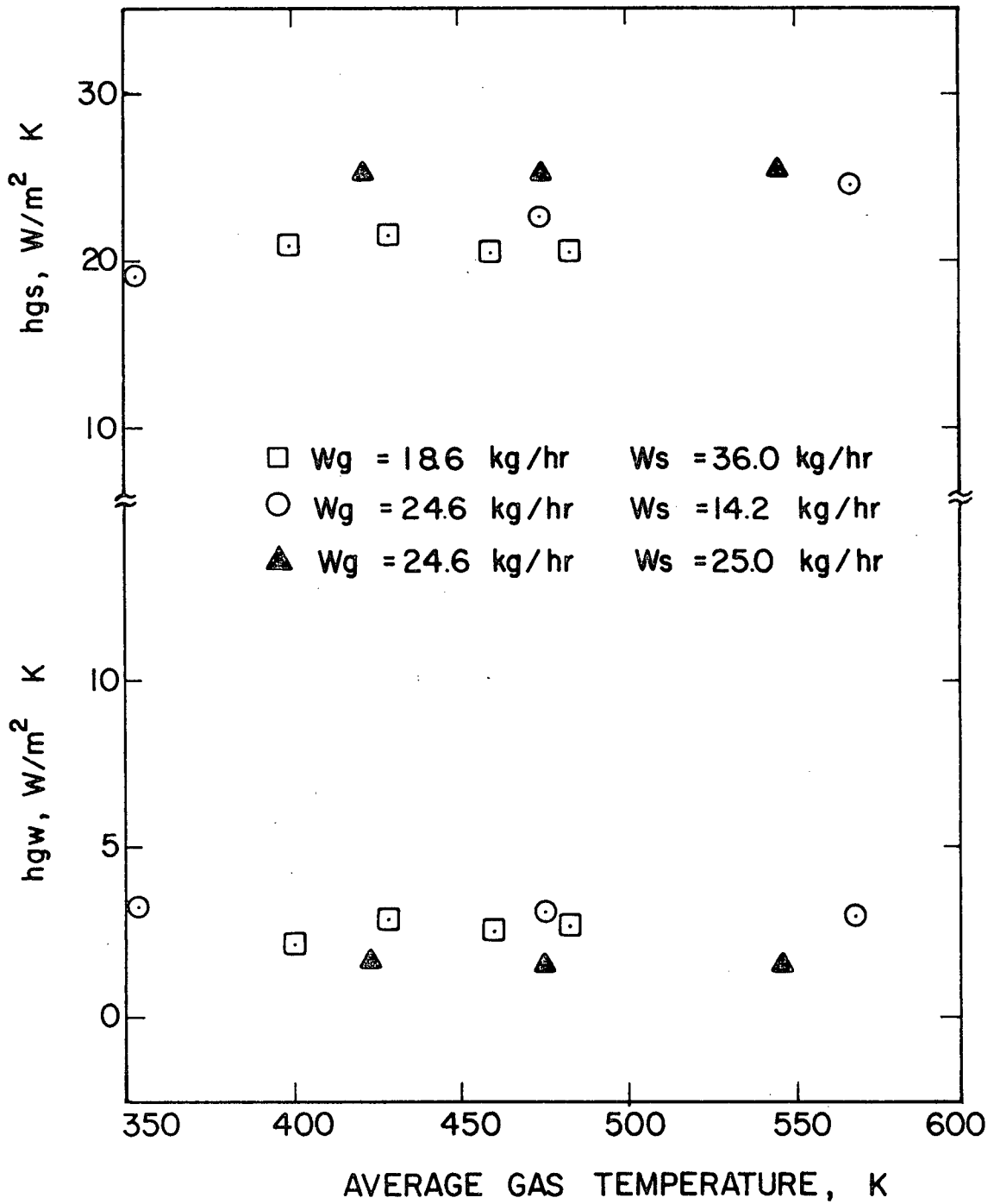
Figure 6-28   Effect of Gas Temperature on Heat Transfer
              Coefficient
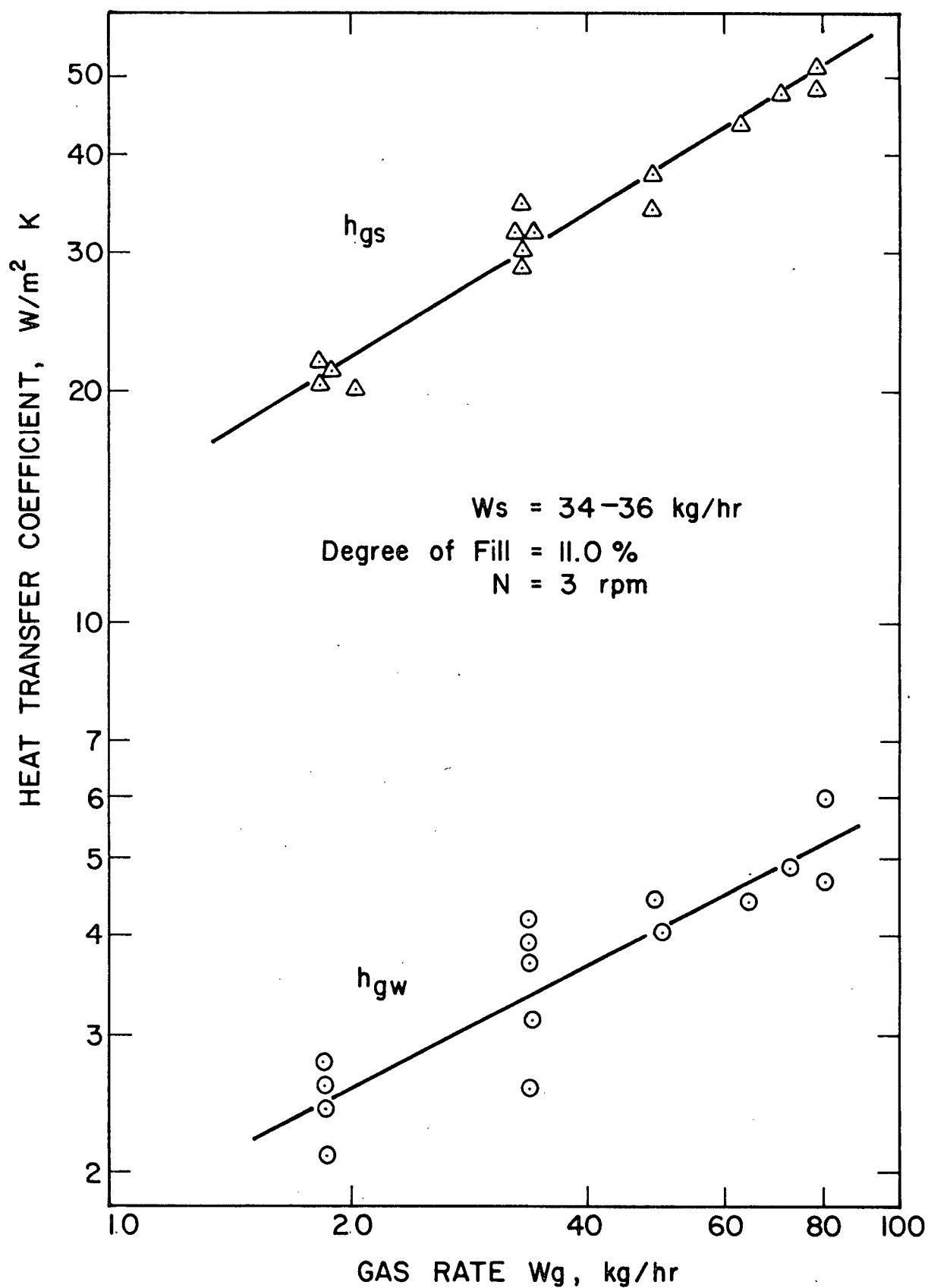
Figure 6-29   Effect of Gas Flow Rate on Heat Transfer
            Coefficient

As was noted above the values of h_{gs} are about an order of magnitude higher than h_{gw}. The higher values of h_{gs} are attributed to two related factors. The coefficient for the gas to solids heat transfer is based on the chord length of a plane bed surface. However the total surface area of particles on top of a static bed can be more than twice the plane surface area depending on particle arrangement. The other significant factor contributing to higher h_{gs} is rapid particle motion in lateral direction, which would prohibit the development of a viscous layer that would exist even on a rough plate, or on the kiln walls, and would present an even larger surface area for heat transfer.

If the thermal resistance of the gas/bed interface is pictured as consisting of two resistances in series, one on the gas side, and the other on the solid bed side, then the strong dependence of h_{gs} on gas flow rate suggests the major resistance for heat flow from the gas phase to the bed is on the gas side. Any means that could reduce this resistance would definitely increase the heat flow. At the normal rotational speed of the rotary kiln the particles roll on the surface at speeds much greater than the circumferential speed of the kiln. Thus, the interface consists of a rolling mass of particles which would create turbulence in the gas phase near the bed surface.

6.10d Effect of Rotational Speed

Figure 6-30 shows the effect of rotational speed on the
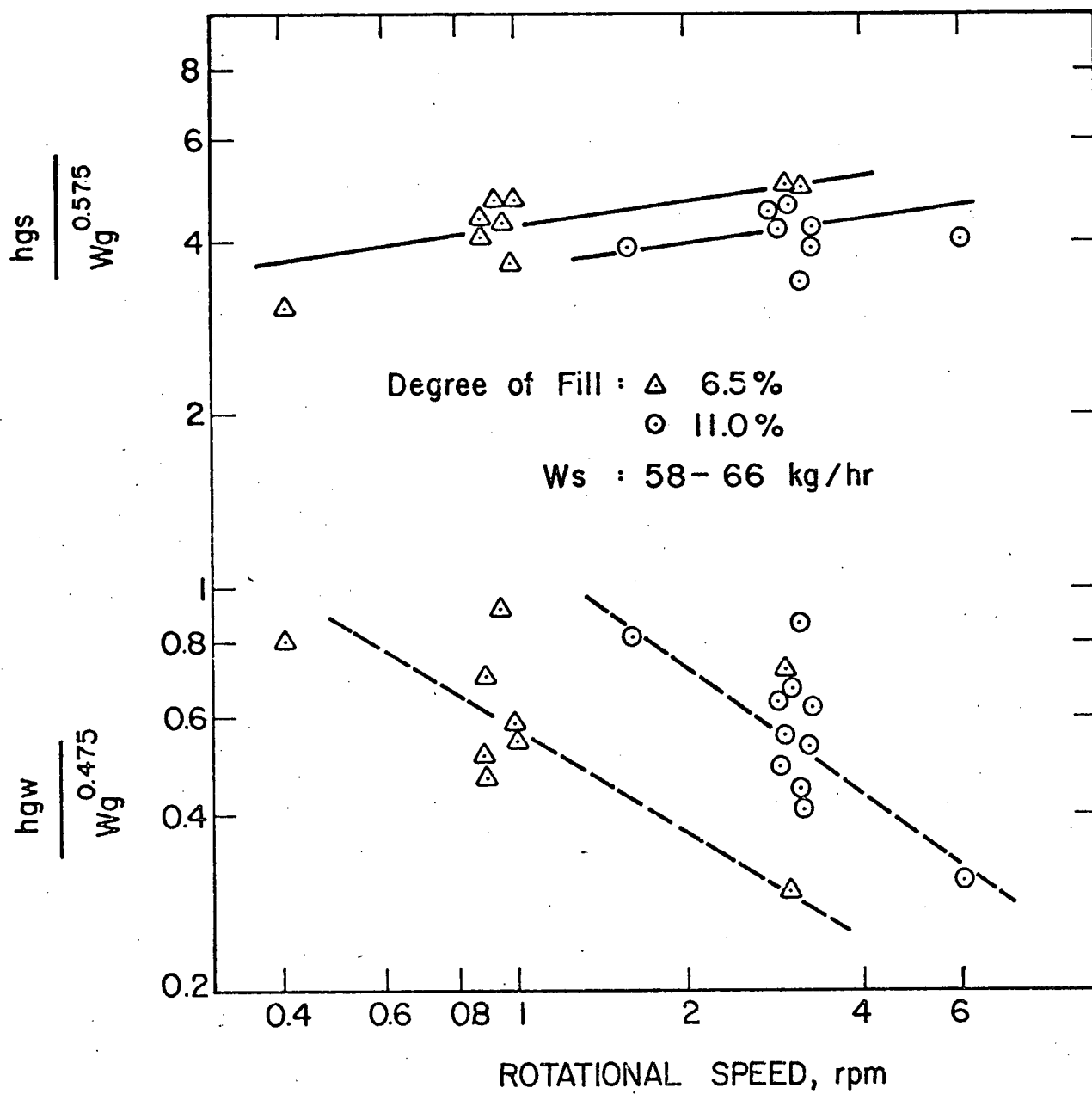
Figure 6-30   Effect of Rotational Speed on Heat
               Transfer Coefficient.

heat transfer coefficients, h_{gs} and h_{gw}. The effect of gas flow rate is excluded by dividing h_{gs} and h_{gw} with $W_g^{0.575}$ and $W_g^{0.475}$ respectively.

As seen in the figure rotational speed has a slightly positive effect on h_{gs}, and a significant negative effect on h_{gw}. The slightly positive effect of N on h_{gs} can be explained as follows. When heat is transferred from the gas to a stationary bed, heat first has to reach the bed surface by convection through a gas film and then penetrate into the bed by conduction. The convective heat transfer coefficient to a stationary bed can be estimated by the equations (66,67) developed for gas flowing over a rough flat plate or through a rough empty tube. As the kiln starts to rotate at low speed, the bed slumps as described in Chapter 2 . In a slumping bed the bed surface remains tranquil between slumps. On the tranquil surface heat is transferred to the exposed burden surface from the gas to create a thin hot layer of particulate material. When the burden slumps the gas "film" near the bed surface is suddenly agitated and the hot solid layer would mix with a layer mass of cooler material, leaving a fresh top surface to absorb heat during the next slump period. The periodic function of gas "film" disturbance and solid mixing certainly increases the heat transfer rate from the gas to the solid bed compared with that in a stationary bed. Under the slumping condition, the bed mixing is then expected to control the heat uptake by the bed. Figure 6-31 illustrates the expected effect of N on h_{gs}
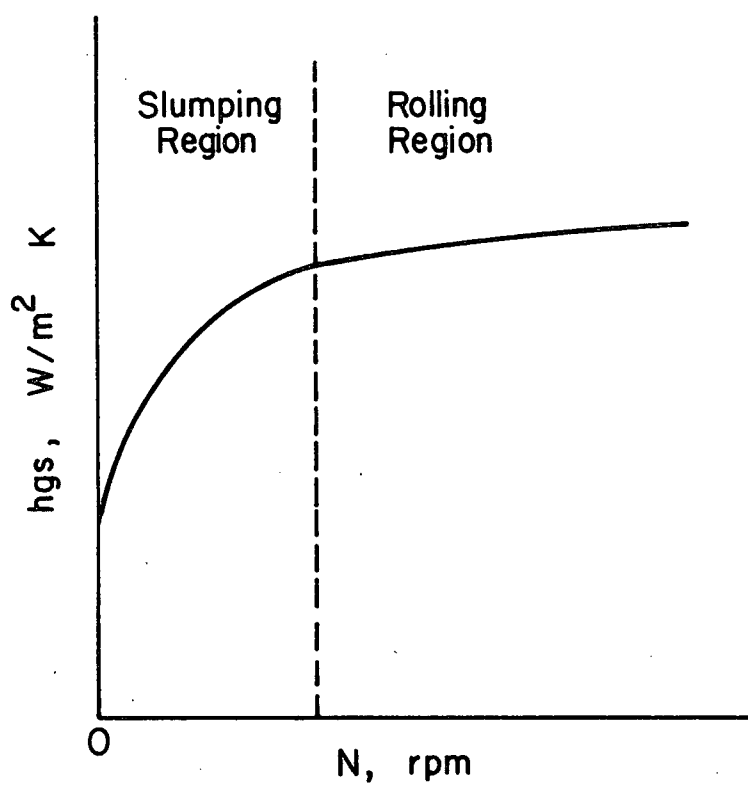
Figure 6-31 Effect of N on h$_{gs}$ in Both Slumping
and Rolling Beds

with several types of bed movement. The coefficient h_{gs} is expected to increase substantially with increasing N until at a speed is reached where rolling starts. Once rolling begins the dominating thermal resistance is thought to shift to the gas side. Particle lateral velocity on the bed surface is high enough to convey any heat received through the gas "film" as described before. In the rolling bed an increase of rotational speed increases the lateral velocity of surface particle as

$$V_1 \propto N^{0.5}$$

as shown in Figure 6-6. Since rotational speeds in this study range from 1 to 6 rpm, the lateral velocity increases by about 2.5 times, which apparently does not alter the gas side resistance markedly. As a result increasing rotational speed in the rolling bed increases the heat transfer coefficients from gas to solids bed only slightly.

The negative effect of increasing the rotational speed on the gas to wall coefficient appeared somewhat surprising. However, Cannon (68) reported the same effect of rotational speed on convective gas-wall heat transfer. His experiments were carried out with air flowing through an 1.52 m long empty rotating pipe, 0.0254 m in diameter. Laminar and transition regions of gas flow were investigated. The most significant effect of rotation was found to be in the transition region. He concluded that pipe rotation tends to stabilize the laminar flow so that transition occurs at higher Reynolds numbers.

This would suggest that, at constant flow conditions (same Reynolds number), increasing rotational speed would decrease the heat transfer coefficient in the transition region. Reynolds number in gas phase varied from 1600 to 7800 in this study, of which most data are in the range of 2000 to 4000 which is not in the fully turbulent region.

By regression analysis the slope of $h_{gs}/W_g^{0.575}$ vs. N is 0.091, and that of $h_{gw}/W_g^{0.475}$ vs. N is -0.297.

6.10e Effect of Degree of Fill

The effects of degree of fill on h_{gs} and h_{gw} are given in Figure 6-32. The ordinate are $h_{gs}/W_g^{0.575}N^{0.091}$ and $h_{gw}/W_g^{0.475}N^{-0.297}$ which exclude the effects of gas flow rate and rotational speed. It appears in the figure that h_{gs} decreases very slightly as the degree of fill increases while h_{gw} is independent of the degree of fill.

The negative effect of η on h_{gs} can be explained as follows. As described above, in the rolling bed, the transfer of heat from the gas to the solids bed can be thought of as comprising two steps. Heat is first transferred to the surface particles which mix with particles of other surface layers before the mixture returns into the bed. The mixed particles will remain in the bed until they emerge again on the bed surface. This suggests that the ratio of bed surface to bed volume is an important factor in the heat transfer process. The bed surface available for gas-bed heat transfer increases at a given size of kiln as the holdup increases according to
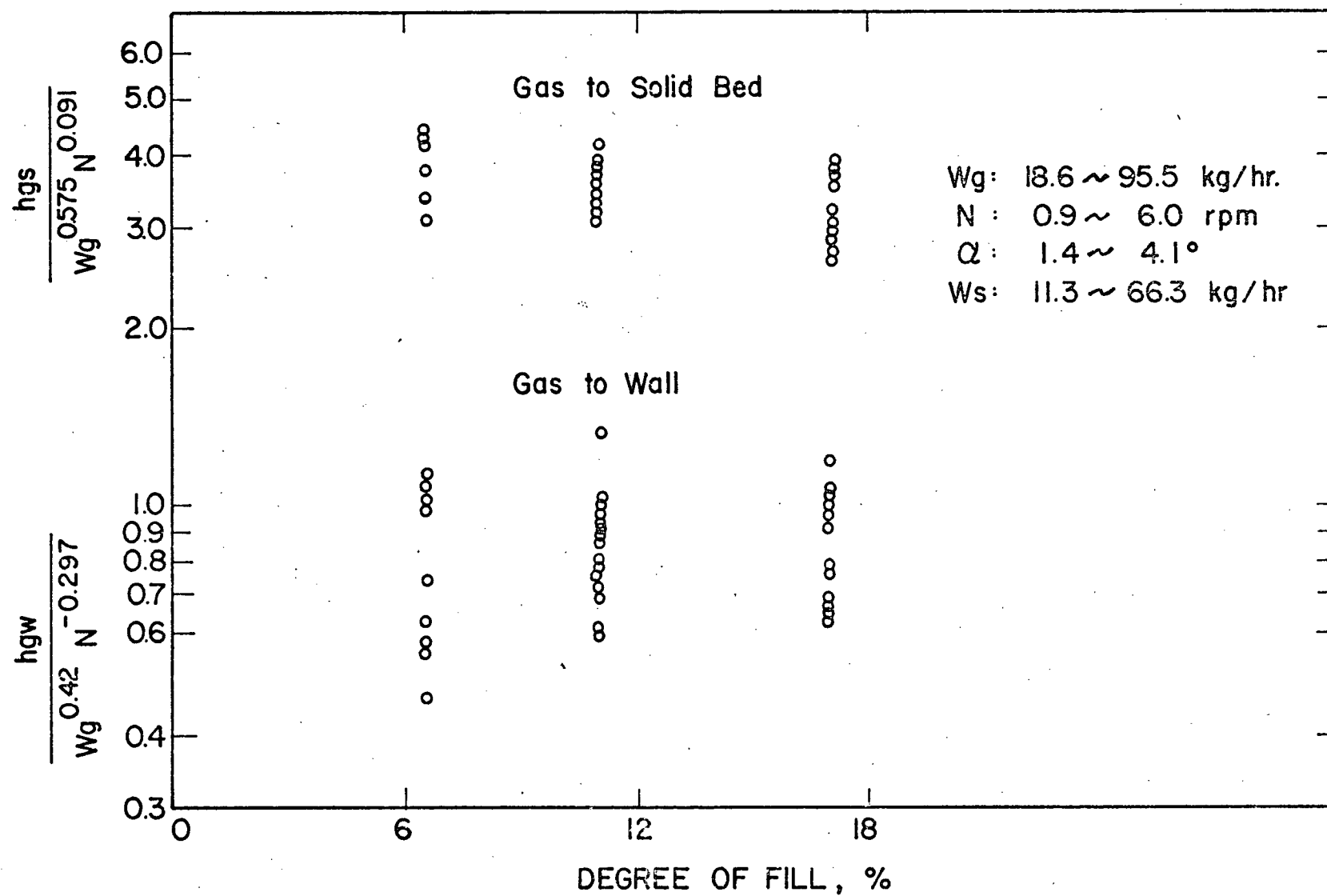
Figure 6-32   Effect of Degree of .Fill on Heat Transfer Coefficient.

$$A_s \propto \eta^{0.27} \qquad\qquad 0.04 < \eta < 0.30$$

however, the ratio of bed surface to bed volume decreases significantly as

$$\frac{\text{Bed surface}}{\text{Bed volume}} \propto \eta^{-0.73}$$

Although the heat transfer rate, q_{gs}, is directly proportional to the bed surface area, experimental data in Table 6-4 for various degrees of fill at the same operating conditions show a much weaker dependence of q_{gs} on A_s. In addition, the temperature differences, $(T_g - T_s)_{lm}$, were found about the same in these three runs. Thus, the heat transfer coefficients, according to

$$h_{gs} = \frac{q_{gs}}{A_s \Delta T_{lm}}$$

have a slightly negative dependence on the degree of fill. The slope of $h_{gs}/W_g^{0.575} N^{0.091}$ vs. η in the log-log plot as shown in Figure 6-32 is -0.171.

It is expected that the gas to wall heat transfer coefficients are independent of the degree of fill.

6.10f Effect of Solid Throughput and Inclination Angle

Figure 6-33 plots the term, $h_{gs}/W_g^{0.575} \eta^{-0.171} N^{0.091}$ against solids throughput with inclination angle as parameter,

Table 6-4

Effect of Degree of Fill on

Heat Transfer Rate and Bed Surface

	A22	A36	A47
η, %	17	11	6.5
A_s (m^2)	0.084	0.075	0.065
q_{gs} (W)	165	150	147
ΔT_{lm} (K)	65	63	66
h_{gs}	30.2	31.7	34.4

W_g 34 ~ 36 kg/hr

N 3 rpm

W_s 34 ~ 36 kg/hr
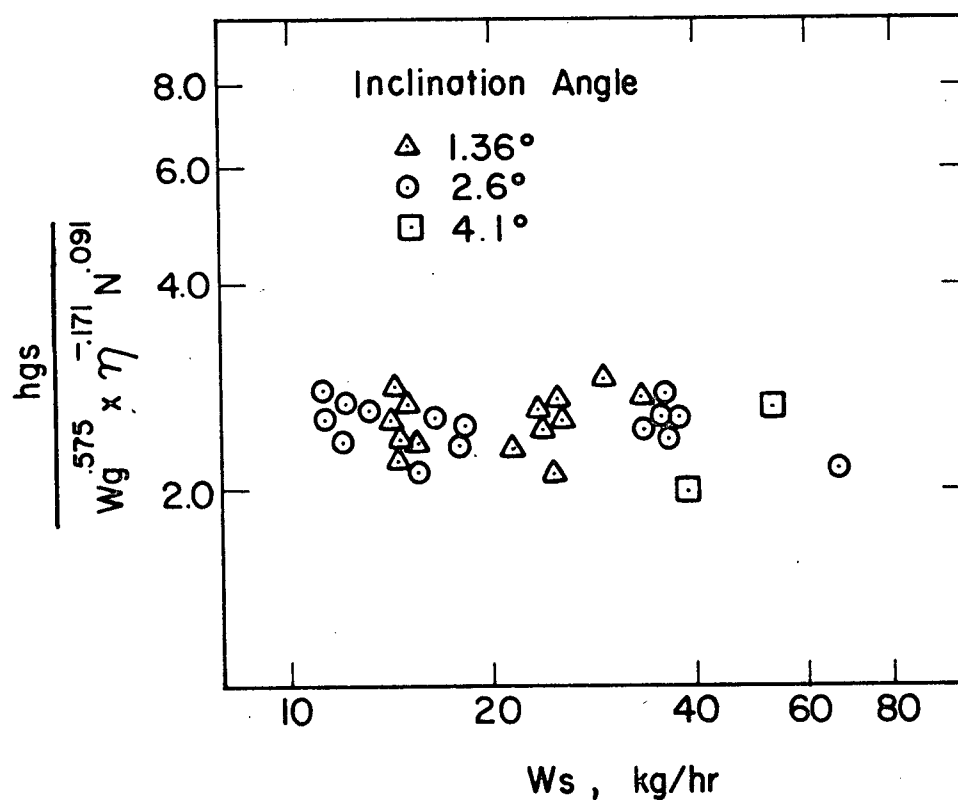
Figure 6-33 Effects of Solid Throughput and Inclination
Angle on Gas-Solids Bed Heat Transfer
Coefficient

while the plot of $h_{gw}/W_g^{0.475}N^{-0.297}$ vs. solid throughput is given in Figure 6-34. The results of regression analysis show that both solid throughput and inclination angle have insignicant effects on h_{gs} and h_{gw}. In a rolling bed, inclination angle would be expected to have no effect on heat transfer. Solid particles move through a rotary kiln as a result of continuous axial movements of particles on the bed surface. Axial velocity of particles is about one order of magnitude less that lateral velocity as seen in Figure 6-6 when particles roll on the bed surface. The effect of this slow axial movement on heat transfer is negligible compared with rapid lateral movements of particles, which are caused by the kilns rotation.

The regression analysis leads to the following equations for gas-solids heat transfer,

$$h_{gs} = 2.44 \ W_g^{0.575}{}_\eta^{-0.171}N^{0.091} \qquad (6-26)$$

and for gas to wall,

$$h_{gw} = 0.822 \ W_g^{0.475}N^{-0.297} \qquad (6-27)$$

6.10g Effect of Particle Size

Limestone with three different particle sizes was used to study the effect of particle size. The three sizes used were 10-20, 20-38 and 28-35 Tyler mesh which corresponds to

Figure 6-34 Effect of Solid Throughput and Inclination
Angle on Gas-Wall Heat Transfer Coefficient

average particle sizes of 1.26, 0.72 and 0.51 mm, respectively. Three runs of experiments were carried out for each of two different air flow rates, 18.6 kg/hr and 34.0 kg/hr. The experiments were carried out at temperatures much below calcining conditions. During the experiments a large amount of fine dust was created when limestone was fed into the kiln. The solid feed rate was originally set at 34 kg/hr, however the solid output at discharge end was measured only 24-27 kg/hr. The dust accounts for 20-30% of feed rate. Most of this dust was immediately carried away when limestone dropped into the bed from the chute and then did not enter the kiln. Over the range covered, the effect of particle size on heat transfer is insignificant as seen in Table 6-5. The narrow size range of particles may be the reason for the insignificant particle size effect. However Brimacombe and Watkinson (69) have also reported little effect on heat flow to limestone in a rotary kiln calciner over particle size range of 0.75 to 2.65 mm. Change in particle size by a factor of 2.5 apparently neither generates further turbulence in the gas "film", nor produces significant increase in actual surface area per plane chord surface area available for heat transfer in a closed-packed array. The Biot numbers for the three sizes of particles are very small, 0.036, 0.021 and 0.015 (h_p = 20 W/m^{2}K, k_s = 0.692 W/m^{2}K assumed), therefore the temperature within the particles becomes uniform after about one second of exposure to heat transfer.

Heat transfer coefficients from air to the limestone bed

Table 6-5

Gas to Solids Heat Transfer Coefficient

	Ottawa Sand		Limestone	
d_p (mm)	0.73	1.26	0.73	0.5
W_g (kg/hr)				
18.6	20.6-21.6 *	28.9	23.7	22.4
34	30.6-34.6	34.1	34.7	31.4

W_s (limestone)   24.4 - 27 kg/hr

W_s (Ottawa Sand)   34 - 36 kg/hr

N :   3 rpm

* $W/m^2 K$

are about the same as the case of Ottawa sand.

6.10h   Comparison with Previous Work

A comparison was made of the experimental data in the present study on the effect of gas flowrate with two equations recommended in Perry's Chemical Engineering Handbook:

$$h = 0.0981 \ G_g^{0.67} \qquad\qquad (2\text{-}32)$$

and

$$h = 0.0608 \ G_g^{0.46}/D \qquad\qquad (2\text{-}33)$$

G_g represents the gas flowrate per cross section area of the kiln.   Equations 2-32 and 2-33 are plotted in Figure 6-35 with the experimental data obtained in this study. Included in Figure 6-35 are the data of Friedman and Marshall (49) in a rotary dryer.   The data were for the conditions that no flights were used.

The heat transfer coefficients predicted by equations 2-32 and 2-33 lie between the experimental data for h_{gs} and h_{gw}.   Equation 2-32 was given based on the assumption that at high temperature the wall-film resistance to convection heat transfer from the gas to the wall is limiting and that at any point the bed temperature approaches the wall temperature. Although equations 2-32 and 2-33 were recommended for gas to wall heat transfer, these equations have been used for gas to solids bed.   In fact, the present work shows that h_{gs} is about
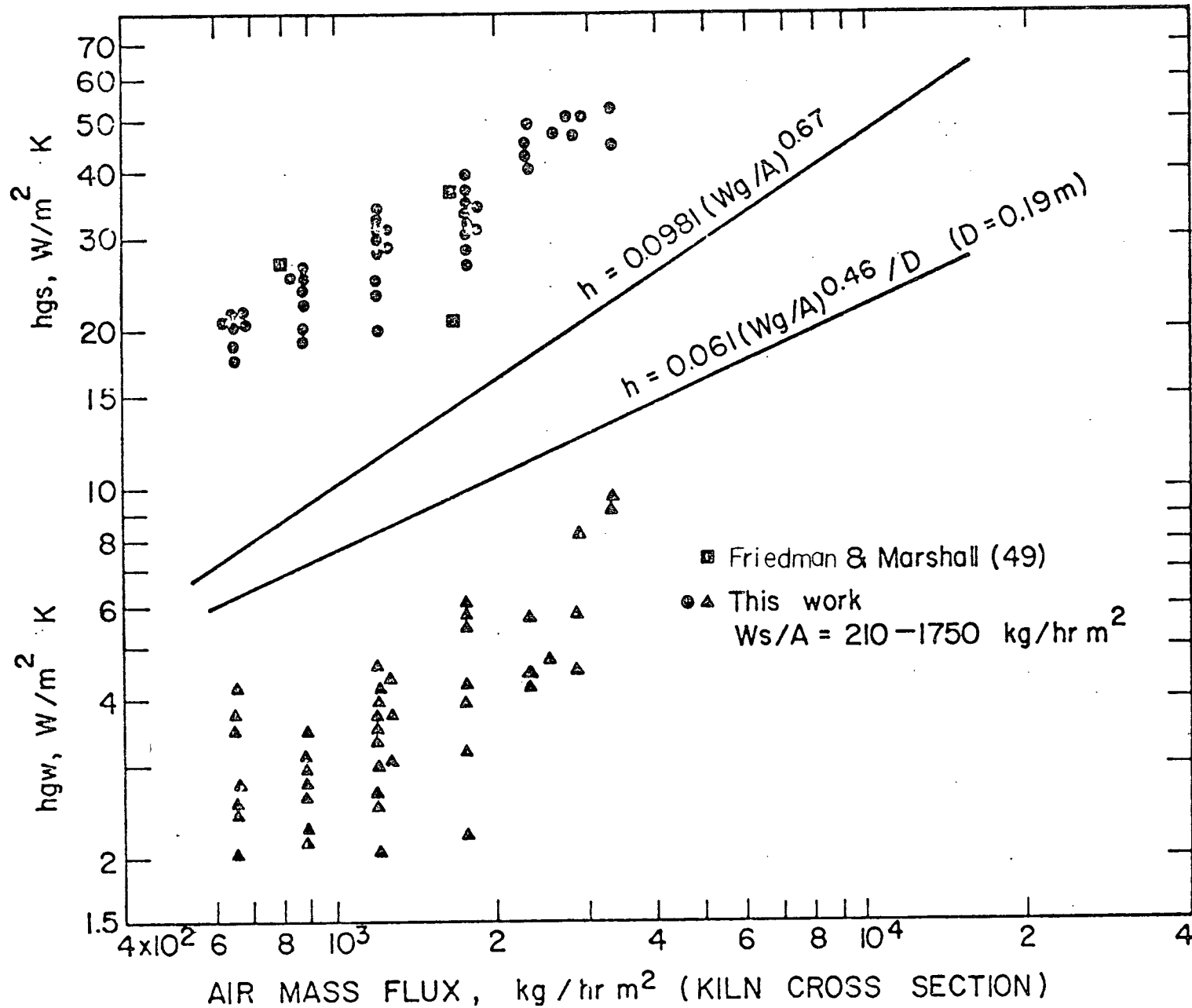
Figure 6-35   Comparison of Experimental Data on Heat Transfer Coefficients.

one order of magnitude higher than h_{gw} as seen in Figure 6-35.
Although h_{gw} shows more scatter than h_{gs}, the magnitude of h_{gw}
is the same as that for air flowing through a non-rotating tube.
Figure 6-36 depicts the heat transfer data by Kreith (55) for
air flowing through a 25.4-mm-ID, 1.52-m-long tube. The ratio
of L/D of the tube he used was 60. In a typical case an air
flow rate of 34 kg/hr at temperature 400 K through an empty
kiln of 0.19 m ID (G_g = 1200 kg/hr-m^2), the size used in this
study, results in a gas-to-wall heat transfer coefficient
1.7 W/m^{2}K according to Figure 6-36 (Nu = 10, Re = 2900). This
calculated value of h_{gw} is the same order of magnitude as, how-
ever, lower than the experimental h_{gw}, 2~4.7 W/m^{2}K, as given in
Figure 6-35. The higher experimental values may result from
the short length of the test section (L/D = 2.8) in the kiln,
compared with the long tube (L/D = 60) used by Kreith.

To rationalize the effect of the short length on heat trans-
fer three runs were carried out in the empty kiln. Table 6-6
shows the results from these three runs, together with the data
from Wes, et al for a 0.6-m-ID, 9.0-m-long empty drum. The
heat transfer coefficients in this work were calculated over
a test section of 0.53 m long, 0.66 m from the gas entry end.
Thus, the test section was located between the distance of
x/D = 3.47 and x/D = 6.25 from the end of the kiln. The air
flow rates for the test runs of this study and Wes et al were
in the transition region with Reynolds number, ranging from 2160 to
4140. The transition flow may complicate the explanation of
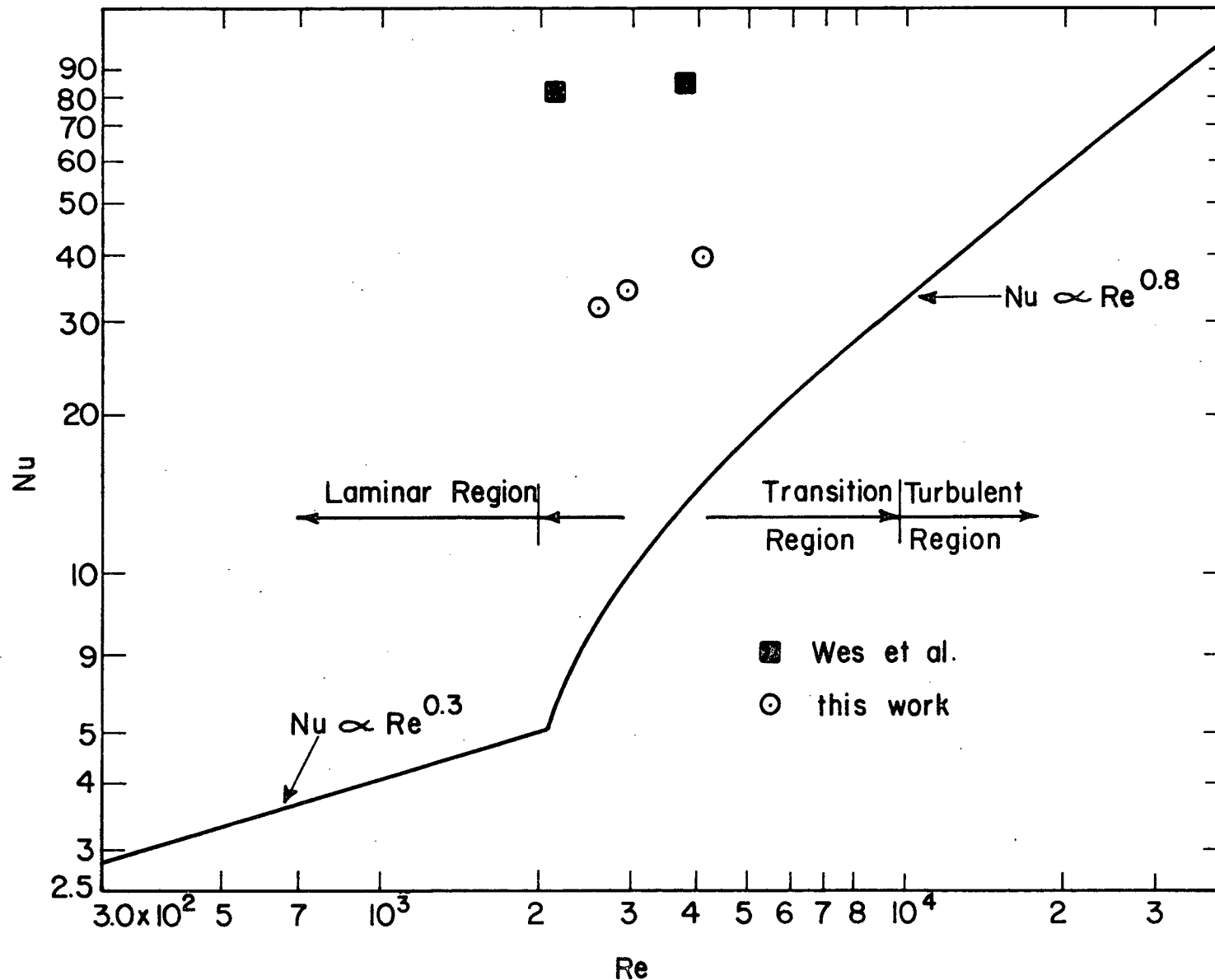
Figure 6-36   Gas-to-Wall Heat Transfer Coefficient in an Empty Kiln

Table 6-6   Comparison of Air-Wall Heat Transfer Coefficients in Empty Kilns

	W_g kg/hr	G_g kg/hr-m^2	Re (-)	h_{gw} W/m^{2}K	Nu_{gw} (-)	Nu_f* (-)	$\dfrac{Nu_{gw}}{Nu_f}$
This work***	34.0	1193	2647	5.40	32.2	8.2	3.9
	34.0	1193	2980	5.66	34.2	10.2	3.4
	50.5	1772	4140	6.67	39.8	15.0	2.7
Wes et al**	95.0	336.3	2160	4.9	80.1	5.5	14.6
	155.0	548.5	3520	5.1	83.4	12.5	6.7

* Taken from Kreith (58) for air flowing through a 25.4-mm-ID, 1.52-m-long heated tube (L/D = 60)

** For a 0.6-m-ID, 9-m-long empty drum (L/D = 15)

*** For a test section of 0.53-m-long

the effect of the entry section. The gas to wall heat transfer coefficients were found about the same for Wes, et al and this study, however Wes et al had the much higher Nusselt number because of larger value of kiln diameter. The values of Nu_f in Table 6-6 are considered for a fully-developed flow and taken from Figure 6-36. The Nusselt numbers in this study were found about 2.7 to 3.9 times Nu_f. The reason for this higher number is mainly due to the entrance effect. Figure 6-37 plots the variation of the local Nusselt number versus x/D in the combined thermal and hydrodynamic entry region of a tube with constant heat rate per unit of length. The curve is for laminar flow (Re = 2100). The test section of the kiln used in this study falls between x/D = 3.47 and 6.25 shown in Figure 6-37. This region gives an average Nusselt number of 11.3 W/m^2K which is 2.6 times the Nusselt number, Nu_f = 4.36, for the fully-developed flow in a tube. This number, 2.6, of Nu_{gw}/Nu_f is for the laminar flow however, it may well be that the same multiple exists for the transition flow.
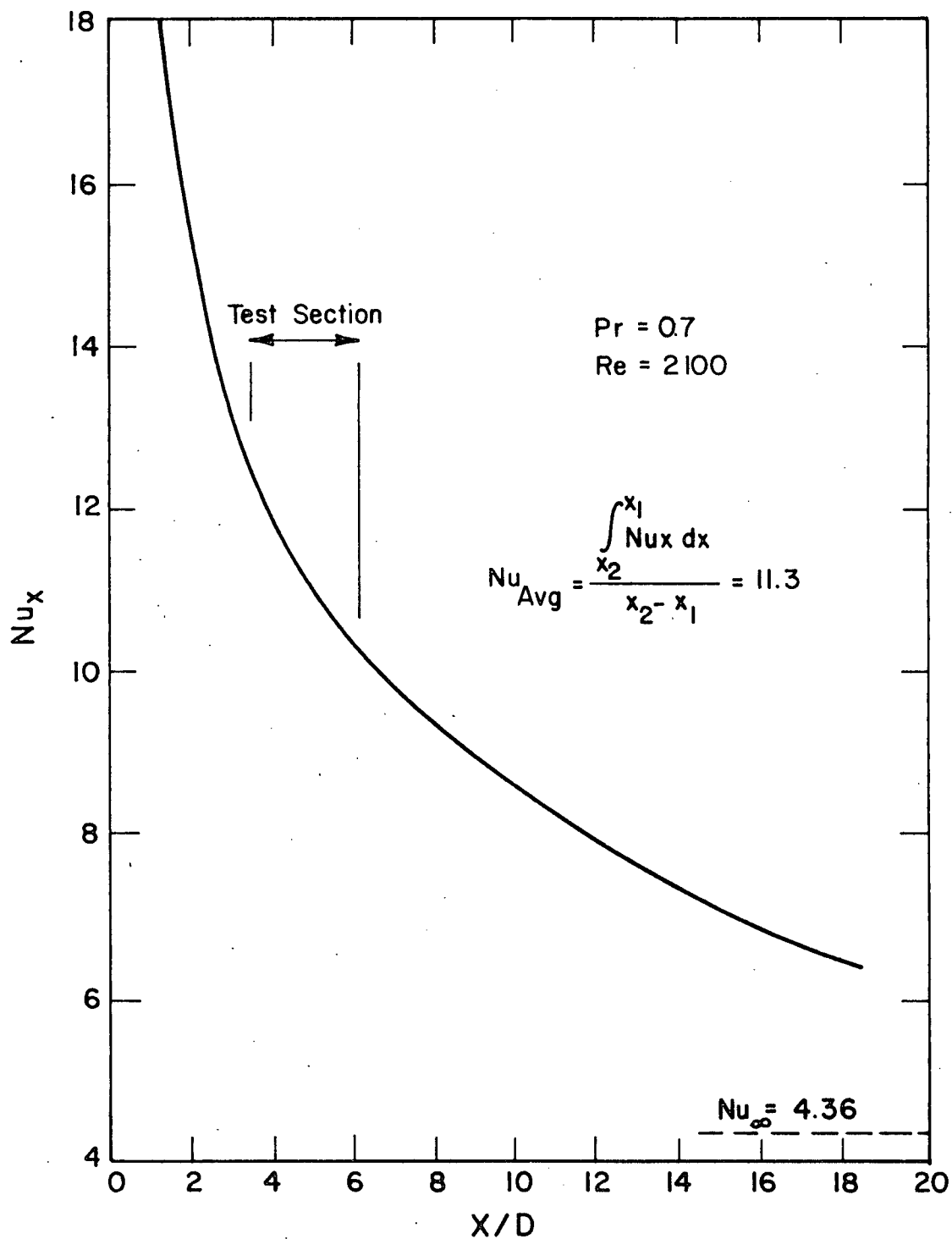
Figure 6-37   Variation of Local Nusselt Number in Thermal
              Entry Region of a Tube with Constant Heat
              Rate Per Unit of Length (65)

6.11 Correlation of Heat Transfer Coefficients

Cannon (68) studied the heat transfer from fluid flowing through a rotating pipe. In his analysis the heat transfer coefficient is a function of the variables listed in the following equation

$$h = f_1 (\omega, L, u_g, \mu_g, \rho_g, C_{pg}, D, k_g)$$

Dimensional analysis of this group of variables yields

$$Nu = f_2 (Re, Re_\omega, L/D, Pr)$$

where $Re_\omega = D^2 W \rho_g / \mu_g$, the rotational Reynolds number.

In a rotary kiln heat transfer is more complicated than that in an empty tube. The heat transfer coefficient is expected to depend on the following group of variables

$$h = f_3 (D, L, N, W_g, \mu_g, C_{pg}, k_g, \rho_g, W_s, d_p, k_s, C_{ps}, \rho_s, \eta, \alpha)$$

Dimensional analysis leads to the following equation,

$$\frac{hD_e}{k_g} = f_4 \left(\frac{D_e^2 \rho \omega_g}{\mu_g}, \frac{W_g}{D_e \mu_g}, \frac{L}{D}, \frac{C_{pg} \mu_g}{k_g}, \eta, \alpha, \frac{W_s}{W_g}, \frac{k_s}{k_g}, \frac{\rho_s}{\rho_g}, \frac{C_{ps}}{C_{pg}} \right) \quad (6-28)$$

where D_e is the equivalent diameter

$$D_e = \frac{4A_{\text{cross section}}}{\text{Wetted Perimeter}} = \frac{1}{2} \left(\frac{2\pi - \beta + \sin\beta}{\pi - \frac{\beta}{2} + \sin\frac{\beta}{2}} \right) \qquad (6\text{-}29)$$

Operating variables are of major interest in this study. Since only one fluid (air) and solids (Ottawa sand and limestone) of slightly different k_s/k_g, C_{ps}/C_{pg} and ρ_s/ρ_g were used in the experiments, the terms, $C_{pg}\mu_g/k_g$, k_s/k_g, ρ_s/ρ_g and C_{ps}/C_{pg} can be neglected in equation 6-28. In addition, the experiments were carried out in a kiln of single size, and the results show that W_s and α have no effects on heat transfer. Therefore equation 6-28 is simplied to equation 6-30.

$$Nu = a_0 Re^{a_1} Re_\omega^{a_2} \eta^{a_3} \qquad (6\text{-}30)$$

where a_0, a_1, a_2, a_3 are coefficients to be determined. Equation 6-30 is applicable to both gas-solid and gas-wall heat transfer.

Multiple linear regression was used to correlate the experimental data. The data of Nu_{gs} yield the following equation for gas to solid bed,

$$\ln Nu_{gs} = -0.777 + 0.535 \ln Re + 0.104 \ln Re_\omega - 0.341 \ln\eta \qquad (6\text{-}31)$$

that is

$$Nu_{gs} = 0.46 Re^{0.535} Re_\omega^{0.104} \eta^{-0.341} \qquad (6\text{-}32)$$

'The result of regression analysis for Nu_{gs} is given in Table 6-7. Figure 6-38 shows the comparison of the experimental data with calculations based on equation 6-32 for gas-solids bed heat transfer.

The same procedure was carried out for the correlation of gas-to-wall Nusselt number. The resultant equation is

$$Nu_{gw} = 1.54 \ Re^{0.575} \ Re_{\omega}^{-0.292} \qquad (6-33)$$

The regression analysis for equation 6-33 is given in Table 6-8. The degree of fill is insignificant for a 95% confidence limit. The comparison of the experimental data with equation 6-33 is given in Figure 6-39. The data for Nu_{gw} is relatively scattered. This is not surprising for experiments in a flow range covering the transition region.

6.12 Scaleup

For purposes of design and modelling, it is of interest to examine predicted heat transfer coefficients for larger size kilns using equations 6-32 and 6-33. Both equations were obtained from experimental results in a kiln of single size, 0.191 m. in diameter. The prediction of the effect of kiln size from these two equations should be considered as a projection only, and is subject to experimental verification in larger size kilns.

Equation 6-32 for Nu_{gs} may be rewritten in the form,

Table 6-7   Result of Regression Analysis for Nu_{gs}

Equation 6-31

$$\ln Nu_{gs} = b_0 + b_1 \ln Re + b_2 \ln Re_\omega + b_3 \ln + b_4 \ln \alpha$$

95% confidence interval

1. For $\ln Nu_{gs}$

    $R^2 = 0.9185$ Standard error = 0.1063

    F - probability = 0.00

2. For independent variables

    Significant variables

	Coefficients	Standard error	F-ratio	F-probability
constant	-0.777	0.356	4.769	0.033
ln Re	0.535	0.039	185.4	0.000
ln Re_ω	0.104	0.031	11.25	0.002
ln η	-0.341	0.057	35.8	0.000

    Insignificant variable

	Partial correlation	F-ratio	F-probability
ln α	0.054	0.1137	0.7344
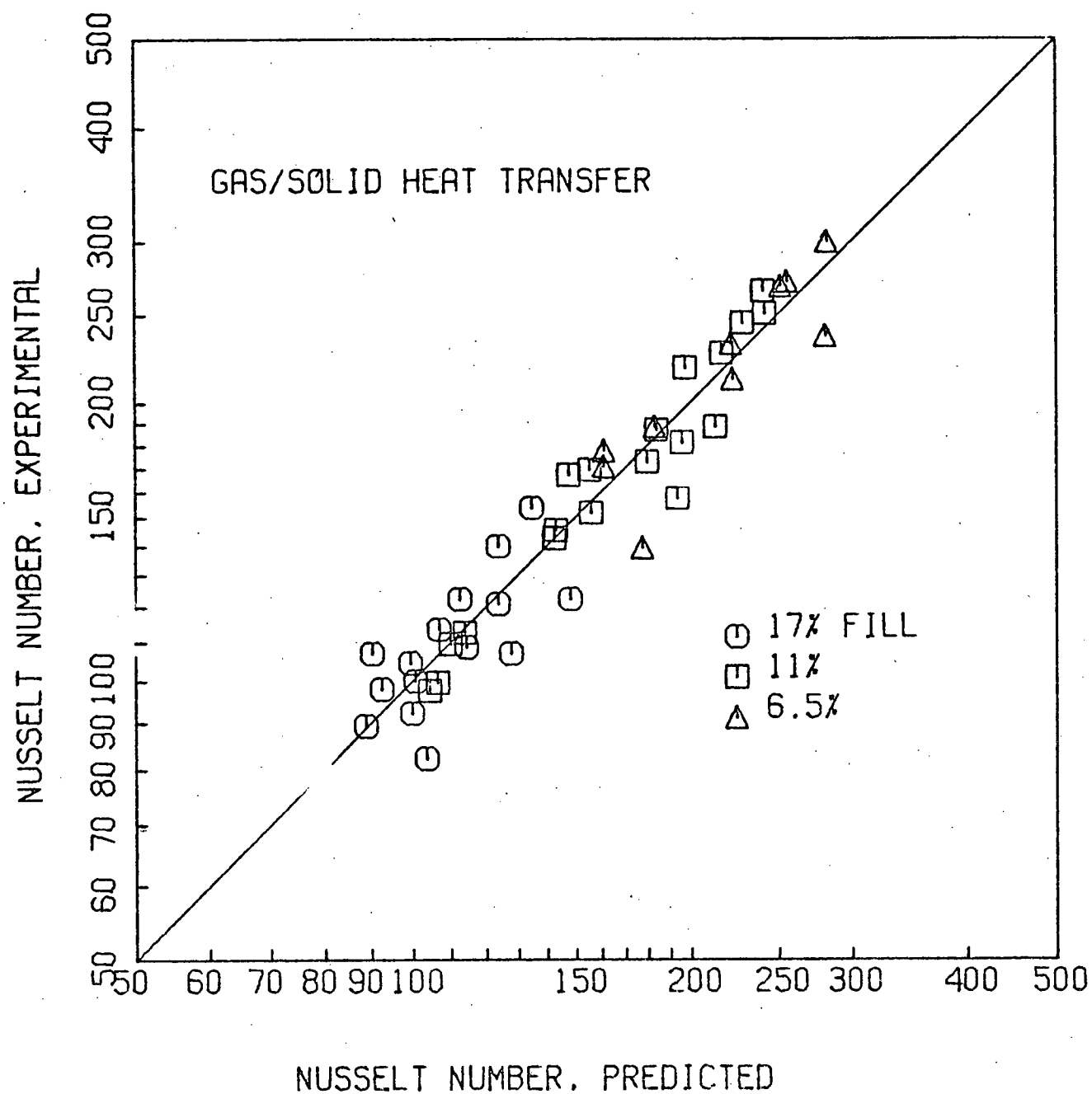
Figure 6-38   Comparison of Experimental Data with Predicted
            Values for N$_{ugs}$.

Table 6-8   Result of Regression Analysis for Nu_{gw}

Equation 6-33

$$\ln Nu_{gw} = a_0 + a_1 \ln Re + a_2 \ln Re_\omega + a_3 \ln \eta + a_4 \ln \alpha$$

1. For $\ln Nu_{gw}$

   $R^2 = 0.6390$ Standard error = 0.2624

   F - probability = 0.00

Significant variables

	Coefficient	Standard error	F-ratio	F-probability
constant	0.432	0.8779	0.2426	0.6303
ln Re	0.575	0.0807	50.79	0.000
ln Re_ω	-0.292	0.0731	15.91	0.003

Insignificant variables

	Partial correlation	F-ratio	F-probability
ln η	0.1322	0.7118	0.4085
ln α	0.1465	0.8769	0.3575
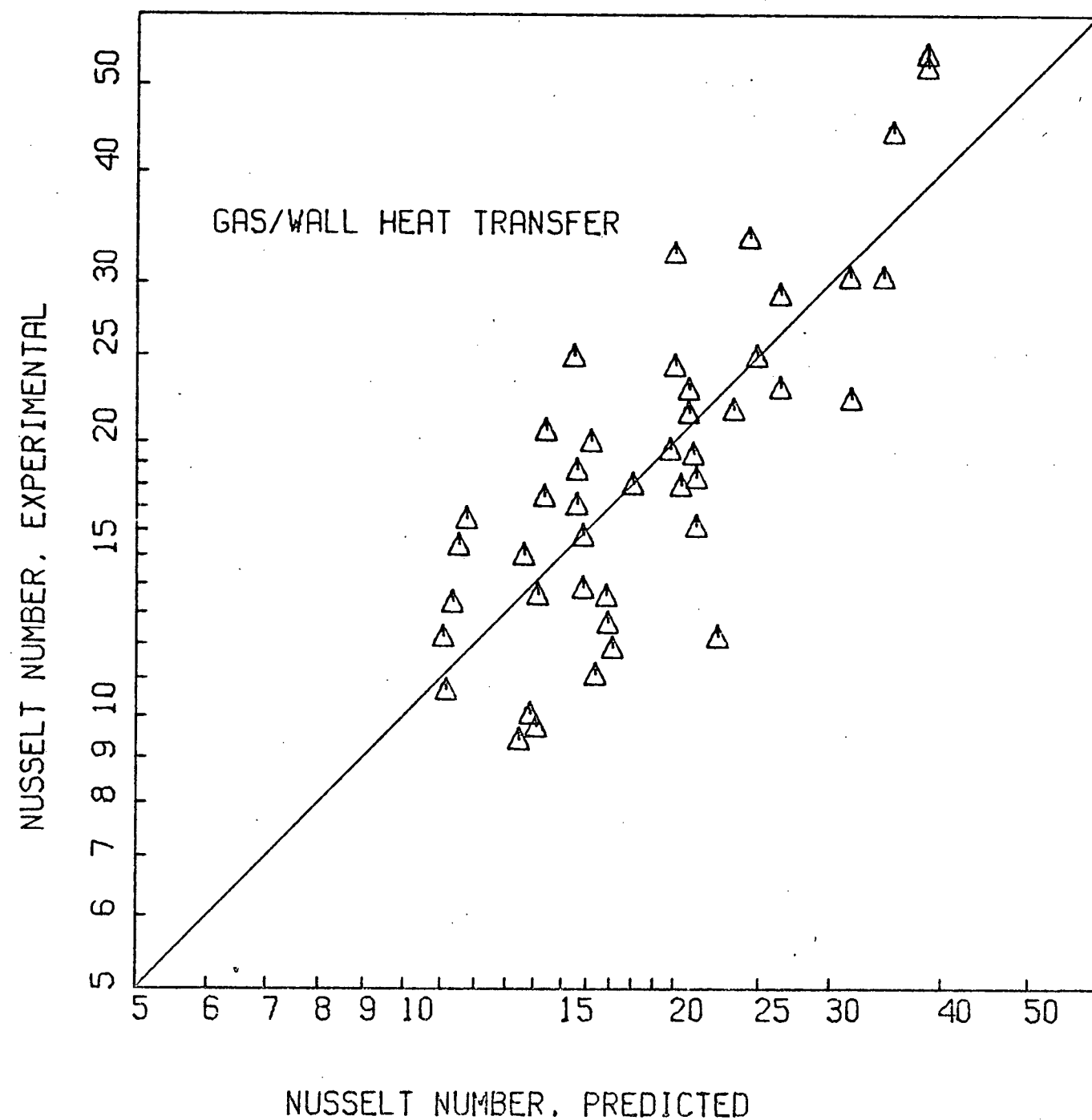
Figure 6-39 Comparison of Experimental Data with
Predicted Values for N_{ugw}.

$$\frac{h_{gs}D_e}{k_g} = 0.46\left(\frac{D_e\bar{u}_g\rho_g}{\mu_g}\right)^{0.535}\left(\frac{D_e^2\omega\rho_g}{\mu_g}\right)^{0.104}\eta^{-0.341}$$

whence the dependence of h_{gs} on D_e is

$$h_{gs} \propto D_e^{-0.257} \qquad\qquad (6-34)$$

Similarly the dependence of h_{gw} on D_e is given as

$$h_{gw} \propto D_e^{-1} \qquad\qquad (6-35)$$

Since the equivalent diameter is directly proportional to the kiln diameter,

$$\frac{D_e}{D} = \frac{2\pi - \beta + \sin\beta}{\pi - \frac{\beta}{2} + \sin\frac{\beta}{2}} = \text{constant for fixed } \eta$$

therefore, the predicted dependence of h_{gs} and h_{gw} on the kiln diameter are

$$h_{gs} \propto D^{-0.257}$$

$$h_{gw} \propto D^{-1}$$

For forced convection in an empty non-rotating tube, the

heat transfer coefficients are dependent on the tube diameter as

$$h \propto D^{-0.2} \text{ for turbulent flow} \tag{6-36}$$

$$h \propto D^{-0.67} \text{ for laminar flow} \tag{6-37}$$

Figure 6-40 plots h_{gs} and h_{gw} versus D based on equations 6-32 and 6-33 at constant mass flux and temperature. The gas mass flux is typical of industrial kilns, where with larger diameters, the gas flow is in the fully turbulent region. Included in the plot are the equations recommended in Perry's handbooks (14, 15)

$$h = 0.0981 \, G_g^{0.67} \tag{2-33}$$

and

$$h = 0.0608 \, G_g^{0.46}/D \tag{2-32}$$

The above two equations were given to predict the heat transfer coefficient from gas to refractory wall in industrial kilns, and have subsequently been used for gas to solid bed by many investigators. As seen in Figure 6-40 equation 2-33 is about one order higher than equation 2-32 for industrial scale kilns. The predicted gas to solids coefficients by equation 2-32 and by equation 2-33 are close to each other at large diameter. The predicted gas to wall coefficient by equation 6-33 are about one half those predicated by equation 6-32.
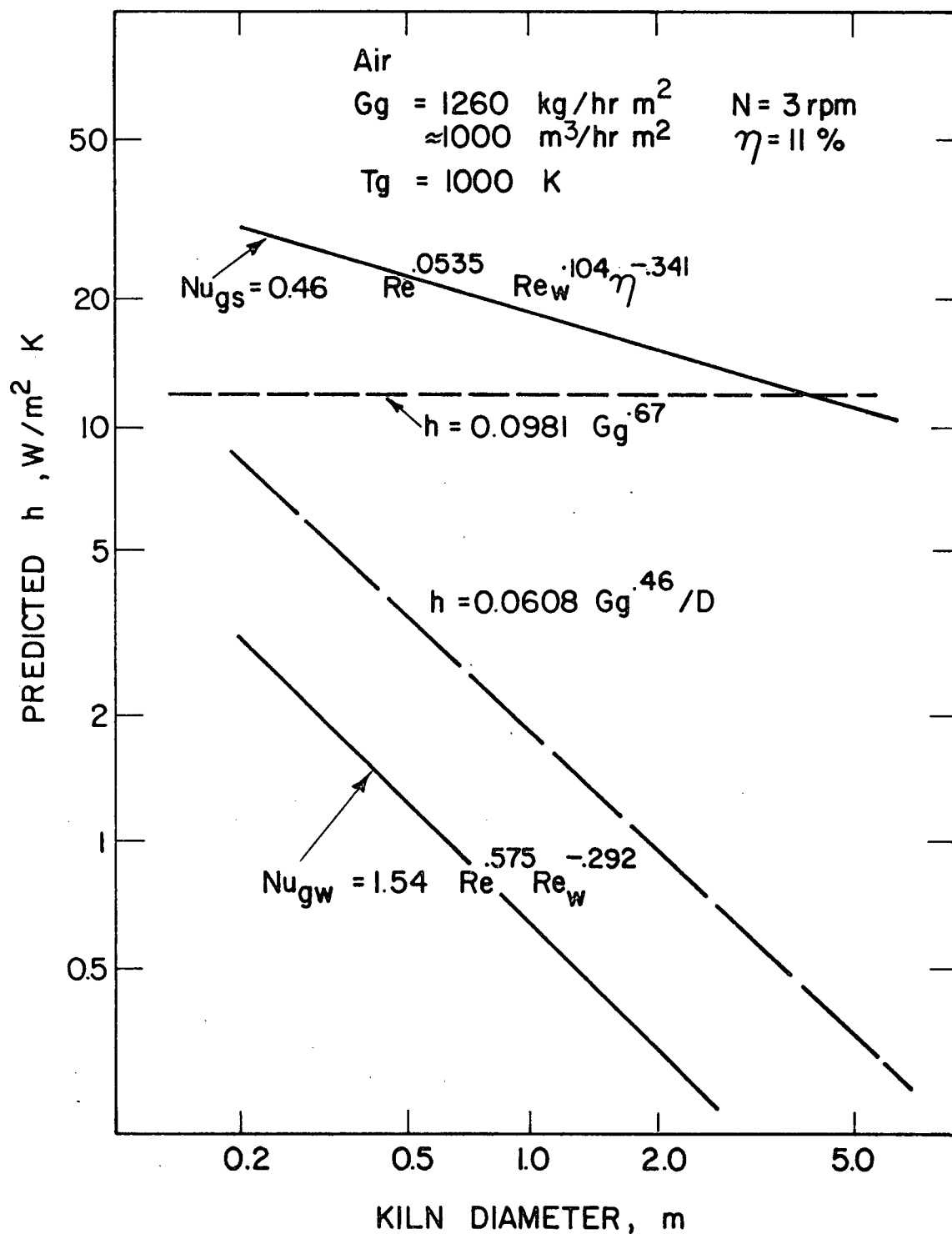
Figure 6-40   Predicted Heat Transfer Coefficients for
               Scaleup

CHAPTER 7

A MODEL FOR GAS TO BED HEAT TRANSFER

The experimental results show that the convective heat
transfer coefficient from the gas to solids is about one order
of magnitude higher than that from gas to wall. The higher
coefficients are attributed to two factors: the motion of
particles on the bed surface and the use of a plane surface area
rather than the true surface used in the calculation of the heat
transfer coefficient.

7.1 True Surface Area

Figure 7-1 shows the heat transfer path from the gas to
the solid bed. The heat transfer rate is defined as

$$Q_{gs} = h_{gs} A_s (T_g - T_s) \tag{7-1}$$

where A_s is the plane area of bed surface and T_s is the bed
temperature. In this equation T_g and T_s are measurable and
A_s is only function of kiln radius and the degree of solid fill.
Therefore, h_{gs} is calculated if Q_{gs} can be measured. However,
this equation expresses only an indirect representation of the
actual heat transfer mechanism. A direct expression for gas-
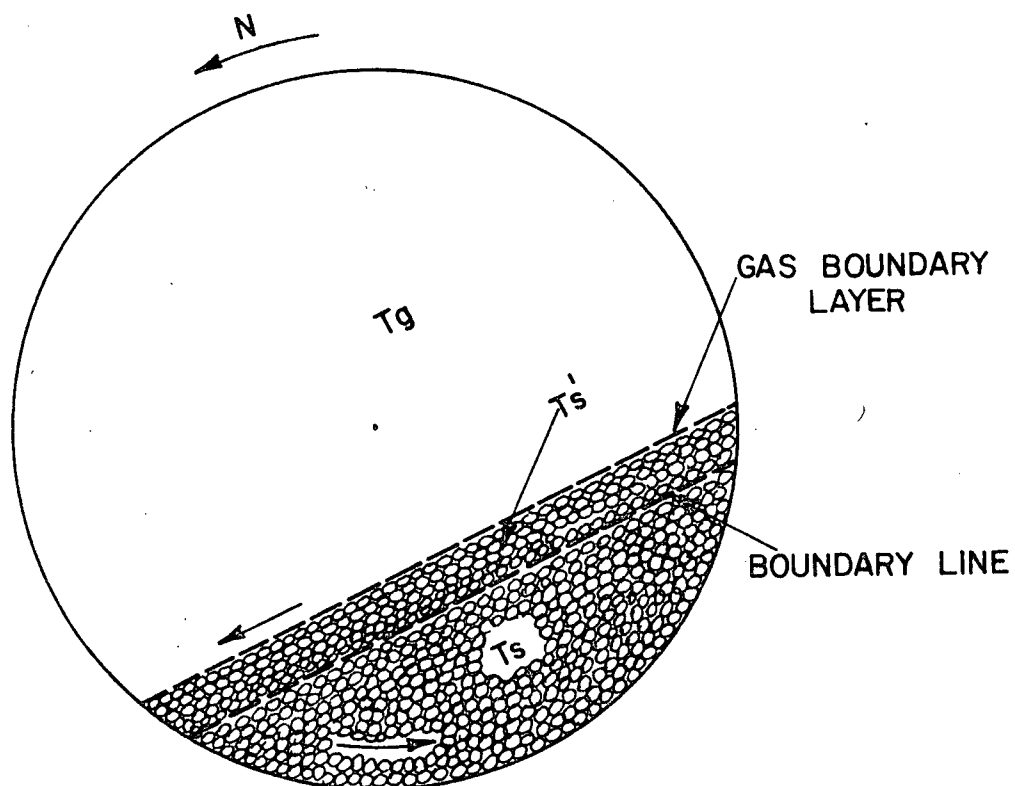
Figure 7-1 Heat Transfer from Gas to Solids Bed

solid heat transfer rate should be

$$Q_{gs} = h'_{gs}A'_{s}(T'_{g}-T'_{s}) \qquad (7\text{-}1A)$$

where A'_{s} is the true exposed surface area of the bed, which is function of particle size, shape and array, and T'_{s} is the bed surface temperature. Since T'_{s} is about the same as T_{s} in the present experiments as will be seen later, the relationship of h_{gs} and h'_{gs} becomes

$$h_{gs} = h'_{gs}\frac{A'_{s}}{A_{s}} \qquad (7\text{-}2)$$

The ratio of A'_{s}/A_{s} in equation 7-2 is obviously important in determining heat transfer coefficient. The values of A'_{s}/A_{s} depend on the types of particle arrays, and is about 1.78 for a cubic array as in Figure 7-2A to 2.42 for a structure as shown in Figure 7-2B. The film study (Section 5.2) shows that Figure 7-2B can best describe the array of larger alumina particles of d_{p} = 6.35 mm. However a cubic array may be used to approximate the condition for Ottawa sand of 0.73 mm.

The second factor which contributes to the higher gas-solid heat transfer coefficient is the motion of surface particles. As described in Chapter 6, the particles roll down on the surface at a speed much higher than the kiln circumferential velocity. The moving particles not only agitate the gas boundary layer adjacent to the bed surface, but also continuously remove

(a)

Side View

S_1

S_2

Top View
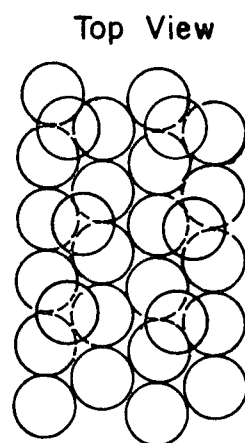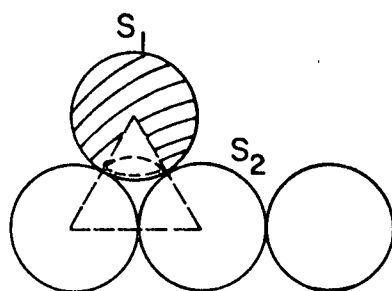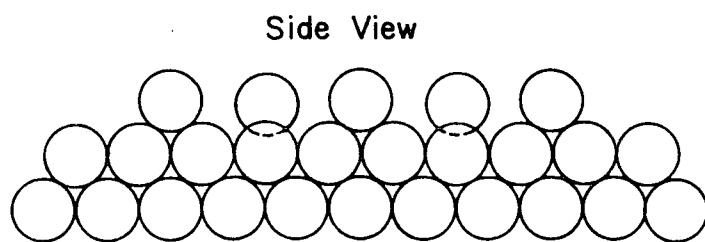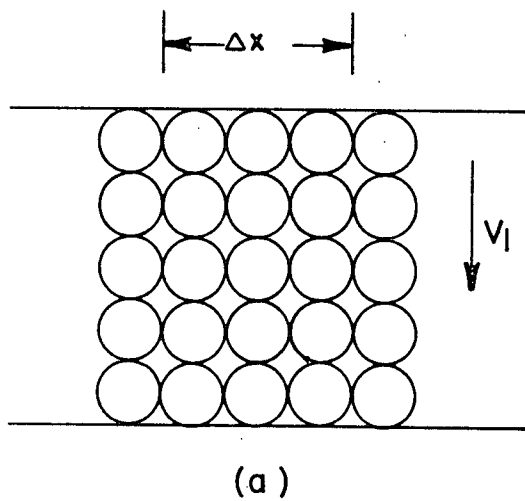
(b)

Figure 7-2 Array of Surface Particles

the heat received by the particles themselves. These phenomena are expected to increase the heat transfer coefficient from the gas to the bed over that of a flat plate for example.

7.2 Individual Particle Heat Transfer

First consider an individual particle in the first layer, just coming out of the bed with a temperature, T_s. It receives heat from the gas while it is rolling on the surface. Part of the received heat may be transferred by conduction to the particles of the adjacent layers. In a low temperature process the conduction heat may compose only a small fraction of the total heat received by the particle.

The equation governing the heat balance of a single particle rolling down the surface is given,

$$V_p \rho_p C_{p_p} \frac{dT}{dt} = h_p S_1 (T_g - T) - h_d S_1' (T - T_s) \tag{7-3}$$

where V_p, ρ_p, C_{p_p} are volume, density and specific heat of particle, respectively.

S_1 and S_1' are exposed and covered surface area of particle in the first layer,

$$S_1' = \pi d_p^2 - S_1$$

The last term of Equation (7-3) accounts for heat transfer to particles below. Since the experiments in this study were carried out at low temperature, the conduction term is

neglected relative to the gas to particle convection.

It is of interest to know whether the temperature within the particle becomes uniform after the particle surface temperature suddenly changes. The thermal diffusivity of Ottawa sand is 0.277×10^{-6} m^2/s and the particle diameter is 0.73 mm. The time (surface time, t_{s_1}) for the particle exposed to the gas stream is about one second. Thus, the value of Fourier modulus at_{s1}/r_p^2 is 2.08. This value shows the particle center temperature is immediately raised to the surface temperature according to Carslaw and Jaeger (70).

Let T_{s_1} be the particle temperature before it returns to the bed, and t_{s_1} is the surface time of the particles in the first layer. Integration of equation 7-3 with the following conditions,

$$
\begin{array}{lll}
t = 0 & T = T_s & \\
& & (7\text{-}4) \\
t_{s_1} & T = T_{s_1} &
\end{array}
$$

gives

$$\frac{T_{s_1} - T_s}{T_g - T_s} = 1 - \exp\left(-\frac{h_p S_1}{V_p \rho_p C_{p_p}} t_{s1} \right) \qquad (7\text{-}5)$$

Ottawa sand used for the experiments has a diameter of 0.73×10^{-3} m, which gives $V_p = 0.204 \times 10^{-9}$ m^3 and $S_1 = 0.837 \times 10^{-6}$ m^2. The values of C_{p_p}, and ρ_p for the sand are 0.603 J/gK and 2527 kg/m^3,

respectively. The gas to particle heat transfer coefficient h_p, and the surface time, t_{s1} are reasonably assumed at 15 W/m^{2}K (Section 7.4) and 1 second respectively. The substitution of the above values yields

$$\frac{h_p S_1}{V_p \rho_p C_{pp}} \, t_{s1} \approx 0.04$$

Thus, equation 7-5 can be approximated as

$$\frac{T_{s1} - T_s}{T_g - T_s} = \frac{h_p S_1 t_{s1}}{V_p \rho_p C_{pp}} \tag{7-6}$$

and equation 7-6 is rewritten as

$$V_p \rho_p C_{pp} (T_{s1} - T_s) = h_p S_1 t_{s1} (T_g - T_s) \tag{7-7}$$

The left-hand side of this equation represents the heat accumulated by a particle while it stays on the aerated bed surface, and the right-hand side represents the heat received by the particle by convection from the gas. For a temperature driving force, $T_g - T_s = 50$ K, the particle temperature is raised only 2 K. Considering the low thermal conductivity of Ottawa sand and the temperature difference of 2 K heat transfer to the particles underneath by conduction will be insignificant.

However, conduction should not be neglected for material of
high thermal conductivity, such as metal pellets in high tempera-
ture processes.

A similar derivation for particles in the secondary layer
of the surface region which ignores heat received and transferred
by conduction results in

$$\frac{T_{s2} - T_s}{T_g - T_s} = 1 - \exp\left(- \frac{h_p S_2}{V_p \rho_p C_{p_p}} t_{s2} \right) \qquad (7-8)$$

The particles in the second layer will have different
surface time and exposed surface area from that in the first
layer.

7.3 Gas to Bed Heat Transfer Coefficient

It is assumed that no particles below the first two
aerated layers of the surface region receive heat by convection
from the gas, where the temperatures of the aerated surface
particles are raised to T_{s1} and T_{s2} from T_s. The heated parti-
cles then mix with the particles in the other surface layers
as they return to the bed. The number of particles emerging
from the bed to the surface region per unit time is

$$F_m = \frac{\pi}{4} M \Delta x \cdot n \left(l_s^2 - 8 R \kappa \cos \frac{\beta}{2} \right) \qquad (7-9)$$

where M is the number of particles per unit volume and κ is
the thickness of the surface region. Δx is a short distance

of kiln length.

The detailed derivation of equation 7-9 is given in the appendix. If the rolling rates of particles in the first and second layers respectively are expressed as,

$$F_1 = m_1 \Delta x V_{11}$$

and   (7-10)

$$F_2 = m_2 \Delta x V_{12}$$

then a thermal balance of the mixing process can be expressed as

$$F_m(T_{sm} - T_s) = F_1(T_{s1} - T_s) + F_2(T_{s2} - T_s)$$ (7-11)

where T_{sm} is the temperature of the mixture before it returns to the bed. After rearrangement, equation 7-11 becomes,

$$T_{sm} - T_s = \frac{F_1}{F_m}(T_{s1} - T_s) + \frac{F_2}{F_m}(T_{s2} - T_s)$$

The following equation is obtained after substituting equations 7-4 and 7-8 in the above equation,

$$\frac{T_{sm} - T_s}{T_g - T_s} = \frac{F_1}{F_m}\left[1 - \exp\left(-\frac{h_p S_1}{V_p \rho_p C_{p_p}} t_{s1}\right)\right] + \frac{F_2}{F_m}\left[1 - \exp\left(-\frac{h_p S_2}{V_p \rho_p C_{p_p}} t_{s2}\right)\right]$$

(7-12)

Therefore, the heat absorbed by the rolling particles is represented by

$$Q_{gs} = F_m \rho_p C_{p_p} V_p (T_{sm} - T_s) \qquad (7-13)$$

Combining equations 7-1, 7-9, 7-12 and 7-13, and letting $A_s = \Delta x \cdot l_s$, one will obtain

$$h_{gs} = \frac{\rho_p V_p C_{p_p}}{l_s} \left\{ m_1 V_{11} \left[1 - \exp\left(-\frac{h_p S_1}{V_p \rho_p C_{p_p}} t_{s1} \right) \right] \right.$$

$$\left. + m_2 V_{12} \left[1 - \exp\left(-\frac{h_p S_2}{V_p \rho_p C_{p_p}} t_{s2} \right) \right] \right\} \qquad (7-14)$$

In order to evaluate h_{gs}, V_1 (or t_s) and h_p must be determined. Unfortunately there is no information in the literature on the relationship of V_1 to other operating parameters. For an ideal system the following equation is derived (see Appendix)

$$\kappa V_{11} = \frac{\pi}{2} n (l_s^2 - 8 R \kappa \cos \frac{\beta}{2}) \qquad (7-15)$$

where κ is the thickness of surface region. The velocity, V_{12}, of particles in the second layer can be approximated by

$$V_{12} = \left(1 - \frac{d_p}{\kappa} \right) V_{11} \qquad (7-16)$$

according to Figure 5-2. In equation 7-15, κ and V_1 are related
to rotational speed N and the degree of fill. Furthermore, the
experimental results in Figure 5-5 show

$$V_{11} \propto \sqrt{N} \qquad\qquad (7-17)$$

However, there is still a need to know κ, which is also unavail-
able in the literature. Based on the film study $V_{11} = 0.24$ m/s
was observed for alumina sphere at 4.78 rpm. It seems reason-
able to assume $V_{11} \simeq 0.20$ m/s at 3 rpm for Ottawa sand and this
value will be used to calculate κ and h_{gs}.

7.4 Gas to Particle Heat Transfer Coefficient

No information on the heat transfer coefficient from gas
to rolling particles, h_p, for a system similar to rotary kiln
was reported in the literature. Since the bed in rotary kiln
is close to the fixed bed system, heat transfer data for the
fixed bed will be used as a guide, although the gas flow pat-
tern is different as described below.

Kunii and Levenspiel (71) reported a correlation of
heat transfer data for fixed bed in terms of Nu_p versus Re_p,
which is reproduced in Figure 7-3. Nu_p and Re_p are defined as,

$$Re_p = \frac{u_o \rho_g d_p}{\mu_g}$$
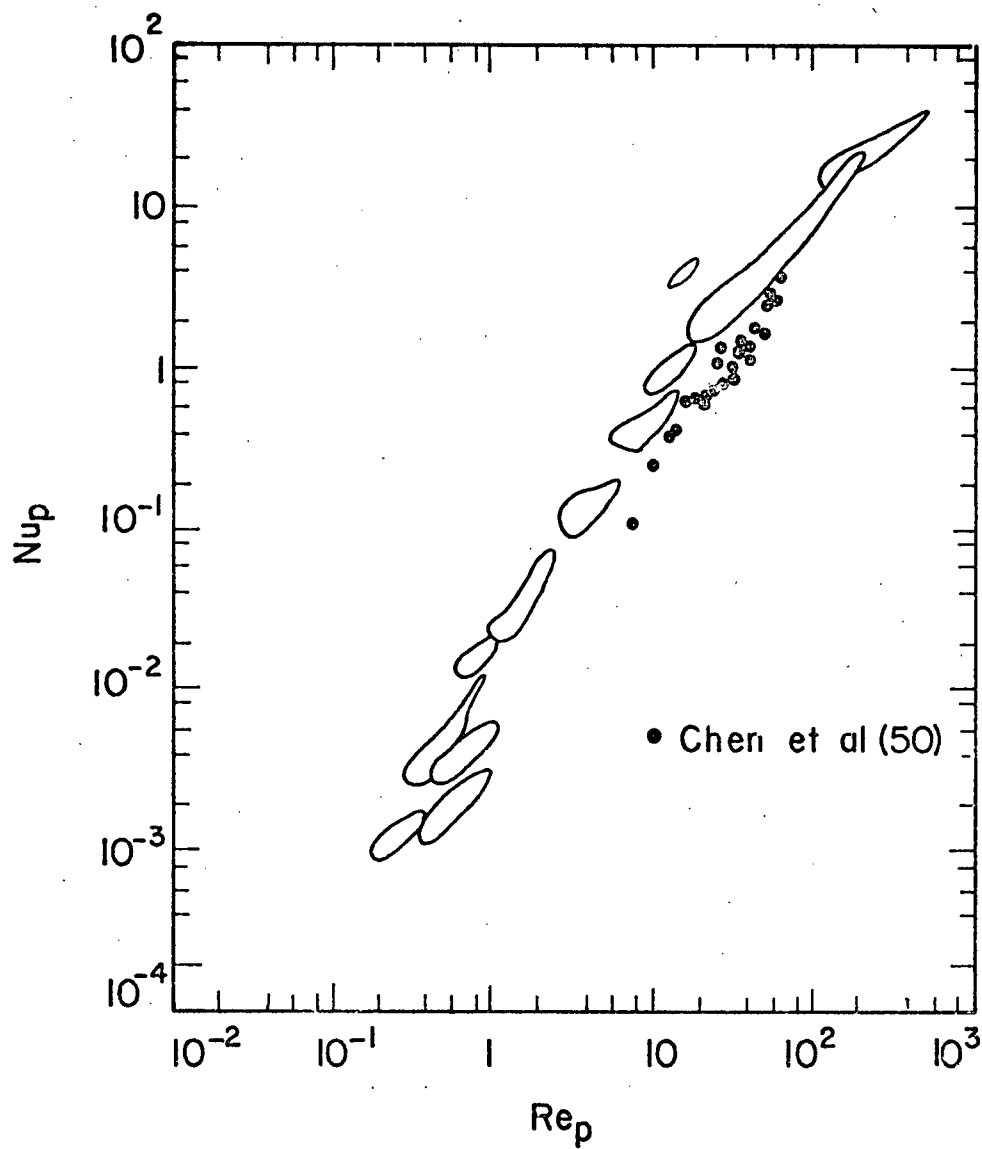
Figure 7-3   Reported Results for Gas-to-Particle
            Heat Transfer in Fixêd Bed.
            (Kunii & Levenspiel, 71).

$$and \qquad Nu_p = \frac{h_{pf} d_p}{k_g} \qquad (7\text{-}18)$$

respectively. u_o is the relative velocity between the particle
and the fluid. To use this approach for the surface of the bed
in the kiln where the aerated particles are rolling perpendi-
cular to the gas flow, u_o in equation 7-18 is defined as

$$u_o = \sqrt{u_g^2 + V_{11}^2} \qquad (7\text{-}19)$$

where u_g is the gas superficial velocity through the empty
space of the kiln.

$$u_g = \frac{W_g/\rho_g}{\pi R^2 (1 - \eta)}$$

The value of u_g is expected to be higher than that of the true
gas velocity near the bed surface.

The gas is flowing over the bed in the rotary kiln
whereas in the fixed bed the gas is flowing through the bed.
So, the effectiveness of gas-particle heat transfer in a rotary
kiln is expected to be lower than that in a fixed bed. The
value of this effectiveness is not known. In a fixed bed each
particle has adjacent particles surrounding it, however, in
rotary kiln about the half surface area of the aerated particles
is exposed to the gas stream. It is, therefore, likely that

h_p for the aerated particle in a rotary kiln is roughly a fraction of h_{pf} in a fixed bed.

Chen et al (50) reported the gas to particle heat transfer in a rotary dryer. In their experiments hot air, instead of flowing through the dryer, was passed through the bed from the wall which was made of plate with holes and pitch covered with a screen. The data of the heat transfer coefficients between gas and particles were found to be in the range of fixed bed. The data are also shown in Figure 7-3.

7.5 Comparison with Experimental Data

The comparison of the experimental data with equation 7-14 is given in Figure 7-4 where h_{gs} is plotted versus W_g. All the experimental data are included. The input data for calculation for equation 7-14 are given in Table 7-1 and the calculated results are given in Table 7-2. Three curves with h_p are taken as ¼, ½ and 1 times that for a fixed bed. The curve with ½ h_{pf} fits the data better than the other two. The value of h_p taken as one half of h_{pf} seems reasonable since only half of surface area of the aerated particle is exposed to the gas stream. If the value of h_p for the aerated particle is taken from $Nu_g = 2$ which corresponds to an isolated sphere at low Reynolds number this results in a much higher value of heat transfer coefficient than h_{pf}, and the prediction of h_{gs} would be considerably higher.

In equation 7-14 the exponential terms are found to be
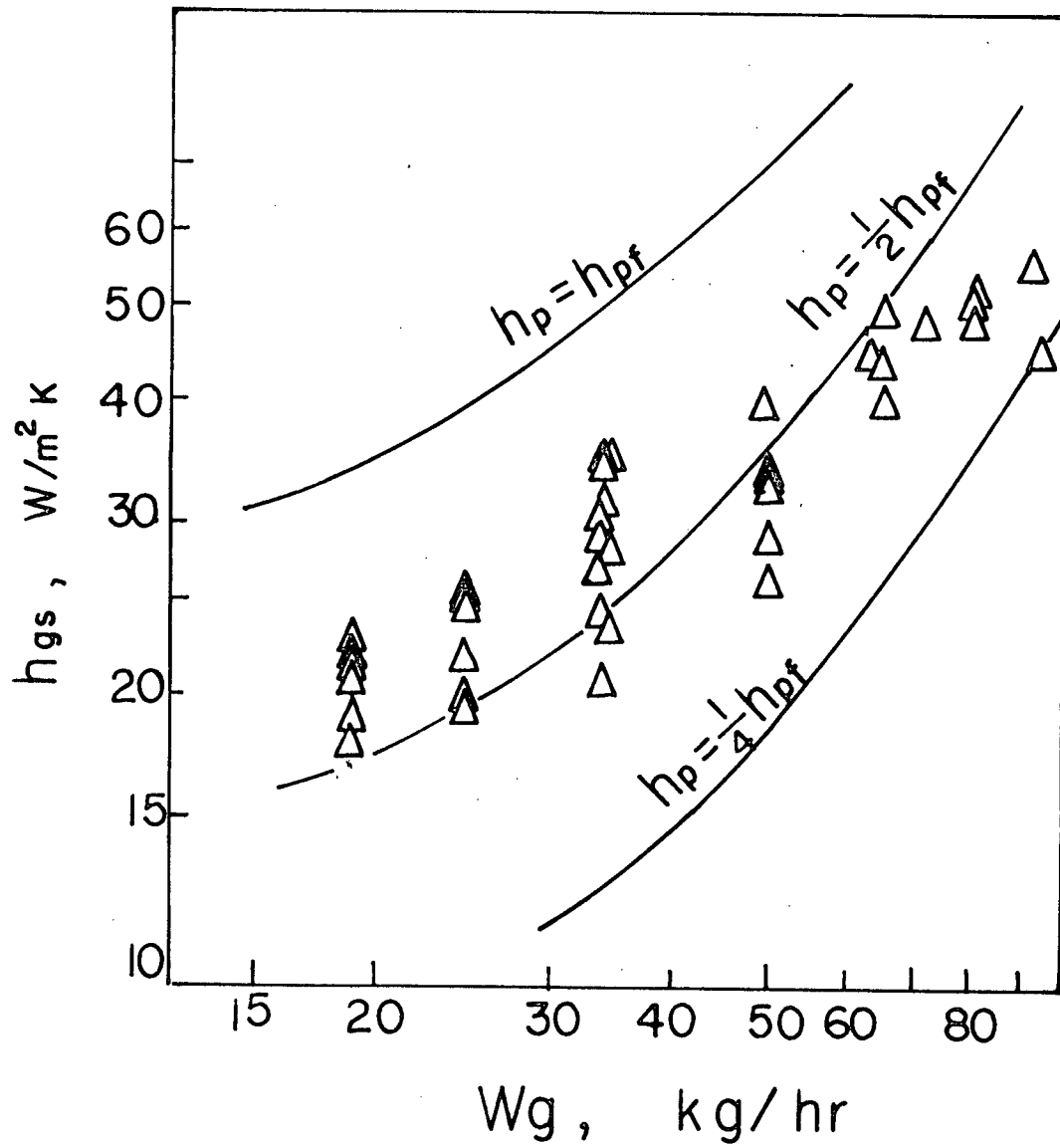
Figure 7-4 Comparison of Theoretical Curve
with Experimental Data.

Table 7-1

Input data for Equation 7-14

For Particle (Ottawa sand)

$$d_p = 0.73 \times 10^{-3} \text{ m}$$

$$\rho_p = 2527.3 \text{ kg/m}^3$$

$$C_{p_p} = 0.603 \text{ J/gK}$$

$$V_p = 0.204 \times 10^{-9} \text{ m}^3$$

$$S_1 = 0.837 \times 10^{-6} \text{ m}^2$$

$$S_2 = 0.042 \times 10^{-6} \text{ m}^2$$

$$m_1 = m_2 = 2.17 \times 10^6 \text{ no. of particles/m}^2$$

For air (at 422 K)

$$\mu_g = 2.369 \times 10^{-5} \text{ kg/m-s}$$

$$\rho_g = 0.833 \text{ kg/m}^3$$

$$k_g = 0.031 \text{ W/m-K}$$

Operating conditions

$$N = 3 \text{ rpm}$$

$$\eta = 11\%$$

$$V_{11} = 0.20 \text{ m/s}$$

Table 7-2

Calculations for Gas-Particle Heat Transfer

W_g	kg/hr	18.6	34	50	70
V_g	m/s	0.245	0.447	0.657	0.92
V_l^+	m/s	0.20	0.20	0.20	0.20
V_o	m/s	0.316	0.490	0.687	0.942
Re_p		8.1	12.6	17.6	24.2
$Nu_p = Nu_p^*$		0.44	0.62	0.90	1.4
h_p	W/m^2K	9.3	13.1	19.1	29.3
h_{gs}	W/m^2K	17.7	24.8	35.8	55.2
$Nu_p = \frac{1}{2}Nu_p^*$		0.22	0.31	0.45	0.70
h_p	W/m^2K	4.65	6.55	9.55	14.65
h_{gs}	W/m^2K	8.85	12.4	17.9	27.6
$Nu_p = \frac{1}{4}Nu_p^*$		0.11	0.16	0.23	0.35
h_p	W/m^2K	2.33	3.28	4.28	7.33
h_{gs}	W/m^2K	4.43	6.2	8.95	13.8
$\kappa \times 10^3$	m	0.369	0.369	0.369	0.369

+   assumed

*   taken from Figure 7-3

quite small. Thus,

$$\frac{h_p S_1}{V_p \rho_p C_{p_p}} \cdot \frac{1}{V_{11}} \approx 0.042$$

$$\frac{h_p S_2}{V_p \rho_p C_{p_p}} \cdot \frac{1}{V_{12}} \approx 0.005$$

for $V_1 = 0.20$ m/s at $N = 3$ rpm. The ratio of these two terms indicates that the top layer probably receives about 8 times as much as heat from the gas than does the second layer, and the second layer could probably be ignored in the above analysis.

The effect of rotational speed on h_{gs} calculated from equation 7-14 is shown in Figure 7-5. The calculated results are given in Table 7-3. The slope of h_{gs} versus N is 0.1 which coincides roughly with the experimental data.

The mathematical model for gas-solid heat transfer has been established from a single particle. In the model two factors which significantly affect the gas to solid bed heat transfer are the particle array on the top bed layer and the gas to rolling particle heat transfer coefficient. The cubic packing array was assumed for Ottawa sand bed. The gas-to-rolling particle heat transfer coefficient, taken as one-half value of that for fixed bed, yields a reasonable prediction for the rotary kiln. To make the model more adaptable further
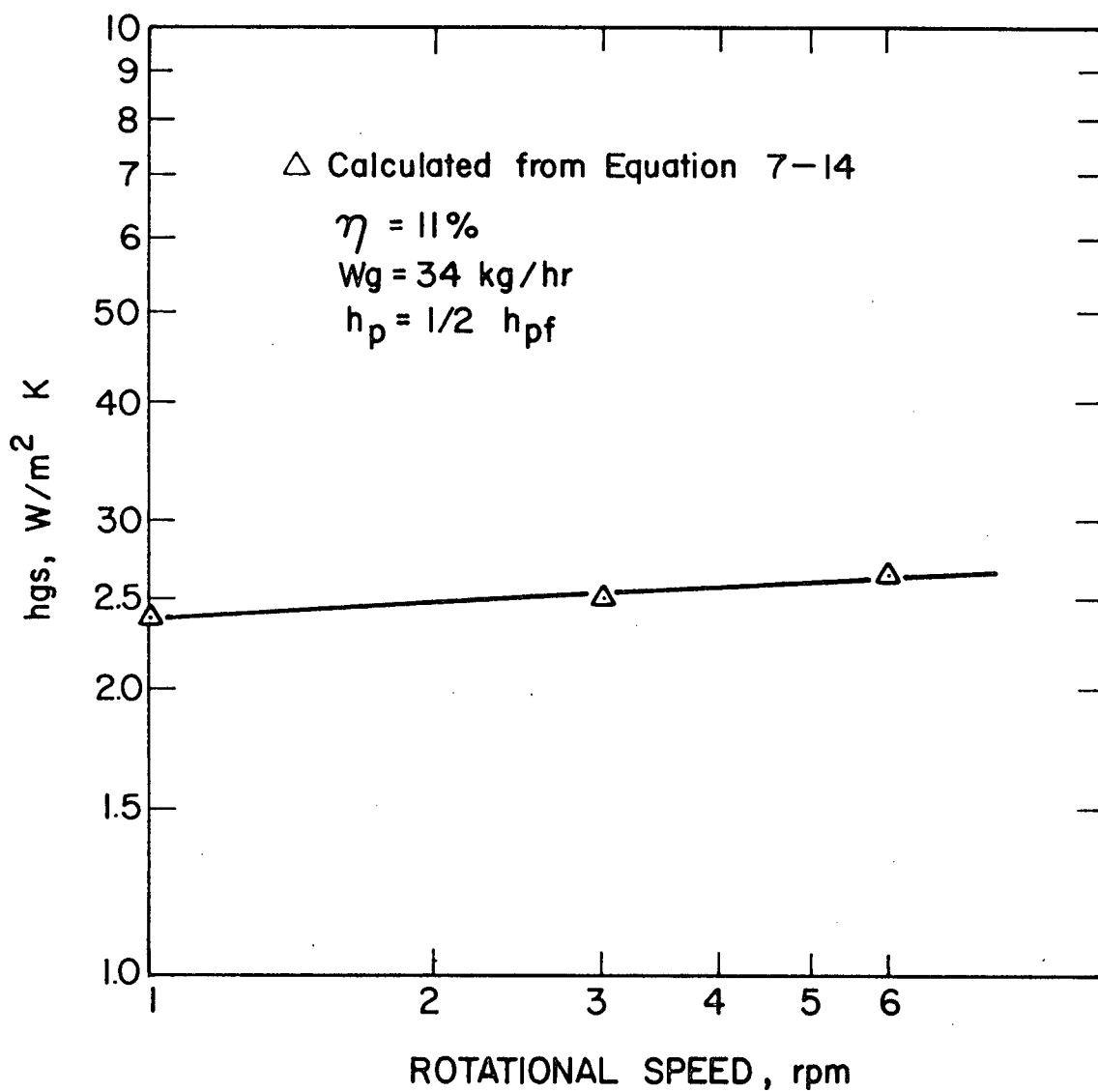
Figure 7-5   Effect of Rotational Speed on Theoretical
Gas-Solids Bed Heat Transfer Coefficient

Table 7-3

Calculation of h_{gs} from Equation 7-14

N (rpm)	1.0	3.0	6.0
V_g m/s	0.447	0.447	0.447
V_l m/s	0.116	0.20^+	0.283
V_o m/s	0.462	0.490	0.529
Re_p	11.8	12.6	13.6
Nu_p^*	0.60	0.62	0.66
$Nu_p = \frac{1}{2} Nu_p^*$	0.30	0.31	0.33
h_p W/m^{2}K	12.7	13.1	14.0
$\kappa \times 10^3$, m	0.221	0.369	0.504
h_{gs} W/m^{2}K	23.8	24.8	26.5

+ assumed

* taken from Figure 7-3

$\eta = 11\%$

$W_g = 34.0$ kg/hr

work on the thickness of the mixing zone and the particle lateral velocity is required. Both κ and V_1 are used to determine the temperature of the mixing particles in the surface region.

CHAPTER 8

MODELLING OF ROTARY KILN HEAT EXCHANGER

As noted in the first two chapters a number of studies
on rotary kiln modelling have been published (5-14), however,
there was a lack of experimental data on heat transfer to in-
corporate into the models. Although Watkinson and Brimacombe
(4) reported some results on heat transfer in a direct-fixed
kiln, 0.406 m inside diameter, their data are still not in a
form readily adapted for scaleup to industrial size kilns.

Kern (15) established a model for heat transfer in a
rotary heat exchanger. In his model , the rotating wall temp-
erature is formulated in terms of gas and solid temperatures
by taking into account the periodic cooling and heating of the
wall. By eliminating the wall temperature, he obtained

$$\frac{dT_g}{dx} = a_1 T_s + a_2 T_g + a_3$$

$$\frac{dT_s}{dx} = b_1 T_s + b_2 T_g + b_3$$

where a_n and b_n are functions of the mass flow rates, rotational speed and the heat transfer coefficients. The heat transfer coefficients were assumed, $h_o = 5$ W/m^{2}K , $h_{sg} = 1.5$ W/m^{2}K (for solid bed to gas), and $h_{sw}/h_{wg} = 3$. The assumed values of heat transfer coefficients do not seem to be reliable in terms of the measured values reported in the present study.

A model of a rotary kiln heat exchanger in the low temperature range where radiation effects can be neglected is presented here. The heat transfer coefficients established in Chapter 6 can be used in the model. Thus, the equations used earlier to calculate heat transfer coefficients from temperature profiles are just inverted to calculate temperature profiles from heat transfer coefficients. The equations governing the heat balances on gas and solid phases over a small differential distance are given as

$$W_g C_{pg} \frac{dT_g}{dx} = h_{gs} l_s (T_g - T_s) + h_{gw} l_w (T_g - T_w) \qquad (8-1)$$

$$W_s C_{ps} \frac{dT_s}{dx} = h_{gs} l_s (T_g - T_s) - h_{sw} l_w' (T_s - T_w) \qquad (8-2)$$

The heat capacities, C_{pg} and C_{ps}, are assumed constant over the temperature range of interest. The wall temperature, T_w, is assumed circumferentially constant at a particular location. This simplifying assumption is justified by the experimental results given in Chapter 6, and by those of reference (4).

The inside refractory temperature (if there is a lining material in the kiln), T_w, in equations 8-1 and 8-2 must be known in order to obtain the gas and solid temperature profiles. Therefore a heat balance over the wall is set up to obtain T_w:

Gas to Wall convection + Solids to Wall convection = Heat loss through Wall by Conduction

$$h_{gw}l_w(T_g-T_w) + h_{sw}l_w'(T_s-T_w) = \frac{2\pi k_w(T_w-T_{wo})}{\ln(R_2/R_1)} \tag{8-3}$$

where T_{wo} is the outside lining temperature. It is further assumed that there is no temperature drop across the metal kiln shell. Therefore, the heat loss through the kiln shell to the surroundings is given by

$$\frac{2\pi k_w(T_w-T_{wo})}{\ln(R_2/R_1)} = h_o l_o(T_{wo} - T_o) \tag{8-4}$$

Substitution of equations 8-3 and 8-4 into equations 8-1 and 8-2 yields two first order linear equations for gas and solids temperatures which can be rewritten as:

$$\frac{dT_g}{dz} = D_1 T_g - D_2 T_s - D_3 T_o \tag{8-5}$$

and

$$\frac{dT_s}{dz} = E_1 T_g - E_2 T_s + E_3 T_o \tag{8-6}$$

where z = x/L, and the coefficients D_n and F_n are functions of mass flow rate and heat transfer coefficients as given in Table 8-1. Kern (15) obtained somewhat similar equations for the gas and solids temperature.

Equations 8-5 and 8-6 can be solved if a set of boundary conditions are given. In this study both the inlet gas and solid temperatures are fixed as

$$z = 0 \qquad T_s = T_{so}$$
$$z = 1 \qquad T_g = T_{gL} \qquad\qquad (8-7)$$

The heat transfer coefficients used in Table 8-1 are calculated from the following equations,

$$h_{gs} = 0.46 \frac{k_g}{D_e} Re^{0.54} Re_w^{0.10} \eta^{-0.34} \qquad (6-31)$$

$$h_{gw} = 1.54 \frac{k_g}{D_e} Re^{0.58} Re_w^{-0.29} \qquad (6-32)$$

and

$$h_{sw} = 11.6 \frac{k_s}{l_w} \left(\frac{nR^2\beta}{a} \right)^{0.3} \qquad (6-26)$$

It is further assumed that the bed height along the kiln is uniform. For a non-uniform bed system, Kramers and Croockewit (29) developed a formula for bed height along the kiln as function of operating parameters. Since the gas-solid heat transfer coefficients depend on the degree of fill, the assumption of

Table 8-1

The Coefficient for Equations 8-5 and 8-6

$$D_1 = B_1 + B_2 - B_2 A_5$$

$$D_2 = B_1 + A_2 A_5 B_2$$

$$D_3 = A_4 A_5 B_2$$

$$E_1 = B_3 + B_4 A_5$$

$$E_2 = B_3 + B_4 - A_2 A_5 B_4$$

$$E_3 = B_4 A_4 A_5$$

where

$$A_1 = \frac{h_o l_o \ln(R_2/R_1)}{2 k_w}$$

$$A_4 = \frac{A_1 A_3}{1 + A_1}$$

$$A_2 = \frac{h_{sw} l'_w}{h_{gw} l_w}$$

$$A_5 = \frac{1}{1 + A_2 + A_4}$$

$$A_3 = \frac{2 k_w}{h_{gw} l_w \ln(R_2/R_1)}$$

$$B_1 = \frac{h_{gs} l_s L}{W_g C_{pg}}$$

$$B_3 = \frac{h_{gs} l_s L}{W_s C_{ps}}$$

$$B_2 = \frac{h_{gw} l_w L}{W_g C_{pg}}$$

$$B_4 = \frac{h_{sw} l'_w L}{W s C p s}$$

uniform bed depth makes the problem simpler. Once the operating parameters (N, α, η, D) are fixed, the solid throughput for a uniform bed system can be calculated from the following equation:

$$W_s = 77.7 \; \tau_L N D^2 \rho_s \; \tan\alpha / \sin\theta \qquad (2-12)$$

where $\qquad \tau_L = \dfrac{D}{2} \left(1 - \cos\dfrac{\beta}{2} \right)$

and $\qquad \eta = \dfrac{1}{2\pi} \left(\beta - \sin\beta \right) \qquad (2-13)$

The gas and solid temperature profiles can be obtained by solving equations 8-5 and 8-6 with equation 8-7. Equation 8-7 gives the boundary conditions at opposite ends of the kiln, which makes an analytical solution difficult. Therefore, Runge Kutta method with trial and error was used. First, T_{go} was assumed at z = 0 and equations 8-5 and 8-6 were solved with boundary conditions $T_s = T_{so}$, $T_g = T_{go}$ at z = 0. Gas temperature at z = 1 was then calculated and compared with T_{gL} as given in equation 8-7. If the calculated gas temperature was not equal to T_{gL}, another value for T_{go} was assumed and the procedure repeated until the calculated gas temperature equal to T_{gL}. A flow chart for computer program is given in Figure 8-1. If both the boundary conditions are set at the same end of the kiln, equations 8-5 and 8-6 can be solved analytically.

A kiln, 3 m I.D. by 80 m long with 0.15 m thick refract-

Figure 8-1   Flow Chart of Computer Program

for Temperature Proliles
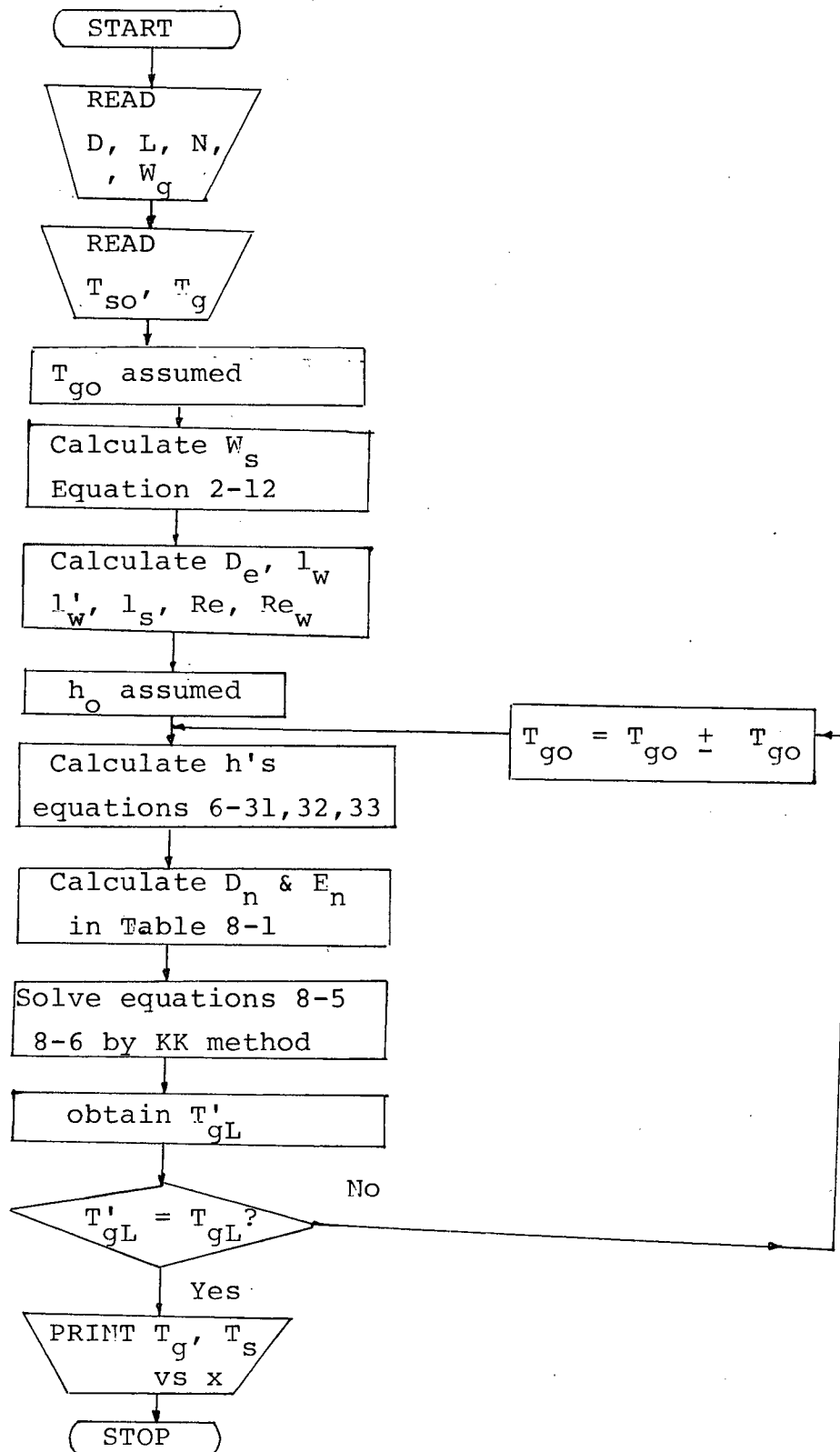
ory lining is selected to illustrate the model. The rotational speed, inclination angle and the degree of fill are chosen so that the solids throughput is about the same order as an industrial lime kiln. The necessary parameters for modelling are collected in Table 8-2. The inlet gas temperature is kept at 500° K, while the inlet solid temperature at the other end of the kiln is fixed at 350 K.

Equations 8-5 and 8-6 for temperature profile are solved with the aid of Table 8-1 for the coefficients. Heat transfer coefficients are calculated from equations 6-26, 31 and 32, while solid throughput is calculated from equation 2-12. The results for gas and solid temperature profiles are depicted in solid lines in Figure 8-2. The temperatures are expressed in dimensionless form, $(T-T_{so})/(T_{g1}-T_{so})$.

Included in Figure 8-2 are the temperature profiles with heat transfer coefficients calculated from the equations recommended in Perry's Chemical Engineering Handbook (46, 47).

$$h = 0.0981 \left(\frac{W_g}{A_c} \right)^{0.67} \qquad (2-32)$$

and

$$h = 0.061 \left(\frac{W_g}{A_c} \right)^{0.46} \Big/ D \qquad (2-33)$$

As expected the local solids temperature increases considerably as the heat transfer coefficients increase. The gas temperature drops accordingly.

Table 8-2   Modelling Parameters

Solid phase : Ottawa sand

Gas phase   : Air

$D = 3$ m $L = 80$ m

$T_{gL} = 500$ K $T_{so} = 350$ K

$h_o = 10$ W/m^{2}K $k_w = 0.043$ W/m^{2}K

$N = 1$ rpm $\alpha = 0.7^o$

$\eta = 11\%$

$\dfrac{W_s}{A} = 2130$ kg/hr-m^2 (kiln cross section)
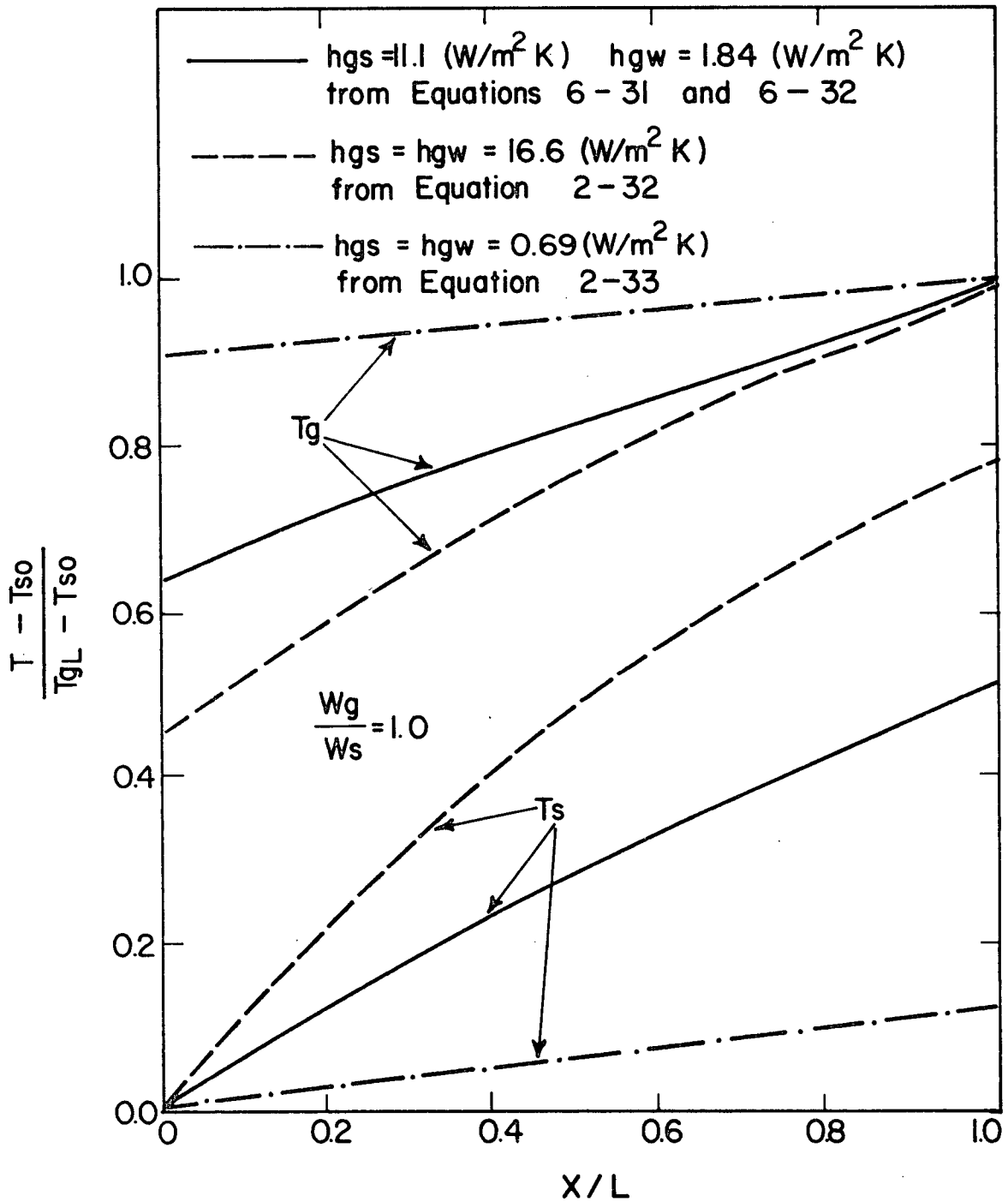
Figure 8-2 Effect of Heat Transfer Coefficient on
Temperature Profiles

Figure 8-3 gives the effect of gas flow rate on the ⸛ ⸝⸝ temperature profile. The results are also as expected. Increasing gas flow rate increases both gas-solid and gas-wall heat transfer coefficient. As a result, the solid temperature increases repidly, however, the gas temperature drops are small due to the high gas flow rate.

The wall temperature for the operating conditions given in Table 8-2 is illustrated in Figure 8-4. Wall temperatures are consistently higher than the solid temperatures along the kiln due to the presence of the thick refractory lining, and low heat loss. For comparison, a rotary kiln of the same dimension having no refractory lining is assumed. The kiln wall is 0.051 m in thickness, made of mild steel having thermal conductivity 45.2 W/m-K. In this case, the wall temperature drops below the solid temperature, and the gas temperature also drops due to high heat loss through the wall. This type of behaviour was found in the present experimental study. The effect of kiln length on the temperature profile is given in Figure 8-5 . For a lime kiln equipped with a preheater, the kiln length of the 3 m I.D. kiln is typically about 50 m. For a short kiln, the exit gas temperature is expectedly, higher than that for a long kiln if the entering gas temperatures are maintained the same for both cases.

The effect of kiln diameter is of most interest to the designer of the kiln. The switch of kiln diameter involves a change of heat transfer coefficients and solid throughput. It may also alter the flow pattern if the rotational speeds are
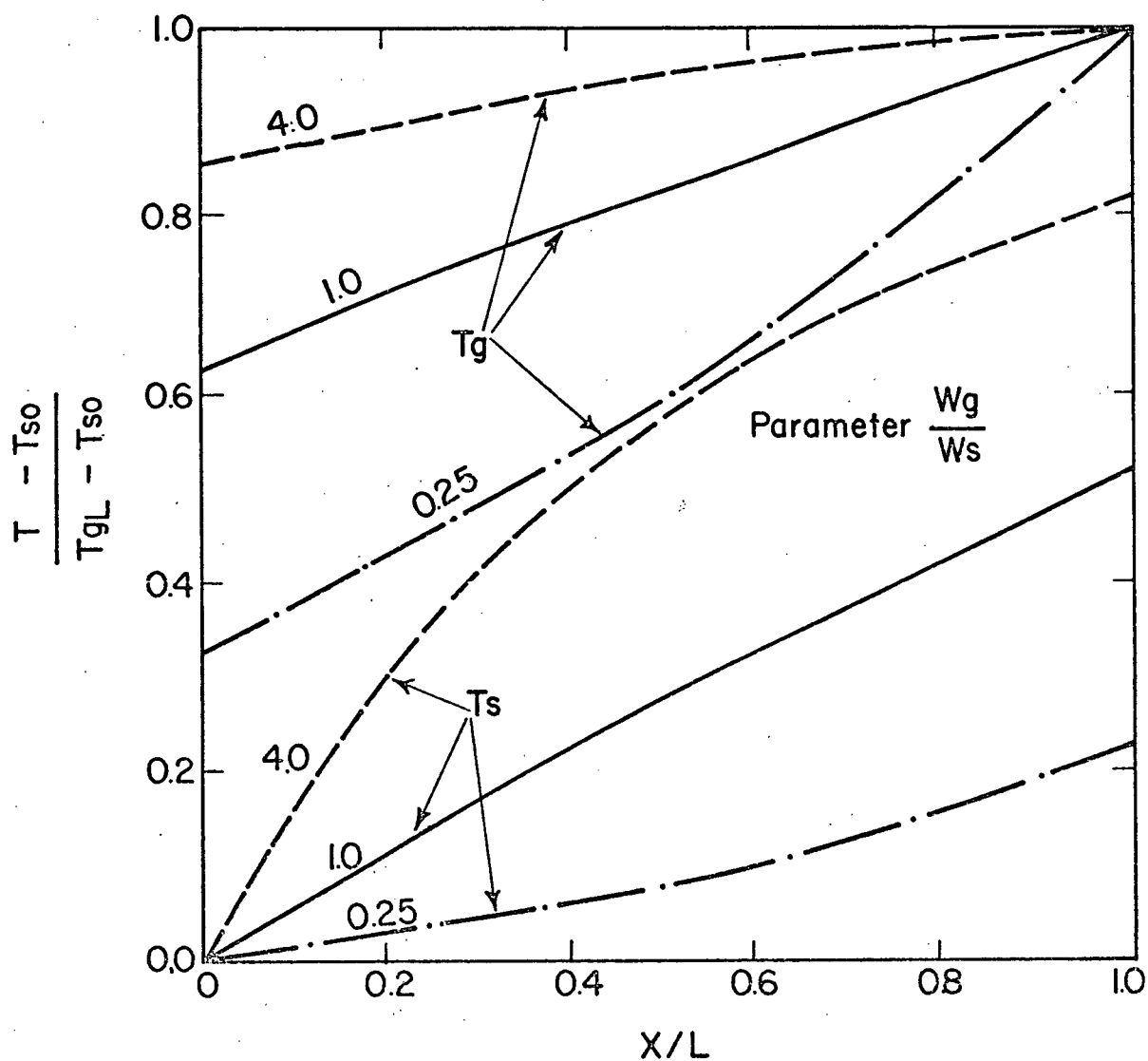
Figure 8-3 Effect of Gas Flow Rate on Modelling
of Rotary Kiln.
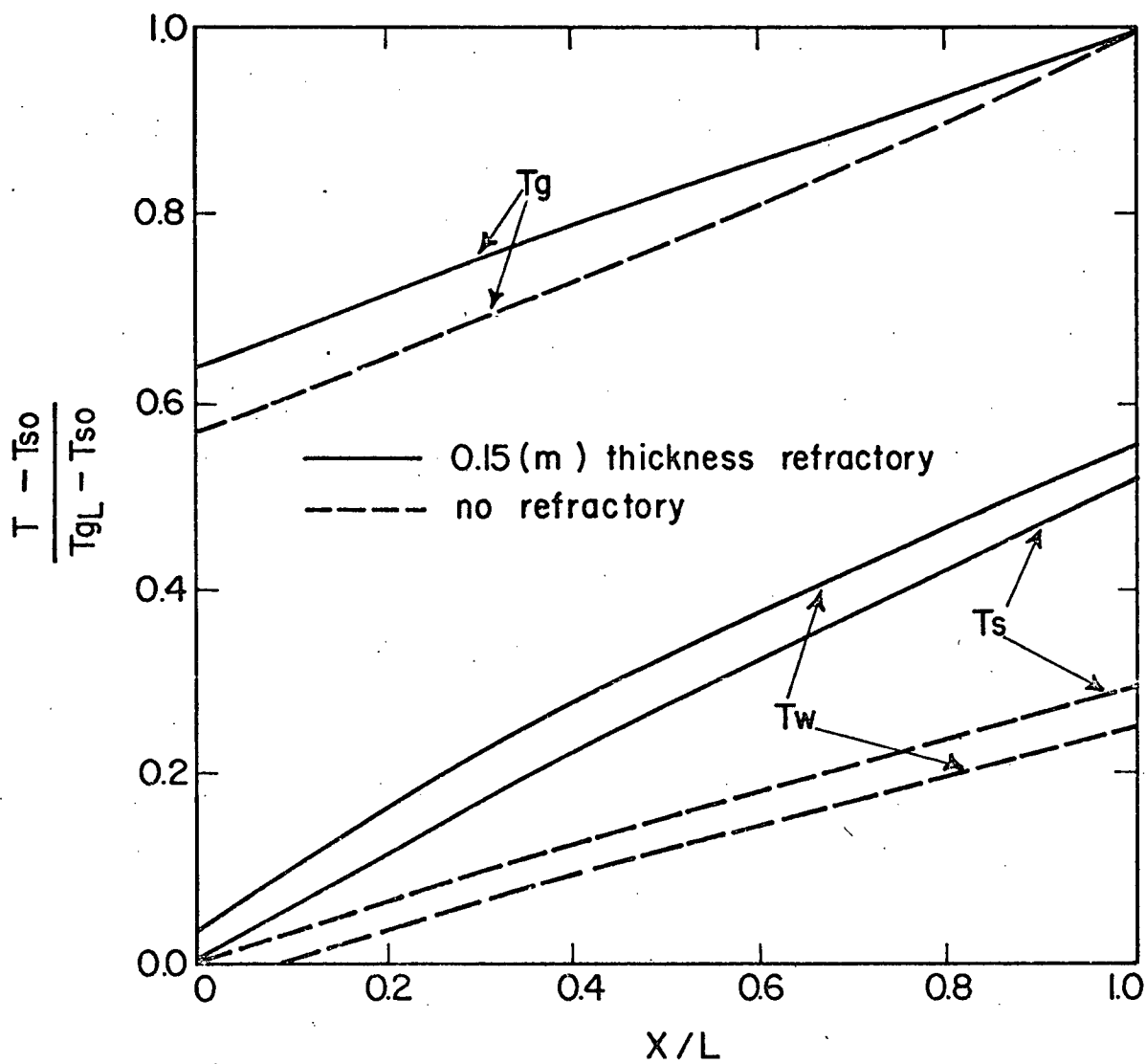
Figure 8-4   Effect of Refractory Insulation on
Modelling of Rotary Kiln.
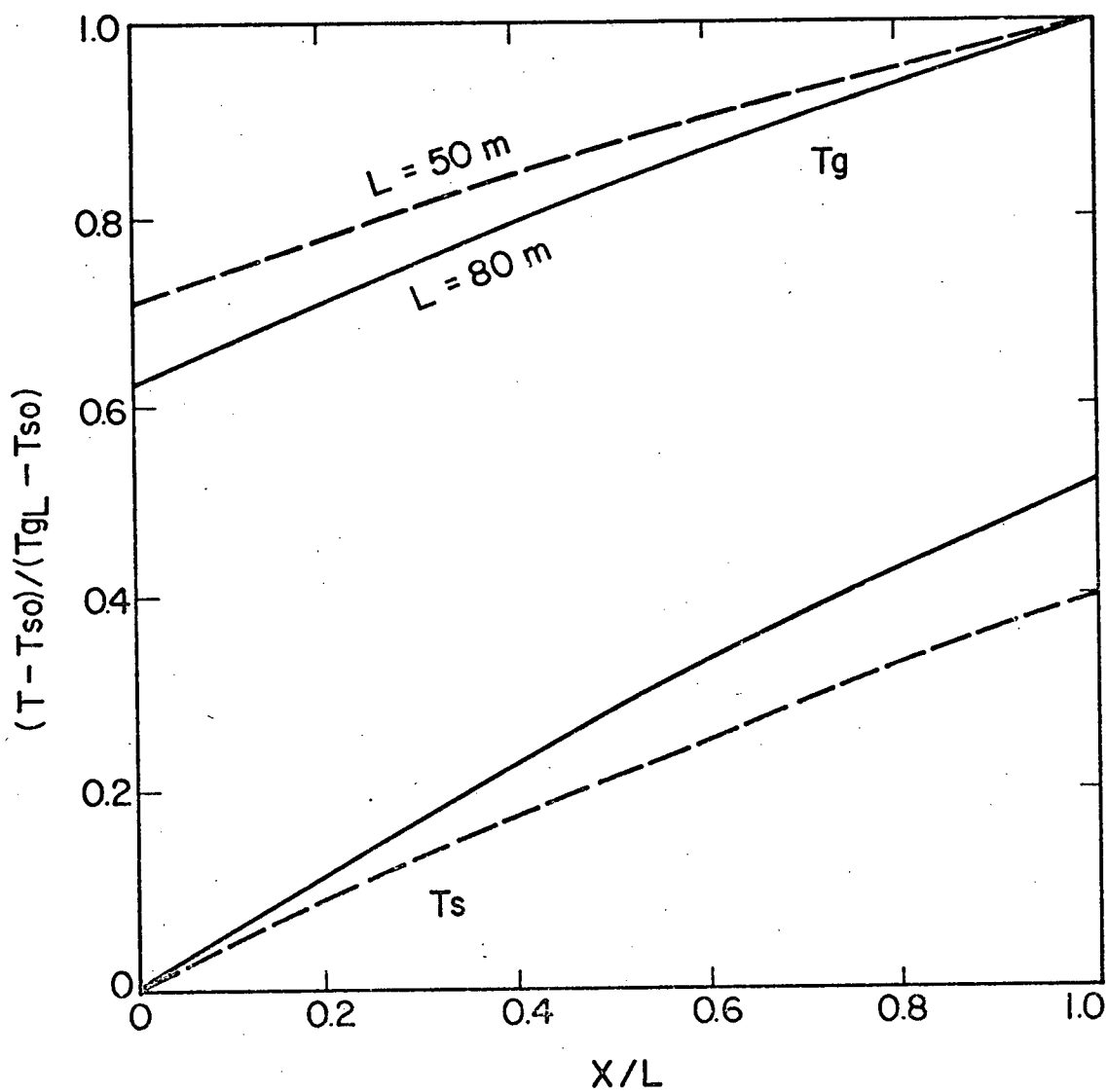
Figure 8-5   Effect of Kiln Length on Modelling of
            Rotary Kiln.

maintained the same. In order to compare the effect of kiln diameter the solid flow pattern in kilns of different diameters should be kept the same, which can be accomplished by maintaining the same Froude number,

$$\frac{N}{N_C} = \frac{N'}{N_C'} = \text{constant or}$$

$$\frac{N}{N'} = \frac{D'}{D} = \text{constant}$$

Therefore, the rotational speed must be adjusted accordingly if the change of the kiln size is necessary. The second factor that should be taken into account is the solid throughput per kiln cross area. This factor will govern the residence time in kilns of the same length. In this calculaton, the solid throughputs per kiln cross section are maintained constant at varying kiln diameters. According to equation 2-12, the inclination angle must be adjusted to keep the same degree of solid fill. Fortunately, the effect of inclination angle on heat transfer is nil.

Figure 8-6 shows the effect of three different kiln diameters, 3 m, 2 m and 1 m for a 50 m long kiln. Both the ratio of N/N_C and solid residence time are kept constant. As seen in the figure, small diameter kilns show high heat transfer efficiency. This is due to higher heat transfer coefficients for small kilns. Figure 8-7 gives the effect of kiln diameter at fixed L/D ratio. Although small kilns have a shorter kiln
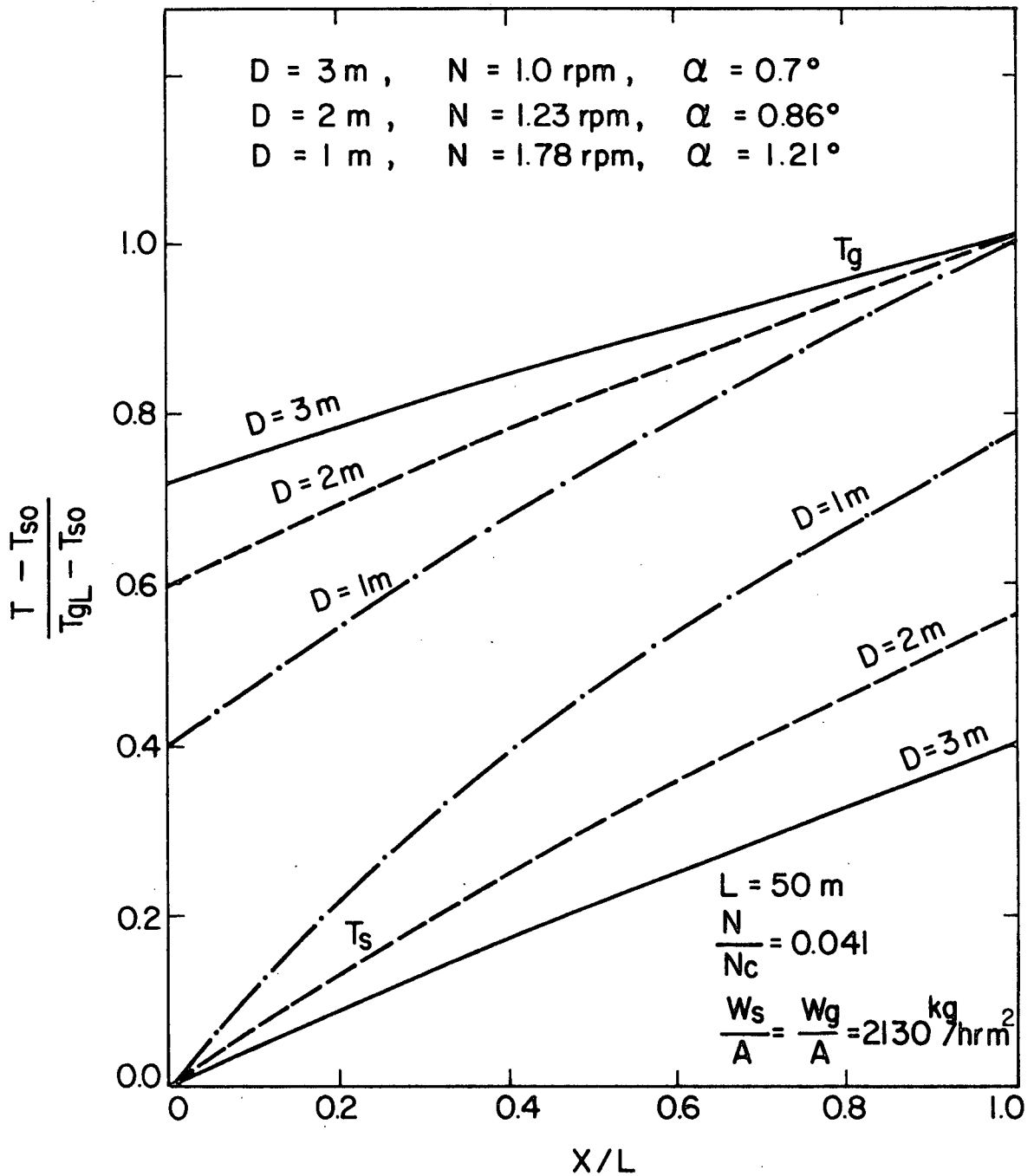
Figure 8-6 Effect of Kiln Diameter on Modelling
of Rotary Kiln Heat Exchanger
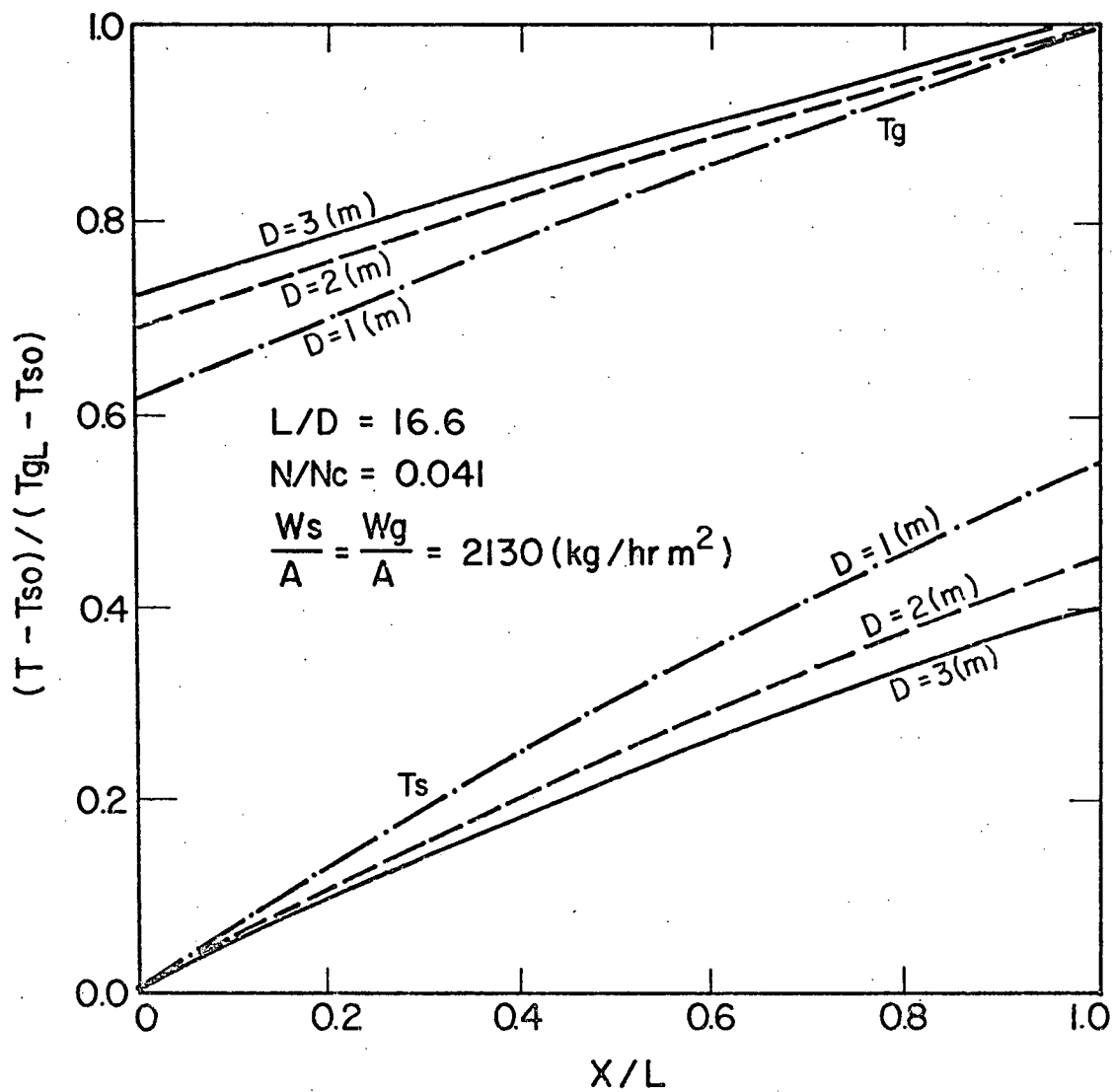
Figure 8-7 Effect of Kiln Diameter on Temperature
Profile at Fixed L/D ratio

length, the strong effect on heat transfer coefficients over-
comes the negative effect of short length.

The model of the rotary kiln heat exchanger has been
developed for low temperature and non-reacting systems. The
high temperature process requires a radiative term added into
Equations 8-1 and 8-2 which will result in non-linear first-
order equations. For a reaction system an additional term,
the heat of reaction, should be added, and the equation for
material balance should be supplemented as well.

CHAPTER 9

CONCLUSIONS

Convective heat transfer from gas to solids bed and wall
has been studied experimentally as a function of operating para-
meters. The parameters covered included temperature level, gas
flow rate, solid throughput, inclination angle, rotational
speed, degree of fill and particle size. Tests were done on
both limestone and Ottawa sand. It was found that the heat
transfer coefficient from the gas to solids bed based on the
plane chord area is roughly an order of magnitude higher than
that from gas to wall. The experimental results show that both
solid throughput and inclination angle have no influence on heat
transfer coefficients and the effect of degree of fill on the
gas to wall heat transfer coefficient is insignificant. The
effect of particle size is negligible, which possibly results
from the narrow range of particle sizes tested. The following
dimensional equations have been obtained for the correlation
of experimental data for Ottawa sand.

$$h_{gs} = 2.44 \, W_g^{0.575} \, \dot{N}^{0.091} \, \eta^{-0.171}$$

and
$$h_{gw} = 0.82 \, W_g^{0.475} N^{-0.297}$$

The higher gas to solids bed heat transfer coefficients partly result from the underestimation of the true surface area used in the calculation of the coefficient. The actual exposed surface area is about twice as much as the plane chord area. Rapid particle velocity on the bed surface contributes significantly to high gas-solids bed heat transfer. It not only agitates the gas adjacent to the bed surface, but also convects heat by virtue of mixing of the fast-rolling particles into the bed. A mathematical model has been developed to describe the influence of particle movement for a rolling bed.

Since the motion of aerated particles was thought to be important for heat transfer, exploratory experiments on measurements of surface time and surface velocity were made. In the rolling bed the lateral velocity of particles on the bed surface increases with the square root of the rotational speed.

Residence time distribution in a rotary kiln was studied briefly. The results show that the solid flow in a rotary kiln can be assumed as a plug flow axially and well-mixed radially.

A simple model of a rotary kiln heat exchanger was constructed to illustrate the effects of kiln parameters on temperature profiles in a low temperature kiln.

CHAPTER 10

RECOMMENDATION FOR FUTURE WORK

Future work on convective heat transfer in a rotary kiln should entail gathering more data relating to particle mechanics - particularly particle velocity on the bed surface. Besides rotational speed, degree of fill may also be a major factor on surface time, ratio of surface time to retention time and thickness of surface layers. The thickness of surface layers and its associated particle velocity in each layer should be investigated to thoroughly understand the heat transfer mechanism, particularly in high temperature processes such as the direct-fired kiln. The experiments could be carried out in a lucite kiln using a high speed camera.

In industrial kilns the slumping type of particle movement may also occur. Since it has been indicated that increased bed surface velocity is one of the major factors that enhances heat transfer coefficients, it is to be expected that gas to solids bed heat transfer will increase significantly as the slumping frequency of particle mass increases until the bed reaches the rolling mode. Further work is also suggested to investigate the heat transfer in the slumping bed, particularly the influence of slumping frequencies which in turn are affected

by rotational speed.

Although the correlation equations for convective heat transfer coefficients for both gas to bed and gas to wall have been obtained in the present study, it is still inadequate for scaleup and design for industrial kilns. It is thus, suggested that the kilns of at least two sizes larger than one used in the present study be tested, so that the effects of diameter, and length to diameter ratio can be demonstrated.

NOMENCLATURE

A	area	m^2
A_s	plane area of bed surface	m^2
A_s'	actual area of bed surface	m^2
A_n	constants, defined in Table 8-1	-
a	heat diffusivity	m^2/s
B_n	constants, defined in Table 8-1	-
C	dimensionless concentration	-
C_p	specific heat	J/gK
c	number of particles per unit weight	kg^{-1}
D	kiln diameter	m
D_n	constants, defined in Table 8-1	-
D	axial dispersion coefficient	m^2/s
d_a	distance per cycle	m
d_p	particle diameter	m
d'	thickness of wall layer	m
E	exit gas distribution	s^{-1}
E_n	constants, defined in Table 8-1	-
F	solid volumetric flow rate	m^3/s
F_m	emerging rate of particles from bed region to surface region	s^{-1}
G_g	gas mass flux based on empty kiln	$kg/hr\text{-}m^2$
g	acceleration of gravity	m/s^2
H	heat flow rate	W
h	heat transfer coefficient	W/m^2K
h_d	conductive heat transfer coefficient	W/m^2K
h_{gs}'	gas-to-bed heat transfer coefficient based on actual surface area	W/m^2K
h'	relative heat transfer coefficient	m^{-1}
k	thermal conductivity	W/mK
L	kiln length	m
l_t	length of test section	m
l_s	bed surface area per unit length	m^2/m
l_w	exposed wall area per unit length	m^2/m

l_w'	covered wall area per unit length	m^2/m
M	number of particles per unit volume	m^{-3}
m	number of particles per unit area	m^{-2}
N	rotational speed	rpm
N_c	critical rotational speed	rpm
n	rotational speed	rps
Q	heat transfer rate	W
q	heat transfer rate per unit length	W/m
R	kiln radius	m
r	radius position	m
S	exposed area of particle surface	m^2
S'	covered area of particle surface	m^2
T	temperature	K
T_{go}	entering gas temperature	K
T_{g1}	exit gas temperature	K
T_{sm}	particle mixing temperature	K
$\bar{t}$	retention time or residence time	s
t_b	bed time	s
t_c	contact time	s
t_s	surface time	s
t_t	cycle time	s
$\bar{t}_\tau$	retention time	s
$\bar{u}$	average axial velocity	m/s
u_o	velocity defined in equation 7-19	m/s
U_o	overall gas-solid heat transfer coefficient	W/m^3K
V_a	axial velocity on bed surface	m/s
V_1	lateral velocity on bed surface	m/s
V_r	radial velocity in the bed region	m/s
W	mass flowrate	kg/hr
x	distance	m
z	x/L	—

Greek letters

α	Kiln inclination angle	radian
α_0	Kiln inclination angle	degree
β	Central angle of the sector occupied by the solid bed	radian
θ	static angle of repose	radian
θ'	dynamic angle of repose	radian
θ_0	dynamic angle of repose	degree
ξ	dimensionless time	–
η	degree of solid fill	–
λ	Angle between inclined bed & horizontal	radian
μ_g	gas absolute viscotiy	Ns/m^2
ν_g	gas kinematic viscosity	m^2/s
ρ_s	particle bulk density	kg/m^3
ρ_p	particle true density	kg/m^3
ρ_g	gas density	kg/m^3
τ	bed height	m
τ_L	bed height at x=L	m
σ	Stefan-Boltzmann constant (5.67×10^{-8})	$W/m^2 K^4$
σ_t	absolute variance	s
σ_θ	relative variance	–
φ	shearing angle	radian
ψ	Angle between bed surface and kiln axis	radian
ω	angular velocity	radian/s
ω_c	critical angular velocity	radian/s
δ_u	parameter defined in Equation 2-31	m
ε_g	gas emissivity	–
ε_s	solid emissivity	–
ε_w	wall emissivity	–
κ	Thickness of surface region	m

Dimensionless Groups

Bi	$\bar{h}D/k_s$	Biot number
Fo	at/r_p	Fourier number
Fr	N/N_c	Froude number
Ga	$\dfrac{d^2 \rho_g^3 g}{\mu^2}$	Gallileo number
N_k	$\dfrac{R \cos\theta}{L \tan\alpha}$	defined in Chapter 2
N_ϕ	$\dfrac{F \sin\theta}{nR^3 \tan\alpha}$	defined in Chapter 2
Nu	$\dfrac{hD}{k_g}$	Nusselt number
Nu_p	$\dfrac{h_{pf}d_p}{k_g}$	particle Nusselt number
Pe	uL/D	Peclet number
Pr	$C_p\mu/k_g$	Prandtl number
Re	$uD\rho_g/\mu_g$	Reynolds number
Re_p	$\dfrac{u_o \rho_g d_p}{\mu_g}$	particle Reynolds number
$Re_{\omega'}$	$\dfrac{D_e^2 \omega \rho_g}{\mu_g}$	Rotating Reynolds number or Taylor number

Subscripts:

g	gas
p	particle
s	bulk solid material, bed
w	exposed wall
w'	covered wall
gs	gas to solid bed
gw	gas to wall
sw	solid bed to covered wall
1	particle in the first exposed layer
2	particle in the second layer

REFERENCES

1. Sugishima, W., 'Plastics Wastes Incineration by Rotary Kiln',
        Fuel Society of Japan, 51 (4), 233 (1972).

2. Wilson, K., 'The SL/RN Process at the Griffith Mine',
        presented at 16th Conference of Metallurgists,
        Vancouver, Canada, August 22-24, 1977.

3. Wachters, L.H.J. and Kramers, H., 'The Calcining of Sodium
        Bicarbonate in a Rotary Kiln', Proc. 3rd European
        Symposium Chemical Reaction Engineering, 77 (1964).

4. Brimacombe, J.K. and Watkinson, A.P., 'Heat Transfer in a
        Direct-Fired Rotary Kiln: I, Pilot Plant and
        Experimentation, II, Heat Flow Results and Their
        Interpretation'. Accepted for Publication Trans.
        A.I.M.E. (1978).

5. Riffaud, J.B., Koehret, B. and Coupal, B., 'Modelling and
        Simulation of an Alumina kiln', Brit. Chem. Engr.
        & Proc. Tech., 17 (5), 413-418 (1972).

6. Manitius, A., Kurcyuse, E., and Kawecki, W., 'Mathematical
        Model of the Aluminum Oxide Rotary Kiln'. IEC,
        Process Des. Develop., 13(2), 132-142 (1974).

7. Lyons, J.W., Min, H.S., Parisot, P.E., and Paul, J.F.,
        'Experimentation with a Wet-Process Rotary
        Cement Kiln via the Analog Computer', I & EC
        Proc. Design and Development, 1 (1), 29-33 (1962).

8. Min, H.S., Parisot, P.E., Paul, J.F., and Lyons, J.W.
        'Computer Simulation of Wet-process Cement Kiln
        Operation', Nometallic Minerals Processing, 35-39,
        September 1962.

9. Wingfield, S.L., Prothero, A. and Auld, J.B. 'A Mathematical
        Model of a Rotary Kiln for the Partial Reduction
        of Iron Ore'. Journal of the Institute of Fuel,
        64-72 March, 1974.

10. Tukamoto, T., Simada, S., Taguchi, T., and Higuchi, J.
        'A Mathematical Model of the Sintering Processes'.
        Tetsu-to-Hagane, 56, 661 (1970), Also BISI 9050.

11. Toyama, S. and Sugeta, T. 'Simulation and Design Study on
        Rotary Kiln of Firing Light Weight Aggregate'.
        Togako Kogako, 33 (10), 1019-1023 (1969).

12. Sass, A., 'Simulation of the Heat-Transfer Phenomena in a
        Rotary Kiln', I & EC Process Design and Develop-
        ment, 6 (4), 532-535 (1967).

13. Imber, M. Ph.D. Thesis 'A Mathematical Analysis of the
           Rotary Kiln Heat Exchanger', Columbia University
           (1958).

14. Vaillant, A., Ph.D. Thesis
           'Thermal Analysis of the Direct Fired Rotary Kiln'.
           Columbia University (1965).

15. Kern, J., 'Heat Transfer in a Rotary Heat Exchanger'.
           Int. J. Heat Mass Transfer, 17, 981-990 (1974).

16. Pearce, K.W., 'A Heat Transfer Model for Rotary Kilns',
           Journal of the Institute of Fuel, 362, December, 1973.

17. Rosa Von J., 'Mathematical Formulation of the Heat Transfer
           in the Rotary Kiln', Zement-Kalk-Gips, Val 23 (8),
           368 (1970).

18. Roberts, F., Taylor, R.F. and Jenkins, T.R., 'High Temperature
           Chemical Reaction Engineering', The Institute of
           Chemical Engineers, London, 1971.

19. Rutgers, R., 'Longitudinal Mixing of Granular Material
           Flowing through a Rotating Cylinder', Chemical
           Engineering Science, 20 (1965), Part I. Descrip-
           tive and Theoretical, p. 1079, Part II. Experi-
           mental, p. 1089.

20. Zablotny, W.W., 'The Movement of the Charge in Rotary Kilns',
           International Chemical Engineering, 5 (2), 360 (1965).

21. Sullivan, I.D., Maier, C.G. and Ralston, D.C., 'Passage
           of Solid Particles through Rotary Cylinder Kilns',
           U.S. Bureau Mines Technical Report, No. 384, (1972).

22. Henein, H., Brimacombe, J.K. and Watkinson, A.P., The
           University of British Columbia, unpublished research.

23. Themelis, N.J., Donaldson, J.W., and Udy, M.C., 'Use of the
           Similarity Principle in Predicting the Optimum
           Performance of Iron Reduction Kilns', The Canadian
           Mining and Metallurgical, Bulletin, p. 434, April,
           1964.

24. Bayard, R.A., 'New Formula Developed for Kiln Time',
           Chemical and Metallurgical Engineering, 52, 100
           March 1945.

25. Saeman, W.C., 'Passage of Solids through Rotary Kilns',
           Chemical Engineering Progress, 47(10), 508 (1951).

26. Pickering, R.W., Feakes, F. and Fitzgerald, M.L., 'Time for Passage of Material through Rotary Kilns', Journal of Applied Chemistry, $\underline{1}$(1) A7 (1951).

27. Varentsor, P.V., Yufa, M.S., 'The Movement of a Bed of Solid Particles in Rotary Kilns', International Chemical Engineering, $\underline{1}$(1), 88 (1961).

28. Vahl, L. and Kingma, W.G., 'Transport of Solids through Horizontal Rotary Cylinders', Chemical Engineering Science, 1(6), 253 (1952).

29. Kramers, H. and Croockewit, P., 'The Passage of Granular Solids Through Inclined Rotary Kilns', Chemical Engineering Science, 1(6), 259 (1952).

30. Abouzeid, A.Z.M.A., Mika, T.S., Sastry, K.V. and Fuerstenau, D.W., 'The Influence of Operating Variables on the Residence Time Distribution for Material Transport in a Continuous Rotary Drum', Powder Technology, $\underline{10}$, 273 (1974).

31. Wes, G.W.J., Drinkenburg, A.A.H., and Stemerding, S., Solids Mixing and Residence Time Distribution in a Horizontal Rotary Drum Reactor', Powder Technology, $\underline{13}$, 177 (1976).

32. Moriyama, A., and Suga, T., 'Axial Dispersion and Residence Time Distribution of Spherical Particles in Rotary Kiln', Tetsu-to-Hagane, $\underline{60}$(9), 1283 (1974).

33. Levenspiel, O., Chemical Reaction Engineering, Wiley, N.Y., 2nd Edition, 1972, Chapter 9.

34. Matsui, Graduation Thesis from Nagoya Institute of Technology, Japan, 1972.

35. Lu, W.M., Shiau, C.Y. and Chen, C.C., 'Study on Mixing of Solid Particles in a Rotary Cylinder with Cross Air Flow', Journal of Chinese Institute of Chemical Engineering, $\underline{4}$, 52 (1973).

36. Sugimoto, M., Endoh, K., and Tanaka, T., 'Behavior of Granular Materials Flowing through a Rotary Cylinder - Effects of Segregation Zones on the Residence Time Distribution of Particles', Kagaku Kogaku, $\underline{31}$(2), 145 (1967).

37. Sugimoto, M., 'Effect of the Balling Filling on the Residence Time Distributions of Particles Flowing through a Rotary Cylinder', Kagaku Kogaku, $\underline{32}$(2), 196 (1968).

38. Suginioto, M., 'An Estimation of the Residence Time Distribution of Particles Flowing through a Rotary Cylinder'. Kagaku Kogaku 32(3), 291 (1968).

39. Kennedy Van Saun Corporation, Danville, Pa., 'Rock Talk Manual', 1974.

40. Hogg, R., Shoji, K. and Austin, L.G., 'Axial Transport of Dry Powders in Horizontal Rotating Cylinders', Powder Technology, 9, 99 (1974).

41. Bowers, T.G. and Read, H.L., 'Heat Transfer in Rotary Kiln', Chemical Engineering Progress Symposium Series 61(57), 340 (1968).

42. Wes, G.W.J., Drinkenburg, A.A.H., and Stemerding, S. 'Heat Transfer in a Horizontal Rotary Drum Reactor', Powder Technology, 13, 185 (1976).

43. Lehmberg, J., Hehl, M., and Schugerl, K., 'Transversal Mixing and Heat Transfer in Horizontal Drum Reactors', presented at the International Conference SPIRE in Arad, Israel, November 30, December 5, 1975.

44. Nikitenko, G.N. 'Heat Transfer from the wall to the Loose Material in Rotary Drum-Type Kilns', Khimicheskaia Promyshlennost Ukrainy 5, 29-32 (1969).

45. Epstein, N. and Mathur, K.B., 'Heat and Mass Transfer in Spouted Beds - A Review', Canadian Society of Chemical Engineering, 49, 467 (1971).

46. Perry & Chilton (Editors-in-Chief) Chemical Engineering Handbook, 4th Edition, p. 20-36, 1973.

47. Perry, J.H. (Editor-in-Chief) Chemical Engineering Handbook, 3rd Edition, p. 831, McGraw-Hill, New York 1950.

48. Gygi, H., 'The Thermal Efficiency of the Rotary Cement Kiln'. Cement and Lime Manufacture, p. 82, April, 1938.

49. Friedman, S.J. and Marshall, W.R.J., 'Studies in Rotary Drying, Part II Heat and Mass Transfer', Chemical Engineering Progress, 45(9), 573 (1949).

50. Chen, C.C., Lu, W.M. and Teng, L.T., 'Heat Transfer in the Through Flow Rotary Dryer', J. of Chinese Institute of Chemical Engineers, 5, 1-6 (1974).

51. Kaiser, V.A. and Lane,J.W., correspondence to Saas 'Simu-
lation of the Heat Transfer Phenomena in a Rotary
Kiln', I & EC Process Design and Development, 7
(2) 318 (1968).

52. Eckert, E.R.G., and Drake, R.M., 'Heat and Mass Transfer',
McGraw Hill, New York, 1959, p. 405.

53. Luethge, J.A., 'Measurement and Control of Temperatures in
Rotary Kilns', Instrumentation Technology, 46,
March 1968.

54. Venkateswaran,V., M.A.Sc. Thesis, 1976, The University of
British Columbia.

55. 1974 ASTM Standard book, E-220 and E-230.

56. Hills, A.W.D. and Paulin, A., 'The Construction and
Calibration of an Inexpensive Microsuction
Pyrometer', Journal of Scientific Instruments
(J. of Physics E) 2, 713 (1969).

57. Brinn, M.S., Friedman, S.J., Gluckert, F.A. and Pigford,
L.R., 'Heat Transfer to Granular Materials', Ind.
Eng. Chem., 40, 1050 (1948).

58. Kreith, F., 'Principles of Heat Transfer', International
Textbook Co., Scranton, Pa. (1969).

59. Irvine, T.F. Jr. and Hartnett, J.P., 'Steam and Air Tables
in SI Units', Hemisphere Pub. Co., Washington (1976).

60. Friedman, S.J. and Marshall, Jr., W.R., 'Studies in Rotary
Drying - Part I - Holdup and Dusting', Chemical
Engineering Progress, 45(3), 482 (1949).

61. Shevtsov, B.I., Kubyshev, N.N., Cherepivskii, A.A. and
Bogdanov, Yu.Yu., 'Determination of the Rate of
Movement of the Charge in Rotary Kiln by means
of Radioactive Isotopes', International Chemical
Engineering, 11(2), 252 (1971).

62. Miskell, F., and Marshall, Jr., W.R., 'A Study of Retention
Time in a Rotary Dryer', Chemical Engineering
Progress, 52(1), 35(1956).

63. Botterill, J.S., Butt, M.H.D., Cain, G.L. and Redish, K.A.,
Proc. Eindhoven Fluidization Symposium, p.442
(1967).

64. Ernest, R., 'Warmeubergang an Warmeaustauschern in Moving
Bed', Chem, Ing. Techn. 32, 17 (1960).

65. Rohsenow W.M. and Hartnett, J.P. (Editors-in-Chief),
        'Handbook of Heat Transfer', McGraw-Hill Inc.,
        N.Y., N.Y. (1973).

66. McAdams, 'Heat Transmission', McGraw-Hill Book Co., 1954.

67. Schlichting, H., 'Boundary Layer Theory', p. 407, McGraw-
        Hill Book Co. Inc., N.Y., 1957.

68. Cannon, J.N., 'Heat Transfer from a fluid flow inside a
        Rotating Cylinder', Ph.D. dissertation, Stanford
        University, 1965.

69. Brimacombe and Watkinson, 'Calcination of Limestone in a
        Rotary Kiln', 17th Conference of Metallurgists,
        CIM, Vancouver, August, 1977.

70. Carslaw, H.S. and Jaeger, J.c., 'Conduction of Heat in
        Solids'. 1947, Oxford.

71. Kunii D. & Levenspiel, O, 'Fluidization Engineering',
        Hohn Wiley & Sons, Inc., New York. 1969.

APPENDIX A

CALIBRATION OF EQUIPMENT

1. Thermocouple Calibration

The iron-constantan thermocouples were calibrated in an oil bath equipped with Haake thermo regulator (Model FS) for temperatures up to 400 K. The millivolt readings were recorded on Watanabe Multicorder recorder (Model 641). In addition, the thermocouples were also calibrated at two temperatures, the melting points for tin and zinc (504.8 K and 692.75 K). The metal granules were first heated in the bath until they melted and the heat was then shut off. The thermocouple was then dipped into the metal bath. The millivolt readings were taken and recorded. The results were shown in Figure A-1. The readings 12.60 mV and 23.00 mV, were obtained for tin and zinc respectively.

Figure A-2 shows the results of thermocouple calibration in the constant temperature baths over the temperature range of 300 to 700 K. The millivolt readings for each thermocouple were fitted by least squares to a quadratic equation of the form,

$$T = a + b \text{ (millivolts)} + c \text{ (millivolts)}^2$$
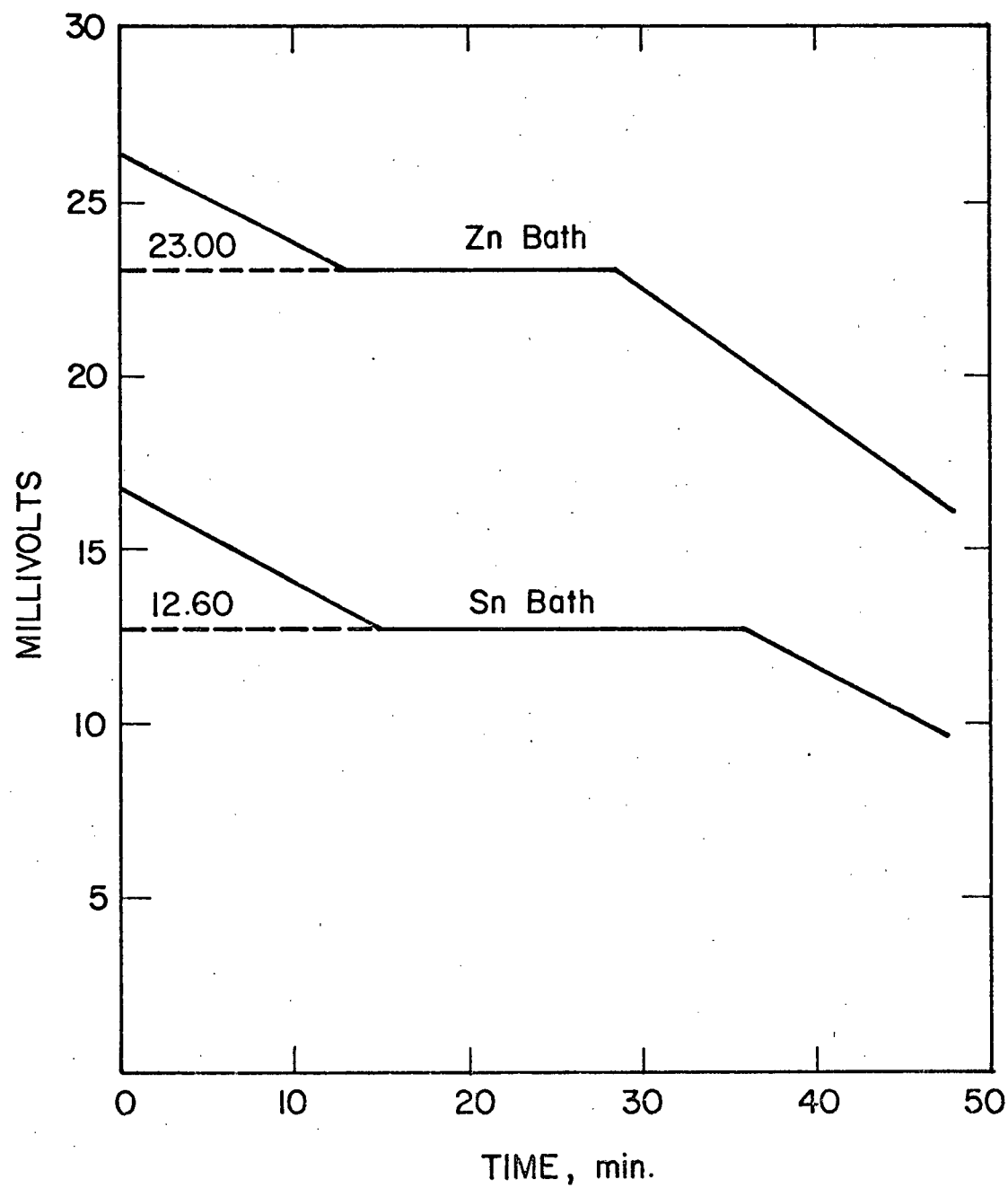
Figure A-1   Calibration of Thermocouple in Metal Baths.
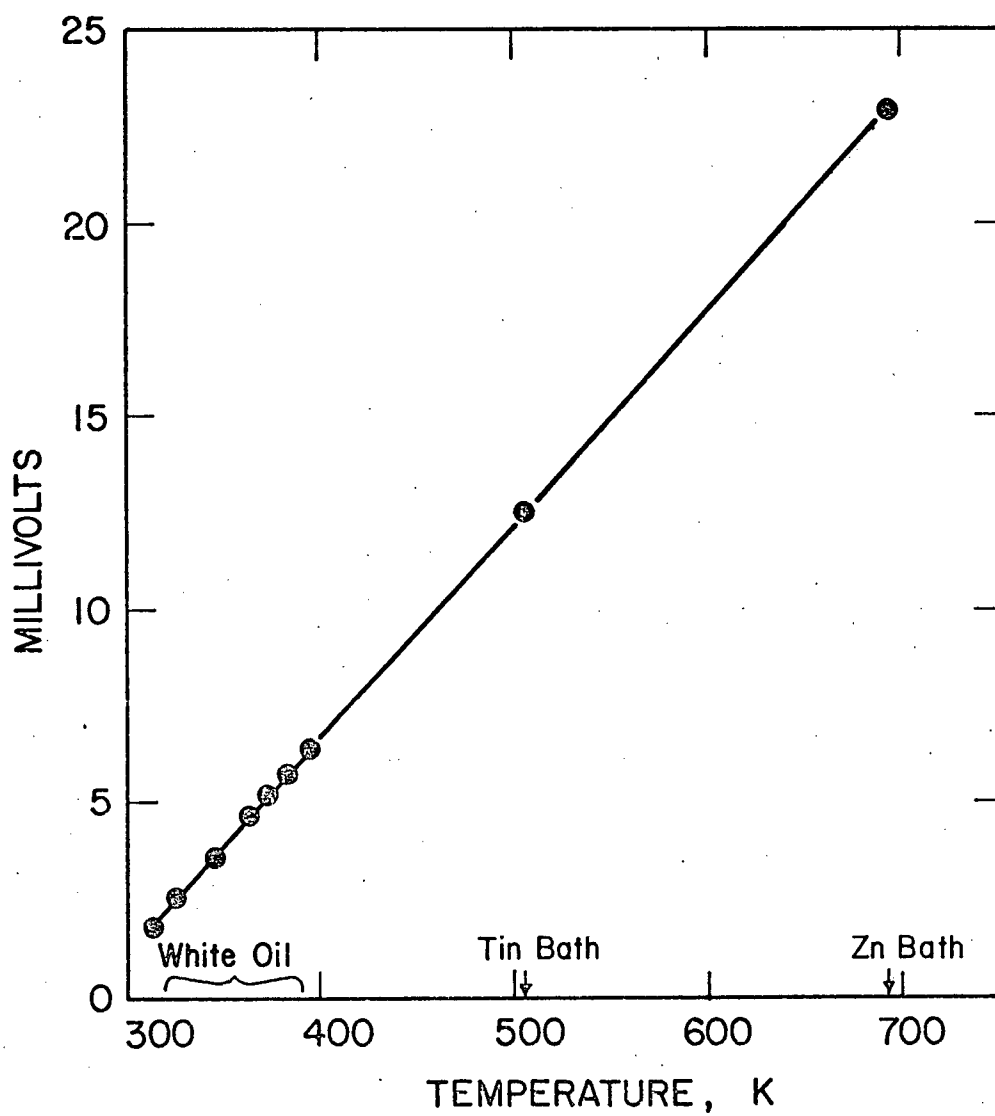
Figure A-2   Calibration of Iron-Constantan
Thermocouples.

The constants for the above equation are given in Table A-1, along with the deviations of the calibrated values from measured values at two temperatures. The measured values were also compared with those tabled in the ASTM Standard manual (55) with the maximum deviation of $\pm$ 1.8 K. The thermocouple data in the manual are given in Table A-2.

2. Calibration of Rotameter

The rotameters were calibrated against gas meters. The calibration curves are given in Figures A-3 and A-4.

Table A-1

Calibration of Thermocouples

THERMOCOUPLE NO.	a	b	c	Deviation K 343°K	Deviation K 504.8 K
A	279.21	17.961	0.0000	0.36	0.70
B	279.55	17.935	0.0003	0.08	0.79
C	278.11	18.187	-0.0111	0.29	0.35
D	277.72	18.197	-0.0108	0.30	0.39
E	277.75	18.425	-0.0224	0.27	0.65
F	280.03	17.875	0.0020	-0.53	0.78
G	278.08	18.158	0.0005	0.30	0.33
H	280.32	17.327	0.0324	0.32	0.80
I	279.87	17.553	0.0062	0.17	0.87
J	277.55	18.189	-0.0101	0.29	0.33
K	279.12	17.681	0.0266	-0.03	0.41
L	276.28	18.736	-0.0346	0.14	0.28
M	278.38	18.047	-0.0022	0.71	0.61
N	269.60	20.980	-0.1348	0.23	-0.81
O	282.91	16.707	0.0367	0.71	0.92
P	277.70	18.104	-0.0034	0.58	0.47
Q	284.13	16.078	0.0910	0.54	0.98
R	273.89	19.869	-0.0529	0.61	-0.10
S	277.80	17.931	0.0108	0.06	0.65
T	268.41	20.874	-0.1174	-0.11	-1.00

$$T \ (K) = a + b(\text{millivolts}) + c(\text{millivolts})^2$$

Table A-2

Thermocouple Data

Reference Temperature
at 0 C.

Voltage millivolt	Temperature C	Temperature K
1.019	20	293.15
1.536	30	303.15
2.058	40	313.15
2.585	50	323.15
3.116	60	333.15
3.649	70	343.15
4.186	80	353.15
4.725	90	363.15
5.268	100	373.15
6.359	120	393.15
7.457	140	413.15
8.560	160	433.15
9.667	180	453.15
10.777	200	473.15
12.998	240	513.15
15.217	280	553.15
16.325	300	573.15
18.537	340	613.15
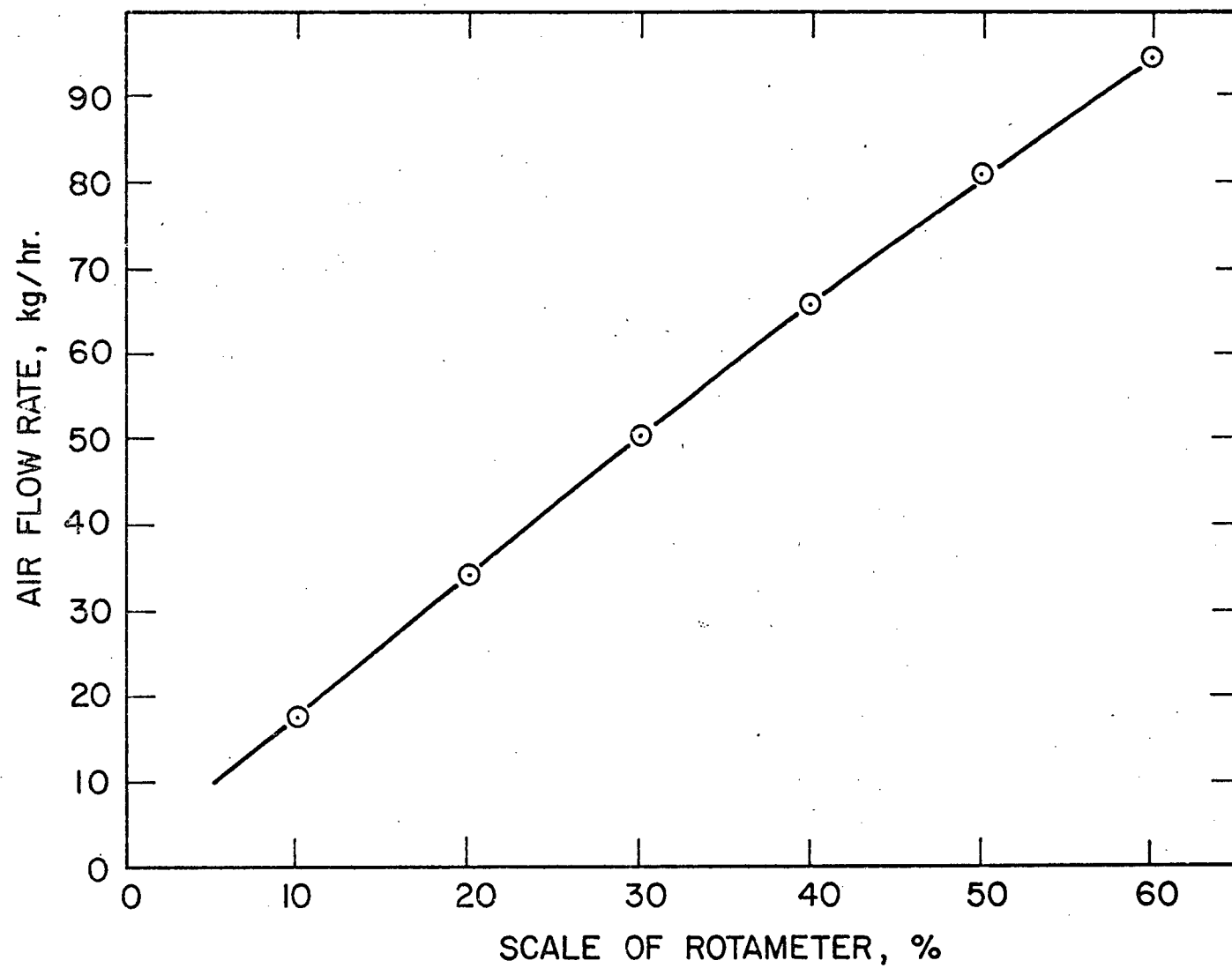
Figure A-3   Air Flow Rate versus Reading on Rotameter Scale (Rotameter 2854).
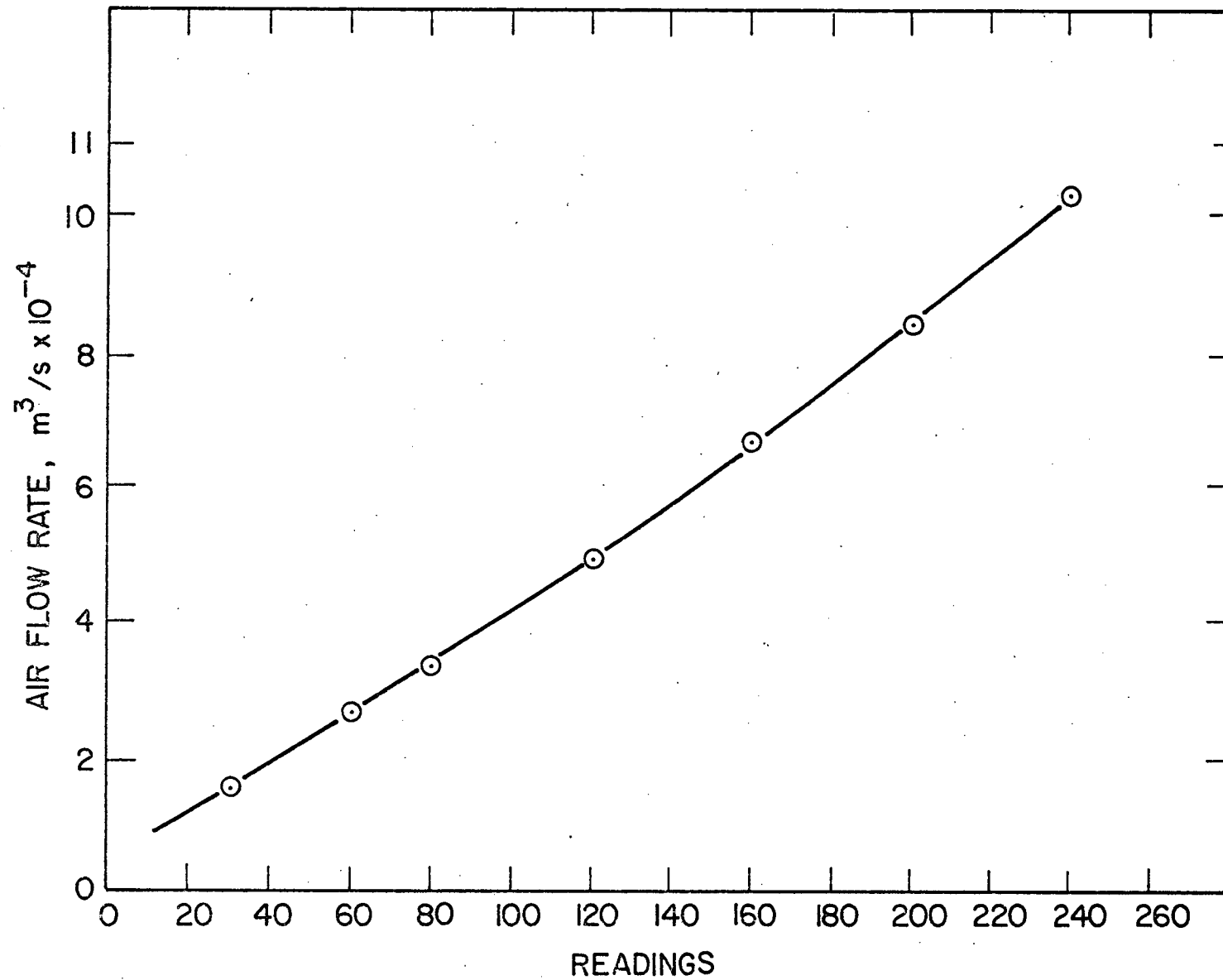
Figure A-4   Suction Rate versus Reading on Rotameter Scale (Rotameter 2487).

APPENDIX B

SURFACE AREA AND SURFACE VELOCITY

1. Determination of A_s'/A_s

The ratio of A_s'/A_s is important in determining heat transfer coefficient. The surface region comprises several surface layers. However, only the first two layers seem to be exposed to gas stream. In order to calculate the ratio of A_s'/A_s, the exposed surface area of individual particles in each of the first two layers have to be determined. The differential surface area of a spherical particle is

$$dS = \frac{d_p^2}{4} \, d\theta \sin\zeta \, d\zeta \qquad (B-1)$$

The array of particles in the first two layers is either a cubic arrangement as given in Figure 7-2B, or a structure as given in Figure 7-2A. In the latter array, the particles in the first layers are shown in Figure B-1. Therefore, the exposed surface of individual particle can be obtained by integrating the following equation.

FIRST LAYER
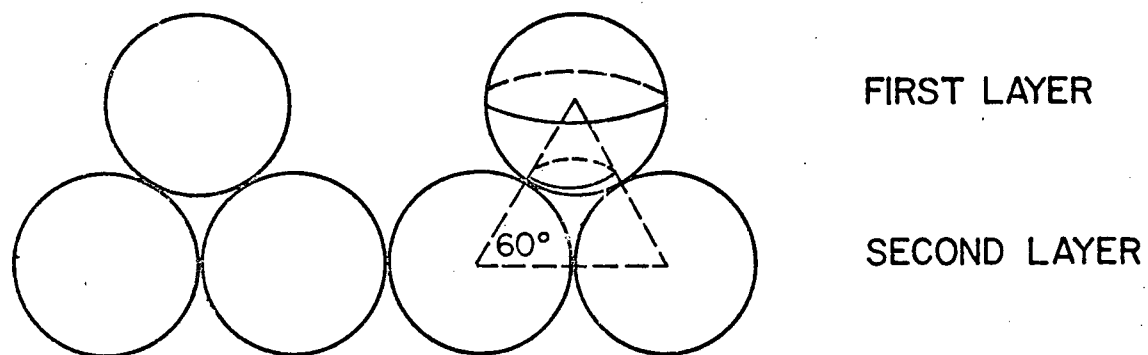
SECOND LAYER

Figure B-1   Particle Configuration in Surface Layers.

$$S_1 = \frac{d_p^2}{4} \int_0^{2\pi} d\theta \int_0^{\frac{5}{6}\pi} \sin\zeta \, d\zeta$$

$$= \frac{\pi d_p^2}{2} \left[1 + \frac{\sqrt{2}}{2} \right] \tag{B-2}$$

Similarly, the exposed area of the second layer particle is

$$S_2 = \frac{1}{2} \cdot \frac{d_p^2}{4} \int_0^{2\pi} d\theta \int_0^{\frac{2\pi}{3}} \sin\zeta \, d\zeta$$

$$= \frac{3\pi}{8} \cdot d_p^2 \tag{B-3}$$

Consider a plane surface with dimension $3d_p$ by $(1 + \frac{\sqrt{2}}{2})d_p$ as shown in Figure 7-2A. There are two particles in the first layer and 6 particles in the second layer. Thus, the ratio of A_s'/A_s is

$$\frac{A_s'}{A_s} = \frac{2S_1 + 6S_2}{3d_p(1+\frac{\sqrt{2}}{2})d_p} = 2.42 \tag{B-4}$$

In a cubic array as shown in Figure 7-2A the aerated area of individual particle in the first layer is represented by

$$S_1 = \frac{\pi}{2} d_p^2 \qquad\qquad (B-5)$$

It is assumed that all the space other than that occupied by the first layer particles are aerated by the second layer particles. Therefore, the total exposed area of the first layer particles in a plane area, $4\,d_p \times 4d_p$ is

$$\frac{\pi}{2} d_p^2 \times 16 = 8\pi d_p^2 \qquad\qquad (B-6)$$

and that of the second layer particles are

$$4d_p \times 4d_p - 16\,\frac{\pi}{4}\,d_p^2 = 4(4 - \pi)d_p^2 \qquad\qquad (B-7)$$

The ratio of A_s'/A_s for a cubic array is

$$\frac{A_s'}{A_s} = \frac{8\pi d_p^2 + 4(4 - \pi)d_p^2}{16\,d_p^2} = 1.78 \qquad\qquad (B-8)$$

2. Particle exchange rate between the bed region and the surface region

The temperature of the aerated surface particles will be raised from T_s to T_{s1} before they return into the bed region. Just before they return to the bed the heated particles

mix with the particles in the other surface layers, which receive no heat from the gas stream. In order to find the temperature of the mixture the rate of the particles emerging out of the bed region must be determined.

Assume the kiln rotates at a speed, N, as shown in Figure B-2. The angular velocity will be $\omega = 2\pi n$ (radians/s). The velocity of the particles normal to the bed surface is

$$V_N = \omega r \sin\zeta \qquad (B-9)$$

Let l_s' be the length of the boundary between the surface region and the bed, and M, the number of particles per unit volume. For a plane area, $\Delta x \dfrac{l_s'}{2}$, the emerging rate of the particles is represented by

$$F_m = M\Delta x \int_0^{l_s'/2} V_N dy \qquad (B-10)$$

where y is the distance from the central line, OA' as shown in Figure B-2. Let h_B' be equal to OA'. Then

$$y = h_B' \tan\zeta$$

and $$r = h_B' \sec\zeta \qquad (B-11)$$

The first equation is derived with respect to ζ and the following equation is obtained

Figure B-2   Emerging Rate of Particles from Bed
            Region to Surface Region

$$dy = h_B' \sec^2 \zeta \, d\zeta \qquad \qquad \text{(B-12)}$$

Therefore, equation B-10 is rewritten and integrated as follows:

$$F_m = M\Delta x \int_0^{\frac{\beta'}{2}} \omega h_B'^2 \tan\zeta \sec^2\zeta \, d\zeta$$

$$= M\Delta x \omega h_B'^2 \left[\frac{1}{2} \sec^2\zeta \right]_0^{\frac{\beta'}{2}}$$

$$= \frac{1}{2} M\Delta x \omega h_B'^2 \tan^2\frac{\beta'}{2}$$

$$= \frac{1}{8} M\Delta x \omega l_S'^2$$

$$= \frac{\pi}{4} nM\Delta x l_S'^2 \qquad \qquad \text{(B-13)}$$

The term, l_S', is the length of the boundary line, and related to kiln diameter and degree of fill. Let κ be the thickness of the surface region. Then

$$h_B' = h_B + \kappa$$

By taking square on both sides, equation B-14 is obtained

$$h_B'^2 = (h_B + \kappa)^2$$

$$= h_B^2 + 2\kappa h_B + \kappa^2 \qquad \qquad \text{(B-14)}$$

Since

$$h_B'^2 = R^2 - \left(\frac{l_s'}{2}\right)^2$$

and

$$h_B = R^2 - \left(\frac{l_s}{2}\right)^2$$

equation B-14 can be rewritten as

$$l_s'^2 = l_s^2 - 8R\kappa\cos\frac{\beta}{2} + \kappa^2 \tag{B-15}$$

By neglecting κ^2, equation B-13 for F_m becomes

$$F_m = \frac{\pi}{4} M\Delta xn(l_s^2 - 8R\kappa\cos\frac{\beta}{2}) \tag{B-16}$$

As indicated in Figure 6-3, the particle velocity in the surface region can be approximated by a linear function as

$$V = \frac{\zeta}{\kappa} V_1 \tag{B-17}$$

where ζ is the distance outward from the boundary between two region as shown in Figure B-3, and V_1 is the surface velocity of particles in the first layer. For a width Δx of the kiln the rate of the particles rolling on the bed surface is represented by
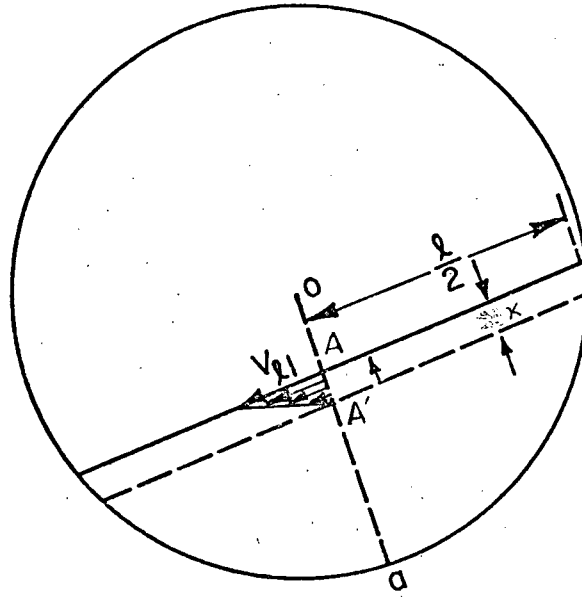
Figure B-3 Particle Velocity Profile in Surface
Region.

$$F_m = M\Delta x \int_0^\kappa V d\zeta$$

$$= \tfrac{1}{2} M\Delta x \kappa V_1 \qquad\qquad (B-18)$$

By equating equation B-16 and equation B-18, one obtain a relationship of κ and V_1 as functions of n.

$$\kappa V_1 = \frac{\pi}{2} n \ (1_s^2 - 8R\kappa\cos\frac{\beta}{2}) \qquad\qquad (B-19)$$

In addition, the surface velocity, V_1 was found as a function of square root of rotational speed, the thickness is then depending on the rotational speed and degree of fill by the following equation

$$\frac{1}{\kappa} \propto \frac{1}{1_s^2}\left[\frac{1}{\sqrt{n}} + 8R\cos\frac{\beta}{2}\right]$$

APPENDIX C

SAMPLE CALCULATIONS

1. Calculation of residence time distribution

The sample calculations for mean residence time, variance, Peclet number and dispersion coefficient are presented. The experimental data for run R2 is given in the first two columns in Table C-1. The concentration, $C(t_i)$ represents

$$C(t_i) = \frac{\dfrac{\text{no. of tracer in the sample}}{\text{no. of total tracer used}}}{\dfrac{\text{wt. of sample}}{\text{wt. of bed}}}$$

In this run, the weight of total color tracer used was 13.7 gm (939 individual tracers). The first sample was collected at t = 8 minute. After the tracers were fed. The weight of the sample was 243.9 g in which 5 tracers were found. The bed weight was 9.4 kg. Thus $C(t_i)$ for the first sample is

$$C(t_i) = \frac{5/939}{243.9/9400} = 0.205$$

With the same procedure the values of $C(t_i)$, i = 2, 3,.....M

Table C-1

Tabulation of Calculation for RTD run (R2)

t_i (min)	$C(t_i)$ (-)	$F(t_i)$ $(min)^{-1}$	$F(t_i)t_i\Delta t_i$	$F(t_i)(t_i-\bar{t})^2\Delta t_i$
8.00	0.205	2.09×10^{-2}	0.042	0.0072
8.25	2.300	23.40	0.483	0.0495
8.50	5.159	54.58	1.158	0.0612
8.75	6.731	68.47	1.498	0.0302
9.00	9.571	97.37	2.190	0.0703
9.25	5.924	60.26	1.394	0.0010
9.50	3.543	36.04	0.859	0.0098
9.75	1.582	16.09	0.392	0.0135
10.00	1.360	13.84	0.346	0.0238
10.25	0.622	6.33	0.162	0.0185
10.50	0.580	5.90	0.155	0.0261
10.75	0.402	4.09	0.102	0.0255
11.00	0.360	3.66	0.101	0.0397
11.25	0.345	3.51	0.099	0.0380
11.50	0.268	2.73	0.079	0.0371
11.75	0.194	1.97	0.058	0.0328
12.00	0.160	1.63	0.041	0.0326
			9.17 (min)	0.453 (min)

are calculated and the results are listed in Table C-1. From

equation 5-5, the exit age distribution function $E(t_i)$ is

defined as

$$E(t_i) = \frac{C(t_i)}{\sum_i C(t_i) \Delta t_i}$$

where

$$\sum_i C(t_i) \Delta t = 9.83 \quad (min)$$

Therefore $E(t_i)$ for the first sample is

$$E(t_i) = \frac{0.205}{9.83} = 0.0209 \quad (min)^{-1}$$

and $E(t_i)$ for all the samples are calculated and tabulated

in the second column in Table C-1. Then the mean residence

time and variance can be calculated from

$$\bar{t} \simeq \sum_{i=1}^{M} t_i E(t_i) \Delta t \tag{5-3}$$

and

$$\sigma_t^2 \simeq \sum_{i=1}^{M} (t_i - \bar{t})^2 E(t_i) \Delta t \tag{5-4}$$

The values of $F(t_i)t_i\Delta t_i$ for each sample is calculated and tabulated in the fourth column in Table C-1. Since the time interval for each sample $\Delta t_i = 0.25$ min, the summation of the values in the fourth column gives

$$\bar{t} = \sum_{i=1}^{M} F(t_i)t_i\Delta t$$

$$= 9.17 \text{ (min)}$$

The mean residence time allows the calculation of $(t_i-\bar{t})^2 F(t_i)$ for each sample. The results are listed in the same table. Therefore,

$$\delta_t^2 = 0.453 \text{ (min)}^2$$

The relative variance and Peclet number are then calculated as

$$\delta_\theta^2 = \frac{\delta_t^2}{\bar{t}^2} = \frac{0.453}{(9.17)^2} = 5.39 \times 10^{-3}$$

and

$$Pe = \frac{2}{\delta_\theta^2} = 371$$

Then the axial dispersion coefficient, D is

$$D = \frac{\bar{u}L}{Pe} = \frac{L^2}{\bar{t}Pe}$$

$$= \frac{2.44^2}{9.17 \times 60 \times 371} = 2.91 \times 10^{-5} \text{ m}^2/\text{s}$$

2. Calculation of the heat transfer Coefficient

The computer program that was used routinely for these calculations is appended. The sample calculation is done for run A16.

The air flow rate and the solid feed rate for the run were 24.6 kg/hr and 14.2 kg/hr respectively. The rotational speed was 1.5 rpm, the inclination angle was 1.2 degree and the solid holdup was 17%. The temperatures of air, sand and wall were measured at x= 1.25 m and 1.78 m from the solid entrance end. The temperature were then interpolated and given in the table in Appendix E. The local heat flows for solids to wall, gas to solids and gas to wall at a given axial location are calculated. The determination of heat flow from solids to bed requires the knowledge of solids to bed heat transfer coefficient which are obtained from Figure 6-26. The diffusivity of Ottawa sand, $a = 0.225 \times 10^{-6}$ m^2/s, the thermal conductivity of Ottawa sand, $k_s = 0.268$ W/mK. The center angle for occupied solids is $\beta = 1.98$ radians. Thus, the value of

$$\frac{nR^2\beta}{a} = \frac{\frac{1.5}{60} \times (0.09525)^2 \times 1.98}{0.226 \times 10^{-6}} = 1987$$

From equation 6-25, the Nusselt number is

$$\frac{h_{sw}l'_w}{k_s} = 11.6 \ (1987)^{0.3} = 113.2$$

and $l'_w = \beta R = 0.189$ m. Thus, the value of h_{sw} is

$$h_{sw} = 113.2 \times 0.268/0.189 = 160.5 \ W/m^2K$$

Since there is a layer of cement about 1 mm thick on the wall, and its thermal conductivity is 0.294 W/mK the equivalent heat transfer coefficient across this layer is $0.294/1.0 \times 10^{-3} = 294 \ W/m^2K$. The overall heat transfer coefficient is

$$h_{sw,o} = \frac{1}{\frac{1}{1605} + \frac{1}{2940}} = 103.8 \ W/m^2K$$

Then the local heat flow from solids bed can be calculated at a given axial location by

$$q_{sw}(x) = h_{sw,o}l'_w \ (T_s - T_w)$$

For instance at x = 1.25 m, T_s = 374.0 K and T_w = 369.2 K, the value of $q_{sw}(x)$ at x = 1.25 m is 57.2 W/m. The heat received by the solids is calculated by

$$\frac{dH_s(x)}{dx} = C_{ps} W_s \frac{dT_s}{dx}$$

where C_{ps} = 0.653 + 0.215x10^{-3}T (J/gK)

Thus C_p = 0.733.   The value of

dT_s/dx was obtained by the Spline function

$$\frac{dT_s}{dx} = 57.3 \ K/m$$

Therefore, the heat received by the solids is

$$\frac{dH_s(x)}{dx} = 14.2 \ \frac{kg}{hr} \ x \ \frac{1000 \ \frac{g}{kg}}{3600 \ \frac{s}{hr}} \ x \ 0.733 \ J/gK \ x \ 57.3 \ K/m$$

$$= 166. \ \ W/m$$

From equation 6-15, the heat transferred from the gas to the solids is

$$q_{gs}(x) = \frac{dH_s(x)}{dx} + q_{sw}(x)$$

$$= 223.2 \text{ W/m}$$

Then, the heat which the gas gives up is calculated from equation 6-8

$$\frac{dH_g(x)}{dx} = C_{pg} \, W_g \, \frac{dT_g}{dx}$$

where

$$C_{pg} = 1.0017 + 0.042 \ T/1000.$$

$$C_{pg} = 1.021 \text{ J/gK}$$

and by the Spline function,

$$\frac{dT_g}{dx} = 45.9 \text{ K/m}$$

Therefore,

$$\frac{dH_g(x)}{dx} = 24.6 \frac{kg}{hr} \times \frac{1000 \ \frac{g}{kg}}{3600 \ \frac{s}{hr}} \times 1.021 \ \text{ J/gK} \times 45.9 \text{ K/m}$$

$$= 320.4 \text{ W/m}$$

From equation 6-16, the local heat flow from the gas to the wall at $x = 1.25$ m is

$$q_{gw} = \frac{dH_g(x)}{dx} - q_{gs}(x)$$

$$= 320.4 - 223.2 = 97.2 \text{ W/m}$$

With the same procedures, the local heat flows at $x = 1.30$, 1.40, 1.50, 1.60 and 1.78 m are also calculated. The results are given in the table on page 261.

The average heat transfer rate per unit length for the test section, $\bar{q}_{gs}$ and $\bar{q}_{gw}$ can be calculated from equations 6-17 and 18, respectively.

$$\bar{q}_{gs} = \int_{x_1}^{x_2} q_{gs}(x)\,dx / (x_2 - x_1)$$

$$= 291.5 \text{ W/m}$$

and

$$\bar{q}_{gw} = \int_{x_1}^{x_2} q_{gw}(x)\,dx / (x_2 - x_1)$$

$$= 107.0 \text{ W/m}$$

where x_1, x_2 are locations for two ends of the test section. $x_2 - x_1 = 0.53$ m.

Therefore, the logarithmic mean heat transfer coeffi-
cients for gas to solids and gas to wall are represented by

$$h_{gs} = \bar{q}_{gs}/l_s (T_g - T_s)_{lm}$$

and

$$h_{gw} = \bar{q}_{gw}/l_w (T_g - T_w)_{lm}$$

respectively, where

$$(T_g - T_s)_{lm} = \frac{(462.0 - 374.0) - (492.0 - 417.0)}{\ln \frac{462.0 - 374.0}{492.0 - 417.0}}$$

$$= 81.3 \text{ K}$$

and

$$(T_g - T_w)_{lm} = \frac{(462.0 - 369.2) - (492.0 - 410.5)}{\ln \frac{462.0 - 369.2}{492.0 - 410.5}}$$

$$= 87.0 \text{ K}$$

In addition,

$$l_s = 2R \sin\frac{\beta}{2}$$

$$= 2 \times 0.09525 \sin\frac{1.98}{2} = 0.175 \text{ m}$$

and

$$l_w = (2\pi - \beta)R$$

$$= (6.28 - 1.98) \times 0.09525 = 0.410 \text{ m}$$

Thus, the heat transfer coefficients from gas to solids and gas to wall are

$$h_{gs} = 291.5/0.175/81.3 = 22.5 \text{ W/m}^2\text{K}$$

and

$$h_{gw} = 107.0/0.41/87.0 = 3.0 \text{ W/m}^2\text{K}$$

COMPUTER PROGRAMS

```
C
C
C      THIS PROGRAM MODELS THE ROTARY KILN BASED ON EQUATIONS
C      8-1 AND 8-2, USING THE CORRELATED HEAT TRANSFER COEFFI-
C      CIENTS.
C
C          NU(GS)=0.46*RE**(0.535)*REW**(0.104)*FILL**(-0.341)
C          NU(GW)=1.54*RE**(0.575)*REW**(-0.292)
C
C      THE CHARGE TEMPERATURE IS FIXED AT 350 K WHILE AIR INLET
C      TEMPERATURE IS 500 K
C
C
C
       DIMENSION Y(3),F(3),O(3),TG(100),TS(100),TW(100),Z(100)
       COMMON D1,D2,D3,E1,E2,E3,TO
       REAL L,KW,KS,N,L1,L2,LS,LO
       PI=3.14159
C
       Y(1)=0.0
       JJ=10
       STEP=0.01
       M=10
       ZI=0.0
       NN=3
       J=0
C    KILN DIMENSION
C
       RO=1.15
       RI=1.0
       D=2.0*RI
       L=D/3.0*50.
C
C      KS     SOLID THERMAL CONDUCTIVITY, W/M K.
C      KW     REFRACTORY THERMAL CONDUCTIVITY.
C      DIFF   DIFFUSIVITY, M2/SEC
C      DENS   SOLID BULK DENSITY, KG/M3
C
       KS=0.268
       KW=0.043
       DIFF=0.225E-06
       DENS=1.602E+03
C
C      N      ROTATIONAL SPEED, RPM.
C      FILL   DEGREE OF FILL.
C      ALPH   INCLINATION ANGLE, DEGREE.
C      BETA   CENTRAL ANGLE OF THE OCCUPIED BED, RADIAN.
C
       N=1.225
       FILL=0.11
       ALPH=0.8570
```

```
       BETA=1.68
       WRITE(6,149)
149    FORMAT(' READY FOR TGO, TSO IN FORMAT 2F5.1')
       READ(5,151) Y(2),Y(3)
       TS1=Y(3)
151    FORMAT(2F5.1)
       ALPHA=ALPH/57.32
       BEE=BETA/2.
       BEE=COS(BEE)
       HB=RI*(1.0-BEE)
C
C      WS : SOLID THROUGHPUT, CALCULATED BY
C
C          WS=1.295*HB*D**2*ALPHA*DENS*N/SIN(THETA)
C
       WS=1.295*HB*D**2.0
       WS=WS*ALPHA/0.454
       WS=WS*DENS*60.*N
       AREA=PI*RI*RI
       WG=WS
       BRE=BETA/2.0
       BRE=SIN(BRE)
C
C      DE: EQUIVALENT DIAMETER.
C
       DE=(2.*PI-BETA)*RI+2.*RI*BRE
       DE=PI*RI*RI*(1.0-FILL)/DE
       DE=4.*DE
       TO=293.
C
C      CALCULATE THE CONTACT AREA PER UNIT LENGTH.
C      L1:  EXPOSED AREA.
C      L2:  COVERED AREA.
C      LS:  BED SURFACE AREA.
C
       L1=(2.*PI-BETA)*RI
       L2=BETA*RI
       LS=2.0*RI*BRE
C
C      CALCULATE OF HEAT TRANSFER COEFFICIENTS
C
       HO=10.0
C
C
C
       NNNN=3
24     IF(NNNN-10) 21,21,22
21     T=(Y(2)-273.1)/1000.
       TT=(Y(3)-273.1)/1000.
```

```fortran
C     VIS:  GAS ABSOLUTE VISCOSITY.
C     VIK:  GAS KINEMATIC VISCOSITY.
C     AKG:  GAS THERMAL CONDUCTIVITY.
C
   23 VIS=1.734+5.274*T-12.22*T**2+25.52*T**3
      VIS=VIS*1.0E-05
C     VIS UNIT  KG/S/M
      VIK=1.347+5.76C*T+1.878*T**2
      VIK=VIK*1.0E-03
C     VIK UNIT  M2/SEC
      AKC=2.423+6.089*T+5.619*T**2-25.20*T**3
      AKG=AKG*1.0E-02
C     AKG UNIT  W/M K
C
      CPG=1.CC17+0.C42*T
      CPS=C.523+1.047*TT
C
C     CALCULATE RE, REW, NUGS AND NUGW.
C     THEN CALCULATE HGS AND HGW.
C
      RE=WG*VIS/PI/DE/360C*4.C
      REW=8.0/60.*PI*DE*N/VIK
      ANKGS=C.46*REW**0.54*REW**0.10*FILL**(-0.34)
      ANKGW=1.54*RE**0.58*REW**(-0.29)
      HGS=ANKGS/DE*AKG
      HGW=ANKGW/DE*AKG
      GO TO 51
   22 HGS=2.44*WG**0.57
      HGS=HGS*FILL**(-C.)71)
      HGS=HGS*KN**0.091
      HGW=C.822*WG**C.48
      HGW=HGW*N**(-0.297)
      HSW=N/60.*RI*RI*BETA/DIFF
   51 HSW=HSW*0.3
      HSW=HSW*11.6
      IF(HSW.GT.1.0E+05) HSW=600.
      HSW=HSW*KS/L2
C
C     CALCULATE PARAMETERS THAT ARE LISTED IN TABLE 8-1.
C
      LC=FC*BETA
      A=RO/RI
      A=ALOG(A)
      A1=HC*LC*A/2./PI/KW
      A2=HSW*L2/HGW/L1
      A3=2.*PI*KW/HGW/L1/A
      A4=A1*A3/(1.+A1)
      A5=1./(1.+A2+A4)

      B1=HGS*LS*L/WG/CPG*3.6
      B2=HGW*L1*L/WG/CPG*3.6
      B3=HGS*LS*L/WS/CPS*3.6
      B4=HSW*L2*L/WS/CPS*3.6
      C1=B1+B2-B2*A5
      D2=B1+A2*A5*R2
      D3=A4*A5*B2
      E1=B3+B4*A5
      E2=B3+B4-A7*A5*R4
      E3=B4*A4*A5
      IF(J-0) 53,53,10
C
C
   53 WRITE(6,100) L,D,RO,RI,L1,L2,LS,LC,DE
  100 FORMAT(' DIMENSION'/' L=',F7.3,'  D=',F6.3,'  RO=',
     1'  RI=',F6.3,'  L1=',F6.3,'  L2=',F6.3,'  LS=',F6.3,
     2'  LC=',F6.3,'  DE=',F6.3)
C
      WRITE(6,200) CPS,CPG,KS,KW,DENS
  200 FORMAT(' PROPERTY'/'  CPS=',E10.4,'  CPG=',E10.4,
     1'  KS=',E10.4,'  KW=',E10.4,'  DENS=',E10.4)
C
      WRITE(6,300) N,FILL,ALPH,WS,WG
  300 FORMAT(' OPERATING VARIABLES'/'  N=',F4.2,'  FILL=',
     1F4.3,'  ALPH=',F4.2,'  WS=',E10.4,'  WG=',E10.4)
C
      WRITE(6,400) A1,A2,A3,A4,A5,B1,B2,B3,B4
  400 FORMAT(' PARAMETERS'/2X,5(E10.4,3X)/2X,5(E10.4,3X))
      WRITE(6,500) D1,D2,D3,E1,E2,E3
  500 FORMAT(2X,5(E10.4,3X)/2X,5(E10.4,3X))
      WRITE(6,600) H0,HGS,HGW,HSW
  600 FORMAT(' HEAT T CCEFF'/3X,4(E10.4,3X))
      WRITE(6,800) RE,REW,ANKGS,ANKGW
  800 FORMAT(' RE=',E10.4,'  REW=',E10.4,'  NGS=',E10.4,'  NGW=',
     1,E1C.4)
C
C
C     USE RUNGE KUTTA METHOD TO SOLVE EQUATIONS.
C
C
   52 DC 1C I=1,JJ
      CALL RK(Y,F,Q,STEP,NN,M)
      J=J+M
      ZZ=J
      Z(I)=ZZ*STEP*L-ZI
      TG(I)=Y(2)
      TS(I)=Y(3)
      TW(I)=(TG(I)+A2*TS(I)+A4*TO)*A5
```

```
      WRITE(6,700) Z(I),TG(I),TS(I),TW(I)
      IF(I.NE.JJ) GO TO 24
  700 FORMAT(1X,F10.3,3(5X,F10.2))
   10 CONTINUE
      TTT=TG(JJ)-TS1
      DO 11 I=1,JJ
      Z(I)=Z(I)/L
      TG(I)=(TG(I)-TS1)/TTT
      TS(I)=(TS(I)-TS1)/TTT
      TW(I)=(TW(I)-TS1)/TTT
      WRITE(6,701) Z(I),TG(I),TS(I),TW(I)
  701 FORMAT(1X,4F10.4)
   11 CONTINUE
      STOP
      END
C
C
C
C     SUBROUTINE AUXRK: EQUATIONS FOR RK CALAULATION.
C
C
      SUBROUTINE AUXRK(Y,F)
      DIMENSION Y(3),F(3)
      COMMON D1,D2,D3,E1,E2,E3,TO
      F(2)=D1*Y(2)-D2*Y(3)-D3*TO
      F(3)=E1*Y(2)-E2*Y(3)+E3*TO
      RETURN
      END
EXECUTION TERMINATED


$SIGNOFF
```

```
C          THIS PROGRAM IS WRITTEN FOR HEAT TRANSFER IN ROTARY
C          KILN.  A KILN OF 8 INCHES OD, 7.5 ID IS USED FOR
C          EXPERIMENT  TO OBTAIN TEMPERATURE PROFILES OF AIR
C          SAND AND WALL ALONG THE KILN.
C          THE MAIN OBJECTIVE IS TC EVALUATE HEAT TRANSFE
C          COEFFICIENTS BASED ON EXPERIMENTAL DATA.
C          NUSSELT AND REYNOLDS NUMBERS ARE ALSO CALULATED.
C
C
C
C          INPUT DATA:
C               RUN,WA,ROT,WS,RIN,HCLDUP
C               MEASURED TEMPERATURES.
C
C          THE INTERPOLATED TEMPERATURES ARE CALCULATED BY
C          THE USE OF SPLINE FUNCTIONS.
C
C
C
C          DIMENSION X(30),LW(7),LS(7),TWE(7),TIE(7),TSE(7),TAE(7)
C          DIMENSION TW(30),TI(30),TS(30),TA(30),TSD(30),TAD(30)
C          DIMENSION S1(30),S2(30),S3(30)
C          DIMENSION QSW(30),QGS(30),QGW(30)
C          DIMENSION QA(30),QS(30),HTCGS(30),HTCGW(30)
C          EQUIVALENCE(S1,QA)
C          EQUIVALENCE(S2,QS)
C          EQUIVALENCE(S3,QGW)
C          COMMON /A/LW,LS,TWE,TIE,TSE,TAE
C          REAL K,LW,LS,NU
C          EXTERNAL FCT
C          DATA DOT/1H./,DOR/1H//
C
C          RUN    RUN NUMBER
C          WA     AIR FLOW RATE THROUGH KILN,     KG/HR
C          WS     SAND FEED RATE,                 KG/HR
C          ROT    ROTATATIONAL SPEED,  RPM
C          RIN    INCLINATIONAL ANGLE, DEGREE
C          HCLDUP     %
C
C          DO 1111 IIII=1,44
C          READ(5,111) RUN,WA,ROT,WS,RIN,HCLDUP
C      111 FORMAT(1X,A4,F5.1,F6.2,F4.1,2X,F4.2,F4.1)
C          WRITE(6,112) RUN,WA,ROT,WS,RIN,HOLDUP
C      112 FORMAT(1H1//////22X,7HRUN NO.,2X,A5//4X,16HAIR FLOW RATE
C         1,F5.1,6H KG/HR,10X,17HROTATIONAL SPEED ,F4.1,4H RPM/4X,
C         216HSAND FEED RATE  ,F5.1,6H KG/HR,10X,19HINCLINATION ANGLE
C         3,F4.1,7H DEGREE/4X,16HHOLDUP             ,F5.1,1X,1H%/)
C          PER=HOLDUP/100.
C
C          LW     THERMOCOUPLE LOCATION FOR WALL TEMPERATURE FROM
C          CHARGE END, M.
```

```
C          LS     THERMOCOUPLE LOCATION FOR AIR AND SOLIDS
C          TEMPERATURES, M
C          TWE    MEASURED WALL TEMPERATURE
C          TIE    MEASURED INSULATION TEMPERATURE
C          TSE    MEASURED SAND TEMPERATURE
C          TAE    MEASURED AIR TEMPERATURE
C
C          LW(2)=0.31
C          LW(3)=0.91
C          LW(4)=1.52
C          LW(5)=2.13
C          LS(2)=0.21
C          LS(3)=0.72
C          LS(4)=1.25
C          LS(5)=1.78
C          LS(6)=2.32
C
C          READ MEASURED TEMPERATURES.
C
C          READ(5,10) (TWE(I),I=2,5),(TIE(I),I=2,5)
C          READ(5,10) (TSE(I),I=2,6),(TAE(I),I=2,6)
C          READ(5,10) TAO,TA6,TSO,TS6,TWO,TW5
C          DO 16 I=2,6
C          WRITE(6,171) LS(I),DOR,TAE(I),TSE(I),DOR
C      171 FORMAT(7X,F4.2,2X,A1,2(F6.0,2X),16X,A1)
C          IF(I.EQ.6) GO TO 16
C          WRITE(6,172) LW(I),DOR,TWE(I),TIE(I),DOR
C      172 FORMAT(7X,F4.2,2X,A1,16X,2(F6.0,2X),A1)
C       16 CONTINUE
C          WRITE(6,173)
C      173 FORMAT(/)
C          X(1)=0.0
C          X(25)=2.4
C          II=24
C          IM=II+1
C          DO 200 I=1,5
C          S2(I)=LS(I+1)
C      200 TAD(I)=TAE(I+1)
C          DO 201 I=1,5
C      201 TSD(I)=TSE(I+1)
C          TAE(1)=TAO
C          TSE(1)=TSO
C          TSE(7)=TS6
C          TAE(7)=TA6
C          DO 202 I=1,4
C          S3(I)=LW(I+1)
C      202 TAD(I)=TWE(I+1)
C          DO 203 I=1,4
C      203 TSD(I)=TIE(I+1)
C          TWE(1)=TWO
```

```
      TWE(6)=TW5                                         C
      TIE(1)=SAINT(4,S3,TSD,X(1),3,S1)                         SGL=RAD*SIN(Z)*2.0
      TIE(6)=SAINT(4,S3,TSD,X(25),3,S1)                        ARC=2.*(3.142-Z)*RAD
      LS(1)=X(1)                                               AREA=3.142*RAD*RAD
      LS(7)=X(25)                                              DE=4.*AREA*(1.-PER)/(SGL+ARC)
      LW(1)=X(1)                                         C
      LW(6)=X(25)                                        C
      A=0.1                                              C     CALCULATE HEAT TRANSFER COEFFICIENTS FROM BED TO WALL, HTCSW.
      DO 11 I=1,II                                       C     A    HEAT DIFFUSIVITY OF SOLID,  0.225X10E-6 M2/SEC FOR
      IF(I.EQ.13) GO TO 11                               C     OTTAWA SAND .
      IF(I.EQ.18) GO TO 11                               C
      IF(I.EQ.12) GO TO 204                                    A=0.225E-06
      IF(I.EQ.17) GO TO 205                                    AA=ROT/60.*RAD**2/A*2.*Z
      X(I+1)=X(I)+A                                            AA=AA**0.3
      GO TO 11                                                 AA=11.6*AA
  204 X(I+1)=1.25                                         C
      X(I+2)=1.3                                          C     TK    THERMAL CONDUCTIVITY,  0.268 W/M K FOR OTTAWA SAND
      GO TO 11                                            C
  205 X(I+1)=1.78                                               TK=0.268
      X(I+2)=1.8                                                EL=2.*Z*RAD
   11 CONTINUE                                                  HTCSW=AA*TK/EL
C                                                               AAA=HTCSW
C                                                         C     ASSUME THERMAL CONDUCTIVITY OF CEMENT 0.294 W/M K AND ITS
C     TO FIND INTERPOLATED TEMPERATURES BASED ON          C     THICKNESS IS 2 MM.
C     MEASURED DATA                                             EQHTC=0.294/1.0*1000.
C                                                               HTCSW=1./HTCSW+1./EQHTC
      CALL SPLINE(LW,TWE,S2,6,X,TW,S1,IM,1001)                  HTCSW=1./HTCSW
      CALL SPLINE(LW,TIE,S2,6,X,TI,S1,IM,1001)                  WRITE(6,175) Z,SGL,ARC,DE,EL,AAA,EQHTC,HTCSW
      CALL SPLINE(LS,TSE,S2,7,X,TS,TSD,IM,1001)          175 FORMAT(/2X,' Z=',F5.2,'    SGL=',F5.2,'   ARC=',F5.2,
      CALL SPLINE(LS,TAE,S2,7,X,TA,TAC,IM,1001)            1' DE=',F5.2,'    EL=',F5.2/'   HTCSW=',F6.1,
C                                                          2'   EQHTC=',F6.1,'   HTCSW OVERALL=',F6.1///)
C                                                         C
      SUMA=0.                                                  DO 150 MM=1,IM
      SUMB=0.                                             C     QA IS AMOUNT OF HEAT RELEASED BY AIR  , W/M
      SUM1=0.0                                                 T=TA(MM)/1000.
      SUM2=0.0                                                 CP=1.0017+0.042*T
      SUM3=0.0                                                 TCP=0.042*(T-0.298)
      EPS=1.0E-05                                              SA=(CP+TCP)*TAC(MM)
      XST=1.0                                                  CA(MM)=1./3.6*SA*WA
      IEND=50                                             C     QS IS THE AMOUNT OF HEAT RECEIVED BY SOLIDS,  W/M
C                                                               T=TS(MM)/1000.
C     CALCULATE THE CENTRAL ANGLE OF THE BED WITH SUBROUTINE    CP=0.653+0.215*T
C     THETA.                                                    TCP=0.215*(T-0.298)
C                                                               SS=(CP+TCP)*TSD(MM)
      CALL THETA(Z,F,DERF,FCT,XST,EPS,IEND,IEK,PER)            QS(MM)=1./3.6*SS*WS
C     KILN RADIUS IS 0.09525 M                            C
      RAD=0.09525                                         C     TO CALCULATE HEAT FLUX FROM BED TO WALL,QSW
C                                                               QSW(MM)=HTCSW*FL*(TS(MM)-TW(MM))
C     DE    EQUIVALENT DIAMETER, M                         C     TO CALCULATE HEAT FLUX FROM GAS TO BED, QGB(MM)
C     SGL   CONTACT LENGTH BETWEEN GAS AND SOLID BED, M
```

```
      QGS(MM)=QSW(MM)+QS(MM)
C     TO CALCULATE HEAT FLUX FROM GAS TO WALL,  QGW(MM)
      QGW(MM)=QA(MM)-QGS(MM)
C
C     TO CALCULATE HTC
C     HTCGS  LCCAL HEAT TRANSFER COEFFICIENTS,  W/M2 K
C     HTCGW   HEAT TRANSFER COEFFICIENT, W/M2 K
      HTCGS(MM)=QGS(MM)/SGL/(TA(MM)-TS(MM))
      HTCGW(MM)=QGW(MM)/ARC/(TA(MM)-TW(MM))
      J=MM
      WRITE(6,115) X(J),TA(J),TS(J),TW(J),TI(J),QSW(J),
     1CS(J),QGS(J)
     1,QA(J),QGW(J)
  115 FCRMAT(2X,F4.2,4(F6.1,2X),5(-0PF7.1,2X))
C
  150 CONTINUE
   10 FORMAT(10F8.3)
C
      II=1
      JJ=25
      WRITE(6,183)
  183 FCRMAT(1H1///)
      DO 500 I=II,JJ
      TSD(I)=QS(I)/(TA(I)-TS(I))/SGL
      TAD(I)=QA(I)-QS(I)
      TAD(I)=TAD(I)/(TA(I)-TW(I))/ARC
      WRITE(6,116) X(I),HTCGS(I),HTCGW(I),TSD(I),TAD(I)
  500 CONTINUE
  116 FCRMAT(2X,F4.2,4F12.2)
      KK=18
      II=13
      KKK=KK-1
      SUM4=0.0
      SUM5=0.0
      SUM6=C.0
      DO 153 I=II,KKK
C
      SEG=X(I+1)-X(I)
      AVG=(HTCGS(I)+HTCGS(I+1))/2.0
      SUMA=SUMA+AVG*SEG
      AVG=(HTCGW(I)+HTCGW(I+1))/2.0
      SUMB=SUMB+AVG*SEG
      AVG=(QGS(I)+QGS(I+1))/2.0
      SUM1=SUM1+AVG*SEG
      AVG=(QGW(I)+QGW(I+1))/2.0
      SUM2=SUM2+AVG*SEG
      AVG=(CS(I)+CS(I+1))/2.0
      SUM4=SUM4+AVG*SEG
      C=(CA(I)+QA(I+1))/2.
      SUM5=SUM5+C*SEG
```

```
      A=QA(I)-QS(I)
      B=QA(I+1)-QS(I+1)
      AVG=(A+B)/2.0
      SUM3=SUM3+AVG*SEG
C
C
  153 CCNTINUE
      QSWT=HTCSW*EL*(TS(16)-TW(16))*0.53
      SUM7=QSWT+SUM4
      SUM8=SUM5-SUM7
      WRITE(6,176) QSWT,SUM4,SUM7,SUM5,SUM8
  176 FCRMAT(/2X,'QSWT=',E10.4,'   QST=',E10.4,'  QGST=',
     1E10.4,'  QGT=',E10.4,'   QGWT=',E10.4)
C
C
C     AHA    MEAN GAS/SCLID HTC DERIVED FROM INTEGRATION
C            OF LOCAL HTC DIVIDED BY KILN TEST SECTION LENGHT.
C     AHB    MEAN GAS/WALL HTC DERIVED FROM INTEGRATION
C            CF LOCAL HEAT TRANSFER CCEFFICIENTS.
C
      JJ=KK
      BB=X(JJ)-X(II)
      AHA=SUMA/BB
      AHB=SUMB/BB
      A=TA(II)-TS(II)
      B=TA(JJ)-TS(JJ)
      C=A-B
      D=A/B
      IF(A.EQ.B) GO TO 161
      T=C/ALOG(D)
      GO TO 162
  161 T=A
C     HBS    LCGARITHM MEAN GAS/SOLID HTC
C     HBW    LOGARITHM MEAN GAS/WALL HTC.
  162 HBS=SUM1/T/SGL/BB
      HBS2=SUM4/T/SGL/BB
      HBS7=SUM7/T/SGL/BB
      WRITE(6,177) A,B,T,HBS7
  177 FCRMAT(/2X,'AIR - SCLID:  DEL T1=',F5.1,'   DEL T2=',F5.1,
     1'   LOG T=',F5.1,'   AIR-SCLID HTC=',F5.2)
      A=TA(JJ)-TW(JJ)
      B=TA(II)-TW(II)
      C=A-B
      D=A/B
      IF(A.EQ.B) GO TO 163
      T=C/ALOG(D)
      GC TO 164
  163 T=A
  164 HBW3=SUM3/T/ARC/BB
      HBW=SUM2/T/ARC/BB
```

250

```
      RATSUM=SUM4/SUM5
      HBW8=SUM8/T/ARC/BB
      WRITE(6,178) A,B,T,HBW8
  178 FORMAT(/2X,'AIR - WALL: DEF T1=',F5.1,'   DEL T2=',F5.1,
     1'   LOG T=',F5.1,'    AIR - WALL HTC=',F5.2)
      WRITE(6,173)
      WRITE(6,10) HBS,HBW,AHA,AHB,HBS2,HBW3,RATSUM,HBS7,HBW8
C
C
C        THE FOLLOWING IS TO CALCULATE NUSSELT NUMBER
C        AND REYNOLDS NUMBER.
C
C        AK    AIR THERMAL CONDUCTIVITY,  J/S M K
C        VIS   AIR VISCOSITY,  N S/M2
C        T     AIR AVERAGE TEMPERATURE IN TEST SECTION
C        RE    REYNOLDS NO.,  V*DEN*DE/VIC
C              = WA/VIC/DE/4./PIE/3600.
C        NU    NUSSELT NO.,    HETRA*DE/AK
C        DE    EQUIVALENT DIAMETER OF KILN, M
C
C
      T=(TA(JJ)+TA(II))/2.0
      TAA=T
      TSS=(TS(II)+TS(JJ))/2.0
      TWW=(TW(II)+TW(JJ))/2.C
      T=(TAA+TSS)/2.0
      CALL PROPTY(T,AK,VIS,DEN)
C
      PIE=3.142
      REW=8./6C.*PIE*DE *DE *ROT*DEN/VIS
      RE=WA/VIS/PIE/DE/3600.*4.
      NU=FPS*CE/AK
      TTT=(TAA+TWW)/2.0
      CALL PROPTY(TTT,AK,VIS,DEN)
      WNU=HBW*DE/AK
      WRITE(6,126) RE,NU,WNU
  126 FORMAT(///5X,12HREYNOLDS NO.,1PE12.3/
     15X,12HNUSSELT   NO.,1PE12.3,1PE12.3)
      WRITE(10,121) RUN,WA,ROT,WS,RIN,HCLOUP
  121 FORMAT(1X,A5,F5.1,F6.2,3X,3F5.1)
      WRITE(11,122) RUN,HBS7,HBW8,RE,NU,WNU,REW
  122 FORMAT(1X,A5,6F12.2)
 1111 CONTINUE
      WRITE(6,129)
  129 FORMAT(1H1)
C
C
C
C        PLOT TEMPERATURE PROFILES VS. KILN LENGTH.
C
C
```

```
      CALL KILNPLOT(RUN,WA,ROT,WS,RIN,HCLOUP)
C
 1001 STOP
      END
C
C
C        SUBROUTINE THETA TO CALCULATE CENTRAL ANGLE OF THE BED.
C
C
      SUBROUTINE THETA(X,F,DERF,FCT,XST,EPS,IEND,IER,PER)
      IER=0
      X=XST
      TOL=X
      CALL FCT(TOL,F,DERF,PER)
      TOLF=100.*EPS
      DO 6 I=1,IEND
      IF(F) 1,7,1
    1 IF(DERF)2,8,2
    2 DX=F/DERF
      X=X-DX
      TOL=X
      CALL FCT(TOL,F,DERF,PER)
      TOL=EPS
      A=ABS(X)
      IF(A-1.0) 4,4,3
    3 TOL=TOL*A
    4 IF(ABS(DX)-TOL) 5,5,6
    5 IF(ABS(F)-TOLF) 7,7,6
    6 CONTINUE
      IER=1
    7 RETURN
    8 IER=2
      RETURN
      END
C
C
C        FUNCTION FOR CENTRAL ANGLE CALCULATION.
C
C
      SUBROUTINE FCT(X,F,DERF,PER)
      PIE=3.14159
      F=X-SIN(2.*X)/2.0-PER*PIE
      DERF=1.-COS(2.*X)
      RETURN
      END
C
C
C        SUBROUTINE PROPTY TO CLACULATE AIR PROPERTY.
C
C
```

```
      SUBROUTINE PROPTY(X,AKK,AVIS,ADEN)                         CALL SYMBOL(XX,A,0.14,14,180.0,-1)
      DIMENSION T(20),DEN(20),CPG(20),VIS(20),VKS(20)           Z=XX*0.5
      DIMENSION P(20),AK(20),PR(20),YF(20)                      XXX=XX-0.15
      DO 20 I=1,11                                              CALL NUMBER(XXX,1.7,0.14,Z,0.0,1)
   20 READ(7,22) T(I),DEN(I),CPG(I),VIS(I),VKS(I),AK(I),PR(I) 11 CONTINUE
   22 FORMAT(7F10.4)                                       C
      DO 25 I=1,11                                          C
      VIS(I)=VIS(I)*1.0E-05                                     Z=250.
      VKS(I)=VKS(I)*1.0E-03                                     DO 20 I=1,7
   25 CONTINUE                                                  Y=I+1
      DO 30 I=1,12                                              CALL SYMBOL(0.0,Y,0.14,15,180.0,-1)
      T(I)=(T(I)+460.)/1.8                                      Z=Z+50.
      DEN(I)=DEN(I)*16.018                                      IF(I.EQ.1) GO TO 20
      CPG(I)=CPG(I)*0.41868E+04                                 Y=Y-0.14
      VIS(I)=VIS(I)*1.4882                                      CALL NUMBER(-0.15,Y,0.14,Z,90.,-1)
      VKS(I)=VKS(I)*0.092903                               20 CONTINUE
      AK(I)=AK(I)*1.7308                                   C
   30 CONTINUE                                                  CALL PLOT(0.40,1.5,+3)
      AKK=SAINT(11,T,AK,X,5,YF)                                 CALL SYMBOL(0.40,1.2,0.14,'DISTANCE FROM SOLID FEED END,'
      AVIS=SAINT(11,T,VIS,X,5,YF)                              1' METER',0.0,35)
      ADEN=SAINT(11,T,DEN,X,5,YF)                               CALL SPLINE(LS,TSE,S2,7,X,TS,S1,IM,1001)
      RETURN                                                    CALL SPLINE(LS,TAE,S2,7,X,TA,S1,IM,1001)
      END                                                  C
C                                                              AAAA=300.
C                                                              DO 50 I=1,25
C                                                              X(I)=X(I)+X(I)
C                                                              TA(I)=(TA(I)-AAAA)/50.+A
C     THIS SUBROUTINE PLOTS THE TEMPERATURE PROFILES           TS(I)=(TS(I)-AAAA)/50.+A
C     FOR AIR, SAND AND WALL VS. KILN LENGTH POSITION.         TW(I)=(TW(I)-AAAA)/50.+A
      SUBROUTINE KILNPLOT(RUN,WA,ROT,WS,RIN,HOLDUP)            TI(I)=(TI(I)-AAAA)/50.+A
C                                                          50 CONTINUE
C                                                          C
      DIMENSION X(30),TA(30),TS(30),TW(30),TI(30)          C
      COMMON /A/LW,LS,TWE,TIE,TSE,TAE                           DO 40 I=2,6
      DIMENSION TAE(8),TSE(8),TWE(8),TIE(8),LS(8),LW(8)        LS(I)=LS(I)+LS(I)
      DIMENSION S1(30),S2(30)                                  TAE(I)=(TAE(I)-AAAA)/50.+A
      REAL LS,LW                                               TSE(I)=(TSE(I)-AAAA)/50.+A
      ILW=1                                                    CALL SYMBOL(LS(I),TAE(I),0.14,30,0.0,-1)
 1002 A=2.0                                                    CALL SYMBOL(LS(I),TSE(I),0.14,3,0.0,-1)
      B=0.0                                                    IF(I.EQ.6) GO TO 40
      CCC=7.0                                                  LW(I)=LW(I)+LW(I)
      CCC=CCC+A                                                TWE(I)=(TWE(I)-AAAA)/50.+A
      CALL PLOT(8.0,0.0,-3)                                    CALL SYMBOL(LW(I),TWE(I),0.14,2,0.0,-1)
      CALL PLOT(0.0,2.0,+1)                                40 CONTINUE
      CALL PLOT(5.0,A,+2)                                  C
      CALL PLOT(5.0,CCC,+1)                                C
      CALL PLOT(B,CCC,+1)                                      CALL PLOT(0.0,TA(1),+3)
      CALL PLOT(B,A,+1)                                        CALL LINE(X,TA,25,-1)
C                                                              CALL PLOT(0.0,TS(1),+3)
      DO 11 I=1,6                                              CALL LINE(X,TS,25,-1)
      XX=I-1
```

```
      CALL PLOT(0.0,TW(1),+3)
      CALL LINE(X,TW,25,-1)
C
      WWW=8.5
      CALL SYMBOL(0.5,WWW,0.14,'RUN NO.                     '
     1,0.0,31)
      CALL SYMBOL(2.96,WWW, 0.14,RUN,0.0,4)
      WWW=WWW-0.2
      CALL SYMBOL(0.5,WWW,0.14,'AIR FLOW RATE          KG/HR '
     1,0.0,31)
      CALL NUMBER(2.96,WWW,0.14,WA,0.0,1)
      WWW=WWW-0.2
      CALL SYMBOL(0.5,WWW,0.14,'SAND THROUGHPUT        KG/HR '
     1,0.0,31)
      CALL NUMBER(2.96,WWW, 0.14,WS,0.0,1)
      WWW=WWW-0.2
      CALL SYMBOL(0.5,WWW,0.14,'ROTATIONAL SPEED       RPM   '
     1,0.0,31)
      CALL NUMBER(2.96,WWW,0.14,ROT,0.0,1)
      WWW=WWW-0.2
      CALL SYMBOL(0.5,WWW,0.14,'INCLINATION ANGLE      DEGREE'
     1,0.0,31)
      CALL NUMBER(2.96,WWW, 0.14,RIN,0.0,1)
      WWW=WWW-0.2
      CALL SYMBOL(0.5,WWW,0.14,'DEGREE OF FILL          %    '
     1,0.0,31)
      CALL NUMBER(2.96,WWW,0.14,HOLDUP,0.0,1)
      WWW=WWW-0.4
      VVV=C.5
      VVW=0.9
      CALL SYMBOL(VVV,WWW,0.14,30,0.0,-1)
      CALL SYMBOL(VVW,WWW,0.14,'AIR ',0.0,4)
      WWW=WWW-0.2
      CALL SYMBOL(VVV,WWW,0.14,3,0.0,-1)
      CALL SYMBOL(VVW,WWW,0.14,'SAND',0.0,4)
      WWW=WWW-0.2
      CALL SYMBOL(VVV,WWW,0.14,2,0.0,-1)
      CALL SYMBOL(VVW,WWW,0.14,'WALL',0.0,4)
C
C
C
C
      IF(ILM.EC.4) GO TO 1001
      ILM=ILM+1
      GO TO 1002
 1001 CALL PLOTND
      STOP
      END
EXECUTION TERMINATED


$SIGNOFF
```

```
C
C
C          THIS PROGRAM PREDICTS GAS-TO-BED HEAT TRANSFER
C          COEFFICIENTS BASED ON THEORETICAL EQUATION 7-14.
C
C
           REAL KA,M1,M2,K,N,L,NUP
C          AIR TEMPERATURE AT 422 K, AIR PROPERTIES ARE AS FOLLOWS...
           PI=3.14159
           PR=0.71
           VISA=2.369E-05
C                         KG/M S
           DENA=0.833
C                    KG/M3
           KA=0.031
C                 W/M K
C          PHYSICAL PROPERTIES OF OTTAWA SAND ARE AS FOLLOWS....
           R=0.09525
           DP=0.73E-03
           VP=PI/6.0*DP**3
           DENF=2527.3
C                       KG/M3
           CPF=0.603
C                    J/G K
C
C
           FILL=0.065
           BETA=1.535
           BETB=BETA/2.
           BETC=COS(BETB)
           BETD=SIN(BETB)
           M1=2.17E+06
           M2=M1
C          UNIT OF M1, M2 ,      NO. OF PARTICLES / M2
C          ASSUME  N=3RPM, K=5.0E-03 M AT 11% OF FILL
           WRITE(6,21)
 21 FORMAT('   READ N IN RPM AND WG IN KG/HR , BOTH IN FORMAT F5.2')
           READ(5,22) N,WG
 22 FORMAT(2F5.2)
           SN=N/60.0
           L=2.*R*BETD
           VL3=0.20
C
           AREA=PI*R*R
           AREA=AREA*(1.-FILL)
           WG=WG/DENA/3600.
           VG=WG/AREA
C
C
           RATIO=N/3.0
```

```
           VL=VL3*RATIO**0.5
           K=PI/4.0*SN*L**2
           K=K/(VL+2.*PI*SN*BETC*R)
           VLL=VL
C
C
           VDC=VP*DENF*CPF*1.0E+03
           S1=PI/2.0*DP*DP
           S2=(1.-PI*DP*DP/4.0*M1)/M2
C
           VL=VL**2+VG**2
           VL=VL**0.5
           RE=DP*VL*DENA/VISA
           WRITE(6,10) RE,VG,VLL,VL
 10 FORMAT('   REP=',F5.1,3E14.4)
           WRITE(6,23)
 23 FORMAT(' READ NUP IN F5.2, VALUE TAKEN FROM KUNII & '
          1'LEVENSPIEL BOOK, P. 212')
           READ(5,11) NUP
 11 FORMAT(F5.2)
           HF=NUP*KA/DP
C
C   CALCULATE PARTICLE VELOCITY AT SECOND LAYER
           UL=VLL*(1.-DP/K)
C
           A1=-HF*S1*L/VDC/VLL
           B1=-HF*S2*L/VDC/UL
           A=EXP(A1)
           B=EXP(B1)
           WRITE(6,15) A1,B1,A,B
 15 FORMAT(4E12.4)
           A=1.-A
           B=1.-B
           A=M1*VLL*A
           B=M2*UL*B
           HGS=VDC/L*(A+B)
           WRITE(6,12) N,K,HF,HGS
 12 FORMAT('   N=',F4.1,'   K=',E10.4,'   HF=',E10.4,'   HGS=',E10.4)
           STOP
           END
EXECUTION TERMINATED
```

$SIGNOFF

```
C
C
C       THIS PROGRAM IS FOR A PLOT OF NUGS(EXP)  VS.  NUGS(PRED)
C       AND FOR NUGW(EXP) VS. NUGW(PRED).
C       THE PLOTS ARE SHOWN IN FIGURES 6-34 & 6-35.
C
        DIMENSION Y(50),X(50),AA(50),SS(50)
        READ(5,11)  (Y(I),X(I),I=1,44)
   11 FORMAT(6X,E12.4,12X,E12.4)
        CC=2.0
        A=0.0
        B=5.757
        C=0.0
        D=5.757
        C=C+CC
        D=D+CC
        CALL PLOT(3.0,2.0,-3)
        CALL PLOT(A,C,+3)
        CALL PLOT(B,C,+2)
        CALL PLOT(B,D,+2)
        CALL PLOT(A,D,+2)
        CALL PLOT(A,C,+2)
        AA(1)=5.0
        DO 21 I=1,15
        AA(I+1)=AA(I)+1.0
   21 CONTINUE
        AA(17)=25.0
        AA(18)=30.0
        AA(19)=40.0
        AA(20)=50.0
        AA(21)=60.0
        AA(22)=70.0
        DO 85 I=1,44
        Y(I)=Y(I)/50.
        Y(I)=ALOG(Y(I))*2.5+CC
        X(I)=X(I)/50.
        X(I)=ALOG(X(I))*2.5
   85 CONTINUE
C
        DO 80 I=1,20
        SS(I)=AA(I)/AA(1)
        SS(I)=ALOG(SS(I))*2.5
   80 CONTINUE
C
        DO 90 I=1,20
        CALL SYMBOL(SS(I),C,0.14,14,180.0,-1)
        ZZ=AA(I)*10.
        GO TO (2,2,2,2,2,2,4,4,4,4,2,4,4,4,4,2,2,2,2,2),I
    4 GO TO 7
    2 TX=SS(I)-0.14
```

```
        TY=CC-0.20
        CALL NUMBER(TX,TY,0.14,ZZ,0.0,-1)
    7 SS(I)=SS(I)+CC
        CALL SYMBOL(A,SS(I),0.14,15,180.0,-1)
        GO TO (3,3,3,3,3,3,5,5,5,5,3,5,5,5,5,3,3,3,3,3),I
    5 GO TO 90
    3 TX=A-0.14
        TY=SS(I)-0.14
        CALL NUMBER(TX,TY,0.14,ZZ,90.,-1)
   90 CONTINUE
        CALL SYMBOL(-0.60,3.0,0.14,'NUSSELT NUMBER, EXPERIMENTAL'
     1,90.,28)
        CALL SYMBOL(1.0,1.2,0.14,'NUSSELT NUMBER, PREDICTED',0.0,25)

        AA(1)=AA(1)*10.0
        DO 95 I=1,15
        CALL SYMBOL(X(I),Y(I),0.14,1,0.0,-1)
   95 CONTINUE
        DO 96 I=16,34
        CALL SYMBOL(X(I),Y(I),0.14,0,0.0,-1)
   96 CONTINUE
        DO 97 I=35,44
        CALL SYMBOL(X(I),Y(I),0.14,2,0.0,-1)
   97 CONTINUE
        CALL PLOT(A,C,+3)
        CALL PLOT(B,D,+2)
        DD=C+2.0
        BB=B-2.0
        EE=BB+0.20
        CALL SYMBOL(BB,DD,0.14,1,0.0,-1)
        CALL SYMBOL(EE,DD,0.14,'17% PILL  ',0.0,10)
        DD=DD-0.25
        CALL SYMBOL(BB,DD,0.14,0,0.0,-1)
        CALL SYMBOL (EE,DD,0.14,'11%',0.0,3)
        DD=DD-0.25
        CALL SYMBOL(BB,DD,0.14,2,0.0,-1)
        CALL SYMBOL (EE,DD,0.14,'6.5%',0.0,4)
        CALL SYMBOL(0.5,6.8,0.14,'GAS/SOLID HEAT TRANSFER',0.0,23)
        READ(5,12)  (Y(I),X(I),I=1,44)
   12 FORMAT(42X,E12.4,12X,E12.4)
C
C
        CC=2.0
        A=0.0
        B=6.2
        C=0.0
        D=6.2
        C=C+CC
        D=D+CC
C
```

```
C
      CALL PLOT(3.0,2.0,-3)
      CALL PLOT(A,C,+3)
      CALL PLOT(B,C,+2)
      CALL PLOT(B,D,+2)
      CALL PLOT(A,D,+2)
      CALL PLOT(A,C,+2)
      AA(1)=5.0
      DO 22 I=1,15
      AA(I+1)=AA(I)+1.0
   22 CONTINUE
      AA(17)=25.0
      AA(18)=30.0
      AA(19)=40.0
      AA(20)=50.0
      AA(21)=60.0
      AA(22)=70.0
C
      DO 81 I=1,20
      SS(I)=AA(I)/AA(1)
      SS(I)=ALOG(SS(I))*2.5
   81 CONTINUE
C
      DO 91 I=1,20
      ZZ=AA(I)
      CALL SYMBOL(SS(I),C,0.14,14,180.0,-1)
      GO TO (1,1,1,1,1,1,6,6,6,6,1,6,6,6,6,1,1,1,1,1),I
    6 GO TO 10
    1 TX=SS(I)
      TY=CC-0.20
      CALL NUMBER(TX,TY,0.14,ZZ,0.0,-1)
   10 SS(I)=SS(I)+CC
      CALL SYMBOL(A,SS(I),0.14,15,180.0,-1)
      GO TO (8,8,8,8,8,8,9,9,9,9,8,9,9,9,9,8,8,8,8,8),I
    8 GO TO 91
    8 TX=A-0.14
      TY=SS(I)
      CALL NUMBER(TX,TY,0.14,ZZ,90.,-1)
   91 CONTINUE
      CALL SYMBOL(-0.60,3.0,0.14,'NUSSELT NUMBER, EXPERIMENTAL'
     1,90.,28)
      CALL SYMBOL(1.0,1.2,0.14,'NUSSELT NUMBER, PREDICTED',0.0,25)
      DO 94 I=1,44
      X(I)=X(I)/AA(1)
      Y(I)=Y(I)/AA(1)
      X(I)=ALOG(X(I))*2.5
      Y(I)=ALOG(Y(I))*2.5+CC
   94 CONTINUE
      DO 99 I=1,44
      CALL SYMBOL(X(I),Y(I),0.14,2,0.0,-1)
```

```
   99 CONTINUE
      CALL PLOT(A,C,+3)
      CALL PLOT(B,D,+2)
      CALL SYMBOL(0.5,6.8,0.14,'GAS/WALL HEAT TRANSFER',0.0,23)
      CALL PLOTND
      STOP
      END
EXECUTION TERMINATED


$COPY *SKIP
```

EXPERIMENTAL   DATA

Run No.	W	N	α	η	W_s
A11	24.6	3.00	1.20	17.0	25.0
A12	24.6	3.00	1.20	17.0	25.0
A13	24.6	3.00	1.20	17.0	25.0
A14	24.6	3.00	1.20	17.0	25.0
A15	24.6	1.50	1.20	17.0	14.2
A16	24.6	1.50	1.20	17.0	14.2
A17	24.6	1.50	1.20	17.0	14.2
A18	18.6	3.00	1.20	15.0	21.0
A19	18.6	1.60	2.20	17.0	29.1
A20	18.6	1.60	1.20	17.0	15.0
A21	34.0	1.50	1.20	17.0	15.0
A22	34.0	3.00	1.20	17.0	34.0
A23	34.0	1.50	1.20	17.0	15.0
A24	34.0	6.00	1.20	17.0	50.5
A25	34.0	1.50	3.40	17.0	39.0
A26	34.0	3.20	2.20	11.0	34.6
A27	50.5	3.20	2.20	11.0	34.0
A28	50.5	3.10	3.00	11.0	52.7
A29	50.0	3.10	1.20	11.0	19.4
A30	50.0	1.60	2.20	11.0	18.2
A31	50.5	6.00	2.20	11.0	66.3
A32	81.0	3.00	2.00	11.0	36.0
A33	65.5	3.00	2.00	11.0	36.0
A34	73.0	3.00	2.00	11.0	36.0
A35	81.0	3.00	2.00	11.0	36.0
A36	34.0	3.00	2.00	11.0	36.0
A37	34.0	3.00	2.00	11.0	36.0
A38	34.0	3.00	2.00	11.0	36.0
A39	34.0	3.00	2.00	11.0	36.0
A40	18.6	3.00	2.00	11.0	36.0
A41	18.6	3.00	2.00	11.0	36.0
A42	18.6	3.00	2.00	11.0	36.0
A43	18.6	3.00	2.00	11.0	36.0
A44	50.0	3.00	2.00	11.0	36.0
A45	65.5	0.90	2.00	6.5	12.0
A46	34.0	1.00	2.00	6.5	13.3
A47	34.0	3.00	2.00	6.5	35.8
A48	65.5	3.00	2.00	6.5	35.8
A49	65.0	0.90	2.00	6.5	11.7
A50	95.5	3.00	2.00	6.5	35.8
A51	95.5	1.00	2.00	6.5	15.8
A52	34.0	1.00	2.00	6.5	11.3
A53	95.5	1.00	2.00	6.5	16.1
A54	81.0	0.95	2.00	6.5	12.0

Run.No.	Ta$_1$	Ta$_2$	Ta$_3$	Ta$_4$	Ta$_5$	Ts$_1$	Ts$_2$	Ts$_3$	Ts$_4$	Ts$_5$	Tw$_1$	Tw$_2$	Tw$_3$	Tw$_4$
A11	450.0	486.0	524.0	574.0	635.0	334.0	356.0	378.0	431.0	521.0	320.0	351.0	397.0	500.0
A12	425.0	460.0	489.0	535.0	592.0	323.0	339.0	356.0	397.0	473.0	314.0	338.0	372.0	445.0
A13	402.0	423.0	457.0	493.0	538.0	321.0	337.0	354.0	392.0	447.0	313.0	333.0	368.0	429.0
A14	372.0	392.0	411.0	436.0	457.0	314.0	327.0	341.0	368.0	405.0	308.0	326.0	352.0	395.0
A15	330.6	340.0	348.3	358.8	372.0	306.7	308.9	312.8	326.7	348.3	301.0	306.0	316.0	333.0
A16	414.0	438.0	462.0	494.0	535.0	341.0	356.0	374.0	417.0	473.0	324.0	347.0	387.5	447.0
A17	470.0	505.0	543.0	594.0	652.0	364.0	383.0	410.0	473.0	554.0	341.0	370.0	425.0	520.0
A18	351.5	378.9	412.2	445.0	488.0	313.9	325.6	338.9	363.9	402.8	308.0	323.0	349.0	395.0
A19	350.0	375.1	405.0	448.0	497.0	312.2	322.2	332.2	355.5	391.7	304.0	317.0	341.0	377.0
A20	365.0	392.8	427.2	464.0	507.0	330.6	340.0	352.8	383.3	424.4	315.5	331.0	363.0	407.0
A21	380.0	398.0	418.0	435.0	455.0	335.0	346.1	360.3	384.4	411.1	319.4	336.0	365.8	401.0
A22	368.0	388.0	407.0	428.0	455.8	320.6	331.1	341.7	363.3	390.0	311.0	326.6	349.6	378.0
A23	383.0	400.8	418.0	437.0	456.0	337.8	348.9	365.0	385.6	412.8	321.0	338.0	365.0	400.0
A24	357.0	374.0	390.6	407.0	430.0	308.3	315.0	322.2	336.7	360.0	302.0	311.6	330.0	355.0
A25	361.0	377.2	391.5	410.0	430.0	305.6	313.6	322.2	338.9	362.1	300.0	313.4	331.0	360.0
A26	370.0	385.0	398.9	414.0	437.0	313.8	323.3	333.3	350.0	376.1	306.0	321.6	340.0	354.8
A27	369.0	380.0	388.9	401.0	413.0	316.7	326.1	334.4	351.7	373.9	306.8	323.0	341.6	366.0
.A28	361.0	371.0	381.1	395.0	410.0	312.8	318.9	327.9	341.7	358.9	304.0	315.5	333.0	353.0
A29	376.0	386.0	396.0	405.0	417.0	320.0	331.1	339.4	353.9	370.6	320.0	338.8	350.0	380.0
A30	378.0	388.0	399.0	410.0	420.5	329.4	341.1	357.2	373.9	394.4	320.0	339.0	360.0	387.0
A31	353.0	365.0	375.6	387.5	404.5	308.3	313.9	321.5	331.7	350.0	302.3	313.6	326.0	345.6
A32	407.0	417.8	425.1	437.5	450.0	333.3	350.6	366.7	391.1	417.3	321.1	347.4	375.5	407.0
A33	393.0	407.0	418.3	431.0	445.0	326.1	341.7	358.3	380.6	407.2	313.0	338.4	367.4	395.0
A34	396.2	412.2	423.3	436.0	448.9	331.7	347.2	362.7	385.8	412.2	315.8	344.0	370.0	402.0
A35	396.8	411.1	422.2	433.0	444.4	326.7	348.9	366.7	388.9	414.2	315.8	345.0	375.5	404.0
A36	366.7	380.6	395.6	415.0	441.0	311.1	322.2	334.4	352.2	378.1	304.5	321.7	339.0	368.0
A37	420.0	445.4	476.7	513.0	560.0	322.8	334.4	369.4	399.7	443.0	312.6	341.1	380.4	425.5
A38	395.0	417.0	440.6	471.0	505.0	318.9	334.4	355.0	380.0	415.3	312.4	335.4	361.0	401.0
A39	420.6	446.5	475.0	512.0	559.0	323.9	343.3	369.4	400.0	445.4	312.0	344.0	380.0	425.5
A40	385.6	417.0	461.1	510.0	560.0	318.3	331.7	352.0	377.8	428.0	311.0	333.0	364.0	413.0
A41	358.3	376.0	410.6	447.0	505.0	308.9	317.8	332.2	348.3	387.2	300.4	317.6	335.0	372.8
A42	351.7	360.0	384.4	413.5	460.0	306.1	312.2	321.7	336.1	366.7	299.0	312.6	327.0	355.8
A43	375.6	400.0	440.0	478.0	535.0	313.3	325.0	345.0	365.0	412.2	306.0	325.0	352.0	397.5
A44	398.0	416.7	433.9	452.5	475.0	323.9	338.9	360.0	384.2	419.4	312.0	338.0	371.0	407.0
A45	412.0	425.0	434.4	441.1	448.0	361.1	373.9	391.7	416.7	434.4	339.8	365.0	400.0	428.0
A46	382.1	397.2	413.3	427.3	444.0	333.3	345.6	361.7	385.7	411.1	314.0	338.4	369.4	400.0
A47	367.8	332.2	398.9	416.0	441.0	312.8	322.8	336.1	352.8	380.0	305.0	323.6	344.2	370.5
A48	400.0	408.0	420.6	432.0	447.0	327.8	341.1	360.0	382.0	409.4	318.0	340.2	369.0	395.0
A49	419.0	427.0	435.0	442.3	448.0	368.9	378.3	397.8	419.4	433.3	349.6	374.4	402.6	430.0
A50	404.0	410.2	417.2	424.0	431.0	375.0	377.8	391.7	407.2	418.9	355.0	374.0	395.0	415.0
A51	406.6	412.2	417.6	422.0	427.0	370.6	377.2	390.6	402.7	418.3	351.4	372.2	393.3	413.0
A52	384.0	398.1	416.7	428.0	443.0	335.5	348.9	368.3	391.7	418.9	319.0	341.5	373.0	405.0
A53	403.3	409.5	414.4	413.5	422.8	374.4	375.6	388.9	404.4	415.6	347.0	369.0	395.0	410.0
A54	419.0	427.0	434.4	442.0	450.0	373.3	381.7	397.2	418.9	435.0	351.0	364.4	400.0	430.0

RUN NO.   A11

x	$T_g(x)$	$T_s(x)$	$T_w(x)$	$\dfrac{dT_g}{dx}$	$\dfrac{dT_s}{dx}$	$q_s(x)$	$q_{gs}(x)$	$q_a(x)$	$q_{gw}(x)$
1.25	520.0	378.0	373.2	84.8	65.1	339.5	446.5	598.4	151.8
1.30	524.4	381.5	377.0	91.9	73.0	381.9	481.1	649.0	167.8
1.40	534.2	389.5	385.4	103.0	87.6	460.3	552.8	728.0	175.1
1.50	544.9	398.9	394.9	109.9	100.4	530.2	619.6	777.4	157.8
1.60	556.0	409.5	405.9	112.6	111.3	591.4	671.2	797.1	125.8
1.78	576.0	431.0	430.4	106.8	126.4	679.5	693.5	757.4	63.9

Z= 0.99   SGL= 0.16   ARC= 0.41   DE= 0.17   EL= 0.19
QSWT=0.4739E+02   QST=0.2801E+03   QGST=0.3275E+03   QGT=0.3939E+03
QGWT=0.6641E+02   HTCGS=27.0   HTCGW= 2.1
RE=2.013E+03   NU=1.202E+02   NUW=1.048E+01

RUN NO.   A12

x	$T_g(x)$	$T_s(x)$	$T_w(x)$	$\dfrac{dT_g}{dx}$	$\dfrac{dT_s}{dx}$	$q_s(x)$	$q_{gs}(x)$	$q_a(x)$	$q_{gw}(x)$
1.25	489.0	356.0	353.9	66.9	48.3	248.7	294.8	471.3	176.5
1.30	492.5	358.5	356.8	71.4	53.2	274.7	314.3	502.9	188.6
1.40	500.0	364.4	363.1	79.6	63.7	329.7	359.1	561.1	202.0
1.50	508.4	371.3	370.4	86.9	74.8	389.0	409.2	612.8	203.5
1.60	517.4	379.4	378.9	93.2	86.7	452.6	461.9	657.8	195.9
1.78	535.0	397.0	397.5	102.2	109.7	578.5	566.5	722.0	155.5

Z= 0.99   SGL= 0.16   ARC= 0.41   DE= 0.17   EL= 0.19
QSWT=0.1072E+02   QST=0.2141E+03   QGST=0.2248E+03   QGT=0.3240E+03
QGWT=0.9912E+02   HTCGS=19.6   HTCGW= 3.4
RE=2.108E+03   NU=9.350E+01   NUW=1.630E+01

RUN NO.   A13

x	$T_g(x)$	$T_s(x)$	$T_w(x)$	$\dfrac{dT_g}{dx}$	$\dfrac{dT_s}{dx}$	$q_s(x)$	$q_{gs}(x)$	$q_a(x)$	$q_{gw}(x)$
1.25	452.0	354.0	349.9	66.5	48.3	248.6	341.2	466.4	125.2
1.30	455.4	356.5	352.9	69.1	53.5	275.9	358.5	485.0	126.5
1.40	462.5	362.4	359.3	73.8	63.2	326.7	395.4	518.2	122.8
1.50	470.1	369.1	366.5	77.7	71.8	372.6	432.2	546.2	114.1
1.60	478.1	376.7	374.4	80.9	79.3	413.4	465.1	569.0	103.9
1.78	493.0	392.0	390.6	84.8	90.1	473.9	506.3	596.9	90.7

Z= 0.99   SGL= 0.16   ARC= 0.41   DE= 0.17   EL= 0.19
QSWT=0.3160E+02   QST=0.1974E+03   QGST=0.2290E+03   QGT=0.2879E+03
QGWT=0.5891E+02   HTCGS=27.2   HTCGW= 2.7
RE=2.181E+03   NU=1.354E+02   NUW=1.325E+01

RUN NO. A14

1.25	411.0	341.0	338.7	40.5	36.8	188.1	220.7	283.2	62.5
1.30	413.1	342.9	340.9	42.1	40.2	205.8	234.8	294.8	60.0
1.40	417.4	347.3	345.6	45.0	46.3	237.6	261.0	315.3	54.3
1.50	422.1	352.2	350.9	47.5	51.4	264.5	282.5	332.2	49.7
1.60	426.9	357.5	356.8	49.3	55.5	286.4	297.0	345.6	48.7
1.78	436.0	368.0	368.7	51.5	60.4	313.3	303.1	360.7	57.6

Z= 0.99   SGL= 0.16   ARC= 0.41   DE= 0.17   EL= 0.19
QSWT=0.9579E+01   QST=0.1336E+03   QGST=0.1482E+03   QGT=0.1748E+03
QGWT=0.2658E+02   HTCGS=25.4   HTCGW= 1.8
RE=2.330E+03   NU=1.327E+02   NUW=9.948E+00

RUN NO. A15

1.25	348.3	312.8	310.4	19.8	15.6	44.6	73.1	137.7	64.6
1.30	349.3	313.6	311.3	21.3	17.8	50.8	79.1	148.4	69.3
1.40	351.6	315.6	313.2	23.6	21.9	62.7	91.6	164.6	73.0
1.50	354.0	318.0	315.5	25.0	25.9	74.1	104.2	174.0	69.8
1.60	356.6	320.8	318.2	25.4	29.6	85.0	115.9	176.6	60.7
1.78	361.0	326.7	324.0	23.5	35.9	103.3	135.0	164.0	29.1

Z= 0.99   SGL= 0.16   ARC= 0.41   DE= 0.17   EL= 0.19
QSWT=0.1597E+02   QST=0.3979E+02   QGST=0.5576E+02   QGT=0.8792E+02
QGWT=0.3216E+02   HTCGS=18.9   HTCGW= 4.0
RE=2.593E+03   NU=1.110E+02   NUW=2.336E+01

RUN NO. A16

1.25	462.0	374.0	369.2	45.9	57.2	169.2	226.4	322.6	96.3
1.30	464.3	377.0	372.9	47.7	64.4	190.8	240.9	335.0	94.1
1.40	469.3	384.1	380.3	51.4	76.2	226.5	271.7	361.5	89.9
1.50	474.6	392.2	388.0	55.5	84.4	252.1	302.2	390.6	83.4
1.60	480.4	400.9	395.7	60.0	89.0	267.3	328.7	422.2	93.4
1.78	492.0	417.0	410.5	68.9	88.5	268.1	345.9	485.3	139.4

Z= 0.99   SGL= 0.16   ARC= 0.41   DE= 0.17   EL= 0.19
QSWT=0.2655E+02   QST=0.1279E+03   QGST=0.1545E+03   QGT=0.2112E+03
QGWT=0.5669E+02   HTCGS=22.5   HTCGW= 3.0
RE=2.134E+03   NU=1.119E+02   NUW=1.368E+01

RUN NO.   A17

1.25	543.0	410.0	395.9	82.5	81.5	246.1	523.3	583.5	60.2
1.30	547.2	414.3	400.7	85.6	90.2	272.9	540.9	605.7	64.7
1.40	556.1	424.1	411.0	91.3	105.9	322.2	579.8	646.4	66.6
1.50	565.4	435.4	422.5	96.3	119.5	365.9	618.6	682.4	63.8
1.60	575.3	447.9	435.3	100.7	131.0	403.7	651.8	713.7	61.8
1.78	594.0	473.0	461.2	106.7	146.2	457.0	688.3	757.9	69.6

Z= 0.99   SGL= 0.16   ARC= 0.41   DE= 0.17   EL= 0.19
QSWT=0.1340E+03   QST=0.1931E+03   QGST=0.3270E+03   QGT=0.3610E+03
QGWT=0.3397E+02   HTCGS=30.5   HTCGW= 1.1
RE=1.930E+03   NU=1.323E+02   NUW=4.959E+00

RUN NO.   A18

1.25	410.0	338.9	336.3	60.8	32.1	137.5	193.0	321.6	128.6
1.30	413.1	340.6	338.6	62.1	34.6	148.2	191.1	328.3	137.3
1.40	419.4	344.3	343.2	64.3	39.9	171.4	194.1	340.4	146.3
1.50	425.9	348.6	348.0	66.2	45.7	196.8	208.2	350.6	142.3
1.60	432.6	353.4	352.9	67.7	52.0	224.6	235.7	358.9	123.2
1.78	445.0	363.9	362.3	69.6	64.6	280.9	316.0	365.2	53.2

Z= 0.95   SGL= 0.15   ARC= 0.42   DE= 0.17   EL= 0.18
QSWT=0.6056E+01   QST=0.1031E+03   QGST=0.1142E+03   QGT=0.1852E+03
QGWT=0.7107E+02   HTCGS=18.3   HTCGW= 4.1
RE=1.730E+03   NU=1.044E+02   NUW=2.003E+01

RUN NO.   A19

1.25	405.0	332.2	329.2	68.5	29.9	176.7	235.9	361.9	125.9
1.30	408.5	333.8	331.3	71.9	33.7	199.3	249.1	380.4	131.3
1.40	416.0	337.5	335.6	77.8	40.1	238.2	276.0	411.7	135.7
1.50	424.0	341.8	340.1	82.3	45.1	268.3	301.8	435.6	133.7
1.60	432.4	346.5	344.7	85.3	48.6	289.7	323.8	451.9	128.0
1.78	448.0	355.5	353.9	87.1	51.0	306.0	338.0	462.1	124.1

Z= 0.99   SGL= 0.16   ARC= 0.41   DE= 0.17   EL= 0.19
QSWT=0.1778E+02   QST=0.1381E+03   QGST=0.1559E+03   QGT=0.2272E+03
QGWT=0.7127E+02   HTCGS=22.4   HTCGW= 3.9
RE=1.776E+03   NU=1.211E+02   NUW=2.006E+01

RUN NO.   A20

1.25	427.2	352.8	347.2	69.0	41.1	126.9	239.1	365.6	126.6
1.30	430.7	355.0	350.0	69.1	45.8	141.6	241.5	365.8	124.3
1.40	437.6	360.0	355.7	69.1	53.6	166.2	250.1	366.5	116.5
1.50	444.5	365.6	361.8	69.3	59.3	184.4	261.2	367.6	106.5
1.60	451.4	371.8	368.0	69.6	62.9	196.4	271.8	369.1	97.3
1.78	464.0	383.3	379.7	70.2	64.1	201.5	272.2	372.8	100.6

Z= 0.99   SGL= 0.16   ARC= 0.41   DE= 0.17   EL= 0.19
QSWT=0.4067E+02   QST=0.9447E+02   QGST=0.1351E+03   QST=0.1952E+03
QGWT=0.6008E+02   HTCGS=20.6   HTCGW= 3.4
RE=1.700E+03   NU=1.076E+02   NUW=1.656E+01

RUN NO.   A21

1.25	418.0	360.3	351.2	35.8	36.3	112.6	290.7	346.6	55.9
1.30	419.8	362.2	353.8	35.2	38.8	120.5	285.1	340.9	55.8
1.40	423.2	366.3	359.1	34.3	43.0	133.9	274.6	331.8	57.3
1.50	426.6	370.8	364.7	33.7	46.3	144.2	263.8	325.8	62.0
1.60	430.0	375.5	370.4	33.3	48.5	151.5	251.8	322.9	71.1
1.78	436.0	384.4	380.9	33.6	49.9	156.8	224.6	325.4	100.8

Z= 0.99   SGL= 0.16   ARC= 0.41   DE= 0.17   EL= 0.19
QSWT=0.6340E+02   QST=0.7498E+02   QGST=0.1384E+03   QGT=0.1745E+03
QGWT=0.3611E+02   HTCGS=30.0   HTCGW= 2.7
RE=3.151E+03   NU=1.550E+02   NUW=1.445E+01

RUN NO.   A22

1.25	407.0	341.7	339.0	34.9	29.5	204.8	264.7	337.5	72.8
1.30	408.8	343.3	341.0	35.5	32.7	227.6	278.5	342.9	64.4
1.40	412.4	346.8	344.9	36.9	38.1	265.7	308.1	357.0	48.9
1.50	416.2	350.8	348.8	38.8	42.0	293.6	338.4	375.2	36.8
1.60	420.1	355.2	352.7	41.1	44.5	311.4	367.1	397.7	30.6
1.78	428.0	363.3	359.8	46.4	45.1	317.5	395.1	448.9	53.9

Z= 0.99   SGL= 0.16   ARC= 0.41   DE= 0.17   EL= 0.19
QSWT=0.2375E+02   QST=0.1503E+03   QGST=0.1740E+03   QGT=0.2035E+03
QGWT=0.2941E+02   HTCGS=31.7   HTCGW= 2.0
RE=3.247E+03   NU=1.737E+02   NUW=8.804E+00

RUN NO.   A23

1.25	418.0	365.0	355.7	33.2	32.9	102.2	285.3	321.2	35.9
1.30	419.7	366.6	357.8	33.7	33.1	102.8	275.8	326.3	50.5
1.40	423.1	370.0	362.3	34.7	34.3	107.0	253.0	336.3	78.3
1.50	426.6	373.6	367.0	35.7	36.9	115.2	243.4	346.0	102.5
1.60	430.2	377.4	372.0	36.7	40.7	127.4	234.6	355.4	120.8
1.78	437.0	385.6	381.0	38.4	50.8	159.8	250.6	371.7	121.1

Z= 0.99   SGL= 0.16   ARC= 0.41   DE= 0.17   EL= 0.19
QSWT=0.6797E+02   QST=0.6471E+02   QGST=0.1327E+03   QGT=0.1839E+03
QGWT=0.5125E+02   HTCGS=30.1   HTCGW= 4.0
RE=3.140E+03   NU=1.562E+02   NUW=2.050E+01

RUN NO.   A24

1.25	390.6	322.2	321.1	38.6	19.2	195.6	223.0	373.0	150.0
1.30	392.6	323.2	322.7	41.1	21.1	215.6	227.9	397.2	169.3
1.40	396.9	325.5	326.0	44.7	24.6	251.7	238.8	431.7	193.0
1.50	401.5	328.1	329.3	46.3	27.6	282.5	251.7	447.6	195.9
1.60	406.1	331.0	332.6	46.0	30.0	307.9	266.6	444.9	178.3
1.78	414.0	336.7	338.9	40.6	33.0	340.0	285.7	392.7	107.0

Z= 0.99   SGL= 0.16   ARC= 0.41   DE= 0.17   EL= 0.19
QSWT=-.1634E+02   QST=0.1482E+03   QGST=0.1319E+03   QGT=0.2247E+03
QGWT=0.9282E+02   HTCGS=21.4   HTCGW= 5.9
RE=3.379E+03   NU=1.212E+02   NUW=3.169E+01

RUN NO.   A25

1.25	391.5	322.2	322.3	29.3	22.0	173.5	170.6	283.1	112.5
1.30	393.0	323.3	323.8	30.5	23.8	187.8	179.1	294.2	115.1
1.40	396.2	325.9	326.9	32.7	27.4	216.5	197.5	315.5	118.0
1.50	399.5	328.8	330.3	34.7	31.0	245.2	216.8	335.6	118.8
1.60	403.1	332.1	334.1	36.7	34.6	273.9	235.5	354.6	119.1
1.78	410.0	338.9	341.8	39.9	40.9	325.7	268.1	385.9	117.8

Z= 0.99   SGL= 0.16   ARC= 0.41   DE= 0.17   EL= 0.19
QSWT=-.1507E+02   QST=0.1323E+03   QGST=0.1172E+03   QGT=0.1786E+03
QGWT=0.6144E+02   HTCGS=19.8   HTCGW= 4.1
RE=3.331E+03   NU=1.084E+02   NUW=2.313E+01

RUN NO. A26

1.25	398.9	333.3	331.4	24.6	22.1	155.7	195.3	237.6	42.3
1.30	400.1	334.4	332.9	24.5	23.3	164.0	195.8	236.9	41.1
1.40	402.6	336.9	336.0	25.2	26.2	184.9	203.0	243.2	40.1
1.50	405.2	339.7	339.3	26.9	29.9	211.5	219.5	259.8	40.3
1.60	408.0	342.9	342.8	29.7	34.5	244.0	246.2	286.8	40.7
1.78	414.0	350.0	349.6	37.4	44.6	317.2	324.9	361.7	36.8

Z= 0.84   SGL= 0.14   ARC= 0.44   DE= 0.17   EL= 0.16
QSWT=0.4212E+01   QST=0.1185E+03   QGST=0.1228E+03   QGT=0.1467E+03
QGWT=0.2396E+02   HTCGS =25.1   HTCGW= 1.6
RE=3.159E+03   NU=1.472E+02   NUW=7.930E+00

RUN NO. A27

1.25	388.9	334.4	333.2	21.3	27.6	191.3	215.9	304.7	88.8
1.30	390.0	335.9	334.7	22.7	31.0	214.8	233.0	326.0	88.1
1.40	392.4	339.2	337.8	24.5	35.3	245.3	273.5	351.8	78.3
1.50	394.9	342.8	341.0	24.8	36.5	253.7	291.9	355.1	63.2
1.60	397.3	346.4	344.1	23.4	34.4	239.9	286.3	336.0	49.7
1.78	401.0	351.7	350.3	17.1	22.7	158.7	188.3	245.0	56.7

Z= 0.84   SGL= 0.14   ARC= 0.44   DE= 0.17   EL= 0.16
QSWT=0.2025E+02   QST=0.1187E+03   QGST=0.1389E+03   QGT=0.1719E+03
QGWT=0.3295E+02   HTCGS=35.6   HTCGW= 2.7
RE=4.742E+03   NU=2.024E+02   NUW=1.643E+01

RUN NO. A28

1.25	381.1	327.9	325.3	22.6	21.7	232.1	285.1	324.1	38.9
1.30	382.3	329.0	326.7	23.5	22.4	239.5	287.3	336.9	49.6
1.40	384.7	331.3	329.5	25.1	23.9	255.9	293.7	359.6	66.0
1.50	387.3	333.8	332.4	26.4	25.6	274.2	302.6	378.2	75.6
1.60	390.0	336.4	335.5	27.4	27.4	294.4	314.3	392.8	78.5
1.78	395.0	341.7	341.3	28.5	31.2	335.6	344.7	408.6	64.0

Z= 0.84   SGL= 0.14   ARC= 0.44   DE= 0.17   EL= 0.16
QSWT=0.1505E+02   QST=0.1482E+03   QGST=0.1633E+03   QGT=0.1989E+03
QGWT=0.3567E+02   HTCGS =40.7   HTCGW= 2.8
RE=4.817E+03   NU=2.390E+02   NUW=1.645E+01

RUN NO. A29

1.25	396.0	353.9	351.0	19.0	30.0	119.9	178.4	270.4	92.0
1.30	397.0	355.4	352.8	19.0	30.4	121.3	174.9	270.3	95.4
1.40	398.9	358.5	356.2	19.0	30.9	123.9	170.8	269.6	98.8
1.50	400.7	361.6	359.4	18.9	31.5	126.3	171.5	268.6	97.2
1.60	402.6	364.8	362.4	18.8	32.0	128.5	177.6	267.3	89.7
1.78	406.0	370.6	367.5	18.6	32.7	132.0	194.6	264.0	69.4

Z= 0.84   SGL= 0.14   ARC= 0.44   DE= 0.17   EL= 0.16
QSWT=0.2393E+02   QST=0.6700E+02   QGST=0.9093E+02   QGT=0.1420E+03
QGWT=0.5110E+02   HTCGS=31.2   HTCGW= 5.3
RE=4.573E+03   NU=1.824E+02   NUW=2.800E+01

RUN NO. A30

1.25	399.0	357.2	349.8	22.2	30.7	115.1	249.8	315.4	65.6
1.30	400.1	358.7	351.5	21.8	30.2	113.6	244.6	310.2	65.5
1.40	402.3	361.7	355.1	21.2	30.0	112.7	232.1	301.1	69.0
1.50	404.3	364.7	359.1	20.7	30.5	114.8	216.3	293.8	77.5
1.60	406.4	367.8	363.6	20.3	31.7	119.9	197.5	288.3	90.8
1.78	410.0	373.9	372.1	19.9	36.0	136.5	163.9	282.8	113.9

Z= 0.84   SGL= 0.14   ARC= 0.44   DE= 0.17   EL= 0.16
QSWT=0.5376E+02   QST=0.6322E+02   QGST=0.1170E+03   QGT=0.1564E+03
QGWT=0.3947E+02   HTCGS=39.9   HTCGW= 3.9
RE=4.541E+03   NU=2.148E+02   NUW=2.472E+01

RUN NO. A31

1.25	375.6	321.5	320.1	21.3	16.7	223.9	255.1	304.7	49.6
1.30	376.7	322.4	321.1	22.2	17.3	232.2	259.9	318.0	58.1
1.40	379.0	324.1	323.2	23.4	18.4	247.0	267.5	334.6	67.1
1.50	381.3	326.0	325.5	23.6	19.3	259.5	271.1	337.9	66.8
1.60	383.7	328.0	328.0	22.9	20.1	269.7	269.2	327.9	58.7
1.78	387.5	331.7	333.2	19.3	21.0	282.3	247.7	276.1	28.4

Z= 0.84   SGL= 0.14   ARC= 0.44   DE= 0.17   EL= 0.16
QSWT=0.6145E+01   QST=0.1368E+03   QGST=0.1430E+03   QGT=0.1695E+03
QGWT=0.2649E+02   HTCGS=34.5   HTCGW= 2.1
RE=4.891E+03   NU=2.011E+02   NUW=1.392E+01

RUN NO.   A32

1.25	426.1	366.7	362.9	17.8	38.3	285.7	362.2	411.2	48.9
1.30	427.0	368.7	365.2	18.9	40.8	305.1	375.2	435.9	60.7
1.40	429.0	373.0	369.9	20.7	44.9	336.1	399.4	476.8	77.4
1.50	431.1	377.6	374.6	21.9	47.5	356.5	418.4	506.3	87.8
1.60	433.4	382.4	379.3	22.7	48.6	366.3	428.9	524.3	95.3
1.78	437.5	391.1	388.2	22.9	47.1	356.5	415.0	527.7	112.7

Z= 0.84   SGL= 0.14   ARC= 0.44   DE= 0.17   EL= 0.16
QSWT=0.3282E+02   QST=0.1826E+03   QGST=0.2155E+03   QGT=0.2622E+03
QGWT=0.4671E+02   HTCGS=54.3   HTCGW= 3.6
RE=7.058E+03   NU=2.944E+02   NUW=1.908E+01

RUN NO.   A33

1.25	418.3	358.3	354.8	21.8	36.4	270.3	340.7	406.6	65.9
1.30	419.4	360.2	357.2	22.5	37.9	282.2	342.0	418.7	76.6
1.40	421.7	364.1	361.9	23.5	40.6	302.6	346.9	438.5	91.6
1.50	424.1	368.3	366.5	24.3	42.6	318.2	353.9	452.3	93.4
1.60	426.5	372.6	371.0	24.7	43.9	329.2	362.2	460.1	97.9
1.78	431.0	380.6	378.9	24.6	44.8	336.8	371.2	459.1	87.9

Z= 0.84   SGL= 0.14   ARC= 0.44   DE= 0.17   EL= 0.16
QSWT=0.1890E+02   QST=0.1664E+03   QGST=0.1853E+03   QGT=0.2364E+03
QGWT=0.5106E+02   HTCGS=44.7   HTCGW= 3.8
RE=5.803E+03   NU=2.487E+02   NUW=1.972E+01

RUN NO.   A34

1.25	423.3	362.7	358.4	21.1	35.7	266.2	354.5	437.6	83.1
1.30	424.4	364.5	360.4	22.0	37.7	281.1	364.9	458.1	93.2
1.40	426.7	368.5	364.6	23.6	41.1	307.5	385.7	490.1	104.4
1.50	429.1	372.7	369.1	24.5	44.0	329.3	403.8	510.2	106.3
1.60	431.6	377.3	373.8	24.9	46.1	346.6	415.9	518.3	102.4
1.78	436.0	385.8	383.1	24.2	48.5	365.9	420.8	502.9	82.1

Z= 0.84   SGL= 0.14   ARC= 0.44   DE= 0.17   EL= 0.16
QSWT=0.3949E+02   QST=0.1729E+03   QGST=0.2124E+03   QGT=0.2631E+03
QGWT=0.5078E+02   HTCGS=51.0   HTCGW= 3.7
RE=6.404E+03   NU=2.756E+02   NUW=2.072E+01

RUN NO. · A35

1.25	422.2	366.7	362.3	19.7	34.4	256.6	346.0	454.5	108.5
1.30	423.2	368.5	364.8	19.8	35.9	268.3	342.9	457.1	114.2
1.40	425.2	372.2	369.7	20.1	38.8	290.9	341.5	462.5	121.0
1.50	427.2	376.2	374.5	20.3	41.6	312.6	346.7	468.5	121.8
1.60	429.2	380.5	379.3	20.6	44.3	333.4	353.3	474.9	116.7
1.78	433.0	388.9	387.7	21.1	48.7	368.5	393.0	487.8	94.8

Z= 0.84   SGL= 0.14   ARC= 0.44   DE= 0.17   EL= 0.16
QSWT=0.1895E+02   QST=0.1667E+03   QGST=0.1848E+03   QGT=0.2491E+03
QGWT=0.6435E+02   HTCGS=49.5   HTCGW= 5.3
RE=7.096E+03   NU=2.739E+02   NUW=2.706E+01

RUN NO.   A36

1.25	395.6	334.4	330.6	31.7	27.5	201.9	278.2	306.2	28.1
1.30	397.2	335.8	332.0	32.6	29.0	212.3	289.1	314.8	25.7
1.40	400.6	338.8	335.0	34.4	31.5	231.4	309.4	332.3	22.9
1.50	404.1	342.1	338.3	36.3	33.7	248.0	325.3	350.3	25.0
1.60	407.8	345.6	342.0	38.2	35.5	262.1	334.3	368.9	34.6
1.78	415.0	352.2	349.8	41.7	38.0	281.2	330.9	403.8	72.9

Z= 0.84   SGL= 0.14   ARC= 0.44   DE= 0.17   EL= 0.16
QSWT=0.4098E+02   QST=0.1309E+03   QGST=0.1719E+03   QGT=0.1875E+03
QGWT=0.1562E+02   HTCGS=36.8   HTCGW= 1.0
RE=3.157E+03   NU=2.066E+02   NUW=7.145E+00

RUN NO.   A37

1.25	476.7	369.4	362.1	62.1	52.1	390.0	537.2	604.1	66.9
1.30	479.8	372.0	365.5	62.9	52.1	390.5	523.1	611.4	88.3
1.40	486.2	377.3	372.2	64.8	53.1	398.7	500.9	630.4	129.5
1.50	492.8	382.7	379.0	67.3	55.3	416.4	490.0	655.4	165.4
1.60	499.7	388.4	385.9	70.5	58.7	443.8	494.2	686.5	192.3
1.78	513.0	399.7	398.4	77.7	68.1	517.9	544.3	757.5	213.2

Z= 0.84   SGL= 0.14   ARC= 0.44   DE= 0.17   EL= 0.16
QSWT=0.3904E+02   QST=0.2293E+03   QGST=0.2683E+03   QGT=0.3538E+03
QGWT=0.8550E+02   HTCGS=32.3   HTCGW= 3.2
RE=2.789E+03   NU=1.650E+02   NUW=1.604E+01

RUN NO.   A38

1.25	440.6	355.0	348.4	50.5	42.1	312.6	446.3	489.9	43.6
1.30	443.2	357.1	350.5	52.2	42.5	315.3	449.2	506.0	56.8
1.40	449.5	361.4	355.0	55.1	43.7	325.5	455.6	534.7	79.1
1.50	454.2	365.9	359.9	57.6	45.8	342.0	462.5	558.8	96.2
1.60	460.0	370.6	365.4	59.6	48.7	364.7	470.0	578.3	108.3
1.78	471.0	380.0	376.5	61.9	56.0	421.7	492.9	601.7	108.8

Z= 0.84   SGL= 0.14   ARC= 0.44   DE= 0.17   EL= 0.16
QSWT=0.6391E+02   QST=0.1872E+03   QGST=0.2511E+03   QGT=0.2947E+03
QGWT=0.4353E+02   HTCGS=37.8   HTCGW= 2.0
RE=2.927E+03   NU=1.980E+02   NUW=1.183E+01

RUN NO.   A39

1.25	475.0	369.4	363.2	58.5	49.8	372.1	498.3	568.5	70.3
1.30	477.9	371.9	366.2	59.4	49.2	368.8	484.9	577.2	92.3
1.40	484.0	376.8	372.3	62.4	50.2	377.1	469.5	606.6	137.1
1.50	490.5	382.0	378.7	67.0	53.8	405.6	473.1	652.3	179.2
1.60	497.5	387.7	385.4	73.3	60.1	454.4	500.2	714.1	214.0
1.78	512.0	400.0	398.4	88.9	78.2	594.8	626.6	866.6	240.0

Z= 0.84   SGL= 0.14   ARC= 0.44   DE= 0.17   EL= 0.16
QSWT=0.3579E+02   QST=0.2324E+03   QGST=0.2682E+03   QGT=0.3614E+03
QGWT=0.9320E+02   HTCGS=32.7   HTCGW= 3.6
RE=2.792E+03   NU=1.672E+02   NUW=1.791E+01

RUN NO.   A40

1.25	461.1	352.0	348.3	87.9	38.2	282.5	353.0	466.6	108.6
1.30	465.7	353.9	350.9	95.0	37.7	279.7	340.6	504.7	164.1
1.40	475.7	357.7	356.5	104.8	39.3	291.8	316.4	557.3	240.9
1.50	486.4	361.9	362.7	108.6	44.0	327.6	310.7	578.1	267.4
1.60	497.2	366.6	369.5	106.5	51.9	387.3	328.8	567.2	238.4
1.78	515.0	377.8	383.2	87.6	74.0	556.1	447.1	467.1	20.0

Z= 0.84   SGL= 0.14   ARC= 0.44   DE= 0.17   EL= 0.16
QSWT=-.8945E+01   QST=0.1942E+03   QGST=0.1853E+03   QGT=0.2845E+03
QGWT=0.9921E+02   HTCGS=20.1   HTCGW= 3.5
RE=1.558E+03   NU=1.032E+02   NUW=1.851E+01

RUN NO.   A41

1.25	410.6	332.2	325.7	64.1	22.1	162.1	294.5	338.9	44.4
1.30	413.7	333.3	327.0	60.9	20.2	147.6	273.7	322.3	48.6
1.40	419.7	335.2	330.2	58.6	19.7	144.2	246.0	310.1	64.2
1.50	425.6	337.3	334.1	61.6	23.9	175.2	240.9	326.0	85.1
1.60	432.1	340.1	339.0	69.8	32.7	240.7	264.3	370.0	105.7
1.78	447.0	348.3	349.7	98.1	60.5	447.0	418.9	520.5	101.6

Z= 0.84   SGL= 0.14   ARC= 0.44   DE= 0.17   EL= 0.16
QSWT=0.3483E+02   QST=0.1210E+03   QGST=0.1558E+03   QGT=0.1949E+03
QGWT=0.3909E+02   HTCGS=23.5   HTCGW= 1.9
RE=1.691E+03   NU=1.277E+02   NUW=1.161E+01

RUN NO.   A42

1.25	384.4	321.7	319.7	54.6	19.0	138.2	176.4	288.1	109.7
1.30	387.1	322.7	320.8	53.6	19.1	139.1	175.7	282.8	107.1
1.40	392.4	324.6	323.4	52.6	20.7	151.1	176.9	277.7	100.8
1.50	397.7	326.9	326.3	53.0	24.3	177.0	187.7	280.3	92.5
1.60	403.1	329.5	329.9	54.9	29.7	216.8	209.2	290.3	81.1
1.78	413.5	336.1	337.8	61.9	44.2	324.1	289.5	327.5	38.0

Z= 0.84   SGL= 0.14   ARC= 0.44   DE= 0.17   EL= 0.16
QSWT=0.5679F+01   QST=0.1062E+03   QGST=0.1119E+03   QGT=0.1543E+03
QGWT=0.4242E+02   HTCGS=21.3   HTCGW= 2.6
RE=1.765E+03   NU=1.216E+02   NUW=1.612E+01

RUN NO.   A43

1.25	440.0	345.0	338.4	74.8	32.4	239.2	372.2	396.6	24.4
1.30	443.7	346.6	340.7	72.3	30.5	225.2	344.4	383.3	38.9
1.40	450.7	349.5	345.5	69.1	29.6	218.6	300.0	366.9	66.9
1.50	457.6	352.6	350.9	68.6	32.5	240.4	275.9	364.1	88.2
1.60	464.5	356.2	356.8	70.6	39.2	291.0	278.3	374.8	96.5
1.78	478.0	365.0	368.9	80.6	61.0	455.4	375.7	428.5	52.8

Z= 0.84   SGL= 0.14   ARC= 0.44   DE= 0.17   EL= 0.16
QSWT=0.1880E+02   QST=0.1505E+03   QGST=0.1693E+03   QGT=0.2028E+03
QGWT=0.3350E+02   HTCGS=21.7   HTCGW= 1.4
RE=1.616E+03   NU=1.139E+02   NUW=8.217E+00

RUN NO.   A44

1.25	433.9	360.0	356.1	31.6	40.2	298.9	378.9	450.4	71.5
1.30	435.5	362.0	359.8	32.0	39.7	295.2	359.5	456.4	96.9
1.40	439.7	366.0	364.4	33.1	40.1	299.5	331.6	471.7	140.2
1.50	442.1	370.1	369.9	34.5	42.7	319.3	323.0	491.6	168.6
1.60	445.7	374.6	375.3	36.2	47.3	354.7	339.2	516.0	176.8
1.78	452.5	384.2	385.2	40.1	60.8	458.5	439.1	571.5	132.4

Z= 0.84   SGL= 0.14   ARC= 0.44   DE= 0.17   EL= 0.16
QSWT=0.1965E+01   QST=0.1824E+03   QGST=0.1844E+03   QGT=0.2655E+03
QGWT=0.8111E+02   HTCGS=34.4   HTCGW= 4.8
RE=4.337E+03   NU=1.896E+02   NUW=2.449E+01

RUN NO.   A45

1.25	434.4	391.7	383.7	14.0	42.5	107.3	224.3	262.0	37.7
1.30	435.1	393.9	386.7	14.0	44.6	112.8	217.8	261.6	43.8
1.40	436.5	398.5	392.8	13.7	47.7	120.8	204.8	256.3	51.5
1.50	437.8	403.4	398.8	13.1	49.0	124.6	191.3	245.1	53.8
1.60	439.1	408.3	404.7	12.2	48.8	124.3	176.5	228.0	51.4
1.78	441.1	416.7	414.5	9.8	44.1	112.9	145.1	182.4	37.3

Z= 0.70   SGL= 0.12   ARC= 0.47   DE= 0.18   EL= 0.13
QSWT=0.3534E+02   QST=0.6325E+02   QGST=0.9858E+02   QGT=0.1246E+03
QGWT=0.2605E+02   HTCGS=46.6   HTCGW= 2.8
RE=5.345E+03   NU=2.551E+02   NUW=1.499E+01

RUN NO.   A46

1.25	413.3	361.7	355.6	28.2	40.9	112.6	203.5	273.2	69.7
1.30	414.7	363.8	358.2	27.6	43.6	120.0	204.0	266.5	62.5
1.40	417.4	368.4	363.3	26.5	47.4	130.9	206.4	256.4	50.0
1.50	420.0	373.2	368.4	25.9	49.3	136.5	208.7	250.8	42.1
1.60	422.6	378.2	373.4	25.8	49.3	136.8	208.5	249.7	41.2
1.78	427.3	386.7	382.2	26.7	44.4	123.9	190.8	258.9	68.1

Z= 0.70   SGL= 0.12   ARC= 0.47   DE= 0.18   EL= 0.13
QSWT=0.3827E+02   QST=0.6886E+02   QGST=0.1071E+03   QGT=0.1358E+03
QGWT=0.2967E+02   HTCGS=36.1   HTCGW= 2.3
RE=2.905E+03   NU=2.068E+02   NUW=1.245E+01

RUN NO.   A47

1.25	398.9	336.1	334.9	31.1	27.3	199.4	222.0	300.0	78.0
1.30	400.4	337.5	336.5	30.5	27.6	201.2	217.9	294.2	76.3
1.40	403.5	340.3	340.0	30.1	28.6	208.8	214.1	290.6	76.4
1.50	406.5	343.2	343.5	30.8	30.3	222.0	217.0	297.5	80.5
1.60	409.6	346.4	347.1	32.6	32.8	240.7	227.5	315.0	87.6
1.78	416.0	352.8	354.0	38.6	39.2	288.5	266.5	373.3	106.8

Z= 0.70   SGL= 0.12   ARC= 0.47   DE= 0.18   EL= 0.13
QSWT=-.2667E+01   QST=0.1228E+03   QGST=0.1202E+03   QGT=0.1661E+03
QGWT=0.4592E+02   HTCGS=29.5   HTCGW= 3.0
RE=3.036E+03   NU=1.751E+02   NUW=1.718E+01

RUN NO.   A48

1.25	418.0	360.0	356.5	24.1	40.4	298.4	361.4	449.9	88.5
1.30	419.2	362.0	359.0	25.1	40.6	300.9	356.0	467.4	111.4
1.40	421.8	366.1	363.7	26.5	41.2	305.4	348.2	493.1	144.9
1.50	424.5	370.3	368.2	27.2	41.6	309.3	346.9	506.3	159.5
1.60	427.2	374.4	372.1	27.2	41.9	312.4	354.0	507.C	153.0
1.78	432.0	382.0	378.7	25.5	42.2	316.2	376.6	476.7	100.1

Z= 0.70   SGL= 0.12   ARC= 0.47   DE= 0.18   EL= 0.13
QSWT=0.1992E+02   QST=0.1637E+03   QGST=0.1836E+03   QGT=0.2601E+03
QGWT=0.7651E+02   HTCGS=52.6   HTCGW= 5.4
RE=5.588E+03   NU=3.064E+02   NUW=2.870E+01

RUN NO.   A49

1.25	435.0	397.8	390.1	15.1	41.6	102.7	214.9	279.3	64.4
1.30	435.8	399.9	392.4	15.0	41.7	103.2	212.2	277.8	65.6
1.40	437.2	404.1	397.1	14.7	41.7	103.5	206.0	271.7	65.7
1.50	438.7	408.2	401.7	14.1	41.3	102.7	198.5	261.6	63.2
1.60	440.1	412.3	406.3	13.4	40.5	100.9	189.0	247.6	58.7
1.78	442.3	419.4	414.6	11.5	38.0	95.0	165.7	212.5	46.7

Z= 0.70   SGL= 0.12   ARC= 0.47   DE= 0.18   EL= 0.13
QSWT=0.5078E+02   QST=0.5360E+02   QGST=0.1044E+03   QGT=0.1349E+03
QGWT=0.3056E+02   HTCGS=54.7   HTCGW= 3.5
RE=5.279E+03   NU=2.925E+02   NUW=1.971E+01

RUN NO.   A50

1.25	417.2	391.7	385.5	11.9	25.1	189.4	301.3	322.9	21.7
1.30	417.8	392.9	387.2	11.2	23.1	174.1	277.1	304.6	27.6
1.40	418.8	395.1	390.7	10.4	20.1	152.0	231.2	281.4	50.1
1.50	419.9	397.0	394.3	10.2	18.7	141.2	190.4	275.9	85.5
1.60	420.9	398.8	398.0	10.6	18.8	141.9	156.8	288.2	131.4
1.78	423.0	402.5	404.8	13.1	22.7	171.9	130.1	355.2	225.1

Z= 0.70   SGL= 0.12   ARC= 0.47   DE= 0.18   EL= 0.13
QSWT=0.2607E+02   QST=0.8244E+02   QGST=0.1085E+03   QGT=0.1590E+03
QGWT=0.5044E+02   HTCGS=73.1   HTCGW= 8.4
RE=7.978E+03   NU=3.903E+02   NUW=5.085E+01

RUN NO.   A51

1.25	417.6	390.6	383.9	9.5	24.2	80.3	179.6	258.2	78.6
1.30	418.1	391.8	385.7	9.2	22.6	75.1	166.3	249.1	82.8
1.40	419.0	393.9	389.1	8.6	20.7	69.0	141.1	233.8	92.8
1.50	419.8	396.0	392.6	8.2	20.6	68.8	119.3	222.4	103.1
1.60	420.6	398.1	396.2	7.9	22.3	74.4	103.4	214.9	111.5
1.78	422.0	402.7	402.6	7.8	29.7	99.3	101.3	211.3	109.9

Z= 0.70   SGL= 0.12   ARC= 0.47   DE= 0.18   EL= 0.13
QSWT=0.2677E+02   QST=0.4077E+02   QGST=0.6754E+02   QGT=0.1199E+03
QGWT=0.5232E+02   HTCGS=45.5   HTCGW= 8.2
RE=7.983E+03   NU=2.495E+02   NUW=4.648E+01

RUN NO.   A52

1.25	414.0	368.3	358.9	31.4	42.6	99.9	239.7	303.4	63.8
1.30	415.6	370.5	361.6	31.5	43.5	102.1	234.3	304.9	70.6
1.40	418.7	374.9	366.9	31.4	44.6	105.1	224.4	304.2	79.8
1.50	421.8	379.4	372.0	30.9	45.1	106.4	216.2	298.9	82.7
1.60	424.9	383.8	376.9	29.8	44.7	105.8	209.6	288.8	79.2
1.78	430.0	391.7	385.5	26.7	42.1	100.1	192.7	258.8	66.1

Z= 0.70   SGL= 0.12   ARC= 0.47   DE= 0.18   EL= 0.13
QSWT=0.5821E+02   QST=0.5512E+02   QGST=0.1133E+03   QGT=0.1545E+03
QGWT=0.4115E+02   HTCGS=41.8   HTCGW= 3.4
RE=2.883E+03   NU=2.376E+02   NUW=1.862E+01

RUN NO.   A53

1.25	414.4	388.9	384.3	7.5	31.2	105.4	174.7	204.3	29.5
1.30	414.8	390.5	386.4	7.2	30.9	104.6	165.0	194.7	29.7
1.40	415.5	393.5	390.5	6.9	30.3	102.7	147.3	186.2	38.8
1.50	416.2	396.5	394.3	7.1	29.5	100.3	133.4	191.7	58.3
1.60	416.9	399.4	397.6	7.8	28.6	97.4	124.2	211.3	87.1
1.78	418.5	404.4	402.6	10.4	26.6	90.9	117.5	281.9	164.4

Z= 0.70   SGL= 0.12   ARC= 0.47   DE= 0.18   EL= 0.13
QSWT=0.1750E+02   QST=0.5261E+02   QGST=0.7011E+02   QGT=0.1124E+03
QGWT=0.4234E+02   HTCGS=56.3   HTCGW= 7.7
RE=8.010E+03   NU=3.259E+02   NUW=4.040E+01

RUN NO.   A54

1.25	435.0	397.2	382.4	13.6	38.9	98.4	316.7	314.7	2.0
1.30	435.7	399.2	385.6	13.3	40.6	103.0	303.8	306.9	3.1
1.40	437.0	403.4	392.1	12.9	42.8	108.8	275.3	297.2	21.9
1.50	438.3	407.7	398.7	12.8	43.2	110.0	243.2	295.4	52.2
1.60	439.5	412.0	405.1	13.1	41.7	106.5	207.3	301.3	94.0
1.78	442.0	418.9	415.9	14.4	34.5	88.4	133.3	331.7	198.4

Z= 0.70   SGL= 0.12   ARC= 0.47   DE= 0.18   EL= 0.13
QSWT=0.7056E+02   QST=0.5494E+02   QGST=0.1255E+03   QGT=0.1622E+03
QGWT=0.3668E+02   HTCGS=64.9   HTCGW= 3.9
RE=6.582E+03   NU=3.463E+02   NUW=2.257E+01

RUN NO.   A55

1.25	431.1	394.4	383.5	18.9	46.1	56.4	192.9	269.6	76.7
1.30	432.0	396.7	386.8	18.8	45.0	55.1	178.8	267.3	88.5
1.40	433.9	401.1	393.3	18.2	42.7	52.4	149.8	259.3	109.6
1.50	435.7	405.2	399.4	17.3	40.4	49.6	122.0	246.8	124.8
1.60	437.3	409.1	405.0	16.1	38.0	46.9	98.0	229.8	131.3
1.78	440.0	415.6	413.9	13.2	33.8	41.7	63.4	187.6	124.2

Z= 0.70   SGL= 0.12   ARC= 0.47   DE= 0.18   EL= 0.13
QSWT=0.3834E+02   QST=0.2606E+02   QGST=0.6440E+02   QGT=0.1265E+03
QGWT=0.6206E+02   HTCGS=33.0   HTCGW= 7.0
RE=4.085E+03   NU=1.809E+02   NUW=3.816E+01